

Università degli Studi del Piemonte Orientale
“Amedeo Avogadro”

Dipartimento di Scienze del Farmaco

PhD in Chemistry & Biology
XXXIII cycle a.y. 2020-2021

**Discovery and development
of small molecules
targeting IDO1 and SOCE**

PhD candidate: **Marta Serafini**

Supervised by **Prof. Tracey Pirali**

PhD program coordinator Prof. Gian Cesare Tron



UNIVERSITÀ DEL PIEMONTE ORIENTALE

DOTTORATO DI RICERCA
IN CHEMISTRY & BIOLOGY

Via Duomo, 6
13100 – Vercelli (ITALY)

DECLARATION AND AUTHORISATION TO ANTIPLAGIARISM DETECTION

The undersigned Marta Serafini student of the Chemistry & Biology Ph.D course (XXXIII Cycle)

declares:

- to be aware that the University has adopted a web-based service to detect plagiarism through a software system called “Turnit.in”,
- his/her Ph.D. thesis was submitted to Turnit.in scan and reasonably it resulted an original document, which correctly cites the literature;

acknowledges:

- his/her Ph.D. thesis can be verified by his/her Ph.D. tutor and/or Ph.D Coordinator in order to confirm its originality.

Date: 10/11/2020 Signature: *Marta Serafini*

TABLE OF CONTENTS

PREFACE	7
INTRODUCTION	9
1.1 THE CHANGING LANDSCAPE OF MEDICINAL CHEMISTRY	11
1.2 VIRTUAL SCREENING APPROACH	14
1.3 THE CLICK CHEMISTRY APPROACH	16
1.4 DEUTERIUM APPLICATIONS IN MEDICINAL CHEMISTRY	21
1.5 REFERENCES	24
PART I: STORE-OPERATED CALCIUM ENTRY MODULATORS	31
2.1 A BRIEF INTRODUCTION ON STORE-OPERATED CALCIUM ENTRY	33
2.1.1 ACUTE PANCREATITIS AND SOCE	35
2.1.2 RARE DISEASES RELATED TO SOCE PROTEINS MUTATIONS	36
2.2 OUTLINE OF THE PROJECT	38
2.3 REFERENCES	40
<u>STORE-OPERATED CALCIUM ENTRY (SOCE) AS A THERAPEUTIC TARGET IN ACUTE PANCREATITIS: DISCOVERY AND DEVELOPMENT OF DRUG-LIKE SOCE INHIBITORS</u>	49
3.1 THE REPLACEMENT OF THE ARYLAMIDE OF SYNTA66 AFFORDED THE 1ST CLASS OF MODULATORS	51
3.2 EXPERIMENTAL PART	71
3.3 REFERENCES	94
3.4 AUTHOR CONTRIBUTIONS	98
<u>1,2,4-OXADIAZOLE-BEARING PYRAZOLES AS METABOLICALLY STABLE INHIBITORS OF STORE-OPERATED CALCIUM ENTRY</u>	99
4.1 THE REPLACEMENT OF THE ETHYL ESTER OF PYR3 WITH A 1,2,4-OXADIAZOLE RING AFFORDED THE 2ND CLASS OF MODULATORS	101
4.2 EXPERIMENTAL PART	110
4.3 REFERENCES	121
4.4 CONTRIBUTIONS AND COLLABORATIONS	122
PART II: INDOLEAMINE 2,3-DIOXYGENASE INHIBITORS	123

5.1 A BRIEF INTRODUCTION ON INDOLEAMINE 2,3-DIOXYGENASE	125
5.2 OUTLINE OF THE PROJECT	129
5.3 REFERENCES	131

**SYNTHESIS, DOCKING AND BIOLOGICAL EVALUATION OF A NOVEL CLASS OF
IMIDAZOTHIAZOLES AS IDO1 INHIBITORS** **135**

**DISCOVERY OF HIGHLY POTENT BENZIMIDAZOLE DERIVATIVES AS INDOLEAMINE 2,3-
DIOXYGENASE-1 (IDO1) INHIBITORS: FROM STRUCTURE-BASED VIRTUAL SCREENING TO
IN VIVO PHARMACODYNAMIC ACTIVITY** **153**

UNPUBLISHED RESULTS **241**

8.1 IDENTIFICATION OF COMPOUND VS-15	243
8.2 EXPERIMENTAL SECTION	255
8.3 REFERENCES	266
8.4 CONTRIBUTIONS AND COLLABORATIONS	268

DISCUSSION AND CONCLUSIONS **269**

9.1 THE MODULATION OF STORE-OPERATED CALCIUM ENTRY AS A THERAPEUTIC APPROACH FOR THE TREATMENT OF TUBULAR AGGREGATE MYOPATHY	271
9.2 IDO1 INHIBITORS IN CANCER IMMUNOTHERAPY	272
9.2.1 VS-13 IS A PROMISING CANDIDATE BUT IS AFFECTED BY A LOW METABOLIC STABILITY	273
9.2.3 VS-15 IS CHARACTERIZED BY A PECULIAR BIOLOGICAL PROFILE	275
9.3 REFERENCES	276

PUBLICATIONS **279**

CURRICULUM VITAE **283**

Preface

The research activity of my PhD has been focused on two main projects. The first topic has started in my first year and its central core is the discovery of novel Store-Operated Calcium Entry (SOCE) modulators as potential treatments for calcium related diseases. The second, involving the development of indoleamine 2,3-dioxygenase (IDO) inhibitors in cancer immunotherapy, has started in my second year thanks to a *Fondazione AIRC (Associazione Italiana per la Ricerca sul Cancro) research fellow* that I was awarded. The two-year individual fellowship has helped me to finish my PhD, since I have not benefited from an Italian Ministry of Education fellowship and I was previously paid by funds of my supervisor's lab deriving from industrial commissions. For this reason, *Fondazione AIRC* is deeply acknowledged. Given that the two topics are not related to each other, this thesis has been divided in two parts, named Part I and II. Despite unrelated, the *leitmotif* of both projects can be found in the role played by modern medicinal chemistry in the process of drug discovery and development. Therefore, while a brief introduction on each topic can be found at the beginning of Part I and II, the introduction of my Thesis is focused on the different techniques that a medicinal chemist can rely upon in the search of novel drugs and that have been applied in my research activity.

The compounds described in this Thesis have been synthesized first-hand by me or have been the object of co-supervision of Master students that have carried out their Thesis project in Prof. Pirali's laboratory.

The efforts described herein have resulted in several publications listed at the end of the Thesis. Some of these publications are related to Part I and II and therefore compose the different Chapters. All of these results have been achieved thanks to a number of collaborations both inside the University of Piemonte Orientale and outside. In particular, Prof. Genazzani and Dr. Fallarini's groups from University of Piemonte Orientale, Prof. Ugel from University of Verona, Dr. Pallotta from University of Perugia and their respective research units are deeply acknowledged.

Chapter 1

Introduction

1.1 The changing landscape of medicinal chemistry

The role of medicinal chemists in the process of drug R&D has dramatically changed in the past years.¹ First of all, new technologies have appeared, allowing the synthesis and the *in vitro* screening of large libraries of compounds. A recent review, for example, analyses the lead generation strategies that have led to clinical candidates described in the *Journal of Medicinal Chemistry*: the majority of them (43%) have been designed from previously known molecules, while random high-throughput screening (HTS) has led to the identification of the 29% of the candidates. Structure-based drug design, fragment-based lead generation and DNA-encoding library screening are other important approaches nowadays.² At the same time, the techniques that allow the identification of new targets, such as genomics, proteomics, small interfering RNA, have made their appearance, arising the quest for novel compounds able to target them.³ Besides the increase of both drug targets and available techniques for the design and synthesis of compounds, the knowledge required in drug discovery has enormously expanded as well, increasing the challenge that a modern medicinal chemist has to deal with during his/her everyday life.

The high degree of complexity in drug R&D is reflected in the fact that the number of newly approved drugs has suffered a setback in the last decade, mostly due to a low clinical success rate.⁴ However, this trend does not find a counterpart in the investments that pharmaceutical industry made in developing new entities, but is more likely associated with the lower quality of clinical candidates. A powerful tool to gain insight into the direction in which drug R&D is moving today is represented by the lists of International Non-proprietary Name (INN) by World Health Organization (WHO), which clearly demonstrate that the pharmaceutical market is thriving more than ever. For a new molecular entity, it is mandatory to receive an INN before being approved by the regulatory agencies. When a company applies to the WHO to receive an INN for a new molecule, a name might be proposed by the applicant, following the rules of drug nomenclature. The proposed name is evaluated

by the INN Committee and might be changed before the publication of the official name. The publication of the assigned INN⁵ is made online, in a volume that is downloadable and in which additional information are present, such as the chemical structures, the IUPAC names and the CAS numbers. Therefore, the publication of the assigned INN might represent the first public disclosure of the structure of the candidate being developed by a company. In the last twenty years, the Committee of the WHO in charge of this process has assigned 3456 INNs, with the number of INNs dramatically increased over time, raising from an average of 120 names published per year in the 2000s to a number of 307 INNs in 2020.

Another issue that draws attention by analyzing the structures listed in the INN volumes is represented by the fact that the number of organic drugs listed has been halved from 2000 to 2020 (from 79% of organic drugs on all the INNs to only 41%). At the same time, the percentage of biologic drugs and monoclonal antibodies has increased, and, since 2007, DNA/RNA based and other advanced therapies (*e.g.* gene and cell therapies, oncolytic viruses or bacteria) have made their appearance. Overall, the contribution of these entities accounts for the 52% of all the listed INNs in 2020.

In this changing landscape, therefore, medicinal chemists should reinvent themselves, repurposing their skills in a world in which further actors are now “creating” drugs. While the medicinal chemist has always been part of a multidisciplinary team, participation in a tight network of different disciplines, spanning from biophysics to regulatory affairs, has become more and more important to achieve the goal and develop a successful drug. Besides being obviously experts in organic and medicinal chemistry, other complementary skills include a deep understanding of the biology and of the literature focused on the target disease, a comprehension of the pharmacological tests set up to evaluate the compounds, a knowledge of the factors that influence ADMET profiles of candidates, and the awareness of what is the clinical need associated with the disease, what are the

medicines already in use and, as a consequence, what are the competitive standards of care and what would be the regulatory requirements for the approval.¹

Medicinal chemists are obviously the protagonists in the early phases of drug discovery and the success of a drug largely relies upon the choice made in these early phases, with an eye on the future development of the drug. Indeed, while medicinal chemists are often perceived as “compound makers”, the real mission that should be pursued is to address an unmet clinical need and bring a drug to the approval with the aim to provide a benefit to patients. Indeed, not all medicines are equal, and some drugs stand over the others for the clinical benefits they provide to patients. On this concept, during the lockdown imposed by the COVID-19 pandemic at the beginning of March 2020, I participated in writing a Perspective article published in the *Journal of Medicinal Chemistry*, analysing the medicinal chemistry of Essential Medicines (EMs) through a number of systematic analyses.⁶ EMs are a very selected group of medicines listed by WHO in the Essential Medicines List (EML)⁷ and chosen among all the approved drugs for their highest benefit/risk ratio, as well as their pivotal role for the worldwide health. Today, four States out of five possess a National EML, ensuring that the population of a specific country has access to a drug considered crucial for satisfying their healthcare needs. In analyzing the medicinal chemistry features of this cluster of medicines, it emerged that the requirements usually said to be necessary to make a compound a good candidate are not always fulfilled. While maybe obvious, our analysis concludes that no rules in drug R&D seem to exist: the rules of thumb usually followed in medicinal chemistry serve just to reduce the failure associated with the development of a molecule. For example, we found out that there are EMs bearing 21 stereocenters and are still blockbuster drugs for heart failure treatment (*i.e.* digoxin), that are administered *per os* even if failed 4 Lipinski’s parameters out of 4 (*i.e.* rifapentine), that include multiple structural alerts but are safe enough to be in the market (*e.g.* valproic acid, isoniazide), that are predicted not to cross the blood brain barrier but have been used for decades as general anesthetics (*i.e.* isoflurane, halothane). Therefore, many

exceptions to the known rules exist, no prediction can be easily made on paper and more than ever there is a need for effective strategies that help medicinal chemists to reduce the high degree of attrition in drug R&D.

Among the new available technologies that have enriched the arsenal of medicinal chemists, some of them have been largely explored in my research activity, such as the virtual screening approach to identify new scaffolds, the click chemistry reaction to synthesize large libraries of compounds and the use of deuterium as a strategy to improve the pharmacokinetic and toxicological profiles of a candidate. The application of these techniques in the everyday laboratory life has resulted in a strong knowledge of the latter two fields, stemming in a Book Chapter submitted under invitation to *Advances in Heterocyclic Chemistry*⁸ focused on click chemistry and in a Perspective article published in the *Journal of Medicinal Chemistry* on the use of deuterium in medicinal chemistry.⁹

1.2 Virtual screening approach

In the last decades, two techniques applied in the earlier stages of drug discovery campaigns have contributed to minimize the cost and time associated with identification of candidates: high throughput screening (HTS) and virtual screening (VS). While the first, relying on the automatic testing of thousands of molecules on a specific biological target, has undoubtedly led to the discovery of important drugs,¹⁰ VS provides the advantage of processing millions of compounds without the need to physically synthesize them, enormously expanding the analysed chemical space.¹¹

The term VS was coined in 1997,¹² in spite of the fact that the technique has been known since the '80s. Since then, VS has become very popular and has found wide application in the field of medicinal chemistry. There are two different approaches in VS, ligand-based (LBVS) and structure-based (SBVS). The former is based on the similarity of the screened compounds with known active molecules or common pharmacophores,¹³ relying on the principle that similar compounds are endowed with

similar properties.¹⁴ On the other hand, SBVS exploits the complementarity of the analysed compounds with the protein binding site, using docking procedures, scoring functions and computational algorithms, but necessarily requiring the 3D structure of the target protein.¹⁰ VS sees the automate evaluation of large databases, either as public or commercial or from vendors catalogues, allowing the fast screening of up to 10 million of structures. The considered molecules pass through a virtual funnel in which different filters are applied and candidates are scored at each step. Compounds that survive all the filters are predicted to be the most promising in binding to the target. However, while VS boosts the identification of a hit or lead compound, the molecule still needs to be synthesized or purchased in order to be biologically tested against the target of interest. Moreover, a molecule discovered by VS might require a hit-to-lead optimization to improve its potency or drug-likeness.

Outcome of the application of virtual screening in my research activity

The SBVS technique has represented the starting point of my research activity in the IDO field, thanks to the tight collaboration with Prof. Massarotti from UPO. Indeed, the screening of more than 8 million compounds on IDO1 active site (ZINC database) has allowed their ranking (Chapter 7 and 8).¹⁵ By purchasing and screening the top 50 scored compounds for their inhibitory activity on IDO1, we have discovered two promising hit compounds for our medicinal chemistry campaigns. One of them is a completely novel scaffold, never reported before and endowed with high potency (Chapter 7), while the other has been previously reported as iNOS inhibitor (Chapter 8).¹⁶

1.3 The click chemistry approach

Since the discovery of the click chemistry concept by Kolb, Finn and Sharpless in 2001,¹⁷ the copper catalysed azide-alkyne cycloaddition (CuAAC) has permeated many disciplines, spanning from chemistry to biology and appearing as a fundamental tool in chemical biology.¹⁸

The possibility to synthesize molecules containing a 1,2,3-triazole ring in a simple and effective manner has indeed prompted medicinal chemists to prepare large libraries of triazole-displaying molecules in many early drug discovery programs. Triazole is a very popular heterocyclic ring group in the scientific literature, being the most exploited five-membered nitrogen-containing heterocycle.¹⁹ Two isomeric forms are possible: the 1,2,3- and the 1,2,4-triazole. While the latter is particularly abundant in antimycotic drugs due to its strong coordinating properties, the 1,2,3-triazole has been much less exploited in marketed compounds. Nevertheless, since the discovery of the CuAAC reaction, the 1,2,3-triazole, and especially the 1,4-disubstituted regioisomer, has received an ever-increasing attention and has found wide application.²⁰

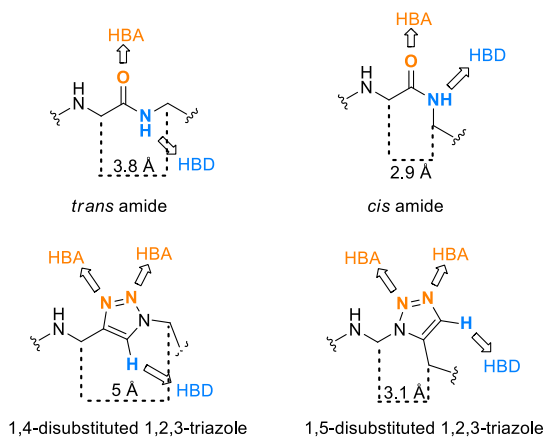
In terms of intermolecular interactions, the 1,4-disubstituted 1,2,3-triazole has a preference for hydrophobic residues in the binding pocket.²¹ Moreover, since it is planar and possesses a strong aromatic character, it is potentially involved in edge-face and face-face stacking, especially with Trp residues in the binding pocket. Furthermore, the triazole might serve as hydrogen bond acceptor in correspondence to the N(2) and N(3), while the C-H, due to the polarization given by the 1,2,3-triazole ring, might behave as hydrogen bond donor (Figure 1). Finally, 1,2,3-triazoles display marked stability towards acidic and basic hydrolysis, oxidative and reductive conditions (reflecting a high aromatic stabilization), and enzymatic degradation. This is the reason why triazole is often used in the **isosteric replacement of amide group**, the latter at times associated with poor hydrolytic stability.²²

In particular, 1,4-disubstituted triazoles are effective isosteres of *trans*-amides, while the 1,5-disubstituted regioisomers mimic *cis*-amides. Both isosteric replacements

suffer from a slight difference in the overall dipole moment and the spatial arrangements of substituents, as shown in Figure 1. Nevertheless, the similarities in planarity and hydrogen-bonding properties between the two groups have established the triazole as a useful non-classical bioisostere of the amide, with the advantage of being resistant to hydrolysis and protease-mediated cleavage.

In particular: (i) the carbonyl oxygen lone pair of the amide bond is substituted by the N(3) lone pair; (ii) the polarized C-H bond (in the 5-position) acts as a hydrogen bond donor as the amide N-H bond; (iii) the electrophilic and polarized C4 is electronically similar to the carbonyl carbon.

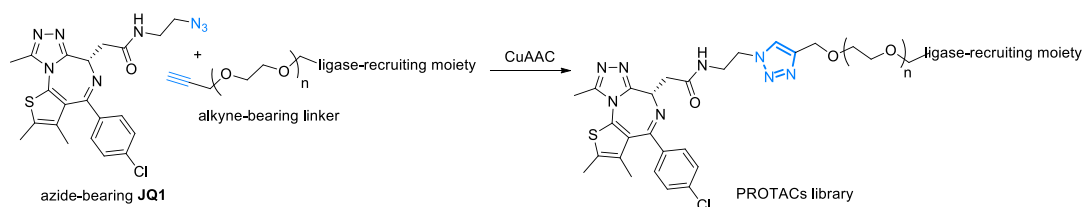
Figure 1. Intermolecular interactions and differences between amides and the 1,2,3-triazole ring.



Besides its exploitation in isosteric amide replacement, the triazole **linker** has also been extensively used to join two building blocks in the generation of hit compounds, twin drugs, both homodimers and heterodimers, and bidentate inhibitors, where the molecule interacts with two different binding sites of the target protein. For example, following the explosion of the Proteolysis Targeting Chimeras (PROTACs) technology, the click chemistry approach has been reported as a powerful tool to modulate the chemistry of the linker moiety.²³ Briefly, PROTACs are bifunctional molecules in which one ligand binds to the protein of interest while the other binds to and recruits an E3 ubiquitin ligase. The recruited E3 ligase induces the transfer of

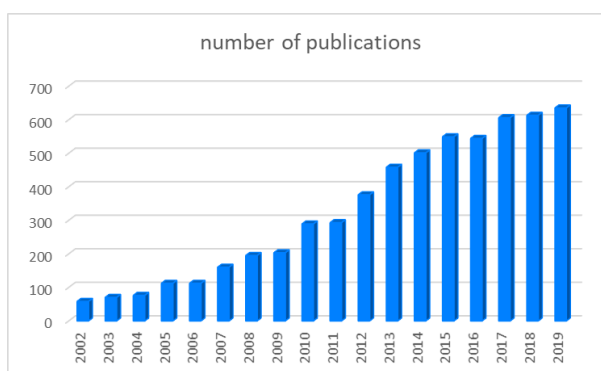
ubiquitin from the ubiquitin-conjugating enzyme E2 to the target protein and the polyubiquitination of the latter results in the degradation by the proteasome system.²⁴ Both the pharmacokinetic and the pharmacodynamic features of PROTACs heavily depend on linker length and structure. Indeed, the formation of the ternary complex between the ligase, the PROTAC and the target protein, a key element to ensure the efficient degradation of the protein of interest, relies upon the appropriate length of the linker. Moreover, the structural features of the linker are responsible for PROTACs solubility and metabolic stability.²⁵ It is foreseen therefore that the exploitation of the click chemistry approach will boost the process of PROTACs optimization, leading to a straightforward and comprehensive study of linker length/activity relationship (Figure 2).

Figure 2. The click chemistry approach applied to the design of PROTAC libraries.



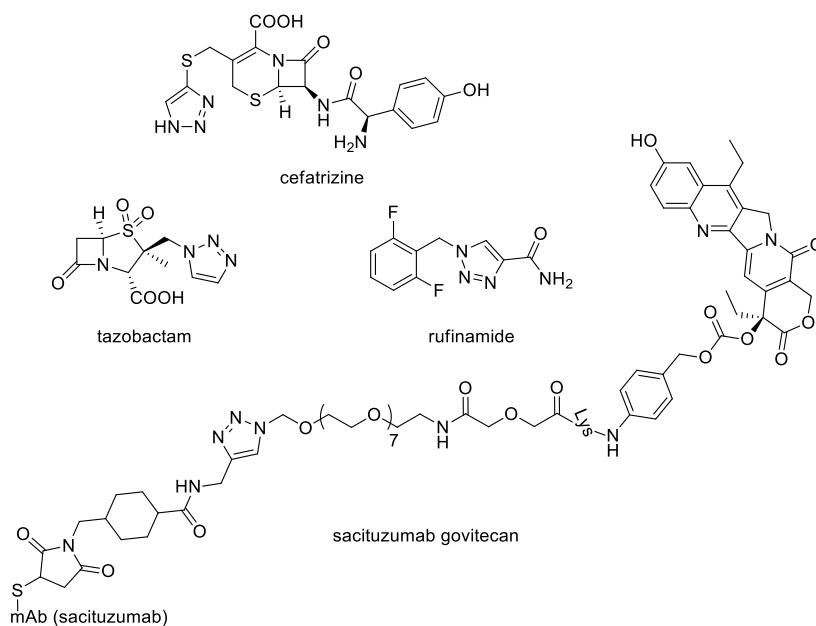
In this context, another example is represented by the use of the triazole ring in the design of antibody-drug conjugates (ADC).²⁶ This has recently led to the approval of sacituzumab govitecan, the first marketed ADC synthesized by click chemistry.²⁷ By analysing the number of publications containing the “1,2,3-triazole” concept from 2002 to 2019, it appears undeniable that click chemistry has made an impact on the medicinal chemistry field (Figure 3). However, despite the increasing number of publications, only few triazoles have been approved by FDA and some others are under clinical development.

Figure 3. Number of publications that result in SciFinder searching “1,2,3-triazole” from 2002 to 2019 and filtering only journals and only English.



Among the approved triazoles, only four 1,2,3-triazole-bearing drugs have been launched on the market so far and only one of them has been discovered through click chemistry approach, represented by the already cited sacituzumab govitecan.²⁷ The remaining three drugs are cefatrizine,²⁸ bearing a 4-monosubstituted triazoles, tazobactam,²⁹ in which a 1-monosubstituted triazole is displayed, and rufinamide,³⁰ containing a 1,4-disubstituted 1,2,3-triazole ring (Figure 4).

Figure 4. Structures of the four approved 1,2,3-triazole-bearing drugs.



While not discovered through click chemistry, synthetic routes exploiting the CuAAC reaction have been further proposed for both tazobactam and rufinamide.³¹ The lack of clinically approved triazoles is not so surprising, as it is well known that since the discovery of a lead compound, around 15-20 years are usually needed for that molecule to hit the market, and this corresponds to the time passed since the disclosure of the click chemistry concept.

Nevertheless, on visual inspection of the INN volumes starting from 2002, it can be seen that there are at least 11 triazole-displaying compounds in clinical development, namely carboxyamidotriazole, mubritinib, solithromycin, tradipitant, molidustat, bomedemstat, radezolid, seviteronel, milvexian, asundexian and tilpiseritib.

While the rate of success of the molecules published in the INN lists is around 18% of all the molecules that applied to the WHO to receive an INN, it is likely that in the future we will witness the launching on the market of at least some of these triazole-containing clinical candidates, strengthening the utility of the click chemistry approach in drug R&D.

Outcome of the application of click chemistry in my research activity

In my research activity the click chemistry approach has been extensively used in the search of SOCE modulators^{32,33} (Chapter 3) and in the synthesis of a class of imidazothiazoles as IDO1 inhibitors (Chapter 6).³⁴ In particular, the application of this technique and the random synthesis of libraries of compounds are particularly suited to the field of SOCE modulators, as the key components of SOCE machinery have been identified only recently and scarce crystallographic data are available³⁵ to allow the rational design of novel modulators. Moreover, by exploiting click chemistry, the amide shared by most of the reported SOCE inhibitors was substituted by the triazole ring, allowing to go beyond the prior art and to secure enough structural novelty to guarantee intellectual property. This resulted in a filed patent application where I appear as co-inventor.^{33b} Overall, the synthetic efforts led to the generation of 160 triazole-bearing compounds and the identification of two promising lead compounds with *in vivo* efficacy in acute pancreatitis. The relatively

short time in which these goals have been achieved further demonstrated the utility and feasibility of the click chemistry approach.

1.4 Deuterium applications in medicinal chemistry

Very recently, a new isosteric replacement has made its appearance in the medicinal chemistry field. Deuterium (D), the heavy and non-radioactive isotope of protium, (herein named hydrogen (H) for the sake of simplicity), can be used to replace H in chemical compounds as a means of improving known active molecules and already approved drugs (*i.e.* deuterium switch) or as a tool in the generation of new lead compounds (*i.e.* without an hydrogenated counterpart on the market).³⁶ Compared to H, D displays a smaller molar volume (by 0.140 cm³/mol per atom), less lipophilicity ($\Delta \log P_{\text{oct}} = -0.006$) and slightly different pKa.³⁷ Most and foremost, C-D bonds are shorter by 0.005 Å compared to C-H bonds and therefore the transition state for bond cleavage requires a higher activation energy, with a reaction rate, indicated as the k constant, slower ($k_{\text{H}} > k_{\text{D}}$).

The phenomenon, known as deuterium kinetic isotope effect (DKIE) and quantified as the ratio of the rate constants for the reaction rate ($k_{\text{H}}/k_{\text{D}}$),³⁸ accounts for the difference in terms of stability of isotopically-substituted molecules. Typically values of DKIE range from 1, in case of reactions where deuterium has no effect, to 7-9. It follows that DKIE can be exploited in reducing the rate of enzyme-catalysed transformations, if the C-H bond cleavage is at least partially rate-limiting.

Indeed, the most straightforward application of deuterium is represented by the slowdown of drug metabolism, especially through oxidative processes such as those reactions mediated by cytochrome P450 family.³⁹ In particular, high DKIE are detected for dealkylations of ethers and amides (>2), a lower DKIE is usually associated with amine *N*-dealkylation (<2), while DKIE for oxidation of alkyl groups is highly influenced by the rate-limiting step in the specific reaction involved. Last, heteroatom oxygenations, epoxidations and aryl hydroxylations, in which no C-H bond cleavage occurs in the enzyme catalysis, usually display DKIE close to 1.

Besides CYP family, also reactions catalysed by aldehyde oxidase (AO),⁴⁰ involved in the oxidation of the formyl carbon of aldehydes and of α -carbons next to nitrogens in heteroaromatic ring systems, and monoamine oxidases (MAO)⁴¹ enzymes can be affected by DKIE.

Therefore, on one hand the substitution of H with D can slowdown metabolism, improving the pharmacokinetic profile of a molecule. On the other, this isosteric substitution represents the most conservative example of isosteric replacement, since deuterium has the same 3D surface, shape and steric flexibility of hydrogen.³⁷ It is not surprising that most of deuterium-substituted compounds retain the same biochemical potency and selectivity compared to the parent hydrogenated molecule. While the first deuterated compounds have been reported in the 1960s,⁴² the field has exploded in 2017, when the first deuterated drug, deutetrabenazine, was approved by FDA⁴³ for Huntington's disease chorea's and tardive dyskinesias, the same indication of the parent hydrogenated drug tetrabenazine. This approval has represented a surprising breakthrough in the field, considering that the patent of tetrabenazine was still in force at the time and the trial on which deutetrabenazine relied was *versus* placebo, without a head-to-head comparison between the two molecules. Moreover, the only advantage ensured by the deuterated analogue was the reduction of the daily administration, from three to two.⁴⁴ Nevertheless, the success of deutetrabenazine has encouraged the enthusiasm and the investments of the industry, with several companies having as their core business the development of novel deuterated compounds.⁴⁵

At least 14 different deuterated molecules have entered clinical trials: 10 of them derive from a deuterium switch of already marketed drugs, two are nutritional compounds and the remaining two are *de novo* deuterated molecules without a known hydrogenated counterpart. The latter two examples highlight that nowadays a common strategy is the inclusion of the deuterated forms of molecules on which industry had invested in in the Markush formula and in the claims of the related

patents. Deuterium will soon therefore establish its role in the routine process of drug R&D.

In this respect, the most obvious advantage that this isosteric replacement provides is the optimization of the PK profile in the lead optimization process. Generally speaking, the slowdown of metabolism is reflected in an increase in AUC, C_{\max} and $t_{1/2}$ and a reduction of clearance, while T_{\max} is less influenced and the increase in bioavailability occurs only sometimes, putatively depending on the importance of first-pass effect. However, the translation of the *in vitro* effect on metabolism into *in vivo* settings is not always straightforward due to several factors difficult to be predicted, such as the presence of competing elimination mechanisms (*e.g.* urinary/biliary excretion of unchanged drug). Another obstacle is represented by the differences among the animal species and indeed it often happens that an improvement in a species will not be reflected in another, or ultimately in humans. Another phenomenon to be taken into consideration is the possibility of metabolic switching. The deuterium incorporated in a soft spot enhances the rate of metabolism in other sites of the molecule, without leading therefore to an overall advantage in slowing down metabolism, or paradoxically leading to an enhanced metabolism. When this event occurs, simultaneous deuteration or pan-deuteration of the molecule is required to gain a significant effect on metabolism.^{36a}

Other less obvious applications of deuterium are (i) to avoid the formation of toxic metabolites (*i.e.* ifosfamide);⁴⁶ (ii) to reduce drug-drug interactions (*i.e.* paroxetine);⁴⁷ (iii) to increase the formation of active metabolites of prodrugs (*i.e.* clopidogrel);⁴⁸ (iv) to slowdown chemical processes such as epimerization (*i.e.* thalidomide and analogues, telaprevir).⁴⁹

Outcome of the application of deuterium in my research activity

In my research activity, deuterium switch has been largely applied as a means to improve PK profile of an already approved drug on the market. The project has been carried out within an industrial partnership and has resulted in a patent application,

in which I am one of the inventors, filed to the Italian Patent Office (N. 102019000004341, 26/03/2019). While no further details can be disclosed in this thesis, this experience provided me with a deep knowledge of the field, resulting in a Perspective article on the use of deuterium in medicinal chemistry and leading to the application of the technique in the improvement of the metabolic liabilities of IDO1 inhibitors (Chapter 7 and 9).¹⁵

1.5 References

1. Lombardino, J. G.; Lowe, J. A. The role of the medicinal chemist in drug discovery – Then and now. *Nat. Rev. Drug Discov.* **2004**, *3*, 853-862.
2. Brown, D. G.; Boström, J. Where do recent small molecule clinical development candidates come from? *J. Med. Chem.* **2018**, *61*, 9442-9468.
3. Eder, J.; Sedrani, R.; Wiesmann, C. The discovery of first-in-class drugs: origins and evolution. *Nat. Rev. Drug Discov.* **2014**, *13*, 577-587.
4. Carney, S. How can we avoid the productivity gap? *Drug Discov. Today* **2005**, *10*, 1011-1013.
5. <https://www.who.int/medicines/publications/druginformation/innlists/en/> (accessed on Nov 2020).
6. Serafini, M.; Cargnin, S.; Massarotti, A.; Pirali, T.; Genazzani, A. A. Essential medicinal chemistry of essential medicines. *J. Med. Chem.* **2020**, *63*, 10170-10187.
7. <https://www.who.int/medicines/publications/essentialmedicines/en/> (accessed on Oct 2020).
8. Serafini M.; Pirali, T.; Tron, G. C. Click 1,2,3-triazoles in drug discovery and development: from the flask to the clinic? *Advances in Heterocyclic Chemistry* **2020**, *134* (article in press; DOI: 10.1016/bs.aihch.2020.10.001).
9. a) Pirali, T.; Serafini, M.; Cargnin, S.; Genazzani, A. Applications of deuterium in medicinal chemistry. *J. Med. Chem.* **2019**, *62*, 5276-5297; b)

- Cargnin, S.; Serafini, M.; Pirali, T. A primer of deuterium in drug design. *Future Med. Chem.* **2019**, *11*, 2039-2042.
10. Maia, E. H. B.; Assis, L. C.; Alves de Oliveira, T.; Marques da Silva, A.; Taranto, A. G. Structure-based virtual screening: from classical to artificial intelligence. *Front. Chem.* **2020**, *8*, 343-360.
11. Gimeno, A.; Ojeda-Montes, M. J.; Tomás-Hernández, S.; Cereto-Massagué, A.; Beltrán-Debón, R.; Mulero, M.; Pujadas, G.; Garcia-Vallvé, S. The light and dark sides of virtual screening: what is there to know? *Int. J. Mol. Sci.* **2019**, *20*, 1375-1398.
12. Horvath, D. A virtual screening approach applied to the search for trypanothione reductase inhibitors. *J. Med. Chem.* **1997**, *40*, 2412-2423.
13. Lavecchia, A.; Di Giovanni, C. Virtual screening strategies in drug discovery: a critical review. *Curr. Med. Chem.* **2013**, *20*, 2839-2860.
14. Johnson, M. A.; Maggiora, G. M. Concepts and Applications of Molecular Similarity; Wiley: New York, NY, USA, 1990.
15. Serafini, M.; Torre, E.; Aprile, S.; Del Grosso, E.; Gesù, A.; Griglio, A.; Colombo, G.; Travelli, C.; Paiella, S.; Adamo, A.; Orecchini, E.; Coletti, A.; Pallotta, M. T.; Ugel, S.; Massarotti, A.; Pirali, T.; Fallarini, S. Discovery of highly potent benzimidazole derivatives as indoleamine 2, 3-dioxygenase-1 (IDO1) inhibitors: from structure-based virtual screening to *in vivo* pharmacodynamic activity. *J. Med. Chem.* **2020**, *63*, 3047-3065.
16. Zhong, H. J.; Liu, L. J.; Chong, C. M.; Lu, L.; Wang, M.; Chan, D. S.; Chan, P. W.; Lee, S. M.; Ma, D. L.; Leung, C. H. Discovery of a natural product-like iNOS inhibitor by molecular docking with potential neuroprotective effects *in vivo*. *PLoS One* **2014**, *9*, e92905.
17. Kolb, H. C.; Finn, M. G.; Sharpless, K. B. Click chemistry: diverse chemical function from a few good reactions. *Angew. Chem. Int. Ed. Engl.* **2001**, *40*, 2004-2021.

18. Thirumurugan, P.; Matosiuk, D.; Jozwiak, K. Click chemistry for drug development and diverse chemical-biology applications. *Chem. Rev.* **2013**, *113*, 4905-4979.
19. Bozorov, K.; Zhao, J.; Aisa, H. A. 1,2,3-Triazole-containing hybrids as leads in medicinal chemistry: A recent overview. *Bioorg. Med. Chem.* **2019**, *27*, 3511-3531.
20. a) Meghani, N. M.; Amin, H. H.; Lee, B. J. Mechanistic applications of click chemistry for pharmaceutical drug discovery and drug delivery. *Drug Discov. Today* **2017**, *22*, 1604-1619; b) Tron, G.C.; Pirali, T.; Billington, R. A.; Canonico, P. L.; Sorba, G.; Genazzani, A. A. Click chemistry reactions in medicinal chemistry: applications of the 1,3-dipolar cycloaddition between azides and alkynes. *Med Res Rev.* **2008**, *28*, 278-308; c) Meldal, M.; Tornøe, C. W. Cu-catalyzed azide-alkyne cycloaddition. *Chem. Rev.* **2008**, *108*, 2952-3015.
21. Massarotti, A.; Aprile, S.; Mercalli, V.; Del Grosso, E.; Grosa, G.; Sorba, G.; Tron, G. C. Are 1,4- and 1,5-disubstituted 1,2,3-triazoles good pharmacophoric groups? *ChemMedChem* **2014**, *9*, 2497-2508.
22. Kumari, S.; Carmona, A. V.; Tiwari, A. K.; Trippier, P. C. Amide bond bioisosteres: strategies, synthesis, and successes. *J. Med. Chem.* **2020**, <https://doi.org/10.1021/acs.jmedchem.0c00530>.
23. Wurz, R. P.; Dellamaggiore, K.; Dou, H.; Javier, N.; Lo, M.-C.; McCarter, J. D.; Mohl, D.; Sastri, S.; Lipford, J. R.; Cee, V. J. A "click chemistry platform" for the rapid synthesis of bispecific molecules for inducing protein degradation. *J. Med. Chem.* **2018**, *61*, 453-461.
24. Toure, M.; Crews, C. M. Small-molecule PROTACS: new approaches to protein degradation. *Angew. Chem. Int. Ed. Engl.* **2016**, *55*, 1966-1973.
25. Goracci, L.; Desantis, J.; Valeri, A.; Castellani, B.; Eleuteri, M.; Cruciani, G. Understanding the metabolism of proteolysis targeting chimeras (PROTACs):

- the next step toward pharmaceutical applications. *J. Med. Chem.* **2020**, <https://doi.org/10.1021/acs.jmedchem.0c00793>.
26. Pickens, C. J.; Johnson, S. N.; Pressnall, M. M.; Leon, M. A.; Berkland, C. J. Practical considerations, challenges, and limitations of bioconjugation *via* azide-alkyne cycloaddition. *Bioconjug. Chem.* **2018**, *29*, 686-701.
27. a) Syed, Y. T. Sacituzumab govitecan: first approval. *Drugs* **2020**, *80*, 1019-1025; b) Moon, S. J.; Govindan, S. V.; Cardillo, T. M.; D'Souza, C. A.; Hansen, H. J.; Goldenberg, D. M. Antibody conjugates of 7-ethyl-10-hydroxycamptothecin (SN-38) for targeted cancer chemotherapy. *J. Med. Chem.* **2008**, *51*, 6916-6926.
28. a) Dunn, G. L.; Hoover, J. R.; Berges, D. A.; Taggart, J. J.; Davis, L. D.; Dietz, E. M.; Jakas, D. R.; Yim, N.; Actor, P.; Uri, J. V.; Weisbach, J. A. Orally active 7-phenylglycyl cephalosporins. Structure-activity studies related to cefatrizine (SK&F 60771). *J. Antibiot. (Tokyo)*. **1976**, *29*, 65-80; b) Ratti, L.; dall'Asta, L. Process for the preparation of cefatrizine 1,2-propylene glycolate Biochimica O. P. O. S. SpA, US 4965355, 1990.
29. Pagan-Rodriguez, D.; Zhou, X.; Simmons, R.; Bethel, C. R.; Hujer, A. M.; Helfand, M. S.; Jin, Z.; Guo, B.; Anderson, V. E.; Ng, L. M.; Bonomo, R. A. Tazobactam inactivation of SHV-1 and the inhibitor-resistant Ser130 -->Gly SHV-1 beta-lactamase: insights into the mechanism of inhibition. *J. Biol. Chem.* **2004**, *279*, 19494-19501.
30. Gilchrist, J.; Dutton, S.; Diaz-Bustamante, M.; McPherson, A.; Olivares, N.; Kalia, J.; Escayg, A.; Bosmans, F. Nav1.1 modulation by a novel triazole compound attenuates epileptic seizures in rodents. *ACS Chem Biol.* **2014**, *9*, 1204-1212.
31. Kankan, R. N.; Rao, R.; Birari, D. R. Process for the preparation of rufinamide. US 8183269 B2, May 22, 2012; b) Zhang, P.; Russel, M. G.; Jamison, T. F. Continuous flow total synthesis of rufinamide. *Org. Process Res. Dev.* **2014**, *18*, 1567-1570; c) Attolino, E.; Colombo, L.; Mormino, I.;

- Allegrini, P. Method for the preparation of rufinamide, US 8198459 B2, June, 12, 2012.
32. a) Riva, B.; Griglio, A.; Serafini, M.; Cordero-Sanchez, C.; Aprile, S.; Di Paola, R.; Gugliandolo, E.; Alansary, D.; Biocotino, I.; Lim, D.; Grosa, G.; Galli, U.; Niemeyer, B.; Sorba, G.; Canonico, P. L.; Cuzzocrea, S.; Genazzani, A. A.; Piralì, T. Pyrtriazoles, a novel class of store-operated calcium entry modulators: Discovery, biological profiling, and in vivo proof-of-concept efficacy in acute pancreatitis. *J. Med. Chem.* **2018**, *61*, 9756-9783; b) Modulators of SOCE, compositions and use thereof. Piralì T.; Riva B.; Genazzani A. A. WO 2017/212414 A1. Dec 14, 2017.
33. a) Serafini, M.; Cordero-Sanchez, C.; Di Paola, R.; Bhela, I. P.; Aprile, S.; Purghe, B.; Fusco, R.; Cuzzocrea, S.; Genazzani, A. A.; Riva, B.; Piralì, T. Store-Operated Calcium Entry (SOCE) as a therapeutic target in acute pancreatitis: discovery and development of drug-like SOCE inhibitor. *J. Med. Chem.* **2020**, *63*, 14761-14779; b) Piralì, T.; Riva, B.; Serafini, M.; Aprile, S.; Cordero Sanchez, C. Biphenyl compounds as SOCE modulators, compositions and uses thereof. Filed on February 21, 2020, n. 102020000003692.
34. Serafini, M.; Torre, E.; Aprile, S.; Massarotti, A.; Fallarini, S.; Piralì T. Synthesis, docking and biological evaluation of a novel class of imidazothiazoles as IDO1 inhibitors. *Molecules* **2019**, *24*, pii: E1874.
35. Hou, X.; Pedi, L.; Diver, M.M.; Long, S.B. Crystal structure of the calcium release-activated calcium channel Orai. *Nature* **2012**, *338*, 1308-1313.
36. a) Liu, J. F.; Harbeson, S. L.; Brummel, C. L.; Tung, R.; Silverman, R.; Doller, D. A decade of deuteration in medicinal chemistry. *Annu. Rep. Med. Chem.* **2017**, *50*, 519-542.; b) Tung, R. D. Deuterium medicinal chemistry comes of age. *Future Med. Chem.* **2016**, *8*, 491-494; c) Gant, T. G. Using deuterium in drug discovery: leaving the label in the drug. *J. Med. Chem.* **2014**, *57*, 3595-

- 3611; d) Harbeson, S. L.; Tung, R. D. Deuterium in drug discovery and development. *Annu. Rep. Med. Chem.* **2011**, *46*, 403-471.
37. Meanwell, N. A. Synopsis of some recent tactical application of bioisosteres in drug design. *J. Med. Chem.* **2011**, *54*, 2529-2591.
38. Westheimer, F. H. The magnitude of the primary kinetic isotope effect for compounds of hydrogen and deuterium. *Chem. Rev.* **1961**, *61*, 265-273.
39. a) Guengerich, F. P. Kinetic deuterium isotope effects in cytochrome P450 reactions. *Methods Enzymol.* **2017**, *596*, 217-238; b) Guengerich, F. P. Kinetic deuterium isotope effects in cytochrome P450 oxidation reactions. *J. Label. Compd. Radiopharm.* **2013**, *56*, 428-431.
40. Sharma, R.; Strelevitz, T. J.; Gao, H.; Clark, A. J.; Schildknegt, K.; Obach, R. S.; Ripp, S. L.; Spracklin, D. K.; Tremaine, L. M.; Vaz, A. D. N.; Deuterium isotope effects on drug pharmacokinetics. I. System-dependent effects of specific deuteration with aldehyde oxidase cleared drugs. *Drug Metab. Dispos.* **2012**, *40*, 625-634.
41. Malmjöf, T.; Rylander, D.; Alken, R. G.; Schneider, F.; Svensson, T. H.; Cenci, M. A.; Schilström, B. Deuterium substitutions in the L-DOPA molecule improve its anti-akinetic potency without increasing dyskinesias. *Exp Neurol.* **2010**, *225*, 408-415.
42. a) Belleau, B.; Burba, J.; Pindell, M.; Reiffenstein, J. Effect of deuterium substitution in sympathomimetic amines on adrenergic responses. *Science* **1961**, *133*, 102-104; b) Elison, C.; Rapoport, H.; Laursen, R.; Elliott, H. W. Effect of deuteration of N--CH₃ group on potency and enzymatic N-demethylation of morphine. *Science* **1961**, *134*, 1078-1079.
43. Schmidt, C. First deuterated drug approved. *Nat. Biotechnol.* **2017**, *35*, 493-494.
44. a) Claassen, D. O.; Carroll, B.; De Boer, L. M.; Wu, E.; Ayyagari, R.; Gandhi, S.; Stamler, D. Indirect tolerability comparison of deutetrabenazine and tetrabenazine for Huntington disease. *J. Clin. Mov. Disord.* **2017**, *4*, 3-13; b)

- Rodrigues, F. B.; Duarte, G. S.; Costa, J.; Ferreira, J. J.; Wild, E. J. Tetrabenazine versus deutetrabenazine for Huntington's disease: twins or distant cousins? *Mov. Disord. Clin. Pract.* **2017**, *4*, 582-585.
45. a) Timmins, G. S. Deuterated drugs: where are we now? *Expert Opin. Ther. Pat.* **2014**, *24*, 1067-1075; b) Timmins, G. S. Deuterated drugs; updates and obviousness analysis. *Expert Opin. Ther. Pat.* **2017**, *27*, 1353-1361.
46. Calinski, D. M.; Zhang, H.; Ludeman, S.; Dolan, M. E.; Hollenberg, P. F. Hydroxylation and *N*-dechloroethylation of ifosfamide and deuterated ifosfamide by the human cytochrome p450s and their commonly occurring polymorphisms. *Drug Metab. Dispos.* **2015**, *43*, 1084-1090.
47. Uttamsingh, V.; Gallegos, R.; Liu, J. F.; Harbeson, S. L.; Bridson, G. W.; Cheng, C.; Wells, D. S.; Graham, P. B.; Zelle, R.; Tung, R. Altering metabolic profiles of drugs by precision deuteration: reducing mechanism-based inhibition of CYP2D6 by paroxetine. *J. Pharmacol. Exp. Ther.* **2015**, *354*, 43-54.
48. Zhu, Y.; Zhou, J.; Jiao, B. Deuterated clopidogrel analogues as a new generation of antiplatelet agents. *ACS Med. Chem. Lett.* **2013**, *4*, 349-352.
49. a) Maltais, F.; Jung, Y. C.; Chen, M.; Tanoury, J.; Perni, R. B.; Mani, N.; Laitinen, L.; Huang, H.; Liao, S.; Gao, H.; Tsao, H.; Block, E.; Ma, C.; Shawgo, R. S.; Town, C.; Brummel, C. L.; Howe, D.; Pazhanisamy, S.; Raybuck, S.; Namchuk, M.; Bennani, Y. L. In vitro and in vivo isotope effects with hepatitis C protease inhibitors: enhanced plasma exposure of deuterated telaprevir versus telaprevir in rats. *J. Med. Chem.* **2009**, *52*, 7993-8001; b) Jacques, V.; Czarnik, A. W.; Judge, T. M.; Van der Ploeg, L. H.; DeWitt, S. H. Differentiation of antiinflammatory and antitumorigenic properties of stabilized enantiomers of thalidomide analogs. *Proc. Natl. Acad. Sci. U. S. A.* **2015**, *112*, E1471-E1479.

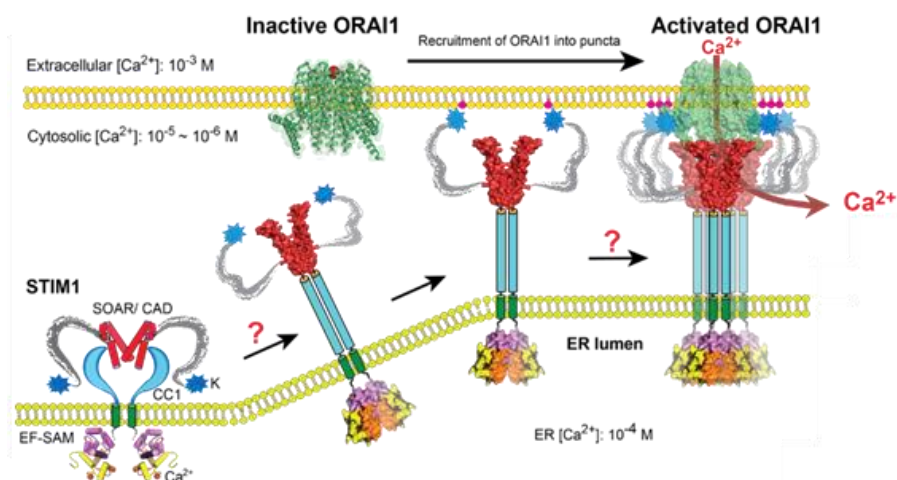
PART I
STORE-OPERATED CALCIUM
ENTRY MODULATORS

2.1 A brief introduction on Store-Operated Calcium Entry

The ubiquitous second messenger calcium is a central regulator of a plethora of physiological processes, spanning from fertilization of oocytes, to cell death, mobility, secretion and gene expression. Infinitesimal oscillations of this ion concentration in the different cell compartments control these multitude of processes. This is the reason why every cell maintains a huge gradient between the plasma membrane or the intracellular calcium repository and the cytoplasm, with various pumps and exchangers in charge of finely regulating its levels.¹ A central mechanism in calcium homeostasis is represented by the Store-Operated Calcium Entry (SOCE), *i.e.* the influx of calcium across the plasma membrane activated by the depletion of this ion in the Endoplasmic Reticulum (ER).² SOCE is mediated mainly, although not exclusively, by two protein families: STIM and Orai. STIM1 and its homologue STIM2 are single-span membrane proteins residing on the ER membrane and act as sensors of calcium levels. Orai are a family of specialized ion channels (Orai1, Orai2 and Orai3) located on the plasma membrane³ and also known as Ca²⁺ release-activated Ca²⁺ (CRAC) channels. When a depletion of calcium from the ER stores occurs, STIM undergoes a conformational change leading to self-association into puncta and migration near the plasma membrane. There, interaction with Orai promotes the opening of the channel and the subsequent influx of calcium (Figure 1). The empty ER stores are then refilled by SERCA pump.⁴

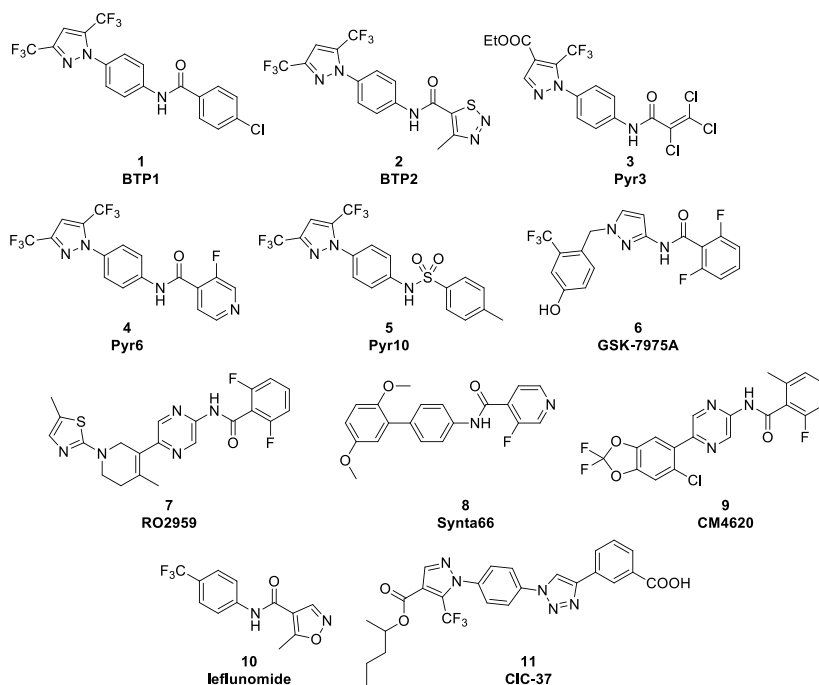
Due to its prominent role in encoding calcium signals, SOCE is implicated in several human disorders, including cancer,⁵ inflammatory bowel diseases,⁶ allergy⁷ and acute pancreatitis.⁸ Therefore, it is not surprising that this cellular pathway has become a popular target for the therapeutic treatment of several pathological conditions.

Figure 1. Cellular mechanism of SOCE (Taken from Ma et al. 2015).⁹



Over the years, many small molecules able to modulate SOCE have been reported.¹⁰ The earliest modulators are SKF-96365,¹¹ 2-APB and its derivatives¹² and bis(trifluoromethyl)pyrazoles compounds, initially named BTP (BTP1 (1), BTP2 (2), Figure 2),¹³ followed by Pyrs (Pyr3 (3), Pyr6 (4), Pyr10 (5), Figure 2).¹⁴ Among others, GSK-7975A (6, Figure 2),¹⁵ RO2959 (7, Figure 2)¹⁶ and Synta66 (8, Figure 2)^{7,8} have been extensively used as chemical probes. More recently, two compounds have entered clinical development, CM4620 (9, Figure 2) for acute pancreatitis (phase 2 completed)¹⁷ and PRCL-02 for psoriasis (phase 2 completed),¹⁸ whose structure has not been disclosed. These are not the only SOCE inhibitors that are in human use. Indeed, a virtual screening made on FDA-approved drugs recently unveiled that two approved drugs are also SOCE inhibitors with relevant activity at therapeutic doses,¹⁹ the pro-drug leflunomide (10, Figure 2),²⁰ and its active form teriflunomide.²¹ The two compounds are approved for the treatment of rheumatoid arthritis and multiple sclerosis, respectively and teriflunomide is a DHODH inhibitor, while leflunomide is devoid of *in vitro* activity on this enzyme. Last, our group of research has contributed to the development of drug-like SOCE modulators by reporting pyrtriazoles, among which the most promising candidate is CIC-37 (11, Figure 2).²²

Figure 2. Structures of SOCE inhibitors reported in the literature.



2.1.1 Acute pancreatitis and SOCE

Among the diseases caused by an hyperactivation of SOCE, acute pancreatitis (AP) has been extensively studied. This condition is an inflammatory life-threatening disorder, characterized by an auto-digestion of the pancreas that causes inflammation, oedema, vacuolization, necrosis, and, in the worst scenario, induces injury of remote extra-pancreatic organs. AP represents an urgent and unmet need since it affects about 35 individuals per 100,000 person-years worldwide,²³ with a mortality rate between 1.5% and 4.2%, and no effective pharmacological treatment is available.^{23,24}

Among the triggers of AP is an intracellular Ca^{2+} overload in pancreatic acinar cells (PACs) that induces the uncontrolled release of intracellular digestive pro-enzymes. While there are numerous mechanisms that control intracellular Ca^{2+} concentrations, SOCE appears to have a pivotal role in the induction of Ca^{2+} overload in PACs.²⁵ Other crucial proteins known to participate in SOCE are transient receptor potential canonical (TRPC) channels,²⁶ which were previously believed to be the primary

contributors of Ca^{2+} rise in PACs, and therefore the main responsible for AP.²⁷ Yet, more recent studies have demonstrated that the metabolic alcohol products, that are among the mediators of acinar cell damage, induce the opening of IP_3Rs , Ca^{2+} channels located in the ER, resulting in the depletion of the ER stores and in the activation of STIM1.²⁸ This event leads to Ca^{2+} entry through Orai1 opening, sustaining toxic intracellular Ca^{2+} elevation and pointing to Orai1 as a key culpable for AP damage.²⁸

In the context of AP, Gerasimenko *et al.* demonstrated that the selective CRAC channel blocker, GSK-7975A (**6**, Figure 2), with no inhibitory activity on TRP-channel currents, is able to decrease the overload of cytosolic Ca^{2+} in a concentration-dependent manner and to prevent the activation of the necrotic cell death pathway in both mouse and human PACs,^{9b} confirming the involvement of Orai in AP and its druggability. Furthermore, GSK-7975A, together with CM4620 (**9**, Figure 2), were demonstrated to be protective in three different murine models of chemically induced AP.^{9a, 29} As previously mentioned, CM4620 has entered clinical trials,¹⁷ with a Phase 2 trial for AP already completed and an ongoing Phase 1/2 trial for a rare condition in which AP is triggered by asparaginase treatment (asparaginase-associated AP). This rare condition (incidence between 7 and 18%) is a well-known complication of childhood acute lymphoblastic leukaemia treatment, that is often responsible for the early discontinuation of drug treatments.^{25b} As the increase in Ca^{2+} induced by asparaginase and the related necrosis of PACs depend on CRAC channels, recent findings have described the inhibition of CRAC channels as the most promising therapeutic approach in this pathology.^{25a, 30}

2.1.2 Rare diseases related to SOCE proteins mutations

There are some rare genetic diseases that arise as a consequence of mutations in genes encoding for Orai or STIM proteins. On one hand, mutations that lead to loss-of-function activity of SOCE components cause a form of Severe Combined ImmunoDeficiency (SCID)-like disorder.³¹ On the other, mutations that lead to gain-

of-function activity of either Orai or STIM have been connected to tubular aggregate myopathy (TAM), a disorder that affected skeletal muscle and platelets.³² This condition is an ultra-rare disease, currently without pharmacological treatments that heavily impairs the quality of life of patients. Considering the rarity of the disorder, its prevalence is still unknown and no patient registries are available, despite we are aware that in Italy there is a family in which a mutation has occurred and, as an estimation, at least 20 person are affected by the pathology.

In TAM, the calcium overload that mainly affected muscles and platelets clinically leads to myalgias, cramps, muscle stiffness and coagulation disorders.³³

Prompted by the will of get better insight in the biology of this rare disease, our research group has previously developed and characterized a knock-in mouse model bearing one of the most frequent TAM mutations in Italy, STIM1^{I115F}.³⁴ This mutation is located in one of the two EF-hand motifs, the intraluminal STIM1 structural domains that bind calcium in the ER, and has been clinically associated with TAM syndrome.

The transgenic mice are fertile, and the mutation is inherited by the 50% of the offspring. Compared to wild-type mice, they are lighter, as a result of the decreased muscle weight, and their performance in motor coordination and speed activity are highly impaired. In myotubes, an overactivation of SOCE is observed and maintained for the entire lifespan. Moreover, the mouse model displays a platelet dysfunction, with a marketed reduction in the number of platelets leading to an increased bleeding time.

While our model is not the only TAM model developed,³⁵ it has never been proven that the restore of calcium entry to physiological levels in those compartments mostly affected might provide a clinical benefit in this pathology. Ultimately, therefore, the demonstration that a SOCE inhibitor might reduce the clinical signs of TAM would postulate a possible therapeutic approach in the disease, that is characterized by a strong unmet clinical need.

2.2 Outline of the project

This project stems from a class of pytriazoles as SOCE modulators, synthesized using the click chemistry approach and published by our research group in 2018.²² The most promising SOCE inhibitor identified among this class was compound CIC-37 (**11**, Figure 2), displaying an IC₅₀ value of 4.4 μM in Hek cells, a human embryonic kidney cell line in which Orai1 and STIM1 isoforms are highly expressed. CIC-37 also possesses a good *in vitro* plasma stability, with a residual substrate of 97.8% after 30 minutes despite the presence of an ester moiety (Figure 3). Despite its good *in vitro* stability, the *in vivo* half-life of CIC-37 (mouse, *i.p.*) is 1.3 hours, with a clearance of 17 L/h/Kg and a volume of distribution of 32 L/kg. The plasma concentrations reached of around 1.2 μM and the PK profile makes the compound suitable for exerting a therapeutic potential in an acute condition. Therefore, to further validate the *in vivo* inhibition of SOCE, the efficacy of the compound was demonstrated in an animal model of acute pancreatitis induced by cerulein, in which the compound has proved to significantly ameliorate inflammation and oedema of pancreatic tissues.

However, the main goal of the development of SOCE inhibitors resides in the identification of a compound compatible with the chronic treatment of TAM. Despite preliminary results show that CIC-37 is able to reduce Ca²⁺-entry *ex vivo* in a muscle biopsy obtained from the TAM mouse model, the PK profile is incompatible with the chronic treatment that this pathology requires.

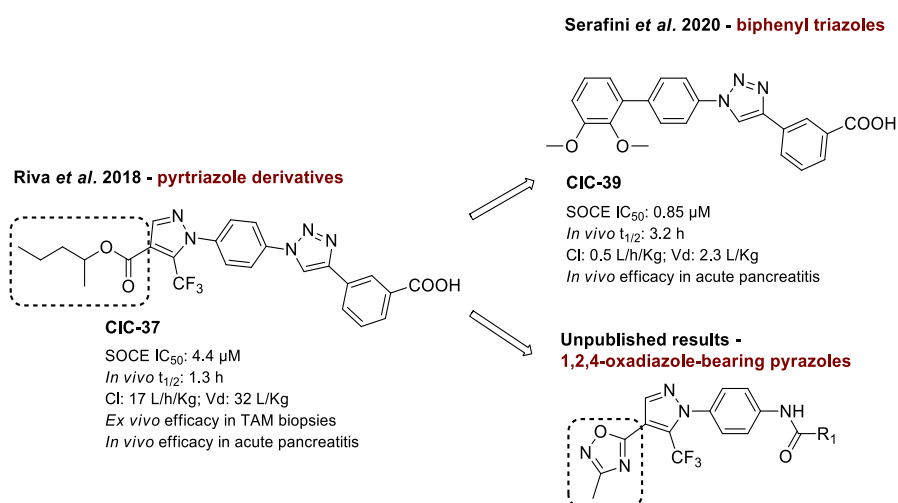
Therefore, with the objective to find more drug-like SOCE inhibitors, we undertook subsequent medicinal chemistry campaigns aimed at developing SOCE modulators with optimized features for the set-up of an *in vivo* chronic experiment lasting one-to-twelve months in the mouse model of TAM.³⁴

In this context, a first class of modulators, represented by the biphenyl triazoles, has been synthesized and developed (Chapter 3). Very promisingly, the identified lead compound, CIC-39 (Figure 3), possesses *in vitro* IC₅₀ value on SOCE in the nanomolar range, improved PK profiles and *in vivo* efficacy in a mouse model of

acute pancreatitis.³⁶ Thanks to the prolonged half-life and the good volume of distribution, CIC-39 is a candidate to be evaluated in the mouse model of TAM. The class of biphenyl triazoles has been patented^{36b} and published in *Journal of Medicinal Chemistry*.^{36a}

Moreover, among the features that hampered the future development of CIC-37 in the mouse model of TAM, the ester moiety remains the main drawback, being the hydrolysis of this group the metabolic transformation that occurs after *in vivo* administration. Therefore, in the search of more drug-like SOCE inhibitors, we have identified a class of pyrazoles bearing a 1,2,4-oxadiazole ring (Figure 3) as a stable isostere of the ester group³⁷ (Chapter 4).

Figure 3. Outline of the project.



2.3 References

1. a) Carafoli, E.; Santella, L.; Branca, D.; Brini, M. Generation, control, and processing of cellular calcium signals. *Crit. Rev. Biochem. Mol. Biol.* **2001**, *36*, 107-260; b) Berridge, M. J.; Bootman, M. D.; Roderick, H. L. Calcium signalling: dynamics, homeostasis and remodelling. *Nat. Rev. Mol. Cell Biol.* **2003**, *4*, 517-529.
2. Putney, J. W. A model for receptor-regulated calcium entry. *Cell Calcium* **1986**, *7*, 1-12.
3. a) Putney, J. W. Origins of the concept of store-operated calcium entry. *Front. Biosci. (Schol Ed)*. **2011**, *3*, 980-984; b) Putney, J. W. The physiological function of store-operated calcium entry. *Neurochem. Res.* **2011**, *36*, 1157-1165; c) Berna-Erro, A.; Woodard, G. E.; Rosado, J. A. Orais and STIMs: physiological mechanisms and disease. *J. Cell. Mol. Med.* **2012**, *16*, 407-424.
4. a) Lewis, R. S. The molecular choreography of a store-operated calcium channel. *Nature* **2007**, *446*, 284-287; b) Darbellay, B.; Arnaudeau, S.; König, S.; Jousset, H.; Bader, C.; Demaurex, N.; Bernheim, L. STIM1- and Orai1-dependent store-operated calcium entry regulates human myoblast differentiation. *J. Biol. Chem.* **2009**, *284*, 5370-5380.
5. a) Khan, H. Y.; Mpilla, G. B.; Sexton, R.; Viswanadha, S.; Penmetsa, K. V.; Aboukameel, A.; Diab, M.; Kamgar, M.; Al-Hallak, M. N.; Szlachky, M.; Tesfaye, A.; Kim, S.; Philip, P. A.; Mohammad, R. M.; Azmi, A. S. Calcium release-activated calcium (CRAC) channel inhibition suppresses pancreatic ductal adenocarcinoma cell proliferation and patient-derived tumor growth. *Cancers* **2020**, *12*, 750-764; b) Xie, J.; Pan, H.; Yao, J.; Zhou, Y.; Han, W. SOCE and cancer: recent progress and new perspectives. *Int. J. Cancer* **2016**, *138*, 2067-2077; c) Guéguinou, M.; Harnois, T.; Crottes, D.; Uguen, A.; Deliot, N.; Gambade, A.; Chantôme, A.; Haelters, J. P.; Jaffrès, P.A.; Jourdan, M. L.; Weber, G.; Soriani, O.; Bougnoux, P.; Mignen, O.;

- Bourmeyster, N.; Constantin, B.; Lecomte, T.; Vandier, C.; Potier-Cartreau, M. SK3/TRPC1/Orai1 complex regulates SOCE-dependent colon cancer cell migration: a novel opportunity to modulate anti-EGFR mAb action by the alkyl-lipid ohmline. *Oncotarget* **2016**, *7*, 36168-36184.
6. Di Sabatino, A.; Rovedatti, L.; Kaur, R.; Spencer, J. P.; Brown, J. T.; Morisset, V. D.; Biancheri, P.; Leakey, N. A. B.; Wilde, J. I.; Scott, L.; Corazza, G. R.; Lee, K.; Sengupta, N.; Knowles, C. H.; Gunthorpe, M. J.; McLean, P. G.; MacDonald, T. T.; Kruidenier, L. Targeting gut T cell Ca²⁺ release activated Ca²⁺ channels inhibits T cell cytokine production and T-Box transcription factor T-Bet in inflammatory bowel disease. *J. Immunol.* **2009**, *183*, 3454-3462.
 7. Ng, S. W.; di Capite, J.; Singaravelu, K.; Parekh, A. B. Sustained activation of the tyrosine kinase Syk by antigen in mast cells requires local Ca²⁺ influx through Ca²⁺ release-activated Ca²⁺ channels. *J. Biol. Chem.* **2008**, *283*, 31348-31355.
 8. a) Wen, L.; Voronina, S.; Javed, M. A.; Awais, M.; Szatmary, P.; Latawiec, D.; Chvanov, M.; Collier, D.; Huang, W.; Barrett, J.; Begg, M.; Stauderman, K.; Roos, J.; Grigoryev, S.; Ramos, S.; Rogers, E.; Whitten, J.; Velicelebi, G.; Dunn, M.; Tepikin, A. V.; Criddle, D. N.; Sutton, R. Inhibitors of ORAI1 prevent cytosolic calcium-associated injury of human pancreatic acinar cells and acute pancreatitis in 3 mouse models. *Gastroenterology* **2015**, *149*, 481-492; b) Gerasimenko, J. V.; Gryshchenko, O.; Ferdek, P. E.; Stapleton, E.; Hébert, T. O.; Bychkova, S.; Peng, S.; Begg, M.; Gerasimenko, O. V.; Petersen, O. H. Ca²⁺ release-activated Ca²⁺ channel blockade as a potential tool in antipancreatitis therapy. *Proc. Natl. Acad. Sci. U. S. A.* **2013**, *110*, 13186-13191.
 9. Ma, G.; Wei, M.; He, L.; Liu, C.; Wu, B.; Zhang, S. L.; Jing, J.; Liang, X.; Senes, A.; Tan, P.; Li, S.; Sun, A.; Bi, Y.; Zhong, L.; Si, H.; Shen, H.; Y.; Li, M.; Lee, M. S.; Zhou, W.; Wang, J.; Wang, Y.; Zhou, Y. Inside-out Ca²⁺

signalling prompted by STIM1 conformational switch. *Nat. Commun.* **2015**, *6*, 7826-7840.

10. a) Stauderman, K. A. CRAC channels as targets for drug discovery and development. *Cell Calcium* **2018**, *74*, 147-159; b) Tia, C.; Du, L.; Zhou, Y.; Li, M. Store-operated CRAC channel Inhibitors: opportunities and challenges. *Future Med. Chem.* **2016**, *8*, 817-832; c) Pevarello, P.; Cainarca, S.; Liberati, C.; Tarroni, P.; Piscitelli, F.; Severi, E. Small-molecule inhibitors of store-operated calcium entry. *Chem. Med. Chem.* **2014**, *4*, 706-718; d) Sweeney, Z. K.; Minatti, A.; Button, D. C.; Patrick, S. Ca²⁺ release-activated Ca²⁺ channel inhibitors. *Pharm. Pat. Anal.* **2009**, *3*, 171-182; e) Sweeney, Z. K.; Minatti, A.; Button, D. C.; Patrick, S. Small-molecule inhibitors of store-operated calcium entry. *Chem. Med. Chem.* **2009**, *4*, 706-718.
11. a) Singh, A.; Hildebrand, M. E.; Garcia, E.; Snutch, T. P. The transient receptor potential channel antagonist SKF96365 is a potent blocker of low-voltage T-type calcium channels. *Br. J. Pharmacol.* **2010**, *160*, 1464-1475; b) Merrit, J. E.; Armstrong, W. P.; Benham, C. D.; Hallam, T. J.; Jacob, R.; Jaxa-Chamiec, A.; Leigh, B. K.; McCarthy, S. A.; Moores, K. E.; Rink, T. J. SKF-96365, a novel inhibitor of receptor-mediated calcium entry. *J. Biochem.* **1990**, *271*, 515-522.
12. a) Bootman, M. D.; Collins, T. J.; Mackenzie, L.; Roderick, H. L.; Berridge, M. J.; Peppiatt, C. M. 2-Aminoethoxydiphenyl borate (2-APB) is a reliable blocker of store-operated Ca²⁺ entry but an inconsistent inhibitor of InsP3-induced Ca²⁺ release. *FASEB J.* **2002**, *16*, 1145-1150; b) Goto, J.; Suzuki, A. Z.; Ozaki, S.; Matsumoto, N.; Nakamura, T.; Ebisui, E.; Fleig, A.; Penner, R.; Mikoshiba, K. Two novel 2-aminoethyl diphenylborinate (2-APB) analogues differentially activate and inhibit store-operated Ca²⁺ entry via STIM proteins. *Cell Calcium* **2010**, *47*, 1-10.

13. Djuric, S.W.; BaMaung, N.Y.; Basha, A.; Liu, H.; Luly, J.R.; Madar, D.J.; Scioyyi, R.J.; Tu, N.P.; Wagenaar, F.L.; Zhoun, X.; Ballaron, S.; Bauch, J.; Chen, Y-W.; Chiou, X.G.; Fey, T.; Gauvin, D.; Gubbins, E.; Hsieh, G.C.; Marsh, K.C.; Mollison, K.W.; Pong, M.; Shaughnessy, T.K.; Sheets, M.P.; Smith, M.; Trevillyan, J.M.; Warrior, U.; Wegner, C.D.; Carter, G.W. 3,5-Bis(trifluoromethyl)pyrazoles: a novel class of NFAT transcription factor regulator. *J. Med. Chem.* **2000**, *43*, 2975-2981.
14. a) Schleifer, H.; Doleschal, B.; Lichtenegger, M.; Oppenrieder, R.; Derler, I.; Frischauf, I.; Glasnov, T. N.; Kappe, C. O.; Romanin, C.; Groschner, K. Novel pyrazole compounds for pharmacological discrimination between receptor-operated and store-operated Ca²⁺ entry pathways. *Br. J. Pharmacol.* **2012**, *167*, 1712-1722; b) Law, M.; Morales, J. L.; Mottram, L. F.; Iyer, A.; Peterson, B. R.; August, A. Structural requirements for the inhibition of calcium mobilization and mast cell activation by the pyrazole derivative BTP2. *Int. J. Biochem. Cell Biol.* **2011**, *43*, 1228-1239.
15. Derler, I.; Schindl, R.; Fritsch, R.; Heftberger, P.; Riedl, M.C.; Begg, M.; House, D.; Romanin, C. The action of selective CRAC channel blockers is affected by the Orai pore geometry. *Cell Calcium* **2013**, *53*, 139-151.
16. Chen, G.; Panicker, S.; Lau, K.Y.; Apparsundaram, S.; Patel, V. A.; Chen, S. L.; Soto, R.; Jung, J. K. C.; Ravindran, P.; Okuhara, D.; Bohnertd, G.; Che, Q.; Rao, P.E.; Allard, J. D.; Badi, L.; Bitter, H-M.; Nunn, P. A.; Narula, S. K.; DeMartino, J. A. Characterization of a novel CRAC inhibitor that potently blocks human T cell activation and effector functions. *Mol. Immunol.* **2013**, *54*, 355-367.
17. a) CM4620 Injectable Emulsion Versus Supportive Care in Patients With Acute Pancreatitis and SIRS. Status: completed. ClinicalTrials.gov Identifier: NCT03401190. Last update: May 3, 2019 (accessed on Nov 4, 2020); b) Study of CM4620 to Reduce the Severity of Pancreatitis Due to

- Asparaginase. Status: recruiting. ClinicalTrials.gov Identifier: NCT04195347. Last update: September 10, 2020 (accessed on Nov 4, 2020).
18. A Study of PRCL-02 in Moderate to Severe Chronic Plaque Psoriasis. Status: completed, has results. ClinicalTrials.gov Identifier: NCT03614078. Last update: March 30, 2020 (accessed on Nov 4, 2020).
 19. Rahman, S.; Rahman, R. Unveiling some FDA-approved drugs as inhibitors of the store-operated Ca^{2+} entry pathway. *Sci. Rep.* **2017**, *7*, 12881-12893.
 20. a) Breedveld, F. C.; Dayer, J. M. Leflunomide: mode of action in the treatment of rheumatoid arthritis. *Ann. Rheum. Dis.* **2000**, *59*, 841-849; b) Schattenkirchner, M. The use of leflunomide in the treatment of rheumatoid arthritis: an experimental and clinical review. *Immunopharmacology* **2000**, *47*, 291-298.
 21. a) Palmer, A. M. Teriflunomide, an inhibitor of dihydroorotate dehydrogenase for the potential oral treatment of multiple sclerosis. *Curr. Opin. Invest. Drugs* **2010**, *11*, 1313-1323; b) Davis, J. P.; Cain, G. A.; Pitts, W. J.; Magolda, R. L.; Copeland, R. A. The immunosuppressive metabolite of leflunomide is a potent inhibitor of human dihydroorotate dehydrogenase. *Biochemistry* **1996**, *35*, 1270-1273.
 22. a) Riva, B.; Griglio, A.; Serafini, M.; Cordero-Sanchez, C.; Aprile, S.; Di Paola, R.; Gugliandolo, E.; Alansary, D.; Biocotino, I.; Lim, D.; Grosa, G.; Galli, U.; Niemeyer, B.; Sorba, G.; Canonico, P. L.; Cuzzocrea, S.; Genazzani, A. A.; Piralì, T. Pyrtriazoles, a novel class of store-operated calcium entry modulators: Discovery, biological profiling, and in vivo proof-of-concept efficacy in acute pancreatitis. *J. Med. Chem.* **2018**, *61*, 9756-9783; b) Modulators of SOCE, compositions and use thereof. Piralì T.; Riva B.; Genazzani A. A. WO 2017/212414 A1. Dec 14, 2017.
 23. Lee, P. J.; Papachristou, G. I. New insights into acute pancreatitis. *Nat. Rev. Gastroenterol. Hepatol.* **2019**, *16*, 479-496.

24. Forsmark, C. E.; Vege, S. S.; Wilcox, C. M. Acute pancreatitis. *N. Engl. J. Med.* **2016**, *375*, 1972-1981.
25. a) Gerasimenko, J. V.; Gerasimenko, O. V.; Petersen, O. H. The role of Ca^{2+} in the pathophysiology of pancreatitis. *J. Physiol.* **2014**, *592*, 269-280; b) Gerasimenko, J. V.; Peng, S.; Tsugorka, T.; Gerasimenko, O. V. Ca^{2+} signalling underlying pancreatitis. *Cell Calcium* **2018**, *70*, 95-101.
26. a) Ong, H. L.; Ambudkar, I. S. Molecular determinants of TRPC1 regulation within ER-PM junctions. *Cell Calcium* **2015**, *58*, 376-386; b) Ong, H. L.; de Souza, L. B.; Ambudkar, I. S. Role of TRPC channels in store-operated calcium entry. *Adv. Exp. Med. Biol.* **2016**, *898*, 87-109.
27. a) Kim, M. S.; Lee, K. P.; Yang, D.; Shin, D. M.; Abramowitz, J.; Kiyonaka, S.; Birnbaumer, L.; Mori, Y.; Muallem, S. Genetic and pharmacologic inhibition of the Ca^{2+} influx channel TRPC3 protects secretory epithelia from Ca^{2+} -dependent toxicity. *Gastroenterology* **2011**, *140*, 2107-2115; b) Parekh, A. B.; Putney, J. W. Store-operated calcium channels. *Physiol. Rev.* **2005**, *85*, 757-810.
28. a) Lur, G.; Sherwood, M. W.; Ebisui, E.; Haynes, L.; Feske, S.; Sutton, R.; Burgoyne, R. D.; Mikoshiba, K.; Petersen, O. H.; Tepikin, A. V. InsP_3 receptors and Orai channels in pancreatic acinar cells: co-localization and its consequences. *Biochem. J.* **2011**, *436*, 231-239; b) Gukovskaya, A. S.; Pandol, S. J.; Gukovsky, I. New insights into the pathways initiating and driving pancreatitis. *Curr. Opin. Gastroenterol.* **2016**, *32*, 429-435.
29. Waldron, R. T.; Chen, Y.; Pham, H.; Go, A.; Su, H. Y.; Hu, C.; Wen, L.; Husain, S. Z.; Sugar, C. A.; Roos, J.; Ramos, S.; Lugea, A.; Dunn, M.; Stauderman, K.; Pandol, S. J. The Orai Ca^{2+} channel inhibitor CM4620 targets both parenchymal and immune cells to reduce inflammation in experimental acute pancreatitis. *J. Physiol.* **2019**, *597*, 3085-3105.
30. Peng, S.; Gerasimenko, J. V.; Tsugorka, T.; Gryshchenko, O.; Samarasinghe, S.; Petersen, O. H.; Gerasimenko, O. V. Calcium and adenosine triphosphate

control of cellular pathology: asparaginase-induced pancreatitis elicited via protease-activated receptor 2. *Philos. Trans. R. Soc. Lond. B. Biol. Sci.* **2016**, *371*, 20150423.

31. a) Feske, S. CRAC channelopathies. *Pflugers Arch.* **2010**, *460*, 417-435; b) Lacruz, R. S.; Feske, S. Diseases caused by mutations in ORAI1 and STIM1. *Ann. NY Acad. Sci.* **2015**, *1356*, 45-79.
32. Böhm, J.; Laporte, J. Gain-of-function mutations in STIM1 and ORAI1 causing tubular aggregate myopathy and Stormorken syndrome. *Cell Calcium* **2018**, *76*, 1-9.
33. Böhm, J.; Chevessier, F.; Koch, C.; Peche, G. A.; Mora, M.; Morandi, L.; Pasanisi, B.; Moroni, I.; Tasca, G.; Fattori, F.; Ricci, E.; Péniisson-Besnier, I.; Nadaj-Pakleza, A.; Fardeau, M.; Joshi, P. R.; Deschauer, M.; Romero, N. B.; Eymard, B.; Laporte, J. Clinical, histological and genetic characterisation of patients with tubular aggregate myopathy caused by mutations in STIM1. *J. Med. Genet.* **2014**, *51*, 824-833.
34. Cordero-Sanchez, C.; Riva, B.; Reano, S.; Clemente, N.; Zaggia, I.; Ruffinatti, F. A.; Potenzieri, A.; Pirali, T.; Raffa, S.; Sangaletti, S.; Colombo, M. P.; Bertoni, A.; Garibaldi, M.; Filigheddu, N.; Genazzani, A. A. A luminal EF-hand mutation in STIM1 in mice causes the clinical hallmarks of tubular aggregate myopathy. *Dis. Model Mech.* **2019**, *13*, dmm041111.
35. a) Gamage, T. H.; Gunnes, G.; Lee, R. H.; Louch, W. E.; Holmgren, A.; Bruton, J. D.; Lengle, E.; Kolstad, T. R. S.; Revold, T.; Amundsen, S. S.; Dalen, K. T.; Holme, P. A.; Tjønnfjord, G. E.; Christensen, G. E.; Westerblad, H.; Klungland, A.; Bergmeier, W.; Misceo, D.; Frengen, E. STIM1 R304W causes muscle degeneration and impaired platelet activation in mice. *Cell Calcium* **2018**, *76*, 87-100; b) Silva-Rojas, R.; Treves, S.; Jacobs, H.; Kessler, P.; Messaddeq, N.; Laporte, J.; Böhm, J. STIM1 overactivation generates a multi-systemic phenotype affecting skeletal muscle, spleen, eye, skin, bones, and the immune system in mice. *Hum. Mol.*

Genet. **2018**, *28*, 1579-1593; c) Grosse, J.; Braun, A.; Varga-Szabo, D.; Beyersdorf, N.; Schneider, B.; Zeitlmann, L.; Hanke, P.; Schropp, P.; Mühlstedt, S.; Zorn, C.; Huber, M.; Schmittwolf, C.; Jagla, W.; Yu, P.; Kerkau, T.; Schulze, H.; Nehls, M.; Nieswandt, B. An EF hand mutation in Stim1 causes premature platelet activation and bleeding in mice. *J. Clin. Invest.* **2007**, *117*, 3540-3550.

36. a) Serafini, M.; Cordero-Sanchez, C.; Di Paola, R.; Bhela, I. P.; Aprile, S.; Purghe, B.; Fusco, R.; Cuzzocrea, S.; Genazzani, A. A.; Riva, B.; Pirali, T. Store-Operated Calcium Entry (SOCE) as a therapeutic target in acute pancreatitis: discovery and development of drug-like SOCE inhibitor. *J. Med. Chem.* **2020**, *63*, 14761-14779; b) Pirali, T.; Riva, B.; Serafini, M.; Aprile, S.; Cordero Sanchez, C. Biphenyl compounds as SOCE modulators, compositions and uses thereof. Filed on February 21, 2020, n. 102020000003692.

37. a) Boström, J.; Hogner, A.; Llinàs, A.; Wellner, E.; Plowright, A. T. Oxadiazoles in medicinal chemistry. *J. Med. Chem.* **2012**, *55*, 1817-1830; b) Goldberg, K.; Groombridge, S.; Hudson, J.; Leach, A. G.; MacFaul, P. A.; Pickup, A.; Poultney, R.; Scott, J. S.; Svenssonb, P. H.; Sweeney, J. Oxadiazole isomers: all bioisosteres are not created equal. *Med. Chem. Commun.* **2012**, *3*, 600-604.

Chapter 3

**Store-Operated Calcium Entry (SOCE) as
a therapeutic target in acute pancreatitis:
discovery and development of drug-like
SOCE inhibitors**

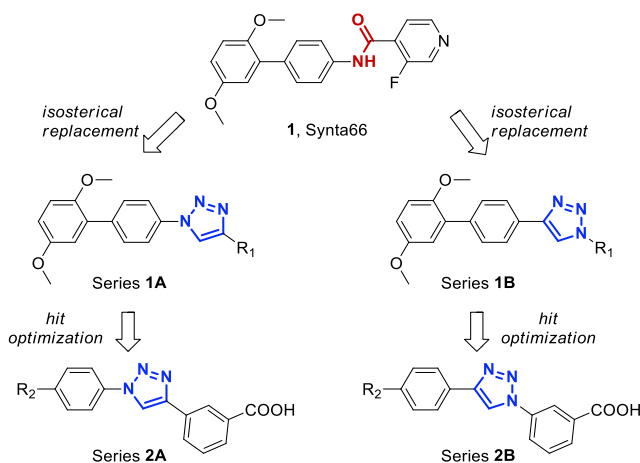
3.1 The replacement of the arylamide of Synta66 afforded the 1st class of modulators

The first class of SOCE modulators¹ has been developed starting from the structure of Synta66, a SOCE inhibitor reported in the literature.

Synta66 (**1**, Figure 1) is a CRAC channel blocker able to inhibit I_{CRAC} (*i.e.* the Ca^{2+} current associated with the ion influx) with an IC_{50} of 1.4-3.0 μM .² Despite the fact that its precise mechanism on SOCE remains unknown, assays performed in siRNA knock-down of Orai1 mast cells have suggested that Synta66 might be selective for the channel.^{2a} Furthermore, experiments in vascular smooth muscle cells have demonstrated that it does not interfere with STIM1 clustering.³ Thanks to its inhibitory activity toward Orai1, an increasing number of *in vitro* and *in vivo* studies have seen Synta66 as a chemical probe to gain better insight in I_{CRAC} biology. Moreover, the compound is selective over a panel of other ion channels or receptors, including Ca^{2+} ATPase pump, voltage-gated Ca^{2+} and Na^{+} channels and TRPC1/5 channels,^{2,3} indicating this molecule as a reliable starting point to develop new SOCE modulators.

Our class of modulators was designed by replacement of the arylamide moiety by a triazole ring,⁴ as depicted in Figure 1.

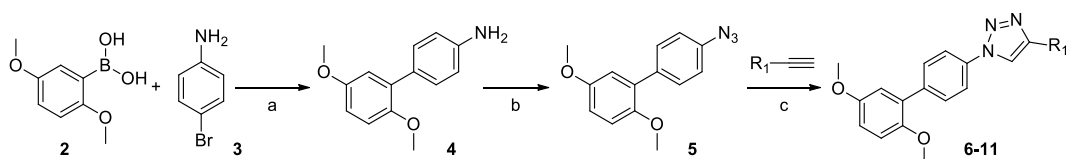
Figure 1. Modifications of Synta66 moieties to synthesize biphenyl triazoles.



The SAR study around 3-fluoropyridine moiety gives less active compounds compared to Synta66 on SOCE

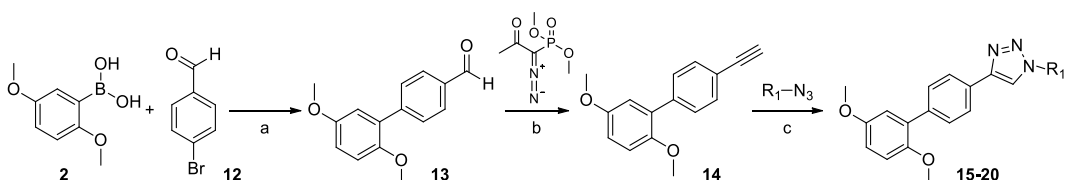
Starting from the structure of Synta66, the amide moiety was substituted with a 1,4-disubstituted 1,2,3-triazole ring by a click chemistry approach.⁵ To this aim, azide **5** and alkyne **14** were prepared according to Scheme 1 and 2. Azide **5** was synthesized starting from (2,5-dimethoxyphenyl)boronic acid and 4-bromoaniline, that reacted in a Suzuki cross-coupling reaction to give intermediate **4** in almost quantitative yield. Compound **4** underwent a diazotization-azidation reaction to afford the desired azide **5** with a yield of 60%. Alkyne **14** was prepared from (2,5-dimethoxyphenyl)boronic acid and 4-bromobenzaldehyde that, after a Suzuki cross-coupling reaction, gave intermediate **13** in quantitative yield that reacted in the presence of Bestmann-Ohira reagent to give **14**.

Scheme 1. Synthesis of compounds **6-11** (series 1A).



Reagents and conditions: (a) K_2CO_3 , $\text{Pd}(\text{OAc})_2$, EtOH, DMF, 80 °C, 3 h, 98%. (b) NaNO_2 , NaN_3 , HCl, H_2O , rt, 5 h, 60%. (c) Sodium ascorbate, $\text{CuSO}_4 \cdot 5\text{H}_2\text{O}$, *t*-BuOH, H_2O , 50 °C, 16 h, 31-65%.

Scheme 2. Synthesis of compounds **15-20** (series 1B).



Reagents and conditions: (a) K_2CO_3 , $\text{Pd}(\text{OAc})_2$, EtOH, DMF, 50 °C, 3 h, 99%. (b) Bestmann-Ohira reagent, K_2CO_3 , MeOH, rt, 18 h, 82%. (c) Sodium ascorbate, $\text{CuSO}_4 \cdot 5\text{H}_2\text{O}$, *t*-BuOH, H_2O , 50 °C, 16 h, 60-99%.

With these two compounds in hand, two click reactions were performed and compounds **6** and **15** (Table 1), displaying the same substructures as the reference compound Synta66, were obtained with a yield of 31% and 60%, respectively. **6** and **15** were tested for activity on SOCE in HEK cells, a human embryonic kidney cell line, at 10 μM by fluorescence microscopy, as described elsewhere.⁶ After 600 seconds, Ca^{2+} was added and intracellular levels were measured. Compared to Synta66, that exhibits an inhibition of $90.8 \pm 1.7\%$, compound **15** inhibited SOCE to a smaller extent ($26.2 \pm 6.5\%$), while **6** showed a percentage of -4.9 ± 21.3 , indicating that the molecule slightly increased Ca^{2+} entry compared to control (Table 1). Therefore, the isosterical replacement of the aryl amide moiety with a triazole ring led to active molecules, albeit the activity was significantly reduced compared to the parent compound Synta66. This is not surprisingly though, since the isosteric replacement of the amide with the triazole slightly changes the topology of the molecules and a structure-activity relationship (SAR) study is usually needed to find the best combination in terms of triazole orientation and nature and position of substituents.

Therefore, prompted by this initial observation, we decided to investigate the SAR around the 3-fluoropyridine ring. To this aim, ten additional molecules were designed and synthesized starting from azide **5** and alkyne **14** that were clicked with five different alkynes and azides, respectively, affording compounds **7-11** (series 1A, Figure 1) and **16-20** (series 1B, Figure 1). All the synthesized triazoles were tested at 10 μM in HEK cells, as described above. Five compounds (**6**, **7**, **8**, **16**, **17**) evoked a variable Ca^{2+} entry, leading to a remarkable standard error and suggesting that they were not able to reliably inhibit SOCE (Table 1). Moreover, only four molecules (**10**, **11**, **18**, **20**) out of twelve inhibited SOCE by a considerable level (arbitrarily chosen to be $> 70\%$). The most active compound, **20** ($87.8 \pm 2.9\%$ of inhibition) showed an inhibitory activity comparable to Synta66 ($90.8 \pm 1.7\%$). Next, we determined the IC_{50} value. **20** showed an IC_{50} of $1.79 \pm 0.14 \mu\text{M}$, revealing approximately a one order of magnitude lower potency compared to Synta66 ($\text{IC}_{50} = 228 \pm 33 \text{ nM}$).

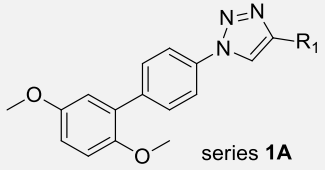
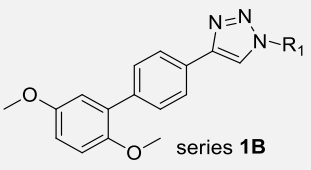
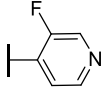
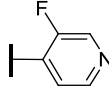
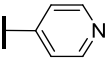
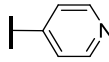
Moreover, **20** was slightly cytotoxic, with a residual cell viability of 71.8% at 10 μ M, a characteristic shared by Synta66 ($75.8 \pm 8.0\%$). To assess the cytotoxicity profile of the biphenyl triazoles, viability assays were performed on other molecules of the first series (10 μ M) and all the compounds showed a cell viability comparable to **20** (data not shown).

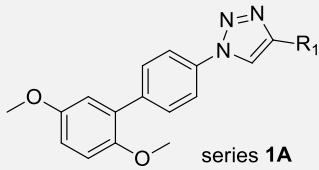
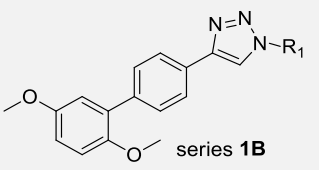
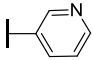
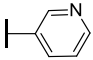
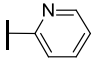
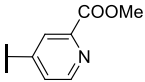
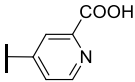
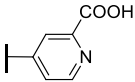
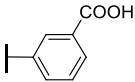
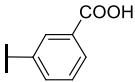
The SAR study around 2,5-dimethoxyphenyl gives compounds as active as Synta66 on SOCE

The above data demonstrate that all the synthesized biphenyl triazoles showed a reduced activity on SOCE compared to Synta66. We therefore synthesized a second series of compounds (series 2A and 2B, Figure 1) where the 2,5-dimethoxyphenyl ring, the only structural motif that had been kept fixed in our preliminary SAR, was extensively modified (Table 2). Given that the most potent compound in the first series featured a 3-carboxyphenyl ring, we decided to select this moiety as the one to keep fixed. The choice was also guided by the fact that this substructure was the preferred substitution in our previous paper reporting pyrtriazoles (CIC-37) and by the perception that the 3-carboxyphenyl substrate is a privileged scaffold in SOCE modulation.⁶

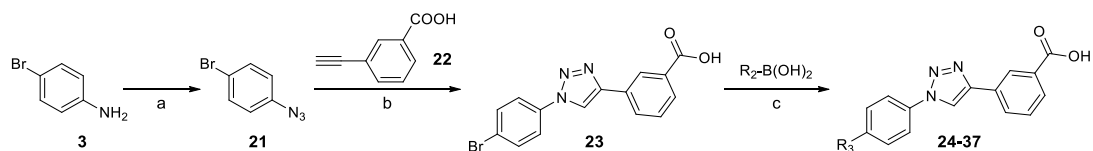
To obtain the second series of biphenyl triazoles, a Suzuki cross-coupling reaction was exploited, starting from two aryl bromides, **23** and **40**, that were coupled with different boronic acids. **23** and **40** were synthesized as depicted in Scheme 3 and 4. Click chemistry reaction between azide **21**, prepared from 4-bromoaniline by diazotization-azidation protocol, and alkyne **22** afforded the aryl bromide **23**, with a yield of 81%. Similarly, **40** was obtained by clicking alkyne **38**, synthesized by reacting 4-bromobenzaldehyde in the presence of Bestmann-Ohira reagent, with azide **39**.

Table 1. First series of compounds and their biological activity in HEK cells.

 series 1A					 series 1B				
Cpd, Yield (%)	R ₁	% SOCE inhibition (10 μM)	% Viability (10 μM)	IC ₅₀ (nM)	Cpd, Yield (%)	R ₁	% SOCE inhibition (10 μM)	% Viability (10 μM)	IC ₅₀ (nM)
1 , Synta66	-	90.8 ± 1.7	75.8 ± 8.0	228 ± 33					
6 , 31%		-4.9 ± 21.3	-	-	15 , 60%		26.2 ± 6.5	-	-
7 , 37%		-12.8 ± 14.4	-	-	16 , 79%		-1.7 ± 12.6	-	-

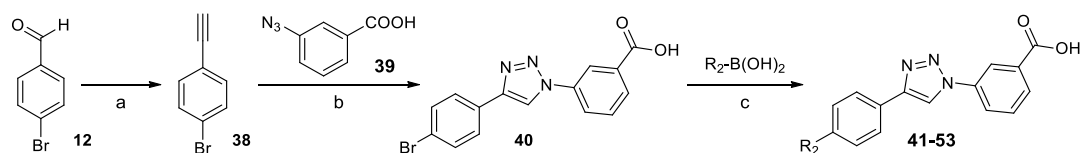
 series 1A					 series 1B				
Cpd, Yield (%)	R ₁	% SOCE inhibition (10 μM)	% Viability (10 μM)	IC ₅₀ (nM)	Cpd, Yield (%)	R ₁	% SOCE inhibition (10 μM)	% Viability (10 μM)	IC ₅₀ (nM)
8 , 65%		-14.0 ± 31.9	-	-	17 , 78%		1.2 ± 33.4	-	-
9 , 50%		0.0 ± 1.5	-	-	18 , 61%		73.5 ± 1.4	-	-
10 , 58%		79.9 ± 4.1	-	-	19 , 75%		57.2 ± 8.3	-	-
11 , 42%		76.2 ± 5.2	-	-	20 , 99%		87.8 ± 2.9	71.8 ± 0.5	1790 ± 143

Scheme 3. Synthesis of compounds **24-37** (series 2A).



Reagents and conditions: (a) NaNO_2 , NaN_3 , HCl , H_2O , rt, 5 h, 81%. (b) Sodium ascorbate, $\text{CuSO}_4 \cdot 5\text{H}_2\text{O}$, *t*-BuOH, H_2O , 50 °C, 48 h, 87%. (c) K_2CO_3 , $\text{Pd}(\text{OAc})_2$, EtOH, DMF, 80 °C, 6 h, 18-86%.

Scheme 4. Synthesis of compounds **41-53** (series 2B).



Reagents and conditions: (a) Bestmann-Ohira reagent, K_2CO_3 , MeOH, rt, 18 h, 54%. (b) Sodium ascorbate, $\text{CuSO}_4 \cdot 5\text{H}_2\text{O}$, *t*-BuOH, H_2O , 50 °C, 16 h, 65%. (c) K_2CO_3 , $\text{Pd}(\text{OAc})_2$, EtOH, DMF, 80 °C, 6 h, 22-99%.

Starting from these two intermediates, twenty-eight Suzuki reactions were performed and compounds **24-37** (series 2A, Figure 1) and **41-53** (series 2B, Figure 1) were synthesized. The reaction between intermediate **40** and (3-hydroxyphenyl)boronic acid was instead not successful and the analogue of compound **29** was not obtained. As described above, all the compounds were initially tested at 10 μM in HEK cells. This second series was significantly more potent compared to the first, and several molecules showed a noteworthy inhibitory activity, with percentage above 80% (data not shown). Therefore, in order to better discriminate between the different candidates, we decided to evaluate the effect of the compounds at 3 μM on SOCE. For those compounds that displayed SOCE inhibitory activity $\geq 70\%$, cell viability assays, this time at 10 μM , were then performed. For those molecules showing an

inhibitory activity $\geq 70\%$ and a cell viability $\geq 85\%$, the IC_{50} values were calculated (Table 2).

The biological results highlighted that removal of both the methoxy substituents from positions 2' and 5' (**24**, $51.0 \pm 31.9\%$; **41**, $1.8 \pm 3.1\%$), or the presence of the solely 2'-methoxy substituent (**25**, $45.9 \pm 14.5\%$; **42**, $12.0 \pm 18.9\%$) caused a significant reduction of activity compared to Synta66 with a remarkable variability. On the other hand, the additional methoxy group at position 4' made the inhibition rise to 50% (**26**, $56.4 \pm 21.0\%$; **43**, $53.0 \pm 3.8\%$). When the same insertion was performed at position 6', for one compound a drop in inhibitory activity occurred (**27**, $25.8 \pm 22.3\%$), while for the other one (**44**) an increase in SOCE was surprisingly observed ($-22.8 \pm 0.9\%$). The compound, tested at a concentration of 3 μM , significantly increased the AUC of calcium entry and the peak amplitude, *i.e.* represents a positive modulator of SOCE (more details on SOCE activators are provided in Chapter 4).

Compound **28** in which the methoxy group is removed from position 2', while bearing a 3'-methoxy substituent, was more active ($85.1 \pm 9.0\%$; Figure 2A) compared to Synta66, while the counterpart **45** was less active ($29.5 \pm 22.7\%$). The substitution of the methoxy group with a hydroxyl (**29**, $0.0 \pm 13.1\%$) or with a thioether (**30**, $23.6 \pm 33.7\%$; **46**, $0.0 \pm 0.7\%$) was instead not tolerated. Compounds **31** and **47** with a 2',3'-dimethoxy phenyl substituent also showed a good activity ($96.5 \pm 2.4\%$ and 93.3 ± 5.1 , respectively; Figure 2A), while, if the two methoxy groups were fused together to form a 1,4-dioxanyl ring, the activity was lower (**32**, $70.9 \pm 7.9\%$ Figure 2A; **48**, $44.1 \pm 17.1\%$). The 3',5'-dimethoxy phenyl substituent provided a good inhibitory activity, as in the case of **33**, that induced an inhibition of $73.8 \pm 11.3\%$ (Figure 2A). On the other hand, **49** had a good inhibitory activity, but due to its remarkable variability ($75.4 \pm 28.8\%$), the compound was not selected for further studies. The inhibition of SOCE was also observed with the 3',4'-dimethoxy phenyl substituent, but to a less extent (**34**, $54.3 \pm 6.3\%$; **50**, $39.6 \pm 7.6\%$). When the substituents in 3' and 4' were fused together in a 6-member 1,4-dioxanyl ring, the

activity rose (**35**, $77.5 \pm 8.2\%$, Figure 2A; **51**, $81.1 \pm 7.0\%$), while the 1,3-dioxolanyl was not tolerated in the case of **52** ($0.0 \pm 4.3\%$) and led to a less active compound with a high standard error in the case of **36** ($67.3 \pm 44.6\%$). Finally, a 2'-fluoro-5'-methoxy phenyl ring provided two compounds with remarkable SOCE inhibitory activity, **37** ($74.7 \pm 6.3\%$) and **53** ($88.9 \pm 7.5\%$), both reported in Figure 2A. In summary, in the second series we were able to discover eight molecules with IC_{50} values in the high nanomolar range (Figure 2B, Table 2).

Figure 2. Effect of Synta66 and selected biphenyl triazoles on SOCE in HEK cells. (A) Average Ca^{2+} -traces of SOCE in the absence or presence of Synta66 or biphenyl triazoles (3 μ M). Traces are the average of 200 cells. (B) Concentration-response curves.

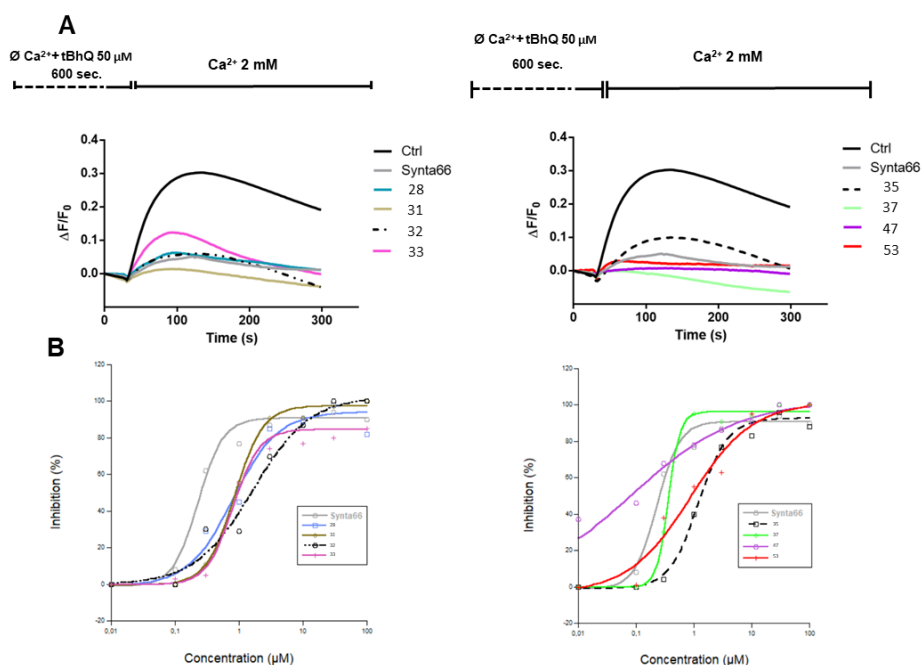
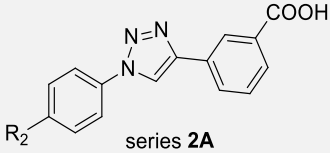
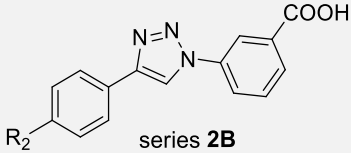
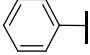
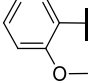
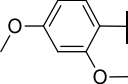
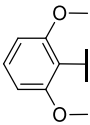
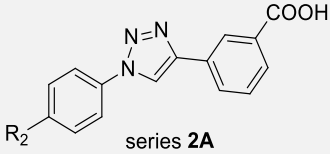
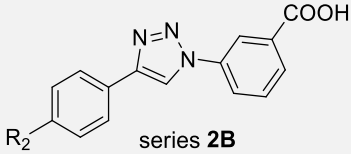
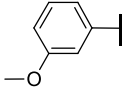
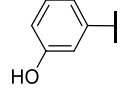
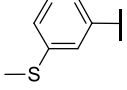
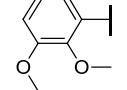
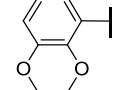
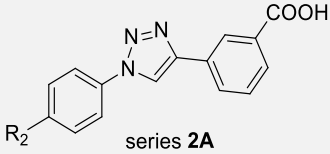
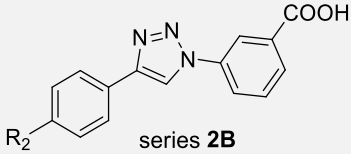
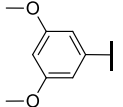
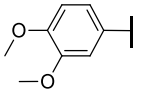
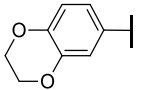
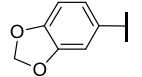
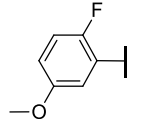


Table 2. Second series of compounds and their biological activity in HEK cells.

 series 2A					 series 2B			
R ₂	Cpd, Yield (%)	% SOCE inhibition (3 μM)	% Viability (10 μM)	IC ₅₀ (nM)	Cpd, Yield (%)	% SOCE inhibition (3 μM)	% Viability (10 μM)	IC ₅₀ (nM)
-	1 , Synta66	86.7 ± 3.7	75.8 ± 8.0	228 ± 33				
	24 , 55%	51.0 ± 31.9	-	-	41 , 55%	1.8 ± 3.1	-	-
	25 , 67%	45.9 ± 14.5	-	-	42 , 22%	12.0 ± 18.9	-	-
	26 , 86%	56.4 ± 21.0	-	-	43 , 98%	53.0 ± 3.8	-	-
	27 , 52%	25.8 ± 22.3	-	-	44 , 46%	-22.8 ± 0.9	-	-

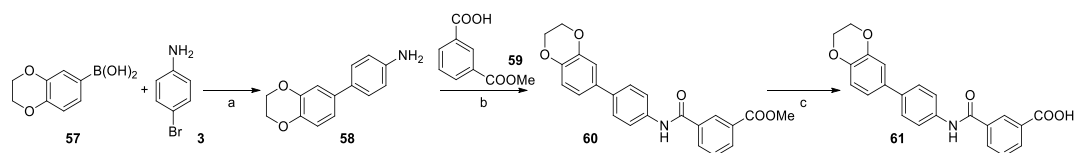
 series 2A					 series 2B			
R ₂	Cpd, Yield (%)	% SOCE inhibition (3 μM)	% Viability (10 μM)	IC ₅₀ (nM)	Cpd, Yield (%)	% SOCE inhibition (3 μM)	% Viability (10 μM)	IC ₅₀ (nM)
	28 , 68%	85.1 ± 9.0	85.1 ± 1.9	807 ± 216	45 , 61%	29.5 ± 22.7	-	-
	29 , 18%	0.0 ± 13.1	-	-	-	-	-	-
	30 , 80%	23.6 ± 33.7	-	-	46 , 99%	0.0 ± 0.7	-	-
	31 , 76%	96.5 ± 2.4	85.6 ± 1.3	851 ± 54	47 , 76%	93.3 ± 5.1	93.1 ± 2.4	781 ± 37
	32 , 76%	70.9 ± 7.9	90.5 ± 1.6	1621 ± 463	48 , 91%	44.1 ± 17.1	-	-

 series 2A					 series 2B			
R ₂	Cpd, Yield (%)	% SOCE inhibition (3 μM)	% Viability (10 μM)	IC ₅₀ (nM)	Cpd, Yield (%)	% SOCE inhibition (3 μM)	% Viability (10 μM)	IC ₅₀ (nM)
	33 , 86%	73.8 ± 11.3	94.3 ± 3.6	802 ± 160	49 , 98%	75.4 ± 28.8	-	-
	34 , 43%	54.3 ± 6.3	-	-	50 , 56%	39.6 ± 7.6	-	-
	35 , 75%	77.5 ± 8.2	93.5 ± 4.4	1198 ± 154	51 , 99%	81.1 ± 7.0	71.7 ± 0.3	-
	36 , 33%	67.3 ± 44.6	-	-	52 , 58%	0.0 ± 4.29	-	-
	37 , 46%	74.7 ± 6.3	91.1 ± 2.9	361 ± 42	53 , 41%	88.9 ± 7.5	92.3 ± 3.1	866 ± 301

The triazole is an indispensable feature of the new class of modulators and reduces off-target effects on DHODH

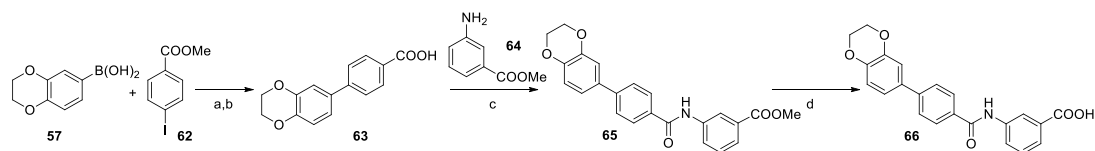
To better elucidate the role of the triazole ring in the interaction with SOCE machinery, we synthesized analogues of **35** displaying the direct (**61**) and the inverse (**66**) amides, according to Scheme 5 and 6. Suzuki cross-coupling reaction between (2,3-dihydrobenzo[*b*][1,4]dioxin-6-yl)boronic acid and 4-bromoaniline afforded amine **58**⁷ that, after coupling with 3-(methoxycarbonyl)benzoic acid and hydrolysis of the methyl ester, yielded compound **61**. (2,3-Dihydrobenzo[*b*][1,4]dioxin-6-yl)boronic acid and methyl 4-iodobenzoate underwent a Suzuki cross-coupling reaction and, after deprotection of the carboxylic group, afforded intermediate **63**. Then, **63** was coupled with methyl 3-aminobenzoate and the methyl ester hydrolysed to give compound **66**.

Scheme 5. Synthesis of compound 61.



Reagents and conditions: (a) K_2CO_3 , $Pd(OAc)_2$, EtOH, DMF, 80 °C, 6 h, 86%. (b) EDCI, DMAP, DIPEA, dry CH_2Cl_2 , rt, 18 h, 77%. (c) NaOH, H_2O , THF, 3 h, 60 °C, 81%.

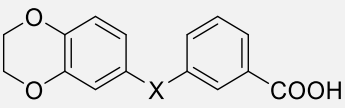
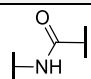
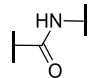
Scheme 6. Synthesis of compound 66.



Reagents and conditions: (a) K_2CO_3 , $Pd(OAc)_2$, EtOH, DMF, 80 °C, 6 h. (b) NaOH, H_2O , THF, 4 h, 60 °C, 85%. (c) EDCI, DMAP, DIPEA, dry CH_2Cl_2 , rt, 18 h, 63%. (d) NaOH, H_2O , THF, 4 h, 60 °C, 61%.

The triazole ring is reputed as a non-classical bioisostere of amides,^{4,5} although we have shown in a number of occasions that this is not necessarily always the case.⁸ To investigate the function of the triazole in this setting, we evaluated the amides of **35** (**61** and **66**). Both molecules displayed a significantly reduced activity compared to the parent compound (Table 3). It should be noticed that such difference was also observed when comparing Synta66 with its triazole-substituted close analogues (**6** and **15**; Table 1).

Table 3. Amide analogues of **35**.

				
Cpd, Yield (%)	X	% SOCE inhibition (3 μ M)	% Viability (10 μ M)	IC ₅₀
61 , 81%		51.8 \pm 9.5	50.3 \pm 0.8	-
66 , 61%		22.6 \pm 5.6	95.3 \pm 3.3	-

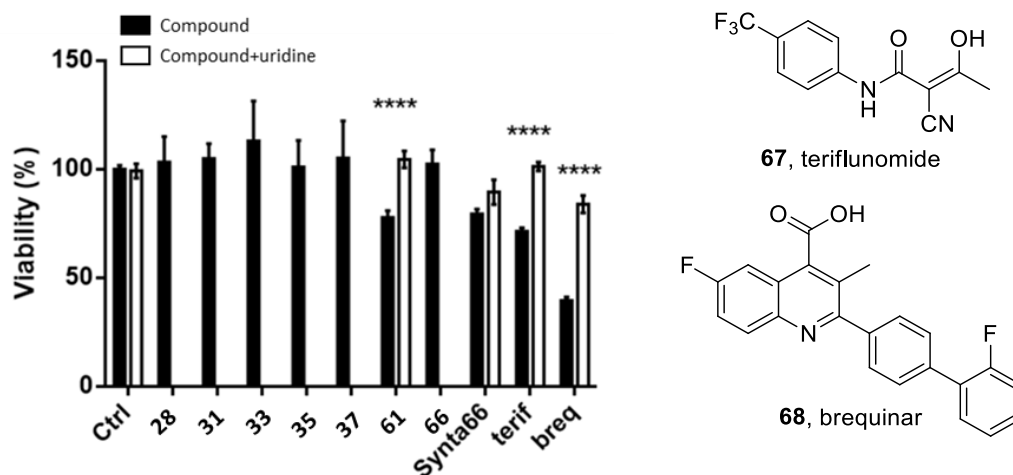
Surprisingly, **61**, despite its low activity on SOCE, showed a significant cytotoxicity, with a residual viability after 24 h of 50% at 10 μ M in HEK cells, in contrast to its inverse amide **66** and **35**, that did not affect cell viability. When attempting to rationalize this cytotoxicity, we noticed that **61** was structurally closely related to dihydroorotate dehydrogenase (DHODH) inhibitors.⁹ Indeed, a *h*DHODH inhibitor usually includes a lipophilic moiety that guarantees the interaction with subsite 1 of the enzyme, together with a carboxylate moiety that interacts with Arg136 residue located in subsite 2, two structural features that can be found in compounds **61** and **66**.

More surprisingly, a recent screening performed on an FDA database has highlighted that teriflunomide (**67**, Figure 3), a DHODH inhibitor approved for multiple sclerosis,¹⁰ is endowed with a considerable inhibitory activity on SOCE ($IC_{50} = 4.3 \pm 1.0 \mu\text{M}$ in HEK cells).¹¹ This led to asking whether **61** was a DHODH inhibitor and whether triazole-bearing analogues shared this feature. To investigate the involvement of DHODH, the cytotoxic activities of the two compounds bearing an amide substructure, **61** and **66**, were evaluated after 72 h at a high concentrations (50 μM) in HEK cells. Also, according to both potency and cell viability of the second series of modulators, five biphenyl triazoles were selected (**28**, **31**, **33**, **35** and **37**), excluding those molecules that differed from these candidates only for the orientation of the triazole ring (**47** and **53**) and these compounds were evaluated under the same conditions for their DHODH selectivity. Alongside, two well-characterized DHODH inhibitors, teriflunomide itself (**67**, Figure 3) and brequinar (**68**, Figure 3)¹² were used as reference compounds. Gratifyingly, the viability profile revealed that the biphenyl triazoles did not impair cell viability even at these high concentrations. For the arylamide-bearing molecules displaying a significant cytotoxicity (**61** and Synta66), the involvement of the *de novo* pyrimidine synthesis pathway was evaluated by supplementing the medium with an excess of uridine that should counterbalance the effect of DHODH inhibition by triggering the *de novo* pathway.¹³ As expected, brequinar and teriflunomide were cytotoxic and their effect was reverted by uridine addition. The cytotoxic effect of **61** was also fully reverted by uridine, supporting our hypothesis that this is a DHODH inhibitor and that the substitution with the triazole ring reduces the off-target effects (Figure 3). While this observation deserves additional investigations, it questions whether other previously reported inhibitors bearing an aryl amide moiety might have promiscuous effects on this enzyme. Indeed, most SOCE inhibitors bear an amide-linkage as part of the pharmacophore.¹⁴ We preliminarily tested CM4620 and found that it was cytotoxic at 50 μM in HEK cells, but this cytotoxicity was not reverted by uridine, suggesting

that it is not a DHODH inhibitor (not shown). A similar lack of effect was also observable for Pyr6, while no other arylamide SOCE inhibitor was tested.

Overall, these data corroborate previous evidence that the amide to triazole substitution is not a merely bioisosteric replacement, as the presence of the triazole prevents off-target effects on DHODH.

Figure 3. Effects of the selected compounds on DHODH. HEK cells were treated for 72 h at the concentration 50 μM with or without uridine (100 μM). Graph shows average \pm SEM of cell viability, peak amplitude and slope of the Ca^{2+} -rise. Student T-test was performed on compounds vs control (**** $p < 4.27 \cdot 10^{-06}$); (terif: teriflunomide, breq: brequinar).



Biphenyl triazoles as sodium salts are more soluble than Synta66

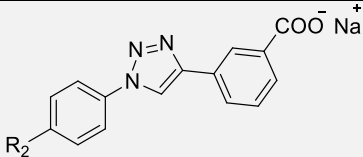
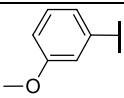
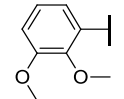
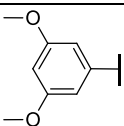
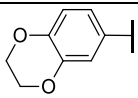
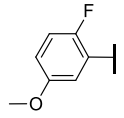
To assess the druggability of the five selected biphenyl triazoles, **28**, **31**, **33**, **35**, **37**, their thermodynamic aqueous solubility was evaluated. Unfortunately, the biphenyl triazoles showed poor aqueous solubility (about 0.20 $\mu\text{g/mL}$, data not shown), comparable to that of Synta66 (0.28 $\mu\text{g/mL}$, Table 4). To overcome this limitation, the candidates were salified as sodium salts and their aqueous solubility was re-assessed (Table 4). Briefly, except for **33**, all the tested biphenyl triazoles salts were

soluble in water in the 0.67-1.53 mg/mL range. The presence of one or two methoxy substituents on the phenyl ring considerably increased the solubility compared to the 1,4-dioxanyl moiety of **35**, as well as the addition of a fluorine atom, that slightly improved the solubility of **37** compared to **28**. Interestingly, the enhanced solubility given by the methoxy substituents is minimally driven by the decrease in hydrophobicity, but rather by the disruption of the molecular symmetry, as shown by the eighty-fold increase aqueous solubility of **31** compared to **33**. In addition, to assess the solubilization of the selected candidates in the aqueous vehicle used for *in vivo* administration, compounds **31** and **37** were dissolved at the nominal concentration of 6 mg/mL in saline solutions containing cosolvents (see methods section). Only **31** gave a limpid solution in saline containing 10% DMSO + 20% PEG400, whose title was confirmed by LC-UV analysis, pointing to this compound as the best candidate for further *in vivo* evaluation.

Biphenyl triazoles are more metabolically stable than Synta66

Next, the *in vitro* metabolic stability of the five candidates (**28**, **31**, **33**, **35** and **37**), was evaluated in mouse liver microsomes (MLM) activated by NADPH by measuring the substrate residual after one hour. For comparative purposes, Synta66 was incubated in the same conditions. All the salified biphenyl triazoles resulted quite stable toward microsomal oxidation, with a residual substrate in the range 75-94% after incubation (Table 4). By contrast, Synta66 resulted considerably less stable toward microsomal metabolism, with a substrate residual of only 15% after incubation, being amide hydrolysis and *O*-demethylation metabolites the most extensive transformations (data not shown).

Table 4. Aqueous solubility and metabolic stability of the selected biphenyl triazoles.

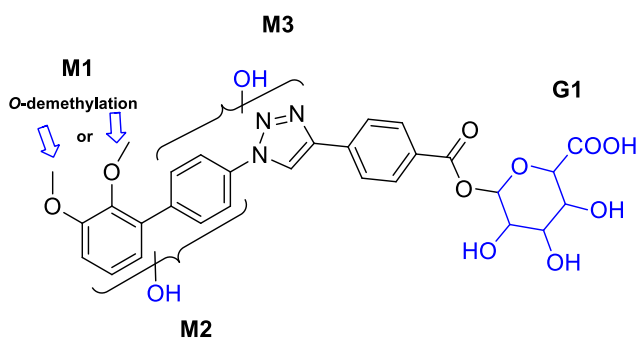
			
R ₂	Cpd	H ₂ O solubility (µg/mL)	Metabolic stability ^b
-	1 , Synta66	0.28	15%
	28_Na	855.57	91%
	31_Na	1528.18 ^a	75%
	33_Na	18.72	92%
	35_Na	668.34	94%
	37_Na	1168.36	93%

^a Soluble at 6 mg/mL in saline containing 10% DMSO + 20% PEG400; ^b Residual substrate after 1-h incubation in MLM.

Next, the structural characterization of the metabolites of **31** was performed by high resolution mass spectrometry (HRMS), processing the raw data with a workflow aimed at drug metabolites identification provided by Compound Discoverer 3.1 software (Thermo Scientific). Overall, data analysis highlighted the occurrence of

three main transformations: *O*-demethylation (M1) followed by hydroxylation (M2 and M3). Furthermore, incubation of **31** with MLM in the presence of uridine diphosphate glucuronic acid (UDPGA) gave the corresponding acyl glucuronide metabolite G1 (Figure 4). Interestingly, data analysis did not highlight the formation of glutathione (GSH) adducts, suggesting that metabolism is not driven toward the formation of reactive species.

Figure 4. Metabolic biotransformation of compound **31** in MLM.

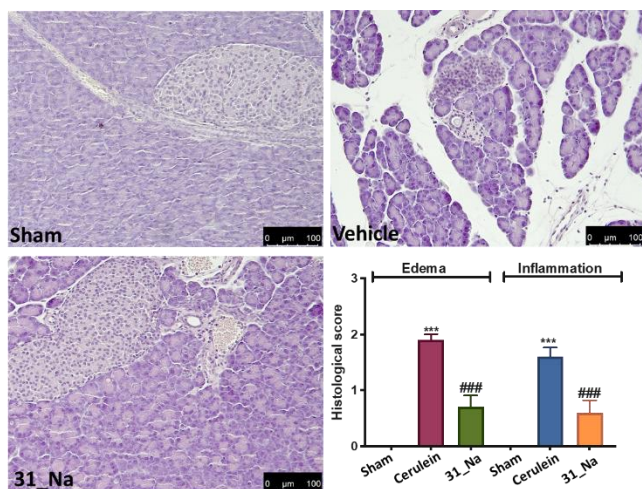


31 is effective in vivo in acute pancreatitis

To further characterize the compound, a pharmacokinetic (PK) analysis was performed in mice. Briefly, mice were injected with **31** (*i.v.*, 7 mg/kg, once) and serial blood sampling was performed. **31** showed a half-life of 3.2 h, with a clearance of 0.5 L/h/Kg, a volume of distribution of 2.3 L/Kg and a C_{max} of 16.8 mg/L.

The PK profile of our candidate prompted us to investigate its efficacy in a cerulein-induced murine model of AP. The compound was administered 30 and 150 minutes after the first cerulein injection at a dose of 10 mg/kg *i.p.* The haematoxylin/eosin (H&E) stainings of the pancreatic tissues collected 5 hours after the first cerulein injection demonstrated that the compound was able to significantly ameliorate the histological scores, with reduction of inflammation and edema typical of this disease (Figure 5), as expected from SOCE inhibitors with profiles compatible with systemic administration.⁶

Figure 5. Evaluation of compound 31 in acute pancreatitis. H&E sections of pancreatic tissues. Analysis were performed in a blinded manner and data represent the mean \pm SEM of 10 mice for each group. *** $p < 0.001$ versus Sham; ### $p < 0.001$ versus cerulein.



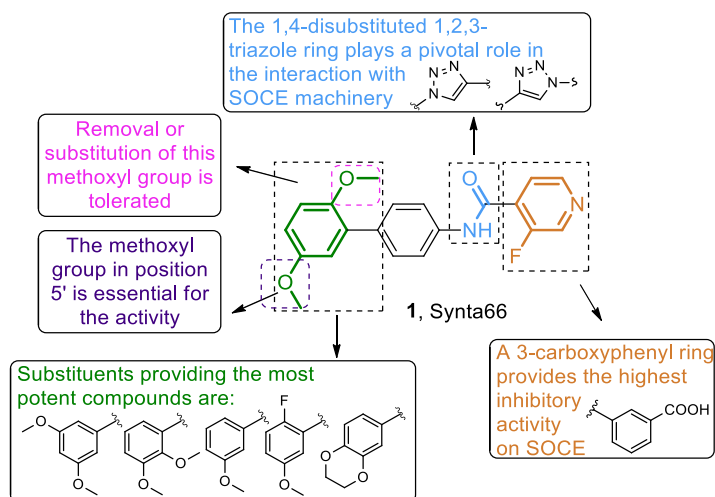
In conclusion, the replacement of the amide with the triazole ring in Synta66, afforded a completely new class of modulators, named biphenyl triazoles.

The synthetic strategy relied on a two-step process based on a click chemistry reaction, followed by a Suzuki coupling. The performed SAR study highlighted that the pharmacophore of this novel class of modulators includes the phenyl ring bearing a methoxyl or methylene ether group in *meta* position, the phenyl ring featuring a carboxylic group in *meta* position and the triazole ring. The latter, when switched into the direct or inverse amide, not only leads a decrease in SOCE inhibition (**61** and **66**), but also to a significant cytotoxicity (**61**), which may in part be reconducted to the fact that arylamide substructures may act on DHODH. The summary of the SAR investigations is schematized in Figure 6.

Our efforts resulted in compound **31** that, compared to Synta66: (i) displays a slightly decreased potency on SOCE ($IC_{50} = 851 \pm 54$ nM vs 228 ± 33 nM) but, importantly, no detectable cytotoxicity in HEK cells up to 60 μ M; (ii) shows a significantly higher *in vitro* metabolic stability in MLM (75% vs 15% of residual substrate after 1 hour);

(iii) is endowed with a carboxylic group that confers high aqueous solubility in the sodium salt form (1528 $\mu\text{g/mL}$ vs 0.28 $\mu\text{g/mL}$). The high metabolic stability confers a favourable PK profile in mice (*i.v.*, $t_{1/2}$ of 3.2 hours) and efficacy in a mouse model of cerulein-induced acute pancreatitis.¹

Figure 6. Graphical representation of SAR study around Synta66.



3.2 Experimental part

General Experimental Methods. Reagents and solvents were used without further purification, although, if required, they were distilled and stored on molecular sieves. Column chromatography was performed on silica gel. The following instrumentation was used: Stuart scientific SMP3 apparatus (melting point), FT-IR Thermo-Nicolet Avatar, FT-IR Bruker Alpha II, Jeol ECP 300 MHz ($^1\text{H-NMR}$), Bruker Avance Neo 400 MHz or Jeol ECP 300 MHz ($^{13}\text{C-NMR}$), Thermo Finningan LCQ-deca XP-plus equipped with an ESI source and an ion trap detector or mass spectrometry (Thermo Scientific Q-Exactive Plus) equipped with an HESI source. Chemical shifts are reported in parts per million (ppm). All lead compounds displayed a purity of 95% or higher, determined by HPLC. Boronic acids, azides and alkynes are commercially available or were synthesized following procedures reported in the literature.

2',5'-Dimethoxy-[1,1'-biphenyl]-4-amine, (4).

4-Bromoaniline **3** (2 g, 11.63 mmol) was solubilized in DMF (23 mL) and ethanol (23 mL) under nitrogen atmosphere. 2,5-(Dimethoxyphenyl)boronic acid **2** (3.17 g, 17.44 mmol), Pd(OAc)₂ (26.1 mg, 0.116 mmol) and K₂CO₃ (3.2 g, 23.26 mmol) were added in order. The mixture was stirred at 80 °C for 3 h and at room temperature overnight. The reaction was then filtered under vacuo over a pad of celite, rinsed with ethanol and evaporated. The crude product was purified by column chromatography using PE/EtOAc 7:3 as eluent, afforded compound **4** as a yellow solid (2.61 g, 11.40 mmol, 98%); ¹H-NMR (300 MHz, CDCl₃): δ 7.39 (d, *J* = 6.9 Hz, 2H), 6.97-6.88 (m, 2H), 6.84 (s, 1H), 6.70 (d, *J* = 6.9 Hz, 2H), 3.82 (s, 3H), 3.76 (s, 3H). MS (ESI): *m/z* 230 [M+H]⁺.

4'-Azido-2,5-dimethoxy-1,1'-biphenyl, (5).

To a solution of 2',5'-dimethoxy-[1,1'-biphenyl]-4-amine (2 g, 8.73 mmol) in water (40 mL) HCl 37% (3.5 mL) was added dropwise and the resulting mixture was cooled down at 0 °C. Then, a solution of NaNO₂ (0.60 g, 8.73 mmol) in water (2 mL) was added and, after 10 min, a solution of NaN₃ (0.68 g, 10.48 mmol) in water (2 mL) was added dropwise. The reaction was stirred at room temperature for 5 h, diluted with EtOAc and washed with water (2x). The organic layer was dried over sodium sulfate and the volatile was removed under vacuo. The crude material was purified by column chromatography using PE/EtOAc 98:2 as eluent, yielded compound **5** as an orange solid (1.33 g, 5.24 mmol, 60%); ¹H-NMR (300 MHz, CDCl₃): δ 8.31 (d, *J* = 7.1 Hz, 2H), 7.75 (d, *J* = 7.1 Hz, 2H), 6.92-6.83 (m, 3H), 3.85 (s, 3H), 3.79 (s, 3H).

General procedure A

Compounds **6-11** were prepared from a suspension of **5** (74 mg, 0.29 mmol, 1 eq) in water (320 μL) and *t*-BuOH (320 μL) and the relative alkyne (0.29 mmol, 1 eq). Reactions were carried out overnight under vigorous stirring at 50 °C in the presence of sodium ascorbate 1M (29 μL) and copper sulfate pentahydrate (0.0029 mmol, 0.01 eq). Evaporation of the volatile and purification by silica gel column chromatography was performed.

4-(1-(2',5'-Dimethoxy-[1,1'-biphenyl]-4-yl)-1H-1,2,3-triazol-4-yl)-3-fluoropyridine, (6).

Following the general procedure A, the reaction of **5** and 4-ethynyl-3-fluoropyridine, after purification (PE/EtOAc 6:4 as eluent), yielded **6** as a yellow solid (34 mg, 0.09 mmol, 31%); mp: 165-166 °C. ¹H-NMR (300 MHz, CDCl₃): δ 8.60-8.50 (m, 3H), 8.31 (d, *J* = 6.1 Hz, 1H), 7.85 (d, *J* = 8.5 Hz, 2H), 7.73 (d, *J* = 8.5 Hz, 2H), 6.97-6.89 (m, 3H), 3.83 (s, 3H), 3.75 (s, 3H). IR (KBr): $\tilde{\nu}$ = 3159, 3058, 2939, 1620, 1490, 1233, 1051, 842, 789 cm⁻¹. MS (ESI): *m/z* 377 [M+H]⁺.

4-(1-(2',5'-Dimethoxy-[1,1'-biphenyl]-4-yl)-1H-1,2,3-triazol-4-yl)pyridine, (7).

Following the general procedure A, the reaction of **5** and 4-ethynylpyridine, after purification (PE/EtOAc 4:6 as eluent), yielded compound **7** as a whitish solid (38 mg, 0.11 mmol, 37%); mp: 185-186 °C. ¹H-NMR (300 MHz, CDCl₃): δ 8.36 (s, 1H), 7.82 (d, *J* = 7.4 Hz, 2H), 7.73-7.64 (m, 4H), 7.52 (s, 1H), 6.97-6.90 (m, 4H), 3.82 (s, 3H), 3.80 (s, 3H). IR (KBr): $\tilde{\nu}$ = 3110, 2930, 2858, 1726, 1499, 1215, 821, 752, 727 cm⁻¹. MS (ESI): *m/z* 359 [M+H]⁺.

3-(1-(2',5'-Dimethoxy-[1,1'-biphenyl]-4-yl)-1H-1,2,3-triazol-4-yl)pyridine, (8).

Following the general procedure A, the reaction of **5** and 3-ethynylpyridine, after purification (PE/EtOAc 5:5, PE/EtOAc 3:7 and PE/EtOAc 2:8 as eluents), yielded compound **8** as a yellow solid (68 mg, 0.19 mmol, 65%); mp: 190-191 °C. ¹H-NMR (300 MHz, CDCl₃): δ 9.11 (s, 1H), 8.63 (s, 1H), 8.31-8.29 (m, 2H), 7.83 (d, *J* = 8.3 Hz, 2H), 7.72 (d, *J* = 8.3 Hz, 2H), 7.43 (s, 1H), 6.97-6.91 (m, 3H), 3.94 (s, 3H), 3.79 (s, 3H). IR (KBr): $\tilde{\nu}$ = 3108, 2996, 2838, 1777, 1501, 1394, 1220, 806, 706 cm⁻¹. MS (ESI): *m/z* 359 [M+H]⁺.

2-(1-(2',5'-Dimethoxy-[1,1'-biphenyl]-4-yl)-1H-1,2,3-triazol-4-yl)pyridine, (9).

Following the general procedure A, the reaction of **5** and 2-ethynylpyridine, after purification (PE/EtOAc 7:3 as eluent), yielded compound **9** as a yellow solid (52 mg, 0.15 mmol, 50%); mp: 166-167 °C. ¹H-NMR (300 MHz, CDCl₃): δ 8.65-8.59 (m, 2H), 8.26 (d, *J* = 8.0 Hz, 1H), 7.85-7.78 (m, 3H), 7.70 (d, *J* = 8.5 Hz, 2H), 7.25 (t, *J*

= 6.6 Hz, 1H), 6.95-6.86 (m, 3H), 3.82 (s, 3H), 3.77 (s, 3H). IR (KBr): $\tilde{\nu}$ = 3106, 2998, 2827, 1761, 1610, 1397, 1289, 810, 704 cm^{-1} . MS (ESI): m/z 359 [M+H]⁺.

4-(1-(2',5'-Dimethoxy-[1,1'-biphenyl]-4-yl)-1H-1,2,3-triazol-4-yl)picolinic acid, (10).

Following the general procedure A, the reaction of **5** and methyl 4-ethynylpicolinate, after purification (PE/EtOAc 4:6 as eluent), yielded methyl 4-(1-(2',5'-dimethoxy-[1,1'-biphenyl]-4-yl)-1H-1,2,3-triazol-4-yl)picolinate as a yellow solid (39 mg, 0.09 mmol, 32%). The compound (39 mg, 0.09 mmol) was solubilized in acetone (390 μL) and water (390 μL). NaOH (7.2 mg, 0.18 mmol) was added and the mixture was stirred at room temperature for 1 h. The volatile was then removed and the crude material was purified by column chromatography using EtOAc/MeOH 7:3 as eluent, yielding compound **10** as a pale yellow solid (21 mg, 0.05 mmol, 58%); mp: 162-163 °C. ¹H-NMR (300 MHz, DMSO-*d*₆): δ 9.72 (s, 1H), 8.70-8.56 (m, 3H), 8.01 (d, J = 8.0 Hz, 2H), 7.75 (d, J = 8.0 Hz, 2H), 7.75 (s, 1H), 6.96 (m, 2H), 3.76 (s, 3H), 3.73 (s, 3H). IR (KBr): $\tilde{\nu}$ = 3158, 2932, 2858, 1726, 1499, 1225, 1075, 812, 758, 716 cm^{-1} . MS (ESI): m/z 403 [M+H]⁺.

3-(1-(2',5'-Dimethoxy-[1,1'-biphenyl]-4-yl)-1H-1,2,3-triazol-4-yl)benzoic acid, (11).

Following the general procedure A, the reaction of **5** and 3-ethynylbenzoic acid, after purification (PE/EtOAc 6:4 as eluent), yielded compound **11** as a pale yellow solid (49 mg, 0.12 mmol, 42%); mp: 177-178 °C. ¹H-NMR (300 MHz, CDCl₃): δ 9.20 (s, 1H), 8.66 (s, 1H), 8.28 (d, J = 8.0 Hz, 1H), 8.04 (d, J = 6.6 Hz, 2H), 7.73 (d, J = 6.6 Hz, 2H), 7.67-7.53 (m, 2H), 7.08 (d, J = 8.0 Hz, 1H), 7.01-6.92 (m, 2H), 3.82 (s, 3H), 3.79 (s, 3H). IR (KBr): $\tilde{\nu}$ = 3155, 2961, 1727, 1497, 1263, 1217, 1073, 810, 756 cm^{-1} . MS (ESI): m/z 402 [M+H]⁺.

2',5'-Dimethoxy-[1,1'-biphenyl]-4-carbaldehyde, (13).

To a solution of 4-bromobenzaldehyde **12** (500 mg, 2.70 mmol) in DMF (8 mL) and water (2 mL) (2,5-dimethoxyphenyl)boronic acid **2** (540 mg, 2.97 mmol), Pd(OAc)₂ (11.2 mg, 0.05 mmol) and K₂CO₃ (933 mg, 6.75 mmol) were added in order under

nitrogen atmosphere and stirred at 50 °C for 3 h. The reaction was filtered under vacuo over a pad of celite, diluted with diethyl ether and washed three times with water. The organic phase was dried over sodium sulfate and evaporated. Purification by column chromatography (PE/EtOAc 98:2) yielded compound **13** as an orange solid (647 mg, 2.67 mmol, 99%). ¹H-NMR (300 MHz, CDCl₃): δ 10.06 (s, 1H), 7.89 (d, *J* = 7.7 Hz, 2H), 7.69 (d, *J* = 7.7 Hz, 2H), 7.08-6.91 (m, 3H), 3.79 (s, 3H), 3.73 (s, 3H). MS (ESI): *m/z* 243 [M+H]⁺.

4'-Ethynyl-2,5-dimethoxy-1,1'-biphenyl, (14).

To a solution of intermediate **13** (636 mg, 2.63 mmol) in MeOH (6 mL), K₂CO₃ (727 mg, 5.26 mmol) and dimethyl (1-diazo-2-oxopropyl)phosphonate (759 mg, 3.95 mmol) were added in order under nitrogen atmosphere. The mixture was stirred at room temperature overnight, then the solvent was removed, water was added and the aqueous layer was extracted with CH₂Cl₂ (3x). The organic phases were collected, dried over sodium sulfate and evaporated. Purification by column chromatography (PE/EtOAc 98:2 as eluent) yielded compound **14** as a white solid (514 mg, 2.16 mmol, 82%). ¹H-NMR (300 MHz, CDCl₃): δ 7.59-7.49 (m, 4H), 6.93-6.85 (m, 3H), 3.86 (s, 3H), 3.76 (s, 3H), 3.10 (s, 1H). MS (ESI): *m/z* 239 [M+H]⁺.

General procedure B

Compounds **15-20** were prepared from a suspension of **14** (0.29 mmol, 1 eq) in water (320 μL) and *t*-BuOH (320 μL) and the relative azide (0.29 mmol, 1 eq). Reactions were carried out overnight under vigorous stirring at 50 °C in the presence of sodium ascorbate 1M (30 μL) and copper sulfate pentahydrate (0.0029 mmol, 0.01 eq). Evaporation of the volatile and purification by silica gel column chromatography was performed.

4-(4-(2',5'-Dimethoxy-[1,1'-biphenyl]-4-yl)-1H-1,2,3-triazol-1-yl)-3-fluoropyridine, (15).

Following the general procedure B, the reaction of **14** and 4-azido-3-fluoropyridine, after purification (PE/EtOAc 7:3 as eluent), yielded compound **15** as a yellow solid (95 mg, 0.25 mmol, 60%); mp: 176-177 °C. ¹H-NMR (300 MHz, CDCl₃): δ 8.75 (s,

1H), 8.64 (d, $J = 6.0$ Hz, 1H), 8.48 (s, 1H), 8.22 (d, $J = 6.0$ Hz, 1H), 7.96 (d, $J = 8.3$ Hz, 2H), 7.66 (d, $J = 8.3$ Hz, 2H), 6.96-6.89 (m, 3H), 3.82 (s, 3H), 3.76 (s, 3H). IR (KBr): $\tilde{\nu} = 3135, 3002, 2837, 1735, 1488, 1216, 1022, 828, 805, 714$ cm⁻¹. MS (ESI): m/z 377 [M+H]⁺.

4-(4-(2',5'-Dimethoxy-[1,1'-biphenyl]-4-yl)-1H-1,2,3-triazol-1-yl)pyridine, (16).

Following the general procedure B, the reaction of **14** and 4-azidopyridine, after purification (PE/EtOAc 9:1 as eluent), yielded compound **16** as a yellow solid (119 mg, 0.33 mmol, 79%); mp: 179-180 °C. ¹H-NMR (300 MHz, DMSO-*d*₆): δ 9.55 (s, 1H), 8.85 (s, 1H), 8.04-8.01 (m, 2H), 7.99 (d, $J = 8.3$ Hz, 2H), 7.66 (d, $J = 8.3$ Hz, 2H), 7.06 (d, $J = 6.9$ Hz, 1H) 6.94-9.93 (m, 3H), 3.77 (s, 3H), 3.74 (s, 3H). IR (KBr): $\tilde{\nu} = 3109, 2961, 2837, 1498, 1488, 1396, 1261, 819, 805, 753$ cm⁻¹. MS (ESI): m/z 359 [M+H]⁺.

3-(4-(2',5'-Dimethoxy-[1,1'-biphenyl]-4-yl)-1H-1,2,3-triazol-1-yl)pyridine, (17).

Following the general procedure B, the reaction of **14** and 3-azidopyridine, after purification (PE/EtOAc 5:5 as eluent), yielded compound **17** as a yellowish solid (117 mg, 0.33 mmol, 78%); mp: 184-185 °C. ¹H-NMR (300 MHz, CDCl₃): δ 9.08 (s, 1H), 8.72 (s, 1H), 8.27-8.21 (m, 2H), 7.95 (d, $J = 8.3$ Hz, 2H), 7.65 (d, $J = 8.3$ Hz, 2H), 7.53 (t, $J = 5.2$ Hz, 1H), 6.96-6.88 (m, 3H), 3.82 (s, 3H), 3.78 (s, 3H). IR (KBr): $\tilde{\nu} = 3108, 2963, 2837, 1585, 1485, 1261, 1025, 820, 805, 700$ cm⁻¹. MS (ESI): m/z 359 [M+H]⁺.

Methyl 4-(4-(2',5'-dimethoxy-[1,1'-biphenyl]-4-yl)-1H-1,2,3-triazol-1-yl)picolinate, (18).

Following the general procedure B, the reaction of **14** and methyl 4-azidopicolinate, after purification (PE/EtOAc 4:6 as eluent), yielded compound **18** as a yellowish solid (107 mg, 0.26 mmol, 61%); mp: 145.5-146.5 °C. ¹H-NMR (300 MHz, (CD₃)₂CO): δ 9.38 (s, 1H), 8.93 (d, $J = 4.6$ Hz, 1H) 8.65 (s, 1H), 8.26 (d, $J = 9.0$ Hz, 1H) 8.05 (d, $J = 8.3$ Hz, 2H), 7.67 (d, $J = 8.3$ Hz, 2H), 7.05 (d, $J = 9.0$ Hz, 1H), 6.95-6.91 (m, 2H), 4.03 (s, 3H), 3.81 (s, 3H), 3.77 (s, 3H). IR (KBr): $\tilde{\nu} = 3160, 2928,$

2840, 1760, 1495, 1466, 1306, 1259, 1200, 828, 732 cm^{-1} . MS (ESI): m/z 417 $[\text{M}+\text{H}]^+$.

4-(4-(2',5'-Dimethoxy-[1,1'-biphenyl]-4-yl)-1H-1,2,3-triazol-1-yl)picolinic acid, (19).

Compound **18** (49 mg, 0.12 mmol) was solubilized in acetone (490 μL) and water (490 μL). NaOH (9.6 mg, 0.24 mmol) was added and the mixture was stirred at room temperature for 2 h. The reaction mixture was diluted with water and HCl 3N was added until pH 4. The aqueous layer was extracted with EtOAc (5x) and the collected organic phases were dried over sodium sulfate and evaporated. Purification by column chromatography (EtOAc/MeOH 8:2 and EtOAc/MeOH 7:3 as eluents) yielded compound **19** as a pale yellow solid (36 mg, 0.09 mmol, 75%); mp: 158-159 $^{\circ}\text{C}$. $^1\text{H-NMR}$ (300 MHz, $\text{DMSO-}d_6$): δ 9.71 (s, 1H), 8.70-8.62 (m, 3H), 8.02 (d, $J = 8.0$ Hz, 2H), 7.63 (d, $J = 8.0$ Hz, 2H), 7.09 (d, $J = 9.6$ Hz, 1H), 6.94-6.92 (m, 2H), 3.80 (s, 3H), 3.76 (s, 3H). IR (KBr): $\tilde{\nu} = 3159, 2931, 2856, 1706, 1490, 1485, 1308, 1260, 1206, 830, 742$ cm^{-1} . MS (ESI): m/z 403 $[\text{M}+\text{H}]^+$.

3-(4-(2',5'-Dimethoxy-[1,1'-biphenyl]-4-yl)-1H-1,2,3-triazol-1-yl)benzoic acid, (20).

Following the general procedure B, the reaction of **14** and 3-azidobenzoic acid, after purification (PE/EtOAc 3:7 as eluent), yielded compound **20** as a yellowish solid (167 mg, 0.42 mmol, 99%); mp: 215-216 $^{\circ}\text{C}$. $^1\text{H-NMR}$ (300 MHz, $(\text{CD}_3)_2\text{CO}$): δ 9.18 (s, 1H), 8.58 (s, 1H), 8.26 (d, $J = 8.0$ Hz, 1H), 8.15 (d, $J = 8.0$ Hz, 1H), 8.05 (d, $J = 6.9$ Hz, 2H), 7.77 (t, $J = 8.0$ Hz, 1H), 7.65 (d, $J = 6.9$ Hz, 2H), 7.04 (d, $J = 9.0$ Hz, 1H), 6.97-6.89 (m, 2H), 3.80 (s, 3H), 3.76 (s, 3H). $^{13}\text{C-NMR}$ (101 MHz; $\text{DMSO-}d_6$): δ 166.9, 153.9, 150.8, 147.9, 138.4, 137.3, 133.5, 130.9, 130.6, 130.3, 129.7, 129.2, 125.5, 124.3, 120.8, 120.2, 116.4, 114.1, 113.7, 56.7, 56.0. IR (KBr): $\tilde{\nu} = 3159, 2931, 1711, 1495, 1312, 1243, 1210, 839, 753$ cm^{-1} . MS (ESI): m/z 402 $[\text{M}+\text{H}]^+$.

1-Azido-4-bromobenzene, (21).

To a solution of 4-bromoaniline (3 g, 17.44 mmol) in water (77 mL) HCl 37% (7 mL) was added dropwise and the resulting mixture was cooled down at 0 °C. Then, a solution of NaNO₂ (1.20 g, 17.44 mmol) in water (3 mL) was added and, after 10 min, a solution of NaN₃ (1.36 g, 20.92 mmol) in water (3 mL) was added dropwise. The reaction was stirred at room temperature for 3 h, diluted with EtOAc and washed with water (2x). The organic layer was dried over sodium sulfate and the volatile was removed under vacuo. Purification by column chromatography (PE/EtOAc 98:2 as eluent) yielded compound **21** as an orange solid (4.86 g, 14.13 mmol, 81%); ¹H-NMR (300 MHz, CDCl₃): δ 7.53-7.44 (m, 2H), 6.97-6.88 (m, 2H).

3-(1-(4-Bromophenyl)-1H-1,2,3-triazol-4-yl)benzoic acid, (23).

To a suspension of 1-azido-4-bromobenzene **21** (2.78 g, 14.04 mmol) in water (26 mL) and *t*-BuOH (26 mL) 3-ethynylbenzoic acid **22** (2.05 g, 14.04 mmol) was added. Then, 1.4 mL of an aqueous solution of sodium ascorbate 1M and copper sulfate pentahydrate (34.9 mg, 0.14 mmol) were added and the mixture was vigorously stirred for 48 h. Evaporation and purification by column chromatography (PE/EtOAc 2:8 and EtOAc/MeOH 8:2 as eluents) yielded compound **23** as a yellow solid (4.22 g, 12.27 mmol, 87%); ¹H-NMR (300 MHz, DMSO-*d*₆): δ 9.54 (s, 1H), 8.51 (s, 1H), 8.14 (d, *J* = 7.7 Hz, 1H), 7.98-7.94 (m, 3H), 7.86-7.83 (d, *J* = 8.8 Hz, 2H), 7.60 (t, *J* = 7.7 Hz, 1H). MS (ESI): *m/z* 343 [M-H]⁻.

General procedure C

Compounds **24-37** were prepared from a solution of **23** (0.29 mmol, 1 eq) in DMF (750 μL) and ethanol (750 μL) under nitrogen atmosphere, in the presence of and the relative boronic acid (0.44 mmol, 1.5 eq). Reactions were carried out at 80 °C overnight in the presence of Pd(OAc)₂ (0.0029 mmol, 0.01 eq) and K₂CO₃ (0.58 mmol, 2 eq). After filtration of the reaction mixture under vacuo over a pad of celite and evaporation of the volatile, purification by silica gel column chromatography was performed.

3-(1-([1,1'-Biphenyl]-4-yl)-1H-1,2,3-triazol-4-yl)benzoic acid, (24).

Following the general procedure C, the reaction of **23** and phenylboronic acid, after purification (PE/EtOAc 4:6 as eluent), yielded compound **24** as a yellow solid (54.5 mg, 0.16 mmol, 55%); mp: 232-234 °C dec. ¹H-NMR (300 MHz, DMSO-*d*₆): δ 9.52 (s, 1H), 8.61 (s, 1H), 8.20 (d, *J* = 6.9 Hz, 1H), 8.09 (d, *J* = 8.3 Hz, 2H), 7.98-7.85 (m, 3H), 7.77 (d, *J* = 8.3 Hz, 2H), 7.63 (t, *J* = 7.5 Hz, 1H), 7.54-7.50 (m, 2H), 7.43 (d, *J* = 7.5 Hz, 1H). ¹³C-NMR (101 MHz; DMSO-*d*₆): δ 167.7, 147.1, 140.9, 139.3, 136.3, 134.5, 132.4, 131.1, 129.8, 129.5, 129.4, 128.5, 128.5, 127.2, 126.6, 120.9, 120.5. IR (neat): $\tilde{\nu}$ = 2922, 2852, 1719, 1687, 1525, 1489, 1299, 1227, 1154, 814, 158, 682 cm⁻¹. MS (ESI): *m/z* 342 [M+H]⁺. HRMS (ESI) *m/z* (M+H)⁺ calcd for C₂₁H₁₆N₃O₂ 342.1237, found 342.1234.

3-(1-(2'-Methoxy-[1,1'-biphenyl]-4-yl)-1*H*-1,2,3-triazol-4-yl)benzoic acid, (25).

Following the general procedure C, the reaction of **23** and (2-methoxyphenyl)boronic acid, after purification (EtOAc as eluent), yielded compound **25** as a yellow solid (72 mg, 0.19 mmol, 67%); mp: 208-209 °C. ¹H-NMR (300 MHz, DMSO-*d*₆): δ 9.45 (s, 1H), 8.56 (s, 1H), 8.18 (d, *J* = 6.9 Hz, 1H), 8.03-7.95 (m, 3H), 7.74 (d, *J* = 8.3 Hz, 2H), 7.53 (t, *J* = 6.9 Hz, 1H), (d, *J* = 8.3 Hz, 2H), 7.24-7.14 (m, 2H), 3.82 (s, 3H). ¹³C-NMR (101 MHz; DMSO-*d*₆): δ 167.9, 156.6, 147.1, 139.0, 135.7, 133.3, 131.1, 130.8, 129.9, 129.8, 129.5, 128.9, 126.6, 122.3, 121.4, 120.6, 120.5, 120.1, 112.3, 56.0. IR (neat): $\tilde{\nu}$ = 3127, 2923, 2851, 1718, 1685, 1595, 1487, 1227, 1024, 756, 745 cm⁻¹. MS (ESI): *m/z* 372 [M+H]⁺. HRMS (ESI) *m/z* (M+H)⁺ calcd for C₂₂H₁₈N₃O₃ 372.1343, found 372.1337.

3-(1-(2',4'-Dimethoxy-[1,1'-biphenyl]-4-yl)-1*H*-1,2,3-triazol-4-yl)benzoic acid, (26).

Following the general procedure C, the reaction of **23** and (2,4-dimethoxyphenyl)boronic acid, after purification (EtOAc/MeOH 9:1 as eluent), yielded compound **26** as a pale yellow solid (100 mg, 0.25 mmol, 86%); mp: 235-236 °C. ¹H-NMR (300 MHz, DMSO-*d*₆): δ 9.47 (s, 1H), 8.56 (s, 1H), 8.17 (d, *J* = 8.2 Hz, 1H), 7.99-7.95 (m, 3H), 7.69 (d, *J* = 9.2 Hz, 2H), 7.62 (t, *J* = 8.2 Hz, 1H) 7.32 (d, *J* = 8.2 Hz, 1H), 6.71 (s, 1H), 6.66 (d, *J* = 6.2 Hz, 1H), 3.83 (s, 3H), 3.81 (s,

3H). ^{13}C -NMR (75 MHz; DMSO- d_6): δ 168.2, 161.1, 157.8, 147.2, 139.1, 135.4, 133.4, 131.5, 131.1, 130.9, 129.7, 129.6, 129.5, 126.6, 121.6, 120.5, 120.1, 106.1, 99.6, 56.2, 55.9. IR (neat): $\tilde{\nu}$ = 3406, 3020, 2929, 1687, 1605, 1499, 1414, 1279, 1161, 1026, 803, 761 cm^{-1} . MS (ESI): m/z 402 $[\text{M}+\text{H}]^+$. HRMS (ESI) m/z $(\text{M}+\text{H})^+$ calcd for $\text{C}_{23}\text{H}_{20}\text{N}_3\text{O}_4$ 402.1448, found 402.1441.

3-(1-(2',6'-Dimethoxy-[1,1'-biphenyl]-4-yl)-1H-1,2,3-triazol-4-yl)benzoic acid, (27).

Following the general procedure C, the reaction of **23** and (2,6-dimethoxyphenyl)boronic acid, after purification (EtOAc/MeOH 9:1 as eluent), yielded compound **27** as a pale yellow solid (60 mg, 0.15 mmol, 52%); mp: 248-250 $^{\circ}\text{C}$ dec. ^1H -NMR (300 MHz, DMSO- d_6): δ 9.40 (s, 1H), 8.55 (s, 1H), 8.15 (d, J = 6.9 Hz, 1H), 7.97-7.95 (m, 4H), 7.84 (d, J = 6.9 Hz, 1H), 7.62-7.58 (m, 1H), 7.47 (d, J = 8.2 Hz, 1H), 7.35 (t, J = 8.2 Hz, 1H), 6.79 (d, J = 8.2 Hz, 1H), 3.71 (s, 6H). ^{13}C -NMR (101 MHz; DMSO- d_6): δ 168.3, 157.6, 147.4, 147.1, 135.5, 135.3, 133.3, 132.7, 130.4, 129.6, 129.3, 126.6, 122.4, 120.5, 119.9, 117.8, 105.0, 56.3. IR (neat): $\tilde{\nu}$ = 3409, 2923, 2834, 1701, 1591, 1400, 1246, 1100, 825, 756 cm^{-1} . MS (ESI): m/z 402 $[\text{M}+\text{H}]^+$. HRMS (ESI) m/z $(\text{M}+\text{H})^+$ calcd for $\text{C}_{23}\text{H}_{20}\text{N}_3\text{O}_4$ 402.1448, found 402.1441.

3-(1-(3'-Methoxy-[1,1'-biphenyl]-4-yl)-1H-1,2,3-triazol-4-yl)benzoic acid, (28).

Following the general procedure C, the reaction of **23** and (3-methoxyphenyl)boronic acid, after purification (EtOAc/MeOH 9:1 as eluent), yielded compound **28** as a white solid (73 mg, 0.20 mmol, 68%); mp: 244-245 $^{\circ}\text{C}$. ^1H -NMR (400 MHz, DMSO- d_6): 9.57 (s, 1H), 8.56 (s, 1H), 8.23 (d, J = 7.4 Hz, 1H), 8.09 (d, J = 8.2 Hz, 2H), 7.96-7.94 (m, 3H), 7.65 (t, J = 7.6 Hz, 1H), 7.43 (t, J = 7.6 Hz, 1H), 7.33 (d, J = 7.6 Hz, 1H), 7.30 (s, 1H), 6.99 (d, J = 7.4 Hz, 1H), 3.86 (s, 3H). ^{13}C -NMR (101 MHz; DMSO- d_6): δ 167.5, 160.3, 147.1, 140.7 (2C), 136.3, 132.2, 131.1, 130.6, 129.9, 129.8, 129.4, 128.7, 126.5, 120.7, 120.6, 119.5, 114.1, 112.7, 55.7. IR (KBr): $\tilde{\nu}$ = 3450, 2837, 1909, 1513, 1244, 1033, 801, 677 cm^{-1} . MS (ESI): m/z 372 $[\text{M}+\text{H}]^+$. For biological evaluation, the sodium salt of **28** was prepared by

dissolving it in THF and adding a 50% aqueous solution of NaOH (1 eq). After stirring at 60 °C for 1 h, the solid precipitate was collected by filtration; mp 182-183 °C dec.

3-(1-(3'-Hydroxy-[1,1'-biphenyl]-4-yl)-1H-1,2,3-triazol-4-yl)benzoic acid, (29).

Following the general procedure C, the reaction of **23** and (3-hydroxyphenyl)boronic acid, after purification (EtOAc/MeOH 9:1 and EtOAc/MeOH 8:2 as eluents), yielded compound **29** as a dark yellow solid (19 mg, 0.05 mmol, 18%); mp: 184-186 °C dec. ¹H-NMR (300 MHz, CD₃OD): δ 8.96 (s, 1H), 8.59 (s, 1H), 8.15 (s, 1H), 8.03 (d, *J* = 7.8 Hz, 1H), 7.92 (d, *J* = 7.4 Hz, 1H), 7.58 (d, *J* = 7.8 Hz, 1H), 7.18-7.15 (m, 3H), 7.04-6.99 (m, 2H), 6.82 (d, *J* = 5.8 Hz, 2H). ¹³C-NMR (101 MHz, DMSO-*d*₆): δ 168.2, 157.0, 133.3, 130.9, 130.6, 130.4, 129.6, 129.4, 129.4, 129.2, 128.8, 128.4, 126.6, 125.2, 122.4, 121.3, 120.8, 120.5, 117.4. IR (neat): $\tilde{\nu}$ = 3406, 2924, 1686, 1613, 1303, 1229, 1034, 887, 757, 700, 683 cm⁻¹. MS (ESI): *m/z* 356 [M-H]⁻. HRMS (ESI) *m/z* (M+H)⁺ calcd for C₂₁H₁₆N₃O₃ 358.1186, found 358.1180.

3-(1-(3'-(Methylthio)-[1,1'-biphenyl]-4-yl)-1H-1,2,3-triazol-4-yl)benzoic acid, (30).

Following the general procedure C, the reaction of **23** and (3-(methylthio)phenyl)boronic acid, after purification (EtOAc/MeOH 9:1 as eluent), yielded compound **30** as a white solid (89.8 mg, 0.23 mmol, 80%); mp: 258-259 °C. ¹H-NMR (300 MHz, DMSO-*d*₆): δ 9.55 (s, 1H), 8.55 (s, 1H), 8.18 (d, *J* = 7.9 Hz, 1H), 8.08 (d, *J* = 9.3 Hz, 2H), 7.97-7.95 (m, 3H), 7.60 (d, *J* = 9.3 Hz, 2H), 7.52 (d, *J* = 7.9 Hz, 1H), 7.45 (t, *J* = 7.9 Hz, 1H), 7.31 (d, *J* = 6.2 Hz, 1H), 2.58 (s, 3H). ¹³C-NMR (75 MHz; DMSO-*d*₆): δ 168.1, 147.3, 140.5, 140.1, 139.8, 136.5, 133.1, 131.1, 130.5, 130.1, 129.8, 129.7, 129.5, 128.8, 126.6, 125.9, 124.5, 123.9, 120.8, 15.2. IR (KBr): $\tilde{\nu}$ = 3450, 3127, 2917, 1521, 1305, 1229, 1043, 838, 696 cm⁻¹. MS (ESI): *m/z* 388 [M+H]⁺. HRMS (ESI) *m/z* (M+H)⁺ calcd for C₂₂H₁₈N₃O₂S 388.1114, found 388.1107.

3-(1-(2',3'-Dimethoxy-[1,1'-biphenyl]-4-yl)-1H-1,2,3-triazol-4-yl)benzoic acid, (31).

Following the general procedure C, the reaction of **23** and (2,3-dimethoxyphenyl)boronic acid, after purification (EtOAc/MeOH 9:1 and EtOAc/MeOH 8:2 as eluents), yielded compound **31** as a yellow solid (88 mg, 0.22 mmol, 76%); mp: 203-204 °C dec. ¹H-NMR (400 MHz, DMSO-*d*₆): δ 9.48 (s, 1H), 8.58 (s, 1H), 8.18 (d, *J* = 7.2 Hz, 1H), 8.05 (d, *J* = 8.4 Hz, 2H), 7.98 (d, *J* = 7.2 Hz, 1H), 7.74 (d, *J* = 8.4 Hz, 2H), 7.64 (t, *J* = 7.6 Hz, 1H), 7.20-7.11 (m, 2H), 7.00 (d, *J* = 7.2 Hz, 1H), 3.87 (s, 3H), 3.60 (s, 3H). ¹³C-NMR (101 MHz; DMSO-*d*₆): δ 168.3, 153.4, 147.3, 146.5, 138.7, 136.0 (2C), 134.2 (2C), 130.9, 129.6, 129.4, 129.3, 126.6, 124.8, 122.4, 120.4, 120.2, 113.3, 60.7, 56.3. IR (neat): $\tilde{\nu}$ = 3165, 2933, 2837, 1700, 1520, 1452, 1258, 1029, 791, 756 cm⁻¹. MS (ESI): *m/z* 402 [M+H]⁺. HRMS (ESI) *m/z* (M+H)⁺ calcd for C₂₃H₂₀N₃O₄ 402.1448, found 402.1440. Sodium salt of **31**: mp 178-179 °C dec.

3-(1-(4-(2,3-Dihydrobenzo[*b*][1,4]dioxin-5-yl)phenyl)-1*H*-1,2,3-triazol-4-yl)benzoic acid, (32).

Following the general procedure C, the reaction of **23** and (2,3-dihydrobenzo[*b*][1,4]dioxin-5-yl)boronic acid, after purification (PE/EtOAc 1:9 and EtOAc/MeOH 9:1 as eluents), yielded compound **32** as a pale yellow solid (88 mg, 0.22 mmol, 76%); mp: 218-220 °C dec. ¹H-NMR (400 MHz, DMSO-*d*₆): δ 9.48 (s, 1H), 8.56 (s, 1H), 8.17 (d, *J* = 5.9 Hz, 1H), 8.03 (d, *J* = 8.5 Hz, 2H), 7.97 (d, *J* = 7.5 Hz, 1H), 7.76 (d, *J* = 8.5 Hz, 2H), 7.62 (t, *J* = 7.5 Hz, 1H), 6.96-6.93 (m, 3H), 4.31-4.29 (m, 4H). ¹³C-NMR (101 MHz; DMSO-*d*₆): δ 167.9, 147.1, 144.4, 141.2, 138.2, 135.9, 133.1, 131.0, 130.4, 129.7, 129.6, 129.4, 129.3, 126.6, 122.6, 121.5, 120.5, 120.1, 117.4, 64.7, 64.3. IR (neat): $\tilde{\nu}$ = 3164, 2922, 2874, 1700, 1467, 1402, 1257, 1213, 1080, 758, 692 cm⁻¹. MS (ESI): *m/z* 400 [M+H]⁺. HRMS (ESI) *m/z* (M+H)⁺ calcd for C₂₃H₁₈N₃O₄ 400.1292, found 400.1283.

3-(1-(3',5'-Dimethoxy-[1,1'-biphenyl]-4-yl)-1*H*-1,2,3-triazol-4-yl)benzoic acid, (33).

Following the general procedure C, the reaction of **23** and (3,5-dimethoxyphenyl)boronic acid, after purification (EtOAc/MeOH 9:1 as eluent),

yielded compound **33** as a white solid (100 mg, 0.25 mmol, 86%); mp: 209-210 °C. ¹H-NMR (400 MHz, DMSO-*d*₆): δ 9.46 (s, 1H), 8.59 (s, 1H), 8.13 (d, *J* = 7.6 Hz, 1H), 8.06 (d, *J* = 8.2 Hz, 2H), 7.99 (d, *J* = 7.6 Hz, 1H), 7.94 (d, *J* = 8.2 Hz, 2H), 7.58 (t, *J* = 7.6 Hz, 1H), 6.89 (s, 2H), 6.55 (s, 1H), 3.84 (s, 6H). ¹³C-NMR (101 MHz; DMSO-*d*₆): δ 170.7, 161.5, 147.5, 141.4, 140.7, 136.5, 130.7, 129.5, 129.3 (2C), 128.8, 128.7, 126.7, 120.7, 120.3, 105.4, 100.4, 55.8 (2C). IR (KBr): $\tilde{\nu}$ = 3558, 3489, 3403, 3160, 2836, 1522, 1152, 1061, 825, 757 cm⁻¹. HRMS (ESI) *m/z* (M+H)⁺ calcd for C₂₃H₂₀N₃O₄ 402.1448, found 402.1441. MS (ESI): *m/z* 402 [M+H]⁺. Sodium salt of **33**: mp 169-170 °C dec.

3-(1-(3',4'-Dimethoxy-[1,1'-biphenyl]-4-yl)-1H-1,2,3-triazol-4-yl)benzoic acid, (34).

Following the general procedure C, the reaction of **23** and (3,4-dimethoxyphenyl)boronic acid, after purification (EtOAc/MeOH 9:1 and EtOAc/MeOH 8:2 as eluents), yielded compound **34** as a pale yellow solid (50 mg, 0.12 mmol, 43%); mp: 244-246 °C. ¹H-NMR (300 MHz, DMSO-*d*₆): δ 9.47 (s, 1H), 8.55 (s, 1H), 8.17 (d, *J* = 7.1 Hz, 1H), 8.03 (d, *J* = 8.2 Hz, 2H), 7.97-7.90 (m, 3H), 7.62 (t, *J* = 7.9 Hz, 1H), 7.33-7.29 (m, 2H), 7.07 (d, *J* = 7.9 Hz, 1H), 3.99 (s, 3H), 3.88 (s, 3H). ¹³C-NMR (101 MHz; DMSO-*d*₆): δ 168.0, 149.7, 149.5, 147.1, 140.8, 135.7, 133.1, 131.9, 131.0, 130.4, 129.7, 129.4, 128.1, 126.5, 120.7, 120.5, 119.5, 112.9, 110.9, 56.2, 56.1. IR (neat): $\tilde{\nu}$ = 3407, 2924, 2851, 1686, 1504, 1227, 1139, 1024, 810, 757 cm⁻¹. MS (ESI): *m/z* 402 [M+H]⁺. HRMS (ESI) *m/z* (M+H)⁺ calcd for C₂₃H₂₀N₃O₄ 402.1448, found 402.1442.

3-(1-(4-(2,3-Dihydrobenzo[*b*][1,4]dioxin-6-yl)phenyl)-1H-1,2,3-triazol-4-yl)benzoic acid, (35).

Following the general procedure C, the reaction of **23** and (2,3-dihydrobenzo[*b*][1,4]dioxin-6-yl)boronic acid, after purification (EtOAc/MeOH 9:1 as eluent), yielded compound **35** as a white solid (87 mg, 0.22 mmol, 75%); mp: 255-256 °C. ¹H-NMR (400 MHz, DMSO-*d*₆): δ 9.48 (s, 1H), 8.56 (s, 1H), 8.18 (d, *J* = 7.5 Hz, 1H), 8.02 (d, *J* = 8.4 Hz, 2H), 7.96 (d, *J* = 7.5 Hz, 1H), 7.86 (d, *J* = 8.4 Hz,

2H), 7.63 (t, $J = 7.5$ Hz, 1H), 7.27-7.24 (m, 2H), 6.97 (d, $J = 8.2$ Hz, 1H), 4.30-4.29 (m, 4H). $^{13}\text{C-NMR}$ (101 MHz; DMSO- d_6): δ 168.0, 147.1, 144.3, 144.1, 140.3, 135.8, 133.1, 132.5, 131.0, 129.7, 129.6, 129.4, 127.9, 126.6, 120.7, 120.4, 120.1, 118.1, 115.7, 64.7, 64.6. IR (KBr): $\tilde{\nu} = 3124, 2873, 1862, 1504, 1302, 1230, 1069, 812, 562$ cm^{-1} . MS (ESI): m/z 400 $[\text{M}+\text{H}]^+$. HRMS (ESI) m/z (M+H) $^+$ calcd for $\text{C}_{23}\text{H}_{18}\text{N}_3\text{O}_4$ 400.1292, found 400.1286. Sodium salt of **35**: mp 196-197 °C dec.

3-(1-(4-(Benzo[*d*][1,3]dioxol-5-yl)phenyl)-1*H*-1,2,3-triazol-4-yl)benzoic acid, (36).

Following the general procedure C, the reaction of **23** and benzo[*d*][1,3]dioxol-5-ylboronic acid, after purification (EtOAc/MeOH 9:1 as eluent), yielded compound **36** as a yellow solid (37 mg, 0.10 mmol, 33%); mp: 263-264 °C. $^1\text{H-NMR}$ (300 MHz, DMSO- d_6): δ 9.51 (s, 1H), 8.54 (s, 1H), 8.17 (d, $J = 7.4$ Hz, 1H), 8.03 (d, $J = 8.5$ Hz, 2H), 7.95 (d, $J = 7.9$ Hz, 1H), 7.87 (d, $J = 8.5$ Hz, 2H), 7.61 (t, $J = 7.4$ Hz, 1H), 7.42 (s, 1H), 7.27 (d, $J = 7.9$ Hz, 1H), 7.04 (d, $J = 7.4$ Hz, 1H), 6.09 (s, 2H). $^{13}\text{C-NMR}$ (101 MHz; DMSO- d_6): δ 168.3, 148.7, 147.8, 147.3, 140.8, 135.9, 133.6, 131.1, 130.5, 129.7, 129.5, 128.3, 126.6, 121.1, 120.1, 120.5, 109.3, 107.7, 101.9, 79.8. IR (KBr): $\tilde{\nu} = 3930, 3552, 3480, 3414, 2922, 1501, 1228, 1041, 936, 812, 614$ cm^{-1} . MS (ESI): m/z 386 $[\text{M}+\text{H}]^+$. HRMS (ESI) m/z (M+H) $^+$ calcd for $\text{C}_{22}\text{H}_{16}\text{N}_3\text{O}_4$ 386.1135, found 386.1129.

3-(1-(2'-Fluoro-5'-methoxy-[1,1'-biphenyl]-4-yl)-1*H*-1,2,3-triazol-4-yl)benzoic acid, (37).

Following the general procedure C, the reaction of **23** and (2-fluoro-5-methoxyphenyl)boronic acid, after purification (EtOAc/MeOH 9:1 as eluent), yielded compound **37** as a white solid (52 mg, 0.13 mmol, 46%); mp: 223-225 °C. $^1\text{H-NMR}$ (400 MHz, DMSO- d_6): δ 9.45 (s, 1H), 8.54 (s, 1H), 8.16 (d, $J = 7.1$ Hz, 1H), 8.08 (d, $J = 7.8$ Hz, 2H), 7.95 (d, $J = 7.1$ Hz, 1H), 7.82 (d, $J = 7.8$ Hz, 2H), 7.64 (t, $J = 7.8$ Hz, 1H), 7.29 (t, $J = 9.2$ Hz, 1H), 7.14 (dd, $J_s = 6.4, 3.2$ Hz, 1H), 7.03-6.99 (m, 1H), 3.83 (s, 3H). $^{13}\text{C-NMR}$ (101 MHz; DMSO- d_6): δ 167.9, 156.3, 155.1, 152.7, 147.2, 136.5, 135.8, 132.9, 131.0, 130.8, 129.6, 129.5, 128.1 (d, $J = 316.3$ Hz), 127.9

(d, $J = 15.1$ Hz), 120.6, 120.5, 117.5 (d, $J = 24.6$ Hz), 115.6 (d, $J = 3.0$ Hz), 115.5 (d, $J = 8.4$ Hz), 56.2. IR (neat): $\tilde{\nu} = 3407, 2923, 1686, 1613, 1502, 1228, 1024, 808, 756, 611$ cm^{-1} . MS (ESI): m/z 390 $[\text{M}+\text{H}]^+$. HRMS (ESI) m/z $(\text{M}+\text{H})^+$ calcd for $\text{C}_{22}\text{H}_{17}\text{FN}_3\text{O}_3$ 390.1248, found 390.1241. Sodium salt of **37**: mp 191-192 °C dec.

1-Bromo-4-ethynylbenzene, (38).

To a solution of 4-bromobenzaldehyde (2.15 g, 11.62 mmol) in MeOH (22 mL) K_2CO_3 (3.21 g, 23.24 mmol) and dimethyl (1-diazo-2-oxopropyl)phosphonate (2.61 g, 17.43 mmol) were added in order under nitrogen atmosphere. The mixture was stirred at room temperature overnight, then the solvent was removed under vacuo, water was added and the aqueous layer was extracted with CH_2Cl_2 (5x). The organic phases were collected, dried over sodium sulfate and evaporated. Purification by column chromatography (PE/EtOAc 9:1 and PE/EtOAc 8:2 as eluents) yielded compound **38** as an orange solid (1.12 g, 6.26 mmol, 54%); $^1\text{H-NMR}$ (300 MHz, CDCl_3): δ 7.45 (d, $J = 8.5$ Hz, 2H), 7.34 (d, $J = 8.5$ Hz, 2H), 3.11 (s, 1H). MS (ESI): m/z 180 $[\text{M}+\text{H}]^+$.

3-(4-(4-Bromophenyl)-1H-1,2,3-triazol-1-yl)benzoic acid, (40).

To a suspension of 1-bromo-4-ethynylbenzene (1 g, 5.52 mmol) in water (6 mL) and *t*-BuOH (6 mL) 3-azidobenzoic acid (0.89 g, 5.52 mmol) was added. Then, 55 μL of an aqueous solution of sodium ascorbate 1M and copper sulfate pentahydrate (13.7 mg, 0.055 mmol) were added and the mixture was vigorously stirred overnight. Evaporation and purification by column chromatography (PE/EtOAc 3:7 and EtOAc as eluents) yielded compound **40** as a pale yellow solid (1.23 g, 3.59 mmol, 65%); $^1\text{H-NMR}$ (300 MHz, $\text{DMSO-}d_6$): δ 9.50 (s, 1H), 8.46 (s, 1H), 8.19 (d, $J = 7.6$ Hz, 1H), 8.06 (d, $J = 7.6$ Hz, 1H), 7.92 (d, $J = 8.5$ Hz, 2H), 7.78-7.69 (m, 3H). MS (ESI): m/z 343 $[\text{M}-\text{H}]^-$.

General procedure D

Compounds **41-53** were prepared from a solution of **40** (0.29 mmol, 1 eq) in DMF (750 μL) and ethanol (750 μL) under nitrogen atmosphere, in the presence of the relative boronic acid (0.44 mmol, 1.5 eq). Reactions were carried out at 80 °C

overnight in the presence of Pd(OAc)₂ (0.0029 mmol, 0.01 eq) and K₂CO₃ (0.58 mmol, 2 eq). After filtration of the reaction mixture under vacuo over a pad of celite and evaporation of the volatile, purification by silica gel column chromatography was performed.

3-(4-([1,1'-Biphenyl]-4-yl)-1H-1,2,3-triazol-1-yl)benzoic acid, (41).

Following the general procedure D, the reaction of **40** and phenylboronic acid, after purification (EtOAc as eluent), yielded compound **41** as a white solid (54 mg, 0.16 mmol, 55%); mp: 205-206 °C. ¹H-NMR (300 MHz, DMSO-*d*₆): δ 9.48 (s, 1H), 8.48 (s, 1H), 8.13-8.03 (m, 5H), 7.83-7.69 (m, 4H), 7.49 (m, 2H), 7.38 (d, *J* = 7.1 Hz, 1H). ¹³C-NMR (101 MHz; DMSO-*d*₆): δ 168.2, 147.6, 140.3, 140.0, 136.9, 130.2, 129.8, 129.7, 129.5, 128.1, 127.7, 127.0, 126.4, 125.9, 122.9, 120.9, 120.3. IR (KBr): $\tilde{\nu}$ = 3104, 2852, 1480, 1399, 1324, 1231, 912, 761, 724 cm⁻¹. MS (ESI): *m/z* 342 [M+H]⁺. HRMS (ESI) *m/z* (M+H)⁺ calcd for C₂₁H₁₆N₃O₂ 342.1237, found 342.1230.

3-(4-(2'-Methoxy-[1,1'-biphenyl]-4-yl)-1H-1,2,3-triazol-1-yl)benzoic acid, (42).

Following the general procedure D, the reaction of **40** and (2-methoxyphenyl)boronic acid, after purification (EtOAc/MeOH 9:1 as eluent), yielded compound **42** as a white solid (24 mg, 0.06 mmol, 22%); mp: 222-223 °C. ¹H-NMR (300 MHz, DMSO-*d*₆): δ 9.41 (s, 1H), 8.51 (s, 1H), 8.19 (d, *J* = 7.7 Hz, 1H), 8.00 (d, *J* = 7.7 Hz, 1H), 7.71-7.62 (m, 3H), 7.37-7.35 (m, 3H), 7.13-7.05 (m, 3H), 3.81 (s, 3H). ¹³C-NMR (101 MHz, DMSO-*d*₆): δ 168.1, 156.7, 147.8, 138.5, 137.1, 130.7, 130.4, 130.3, 129.7, 129.7, 129.5, 129.2, 125.5, 123.4, 121.3, 120.9, 120.2, 112.3, 56.0. IR (KBr): $\tilde{\nu}$ = 3126, 2932, 1658, 1599, 1456, 1323, 1251, 763, 709 cm⁻¹. MS (ESI): *m/z* 372 [M+H]⁺. HRMS (ESI) *m/z* (M+H)⁺ calcd for C₂₂H₁₈N₃O₃ 372.1343, found 372.1346.

3-(4-(2',4'-Dimethoxy-[1,1'-biphenyl]-4-yl)-1H-1,2,3-triazol-1-yl)benzoic acid, (43).

Following the general procedure D, the reaction of **40** and (2,4-dimethoxyphenyl)boronic acid, after purification (EtOAc/MeOH 9:1 as eluent), yielded compound **43** as a yellow solid (114 mg, 0.28 mmol, 98%); mp: 259-260 °C.

¹H-NMR (300 MHz, DMSO-*d*₆): δ 9.41 (s, 1H), 8.47 (s, 1H), 8.13 (d, *J* = 7.4 Hz, 1H), 8.04 (d, *J* = 7.4 Hz, 1H), 7.96 (d, *J* = 7.1 Hz, 2H), 7.71 (d, *J* = 6.6 Hz, 1H), 7.55 (d, *J* = 7.1 Hz, 2H), 7.27 (t, *J* = 7.4 Hz, 1H), 6.67-6.61 (m, 2H), 3.80 (s, 3H), 3.78 (s, 3H). ¹³C-NMR (75 MHz; DMSO-*d*₆): δ 167.6, 160.8, 157.8, 147.9, 138.5, 137.2, 135.9, 131.4, 130.5, 130.2, 129.7, 128.1, 125.6, 123.5, 122.5, 120.8, 120.1, 106.0, 99.6, 56.2, 55.9. IR (KBr): $\tilde{\nu}$ = 3551, 3415, 3124, 2837, 1525, 1312, 1052, 834, 686 cm⁻¹. MS (ESI): *m/z* 402 [M+H]⁺. HRMS (ESI) *m/z* (M+H)⁺ calcd for C₂₃H₂₀N₃O₄ 402.1448, found 402.1440.

3-(4-(2',6'-Dimethoxy-[1,1'-biphenyl]-4-yl)-1*H*-1,2,3-triazol-1-yl)benzoic acid, (44).

Following the general procedure D, the reaction of **40** and (2,6-dimethoxyphenyl)boronic acid, after purification (EtOAc, EtOAc/MeOH 9:1 and EtOAc/MeOH 8:2 as eluents), yielded compound **44** as a pale yellow solid (53 mg, 0.13 mmol, 46%); mp: 215-217 °C dec. ¹H-NMR (300 MHz, DMSO-*d*₆): δ 9.40 (s, 1H), 8.55 (s, 1H), 8.15 (d, *J* = 7.4 Hz, 1H), 8.06 (d, *J* = 7.4 Hz, 1H), 7.96-7.92 (m, 3H), 7.72-7.70 (m, 4H), 7.29 (t, *J* = 7.4 Hz, 1H), 3.69 (s, 6H). ¹³C-NMR (100.1 MHz, DMSO-*d*₆): δ = 167.4, 157.6, 146.9, 137.0, 132.4, 131.9, 130.6, 130.0, 129.8, 129.4, 127.8, 125.9, 125.1, 123.7, 121.8, 120.8, 105.0, 56.2. IR (neat): $\tilde{\nu}$ = 3409, 2920, 2850, 1686, 1399, 1227, 1009, 816, 756, 502 cm⁻¹. MS (ESI): *m/z* 402 [M+H]⁺. HRMS (ESI) *m/z* (M+H)⁺ calcd for C₂₃H₂₀N₃O₄ 402.1448, found 402.1443.

3-(4-(3'-Methoxy-[1,1'-biphenyl]-4-yl)-1*H*-1,2,3-triazol-1-yl)benzoic acid, (45).

Following the general procedure D, the reaction of **40** and (3-methoxyphenyl)boronic acid, after purification (EtOAc/MeOH 9:1 as eluent), yielded compound **45** as a white solid (66 mg, 0.18 mmol, 61%); mp: 216-217 °C. ¹H-NMR (300 MHz, DMSO-*d*₆): δ 9.53 (s, 1H), 8.50 (s, 1H), 8.25 (d, *J* = 7.7 Hz, 1H), 8.07-8.05 (m, 3H), 7.84-7.75 (m, 3H), 7.40-7.27 (m, 3H), 6.96 (d, *J* = 7.7, 1H), 3.84 (s, 3H). ¹³C-NMR (101 MHz, DMSO-*d*₆): δ 166.9, 160.3, 147.7, 141.5, 140.3, 137.3, 133.3, 130.9, 130.5, 129.9, 129.7, 127.8, 126.3, 124.4, 120.8, 120.3, 119.4, 113.8, 112.5, 55.7. IR (KBr): $\tilde{\nu}$ = 3134, 2923, 1689, 1592, 1462, 1319, 1225, 758,

717 cm^{-1} . MS (ESI): m/z 372 $[\text{M}+\text{H}]^+$. HRMS (ESI) m/z $(\text{M}+\text{H})^+$ calcd for $\text{C}_{22}\text{H}_{18}\text{N}_3\text{O}_3$ 372.1343, found 372.1338.

3-(4-(3'-(Methylthio)-[1,1'-biphenyl]-4-yl)-1H-1,2,3-triazol-1-yl)benzoic acid, (46).

Following the general procedure D, the reaction of **40** and (3-(methylthio)phenyl)boronic acid, after purification (PE/EtOAc 5:5 as eluent), yielded compound **46** as a yellowish solid (111 mg, 0.29 mmol, 99%); mp: 225-226 $^{\circ}\text{C}$. $^1\text{H-NMR}$ (300 MHz, $\text{DMSO-}d_6$): δ 9.49 (s, 1H), 8.47 (s, 1H), 8.13-8.03 (m, 4H), 7.83 (d, $J = 8.3$ Hz, 2H), 7.70 (d, $J = 7.7$ Hz, 1H), 7.58 (s, 1H), 7.51 (d, $J = 7.1$ Hz, 1H), 7.43 (t, $J = 7.7$ Hz, 1H), 7.28 (d, $J = 7.7$ Hz, 1H), 2.56 (s, 3H). $^{13}\text{C-NMR}$ (101 MHz, $\text{DMSO-}d_6$): δ 168.2, 147.5, 140.8, 139.8, 139.5, 137.2, 137.0, 130.2, 130.1, 129.9, 129.7, 127.8, 126.4, 125.6, 124.3, 123.7, 123.0, 120.9, 120.3, 15.2. IR (KBr): $\tilde{\nu} = 3525, 3127, 2825, 1688, 1593, 1304, 1043, 818, 757, 696$ cm^{-1} . MS (ESI): m/z 386 $[\text{M}-\text{H}]^-$. HRMS (ESI) m/z $(\text{M}+\text{H})^+$ calcd for $\text{C}_{22}\text{H}_{18}\text{N}_3\text{O}_2\text{S}$ 388.1114, found 388.1107.

3-(4-(2',3'-Dimethoxy-[1,1'-biphenyl]-4-yl)-1H-1,2,3-triazol-1-yl)benzoic acid, (47).

Following the general procedure D, the reaction of **40** and (2,3-dimethoxyphenyl)boronic acid, after purification (EtOAc/MeOH 9:1 and EtOAc/MeOH 8:2 as eluents), yielded compound **47** as a white solid (88 mg, 0.22 mmol, 76%); mp: 189-190 $^{\circ}\text{C}$ dec. $^1\text{H-NMR}$ (400 MHz, $\text{DMSO-}d_6$): δ 9.45 (s, 1H), 8.53 (s, 1H), 8.12-8.04 (m, 4H), 7.70-7.60 (m, 3H), 7.14-6.97 (m, 3H), 3.85 (s, 3H), 3.57 (s, 3H). $^{13}\text{C-NMR}$ (101 MHz, $\text{DMSO-}d_6$): δ 168.3, 153.4, 147.7, 146.5, 138.2, 137.0, 136.8, 135.0, 130.3, 130.0, 129.7, 129.5, 125.7, 124.7, 123.1, 122.4, 120.9, 120.3, 113.0, 60.6, 56.3. IR (neat): $\tilde{\nu} = 3410, 2929, 2834, 1687, 1539, 1400, 1259, 1003, 757, 709, 583$ cm^{-1} . MS (ESI): m/z 402 $[\text{M}+\text{H}]^+$. HRMS (ESI) m/z $(\text{M}+\text{H})^+$ calcd for $\text{C}_{23}\text{H}_{20}\text{N}_3\text{O}_4$ 402.1448, found 402.1440.

3-(4-(4-(2,3-Dihydrobenzo[*b*][1,4]dioxin-5-yl)phenyl)-1H-1,2,3-triazol-1-yl)benzoic acid, (48).

Following the general procedure D, the reaction of **40** and (2,3-dihydrobenzo[*b*][1,4]dioxin-5-yl)boronic acid, after purification (EtOAc/MeOH 9:1 and EtOAc/MeOH 8:2 as eluents), yielded compound **48** as a pale yellow solid (105 mg, 0.26 mmol, 91%); mp: 186-188 °C dec. ¹H-NMR (300 MHz, DMSO-*d*₆): δ 9.42 (s, 1H), 8.49 (s, 1H), 8.11-7.99 (m, 4H), 7.70 (t, *J* = 7.2 Hz, 1H), 7.63 (d, *J* = 7.4 Hz, 2H), 6.93-6.90 (m, 3H), 4.29-4.26 (m, 4H). ¹³C-NMR (101 MHz, DMSO-*d*₆): δ 167.6, 147.8, 144.3, 141.1, 137.7, 137.1, 132.4, 130.5, 130.2, 130.1, 129.4, 127.8, 125.5, 123.7, 122.6, 121.4, 120.8, 120.3, 117.1, 64.6, 64.3. IR (neat): $\tilde{\nu}$ = 3408, 2921, 2873, 1687, 1466, 1400, 1238, 1042, 872, 778 cm⁻¹. MS (ESI): *m/z* 400 [M+H]⁺. HRMS (ESI) *m/z* (M+H)⁺ calcd for C₂₃H₁₈N₃O₄ 400.1292, found 400.1287.

3-(4-(3',5'-Dimethoxy-[1,1'-biphenyl]-4-yl)-1H-1,2,3-triazol-1-yl)benzoic acid, (49).

Following the general procedure D, the reaction of **40** and (3,5-dimethoxyphenyl)boronic acid, after purification (EtOAc/MeOH 9:1 as eluent), yielded compound **49** as a yellow solid (115 mg, 0.29 mmol, 99%); mp: 253-254 °C. ¹H-NMR (300 MHz, DMSO-*d*₆): δ 9.50 (s, 1H), 8.50 (s, 1H), 8.14 (d, *J* = 7.1 Hz, 1H), 8.06-8.04 (m, 3H), 7.82 (d, *J* = 8.2 Hz, 2H), 7.70 (t, *J* = 7.1 Hz, 1H), 6.94-6.87 (m, 2H), 6.52 (s, 1H), 3.82 (s, 3H), 3.78 (s, 3H). ¹³C-NMR (101 MHz; DMSO-*d*₆): δ 167.9, 161.4, 160.3, 147.6, 142.2, 140.2, 137.1, 130.4, 130.0, 129.7, 127.8, 126.3, 123.3, 120.8, 120.3 (2C), 111.9, 105.2, 100.1, 55.8, 55.4. IR (KBr): $\tilde{\nu}$ = 3140, 2838, 1503, 1353, 1204, 1154, 820, 690 cm⁻¹. MS (ESI): *m/z* 402 [M+H]⁺. HRMS (ESI) *m/z* (M+H)⁺ calcd for C₂₃H₂₀N₃O₄ 402.1448, found 402.1439.

3-(4-(3',4'-Dimethoxy-[1,1'-biphenyl]-4-yl)-1H-1,2,3-triazol-1-yl)benzoic acid, (50).

Following the general procedure D, the reaction of **40** and (3,4-dimethoxyphenyl)boronic acid, after purification (EtOAc/MeOH 9:1 and EtOAc/MeOH 8:2 as eluents), yielded compound **50** as a white solid (65 mg, 0.16 mmol, 56%); mp: 253-254 °C dec. ¹H-NMR (300 MHz, DMSO-*d*₆): δ 9.41 (s, 1H), 8.49 (s, 1H), 8.16 (d, *J* = 7.9 Hz, 1H), 8.08-8.02 (m, 3H), 7.79 (d, *J* = 8.0 Hz, 2H),

7.71 (t, $J = 7.9$ Hz, 1H), 7.30-7.27 (m, 2H), 7.06 (d, $J = 7.9$ Hz, 1H), 3.88 (s, 3H), 3.82 (s, 3H). ^{13}C -NMR (101 MHz, DMSO): δ 168.2, 149.6, 149.2, 147.7, 140.3, 137.0, 132.8, 132.4, 130.3, 129.1, 127.8, 127.3, 126.3, 123.2, 120.9, 120.1, 119.3, 112.7, 110.8, 56.2, 56.1. IR (neat): $\tilde{\nu} = 3408, 2927, 1686, 1519, 1399, 1248, 1139, 1011, 804, 757$ cm^{-1} . MS (ESI): m/z 402 $[\text{M}+\text{H}]^+$. HRMS (ESI) m/z $(\text{M}+\text{H})^+$ calcd for $\text{C}_{23}\text{H}_{20}\text{N}_3\text{O}_4$ 402.1448, found 402.1444.

3-(4-(4-(2,3-Dihydrobenzo[*b*][1,4]dioxin-6-yl)phenyl)-1*H*-1,2,3-triazol-1-yl)benzoic acid, (51).

Following the general procedure D, the reaction of **40** and (2,3-dihydrobenzo[*b*][1,4]dioxin-6-yl)boronic acid, after purification (EtOAc as eluent), yielded compound **51** as a pale yellow solid (115 mg, 0.29 mmol, 99%); mp: 192-193 °C. ^1H -NMR (300 MHz, DMSO- d_6): δ 9.49 (s, 1H), 8.49 (s, 1H), 8.22 (d, $J = 8.0$ Hz, 1H), 8.02 (d, $J = 8.5$ Hz, 2H), 7.79-7.77 (m, 3H), 7.27-7.22 (m, 3H), 6.95 (d, $J = 8.0$ Hz, 1H), 4.34-4.28 (m, 4H). ^{13}C -NMR (101 MHz; DMSO- d_6): δ 167.1, 147.7, 145.6, 144.2, 143.8, 143.2, 139.8, 137.2, 133.3, 130.7, 128.0, 127.2, 126.3, 123.3, 120.1, 119.9, 117.9, 116.6, 115.5, 64.7, 64.6. IR (KBr): $\tilde{\nu} = 2880, 2362, 1676, 1483, 1420, 1311, 1252, 800, 752$ cm^{-1} . MS (ESI): m/z 400 $[\text{M}+\text{H}]^+$. HRMS (ESI) m/z $(\text{M}+\text{H})^+$ calcd for $\text{C}_{23}\text{H}_{18}\text{N}_3\text{O}_4$ 400.1292, found 400.1286.

3-(4-(4-(Benzo[*d*][1,3]dioxol-5-yl)phenyl)-1*H*-1,2,3-triazol-1-yl)benzoic acid, (52).

Following the general procedure D, the reaction of **40** and benzo[*d*][1,3]dioxol-5-ylboronic acid, after purification (ether/ethyl acetate 1:9 as eluent) yielded compound **52** as a yellowish solid (65 mg, 0.17 mmol, 58%); mp: 270-271 °C. ^1H -NMR (300 MHz, DMSO- d_6): δ 9.48 (s, 1H), 8.49 (s, 1H), 8.22 (d, $J = 8.2$ Hz, 1H), 8.05-7.94 (m, 3H), 7.79-7.74 (m, 3H), 7.33 (s, 1H), 7.23 (t, $J = 8.2$ Hz, 1H), 7.02 (d, $J = 8.2$ Hz, 1H), 6.11 (s, 2H). ^{13}C -NMR (101 MHz; DMSO- d_6): δ 166.9, 148.5, 147.7, 147.5, 140.1, 137.3, 134.3, 132.5, 130.8, 129.7, 127.8, 127.4, 126.3, 124.3, 120.7, 120.2, 109.1, 107.4, 101.7, 79.8. IR (KBr): $\tilde{\nu} = 3109, 2900, 1736, 1480, 1399,$

1322, 1233, 932, 803 cm^{-1} . MS (ESI): m/z 386 $[\text{M}+\text{H}]^+$. HRMS (ESI) m/z $(\text{M}+\text{H})^+$ calcd for $\text{C}_{22}\text{H}_{16}\text{N}_3\text{O}_4$ 386.1135, found 386.1129.

3-(4-(2'-Fluoro-5'-methoxy-[1,1'-biphenyl]-4-yl)-1*H*-1,2,3-triazol-1-yl)benzoic acid, (53).

Following the general procedure D, the reaction of **40** and (2-fluoro-5-methoxyphenyl)boronic acid, after purification (PE/EtOAc 2:8 as eluent) yielded compound **53** as a yellow solid (46 mg, 0.12 mmol, 41%); mp: 149-150 °C dec. ^1H -NMR (400 MHz, $\text{DMSO}-d_6$): δ 9.52 (s, 1H), 8.51 (s, 1H), 8.25 (d, $J = 8.0$ Hz, 1H), 8.09-8.07 (m, 3H), 7.79 (t, $J = 7.9$ Hz, 1H), 7.72 (d, $J = 8.0$ Hz, 2H), 7.27 (t, $J = 9.2$ Hz, 1H), 7.14 (dd, $J_s = 6.4, 3.2$ Hz, 1H), 7.00-6.96 (m, 1H), 3.83 (s, 3H). ^{13}C -NMR (101 MHz; $\text{DMSO}-d_6$): δ 166.9, 156.2, 155.1, 152.7, 147.6, 137.2, 133.9 (d, $J = 300.0$ Hz), 130.9, 129.9, 129.8, 128.7 (d, $J = 14.6$ Hz), 127.8, 126.0, 124.4, 120.6, 120.5, 117.4 (d, $J = 24.8$ Hz), 115.5 (d, $J = 3.0$ Hz), 115.2 (d, $J = 8.5$ Hz), 56.2. IR (neat): $\tilde{\nu} = 2921, 2581, 2668, 1675, 1480, 1298, 1206, 1038, 807, 752, 674$ cm^{-1} . MS (ESI): m/z 390 $[\text{M}+\text{H}]^+$. HRMS (ESI) m/z $(\text{M}+\text{H})^+$ calcd for $\text{C}_{22}\text{H}_{17}\text{FN}_3\text{O}_3$ 390.1249, found 390.1240.

4-(2,3-Dihydrobenzo[*b*][1,4]dioxin-6-yl)aniline, (58).⁷

To a solution of 4-bromoaniline **3** (300 mg, 1.74 mmol) in ethanol (1.5 mL) and DMF (1.5 mL), (2,3-dihydrobenzo[*b*][1,4]dioxin-6-yl)boronic acid **57** (313 mg, 1.74 mmol), $\text{Pd}(\text{OAc})_2$ (11.7 mg, 0.017 mmol) and K_2CO_3 (481 mg, 3.48 mmol) were added in order. The mixture was heated at 80 °C for 6 h and then was left at rt overnight. The mixture was filtered over a pad of celite and rinsed with MeOH, then the volatile was removed. Purification by column chromatography (PE/EtOAc 8:2 as eluent) yielded compound **58** as a dark yellow oil (339 mg, 1.49 mmol, 86%); ^1H -NMR (300 MHz, CDCl_3): $\delta = 7.38$ (d, $J = 8.2$ Hz, 2H), 7.11 (s, 1H), 7.06 (d, $J = 8.5$ Hz, 1H), 6.94 (d, $J = 8.5$ Hz, 1H), 6.72 (d, $J = 8.2$ Hz, 2H), 4.28-4.27 (m, 4H). MS (ESI): m/z 228 $[\text{M}+\text{H}]^+$.

Methyl

3-((4-(2,3-dihydrobenzo[*b*][1,4]dioxin-6-yl)phenyl)carbamoyl)benzoate, (60).

To a solution of compound **58** (320 mg, 1.41 mmol) in dry CH₂Cl₂ (6.4 mL), 3-(methoxycarbonyl)benzoic acid **59** (254 mg, 1.41 mmol), EDCI (540 mg, 2.82 mmol), DIPEA (723 μL, 4.22 mmol) and DMAP (17 mg, 0.14 mmol), were added in order under nitrogen atmosphere. The reaction was stirred at rt overnight. Then, the mixture was diluted with CH₂Cl₂ and washed with HCl 3N (3x). The organic layer was dried over sodium sulfate and evaporated. Purification by column chromatography (PE/EtOAc 8:2 as eluent) yielded compound **60** as a pale yellow solid (424 mg, 1.09 mmol, 77%); ¹H-NMR (300 MHz, CDCl₃): δ = 8.49 (brs, 1H), 8.21 (d, *J* = 6.3 Hz, 1H), 8.14 (d, *J* = 6.3 Hz, 1H), 7.98 (s, 1H), 7.70 (d, *J* = 7.1 Hz, 2H), 7.62-7.50 (m, 3H), 7.09 (d, *J* = 7.1 Hz, 2H), 6.93 (d, *J* = 7.4 Hz, 1H), 4.29-4.28 (m, 4H), 3.96 (s, 3H). MS (ESI): *m/z* 390 [M+H]⁺.

3-((4-(2,3-Dihydrobenzo[*b*][1,4]dioxin-6-yl)phenyl)carbamoyl)benzoic acid, (61).

Compound **60** (250 mg, 0.64 mmol) was solubilized in THF (2.8 mL). Then, a solution of NaOH (26 mg, 0.64 mmol) in water (2.8 mL) was added and the mixture was heated at 60 °C for 3 h. Water was then added and HCl 3N was added until pH 4. The aqueous layer was extracted with EtOAc (3x) and the collected organic phases were dried over sodium sulfate and evaporated. Purification by column chromatography (EtOAc/MeOH 8:2 as eluent) yielded compound **61** as a white solid (195 mg, 0.52 mmol, 81%); mp: 227-228 °C dec. ¹H-NMR (300 MHz, DMSO-*d*₆): δ 10.44 (brs, 1H), 8.53 (s, 1H), 8.14-8.12 (m, 2H), 7.84 (d, *J* = 8.0 Hz, 2H), 7.64-7.58 (m, 3H), 7.15-7.13 (m, 2H), 6.92 (d, *J* = 8.2 Hz, 1H), 4.28-4.27 (m, 4H). ¹³C-NMR (101 MHz, DMSO-*d*₆): δ 168.8, 165.5, 144.1, 143.3, 138.6, 135.5, 135.4, 133.6, 132.7, 131.6, 129.0, 128.9, 126.8, 121.2, 119.6, 117.9, 115.2 (2C), 64.6 (2C). IR (neat): $\tilde{\nu}$ = 3282, 2922, 1686, 1647, 1495, 1299, 1245, 1072, 801, 695, 527 cm⁻¹. MS (ESI): *m/z* 376 [M+H]⁺. HRMS (ESI) *m/z* (M+H)⁺ calcd for C₂₂H₁₈NO₅ 376.1179, found 376.1173.

4-(2,3-Dihydrobenzo[*b*][1,4]dioxin-6-yl)benzoic acid, (63).

Methyl 4-iodobenzoate **62** (200 mg, 0.76 mmol) was solubilised in ethanol (1.7 mL) and DMF (1.7 mL) under nitrogen atmosphere. (2,3-Dihydrobenzo[*b*][1,4]dioxin-6-yl)boronic acid **57** (137 mg, 0.76 mmol), Pd(OAc)₂ (5.1 mg, 0.0076 mmol) and K₂CO₃ (211 mg, 1.53 mmol) were added in order. The mixture was heated at 80 °C for 6 h and then was left at rt overnight. The reaction was filtered over a pad of celite and rinsed with MeOH, then the volatile was removed, yielding a dark yellow solid. The crude product was used in the next step without further purification. The intermediate was solubilized in THF (2.4 mL) and a solution of NaOH (31 mg, 0.76 mmol) in water (2.4 mL) was added. The mixture was heated at 60 °C for 4 h, then HCl 3N was added until pH 4 and the aqueous layer was extracted with EtOAc (x2). The organic layers were dried over sodium sulfate and evaporated, yielding compound **63** as a white solid (166 mg, 0.65 mmol, 85%); ¹H-NMR (300 MHz, CD₃OD): δ = 8.02 (d, *J* = 7.1 Hz, 2H), 7.56 (d, *J* = 7.1 Hz, 2H), 7.10-7.07 (m, 2H), 6.89 (d, *J* = 8.2 Hz, 1H), 4.30-4.31 (m, 4H). MS (ESI): *m/z* 255 [M-H]⁻.

Methyl 3-(4-(2,3-dihydrobenzo[*b*][1,4]dioxin-6-yl)benzamido)benzoate, (65).

Compound **63** (165 mg, 0.64 mmol) was solubilized in dry CH₂Cl₂ (4 mL) and methyl 3-aminobenzoate **64** (97.3 mg, 0.64 mmol), EDCI (247 mg, 1.29 mmol), DIPEA (331 μL, 1.93 mmol) and DMAP (7.9 mg, 0.064 mmol) were added in order under nitrogen atmosphere. The mixture was stirred at rt overnight, then was diluted with CH₂Cl₂ and washed with HCl 3N (x5). The organic layer was dried over sodium sulfate and evaporated. Purification by column chromatography (PE/EtOAc 8:2 as eluent) yielded compound **65** as a pale yellow solid (157 mg, 0.40 mmol, 63%); ¹H-NMR (300 MHz, CDCl₃): δ = 8.16 (s, 1H), 8.07-8.01 (m, 2H), 7.91 (d, *J* = 6.9 Hz, 2H), 7.82 (d, *J* = 6.6 Hz, 1H), 7.63 (d, *J* = 6.9 Hz, 2H), 7.45 (t, *J* = 6.6 Hz, 1H), 7.13 (d, *J* = 7.7 Hz, 1H), 6.95 (d, *J* = 7.7 Hz, 1H), 4.30-4.29 (m, 4H), 3.91 (s, 3H). MS (ESI): *m/z* 390 [M+H]⁺.

3-(4-(2,3-Dihydrobenzo[*b*][1,4]dioxin-6-yl)benzamido)benzoic acid, (66).

Compound **65** (157 mg, 0.40 mmol) was solubilized in THF (1.7 mL) and a solution of NaOH (16.1 mg, 0.40 mmol) in water (1.7 mL) was added. The mixture was

heated at 60 °C for 4 h and then was left at rt overnight. HCl 3N was added until pH 4 and the aqueous layer was extracted with EtOAc (x2). The collected organic phases were dried over sodium sulfate and evaporated. Purification by column chromatography (EtOAc as eluent) yielded compound **66** as a white solid (91.5 mg, 0.24 mmol, 61%); mp: 234-235 °C dec. ¹H-NMR (300 MHz, DMSO-*d*₆): δ 10.39 (br s, 1H), 8.44 (s, 1H), 8.06-8.00 (m, 3H), 7.77 (d, *J* = 8.2 Hz, 2H), 7.69 (d, *J* = 7.4 Hz, 1H), 7.48 (t, *J* = 7.4 Hz, 1H), 7.25 (d, *J* = 8.2 Hz, 2H), 6.98 (d, *J* = 8.2 Hz, 1H), 4.30-4.29 (m, 4H). ¹³C-NMR (101 MHz, DMSO-*d*₆): δ 167.8, 165.8, 144.3, 144.2, 143.1, 139.9, 133.3, 132.7, 131.9, 129.3, 128.8, 126.5, 124.9, 124.8, 121.6, 120.3, 118.1, 115.9, 64.7, 64.6. IR (neat): $\tilde{\nu}$ = 3310, 2924, 1693, 1650, 1485, 1302, 1069, 811, 752, 677 cm⁻¹. MS (ESI): *m/z* 376 [M+H]⁺. HRMS (ESI) *m/z* (M+H)⁺ calcd for C₂₂H₁₈NO₅ 376.1179, found 376.1172.

3.3 References

1. a) Serafini, M.; Cordero-Sanchez, C.; Di Paola, R.; Bhela, I. P.; Aprile, S.; Purghè, B.; Fusco, R.; Cuzzocrea, S.; Genazzani, A. A.; Riva, B.; Piralì, T. Store-Operated Calcium Entry (SOCE) as a therapeutic target in acute pancreatitis: discovery and development of drug-like SOCE inhibitor. *J. Med. Chem.* **2020**, *63*, 14761-14779; b) Piralì, T.; Riva, B.; Serafini, M.; Aprile, S.; Cordero Sanchez, C. Biphenyl compounds as SOCE modulators, compositions and uses thereof. Filed on February 21, 2020, n. 10202000003692.
2. a) Ng, S. W.; di Capite, J.; Singaravelu, K.; Parekh, A. B. Sustained activation of the tyrosine kinase Syk by antigen in mast cells requires local Ca²⁺ influx through Ca²⁺ release-activated Ca²⁺ channels. *J. Biol. Chem.* **2008**, *283*, 31348-31355; b) Di Sabatino, A.; Rovedatti, L.; Kaur, R.; Spencer, J. P.; Brown, J. T.; Morisset, V. D.; Biancheri, P.; Leakey, N. A. B.; Wilde, J. I.; Scott, L.; Corazza, G. R.; Lee, K.; Sengupta, N.; Knowles, C. H.; Gunthorpe,

- M. J.; McLean, P. G.; MacDonald, T. T.; Kruidenier, L. Targeting gut T cell Ca^{2+} release activated Ca^{2+} channels inhibits T cell cytokine production and T-Box transcription factor T-Bet in inflammatory bowel disease. *J. Immunol.* **2009**, *183*, 3454-3462; c) Xie, Y.; Holmqvist, M.; Mahiou, J.; Ono, M.; Sun, L.; Chen, S.; Zhang, S.; Jiang, J.; Chimmanamada, D.; Fleig, A.; Yu, C.-Y. Method for Modulating Calcium Ion-Release-Activated Calcium Ion Channels. W.O. Patent 009,954, Feb 03, 2005; d) Xie, Y.; Holmqvist, M.; Mahiou, J.; Ono, M.; Sun, L.; Chen, S.; Zhang, S.; Jiang, J.; Chimmanamada, D.; Yu, C.-Y. Compounds for Inflammation and Immune-Related Uses. W.O. Patent 009,539, Feb 3, 2005.
3. Li, J.; McKeown, L.; Ojelabi, O.; Stacey, M.; Foster, R.; O'Regan, D.; Porter, K. E.; Beech, D. J. Nanomolar potency and selectivity of a Ca^{2+} release-activated Ca^{2+} channel inhibitor against store-operated Ca^{2+} entry and migration of vascular smooth muscle cells. *Br. J. Pharmacol.* **2011**, *164*, 382-393.
 4. a) Bonandi, E.; Christodoulou, M. S.; Fumagalli, G.; Perdicchia, D.; Rastelli, G.; Passarella, D. The 1,2,3-triazole ring as a bioisostere in medicinal chemistry. *Drug Discov. Today* **2017**, *22*, 1572-1581; b) Kumari, S.; Carmona, A. V.; Tiwari, A. K.; Trippier, P. C. Amide bond bioisosteres: strategies, synthesis, and successes. *J. Med. Chem.* **2020**, <https://doi.org/10.1021/acs.jmedchem.0c00530>.
 5. a) Tron, G. C.; Pirali, T.; Billington, R. A.; Canonico, P. L.; Sorba, G.; Genazzani, A. A. Click chemistry reactions in medicinal chemistry: applications of the 1,3-dipolar cycloaddition between azides and alkynes. *Med. Res. Rev.* **2008**, *28*, 278-308; b) Jiang, X.; Hao, X.; Jing, L.; Wu, G.; Kang, D.; Liu, X.; Zhan, P. Recent applications of click chemistry in drug discovery. *Expert Opin. Drug Discov.* **2019**, *14*, 779-789.
 6. a) Riva, B., Griglio, A.; Serafini, M.; Cordero-Sanchez, C.; Aprile, S.; Di Paola, R.; Gugliandolo, E.; Alansary, D.; Biocotino, I.; Lim, D.; Grosa, G.;

- Galli, U.; Niemeyer, B.; Sorba, G.; Canonico, P. L.; Cuzzocrea, S.; Genazzani, A. A.; Pirali, T. Pyrtriazoles, a novel class of store-operated calcium entry modulators: discovery, biological profiling, and *in vivo* proof-of-concept efficacy in acute pancreatitis. *J. Med. Chem.* **2018**, *61*, 9756-9783;
- b) Pirali, T.; Riva, B.; Genazzani, A. A. Modulators of SOCE, Compositions and use thereof. W.O. Patent 212,414, Dec 14, 2017.
7. Intermediate **58** has been previously reported in: Parrish, C. A.; Adams, N. D.; Auger, K. R.; Burgess, J. L.; Carson, J. D.; Chaudhari, A. M.; Copeland, R. A.; Diamond, M. A.; Donatelli, C. A.; Duffy, K. J.; Faucette, L. F.; Finer, J. T.; Huffman, W. F.; Hugger, E. D.; Jackson, J. R.; Knight, S. D.; Luo, L.; Moore, M. L.; Newlander, K. A.; Ridgers, L. H.; Sakowicz, R.; Shaw, A. N.; Sung, C.-M. M.; Sutton, D.; Wood, K. W.; Zhang, S.-Y.; Zimmerman, M. N.; Dhanak, D. Novel ATP-competitive kinesin spindle protein inhibitors. *J. Med. Chem.* **2007**, *50*, 4939-4952.
8. a) Pagliai, F.; Pirali, T.; Del Grosso, E.; Di Brisco, R.; Tron, G. C.; Sorba, G.; Genazzani, A. A. Rapid synthesis of triazole-modified resveratrol analogues via click chemistry. *J. Med. Chem.* **2006**, *49*, 467-470; b) Pirali, T.; Pagliai, F.; Mercurio, C.; Boggio, R.; Canonico, P. L.; Sorba, G.; Tron, G. C.; Genazzani, A. A. Triazole-modified histone deacetylase inhibitors as a rapid route to drug discovery. *J. Comb. Chem.* **2008**, *10*, 624-667.
9. a) Lolli, M. L.; Sainas, S.; Pippione, A. C.; Giorgis, M.; Boschi, D.; Dosio, F. Use of human dihydroorotate dehydrogenase (hDHODH) inhibitors in autoimmune diseases and new perspectives in cancer therapy. *Recent Pat. Anticancer Drug Discov.* **2018**, *13*, 86-105. b) Leban, J.; Saeb, W.; Garcia, G.; Baumgartner, R.; Kramer, B. Discovery of a novel series of DHODH inhibitors by a docking procedure and QSAR refinement. *Bioorg. Med. Chem. Lett.* **2004**, *14*, 55-58; c) Munier-Lehmann, H.; Vidalain, P.; Tangy, F.; Janin, Y. L. On dihydroorotate dehydrogenases and their inhibitors and uses. *J. Med. Chem.* **2013**, *56*, 3148-3167.

10. a) Davis, J. P.; Cain, G. A.; Pitts, W. J.; Magolda, R. L.; Copeland, R. A. The immunosuppressive metabolite of leflunomide is a potent inhibitor of human dihydroorotate dehydrogenase. *Biochemistry* **1996**, *35*, 1270-1273; b) Palmer, A. M. Teriflunomide, an inhibitor of dihydroorotate dehydrogenase for the potential oral treatment of multiple sclerosis. *Curr. Opin. Invest. Drugs* **2010**, *11*, 1313-1323.
11. Rahman, S.; Rahman, R. Unveiling some FDA-approved drugs as inhibitors of the store-operated Ca^{2+} entry pathway. *Sci. Rep.* **2017**, *7*, 12881-12893.
12. Peters, G. J.; Sharma, S. L.; Laurensse, E.; Pinedo, H. M. Inhibition of pyrimidine de novo synthesis by DUP-785 (NSC368390). *Invest. New Drugs* **1987**, *5*, 235-244.
13. Sainas, S.; Pippione, A. C.; Lupino, E.; Giorgis, M.; Circosta, P.; Gaidano, V.; Goyal, P.; Bonanni, D.; Rolando, B.; Cignetti, A.; Ducime, A.; Andersson, M.; Järvå, M.; Friemann, R.; Piccinini, M.; Ramondetti, C.; Buccinnà, B.; Al-Karadaghi, S.; Boschi, D.; Saglio, G.; Lolli, M. L. Targeting myeloid differentiation using potent 2-hydroxypyrazolo[1,5- a]pyridine scaffold-based human dihydroorotate dehydrogenase inhibitors. *J. Med. Chem.* **2018**, *61*, 6034-6055.
14. Stauderman, K. A. CRAC channels as targets for drug discovery and development. *Cell Calcium* **2018**, *74*, 147-159.

3.4 Author contributions

Article: Store-Operated Calcium Entry (SOCE) as a therapeutic target in acute pancreatitis: discovery and development of drug-like SOCE inhibitors. *J. Med. Chem.* **2020**, *63*, 14761-14779.

Author 1: Marta Serafini

Performed the synthesis of part the compounds, wrote the paper

Author 2: Celia Cordero-Sanchez

Performed the *in vitro* characterization of the compounds

Author 3: Rosanna Di Paola

Performed the *in vivo* experiments

Author 4: Irene P. Bhela

Performed the synthesis of part of the compounds

Author 5: Silvio Aprile

Performed the evaluation of the metabolism of the compounds

Author 6: Beatrice Purgè

Performed the evaluation of the metabolism of the compounds

Author 7: Roberta Fusco

Contributed data or analysis tools

Author 8: Salvatore Cuzzocrea

Supervision

Author 9: Armando A. Genazzani

Funding acquisition, supervision, designed the experiments

Author 10: Beatrice Riva

Wrote the paper, designed the experiments

Author 11: Tracey Pirali

Wrote the paper, designed the experiments

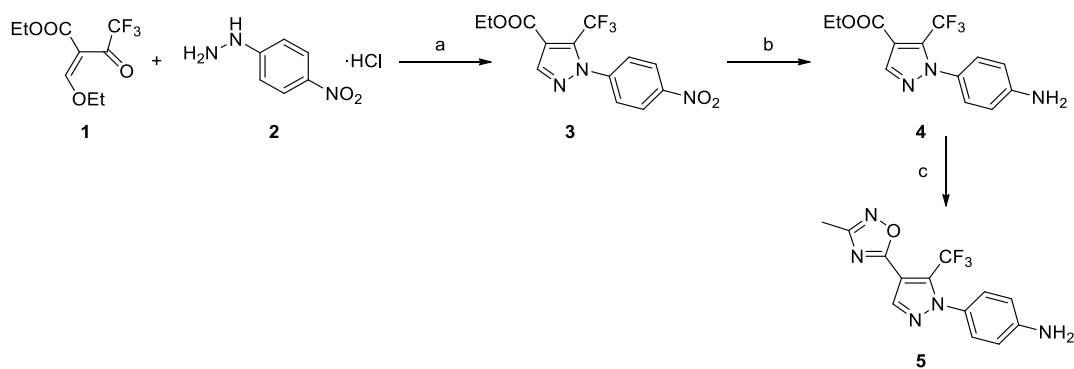
Chapter 4

1,2,4-Oxadiazole-bearing pyrazoles as metabolically stable inhibitors of Store- Operated Calcium Entry

4.1 The replacement of the ethyl ester of Pyr3 with a 1,2,4-oxadiazole ring afforded the 2nd class of modulators

The second class of SOCE modulators is represented by oxadiazole-bearing pyrazoles. Starting from the structure of Pyrs (Figure 2 in Chapter 2), we resorted to bioisosteric replacement with the aim to substitute the ethyl ester moiety displayed on the pyrazole ring of Pyr3 (Scheme 2) with a hydrolytically stable isostere, a 1,2,4-oxadiazole.¹ To this aim, amine **5** was prepared according to Scheme 1. The synthetic route consists of three steps: after a condensation between **1** and **2** and a reduction of the aromatic nitro group, intermediate **4**² was obtained. Then, the ethyl ester reacted with *N*-hydroxyacetamide to afford amine **5** with a yield of 76%.

Scheme 1. Preparation of amine **5**.



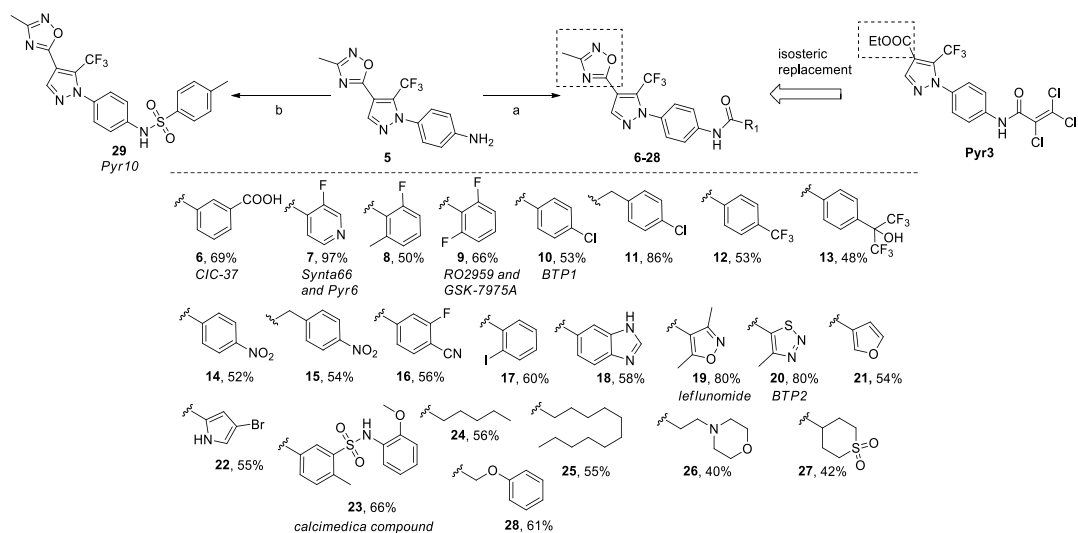
Reagents and conditions: (a) DMF, reflux, 2 h, 96%. (b) H₂, 5% Pd/C, EtOAc, rt, 2 h, 94%. (c) NaH 60%, *N*-hydroxyacetamide, dry THF, 0 °C to rt, 4 h, 76%.

The 2,3,3-trichloroacrylic substructure displayed by Pyr3, despite being involved in providing a certain selectivity over TRPC3 channel, suffers from poor drug-likeness. This substructure was therefore extensively varied in our structure-activity relationship (SAR) study. To this aim, eight coupling reactions were performed (**6-10**, **19-20** and **23**, Scheme 2) based on the prototype substructures displayed by reported SOCE inhibitors, including BTP1, BTP2, Pyr10, GSK-7975A, Synta66,

CM4620, leflunomide and CIC-37. Compound **29**, whose substructure mimics Pyr10, was synthesized according to Scheme 2, from amine **5** and tosyl chloride (TsCl). The structure of SOCE inhibitors from the literature are reported in Figure 2 of Chapter 2.

Moreover, 15 additional coupling reactions were performed (**11-18**, **21-22**, **24-28**, Scheme 2) exploiting different carboxylic acids and further expanding the SAR study.

Scheme 2. Preparation of oxadiazole-bearing pyrazoles **6-29**.



Reagents and conditions: (a) PyBOP, DIPEA, dry CH₂Cl₂, rt, 16-42 h, 40-97%; (in case of compound **6**, see the experimental section); (b) TsCl, pyridine, dry CH₂Cl₂, 0 °C to rt, 5 h, 45%.

With this approach, 24 oxadiazole-bearing pyrazoles were synthesized and tested in (HEK cells for SOCE inhibition. For this, intracellular Ca²⁺ stores of HEK cells were emptied with *t*BhQ (50 μM) in the presence of the compounds at 10 μM concentration. After 600 seconds, Ca²⁺ was added and intracellular levels were measured in fluorescence microscopy with the calcium dye Fura-2. As shown in Table 1, 8 compounds out of 24 were able to reduce calcium entry by more than 50%

compared to control. In particular, the substructures that provided the highest inhibitory activity were those derived from GSK-7975A (**9**, % of SOCE residual activity: $38.6 \pm 4.3\%$), BTP1 (**10**, $40.8 \pm 3.6\%$), leflunomide (**19**, $33.2 \pm 1.9\%$), Pyr2 (**20**, $46.5 \pm 2.8\%$) and Pyr10 (**29**, $47.6 \pm 4.2\%$). Also, compounds **14** ($40.8 \pm 6.9\%$) and **16** ($49.6 \pm 6.5\%$), displaying an electron-withdrawing group in *para* position on the aromatic ring, or **18** ($47.4 \pm 1.0\%$) in which the aromatic ring is fused with an imidazole, afforded a good inhibitory activity. For these compounds, the cell viability was therefore evaluated. To this aim, an MTT assay was performed and the compounds that affected cell viability for more than 25% at 10 μM were discarded (**10**, **18**, **20**). Notably, the remaining 5 compounds (**9**, **14**, **16**, **19**, **29**) were not cytotoxic under these conditions, in contrast to the reference compound, Pyr3, that provided a cell viability of $28.6 \pm 0.5\%$. According to both activity and cytotoxicity, for the selected 5 compounds the IC_{50} values were calculated and are reported in Table 1. The most potent molecule was **9**, with an IC_{50} value of $3.1 \pm 1.4 \mu\text{M}$.

Surprisingly, compound **24** in which the side chain is represented by a linear aliphatic substructure, afforded an increase in calcium entry, with a percentage of SOCE activity of $146.2 \pm 4.5\%$ compared to the control. More in detail, the compound, tested at the concentration of 10 μM , significantly increased the AUC of calcium entry and the peak amplitude, without affecting the slope. We also investigated whether **24** required the triggered opening of the Orai channel to elicit its effect. To do this, we monitored intracellular Ca^{2+} in resting cells in the presence of extracellular Ca^{2+} and we observed that the compound did not elicit any significant calcium entry at 10 μM compared to control in the 300 seconds of observation, suggesting that **24** is a potentiator/enhancer of SOCE. The same effect was also evident at 3 ($118.2 \pm 5.7\%$) and 1 μM ($116.7 \pm 7.1\%$) but was not detected at concentrations above 10. In particular, at 30 and 100 μM , **24** acts as weak SOCE inhibitor, with a percentage of residual activity of about 70%.

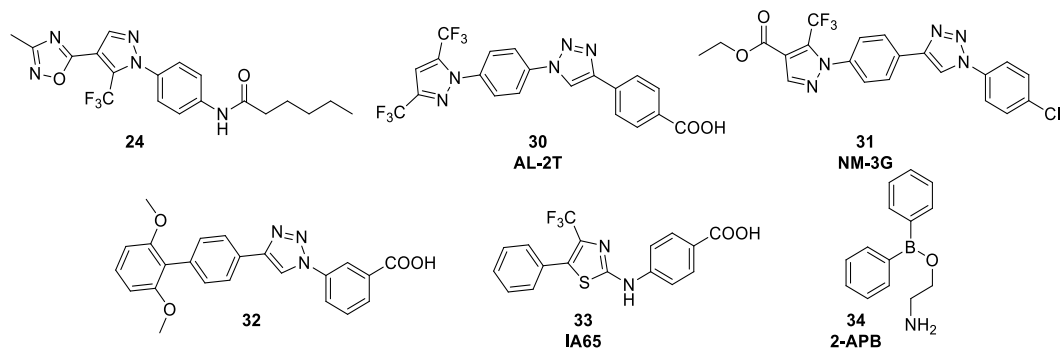
The identification of a SOCE enhancer among a class of inhibitors has been reported in three previously classes of modulators, two of them described by us and

represented by pyrtriazoles (AL-2T (**30**), NM-3G (**31**), Figure 1)² and biphenyl triazoles (compound **32** in Figure 1, also known as compound **44** in Chapter 3),³ and one reported in the literature (IA65 (**33**), Figure 1).⁴

A similar behaviour is also shared by 2-APB (**34**), a well-known inhibitor of IP3 receptors and TRP channels. The compound is a SOCE modifier in Orai1- and Orai3-expressing cells, acting as SOCE enhancer at low concentrations, while high concentrations induce a transient increase followed by complete inhibition.⁵

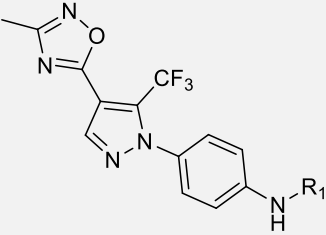
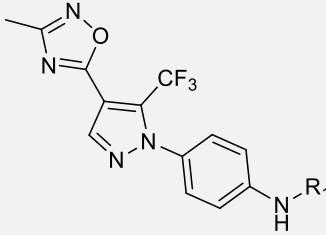
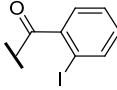
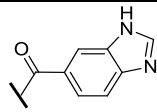
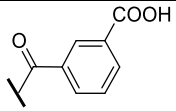
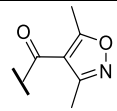
While the 6 enhancers are not structurally related each other, when synthesizing SOCE modulators it often occurs that a minimal structural modification in a class of compounds is able to turn a SOCE inhibitor into a molecule able to increase calcium entry. Despite no crystallographic data are available, the presence of 5 different activators with structural diversity now paves the way to the rational design of positive modulators as either biological tools or active drugs. It should be noted that the binding partner of SOCE inhibitors has not been conclusively ascertained, but the presence of activators strongly suggest that it is the Orai channel. The interaction of SOCE modulators with the ion channel is also supported by a recently published article in which, through computational approaches, a docking pose of Synta66 in the Orai channel has been proposed.⁶ Moreover, azopyrazole-derived CRAC channel inhibitors have been recently reported as the first photoswitchable SOCE modulators able to induce the activation of Orai using light, further supporting the hypothesis that these compounds interact directly with the ion channel.⁷

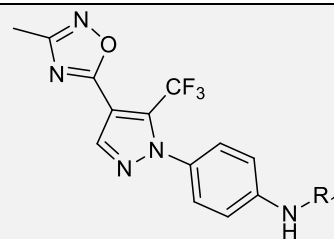
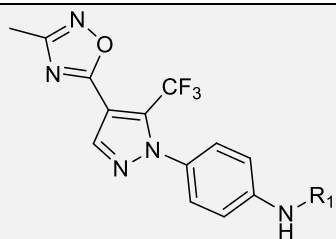
Figure 1. Structures of positive modulators of SOCE reported in the literature.



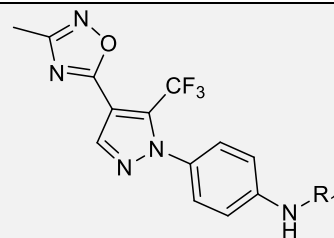
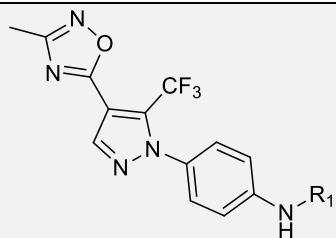
The 5 selected inhibitors (**9**, **14**, **16**, **19**, **29**) and the identified SOCE enhancer (**24**) were then evaluated for their *in vitro* hepatic metabolic stability. To this aim, the candidates were incubated in mouse liver S9 fractions (MLS9) and the residual substrate was measured after one hour. In contrast to Pyr3, which suffered from hydrolysis of the ethyl ester function, being the residual substrate in the same condition equal to 43%,² the oxadiazole-bearing pyrazoles resulted overall more metabolically stable, with only two compounds affording a residual substrate lower than 80% and the remaining molecules higher than 90% after incubation (Table 1). Overall, these results make our class of oxadiazole-bearing pyrazoles more metabolically stable and less cytotoxic compare to the reference compound Pyr3. While the isosteric replacement of the ethyl ester moiety with a 1,2,4-oxadiazole ring provides a certain reduction of potency (IC_{50} value of $0.5 \pm 0.1 \mu\text{M}$ for Pyr3 vs $3.1 \pm 1.4 \mu\text{M}$ for **9**), the most potent analogue **9** retains a good percentage of inhibition, with a residual SOCE activity of $38.6 \pm 4.3\%$, is not cytotoxic, in contrast to Pyr3 that affects cell viability for 72%, and is significantly more stable *in vitro*. Last, in our SAR study, another SOCE enhancer has been identified, adding this compound to the previously reported positive modulators and paving the way for their rational design.

Table 1. Oxadiazole-bearing pyrazoles and their activity on SOCE, IC₅₀ values and cytotoxicity in Hek cells. Residual substrates are determined in MLS9 after 30 minutes incubation.

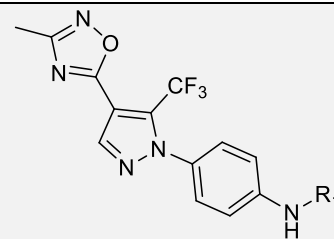
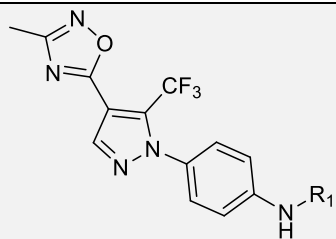
											
Cpd, Yield (%)	R ₁	% SOCE residual activity (10 μM)	% Viability (10 μM)	IC ₅₀ (μM)	MLS9 stability (residual substrate)	Cpd, Yield (%)	R ₁	% SOCE residual activity (10 μM)	% Viability (10 μM)	IC ₅₀ (μM)	MLS9 stability (residual substrate)
Pyr3	-	8.9 ± 0.6	28.6 ± 0.5	0.5 ± 0.1	43%	17 , 60%		53.2 ± 3.9	-	-	-
CIC-37	-	17.5 ± 1.6	93.6 ± 4.6	4.4 ± 1.2	74%	18 , 58%		47.4 ± 1.0	56.5 ± 2.5	-	-
6 , 98%		77.2 ± 3.7	-	-	-	19 , 80%		33.2 ± 1.9	77.7 ± 4.4	9.6 ± 2.5	99%



Cpd, Yield (%)	R ₁	% SOCE residual activity (10 μM)	% Viability (10 μM)	IC ₅₀ (μM)	MLS9 stability (residual substrate)	Cpd, Yield (%)	R ₁	% SOCE residual activity (10 μM)	% Viability (10 μM)	IC ₅₀ (μM)	MLS9 stability (residual substrate)
7 , 97%		53.6 ± 0.9	-	-	-	20 , 80%		46.5 ± 2.8	59.1 ± 6.3	-	-
8 , 50%		56.7 ± 1.3	-	-	-	21 , 54%		61.1 ± 3.9	-	-	-
9 , 66%		38.6 ± 4.3	95.6 ± 8.5	3.1 ± 1.4	>99%	22 , 55%		69.8 ± 2.9	-	-	-
10 , 53%		40.8 ± 3.6	72.9 ± 11.7	-	-	23 , 66%		59.9 ± 4.2	-	-	-



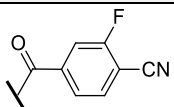
Cpd, Yield (%)	R ₁	% SOCE residual activity (10 μM)	% Viability (10 μM)	IC ₅₀ (μM)	MLS9 stability (residual substrate)	Cpd, Yield (%)	R ₁	% SOCE residual activity (10 μM)	% Viability (10 μM)	IC ₅₀ (μM)	MLS9 stability (residual substrate)
11 , 86%		121.1 ± 2.2	-	-	-	24 , 56%		146.2 ± 4.5	88.5 ± 2.9	-	91%
12 , 53%		110.0 ± 5.9	-	-	-	25 , 55%		53.8 ± 4.4	-	-	-
13 , 48%		109.0 ± 6.5	-	-	-	26 , 40%		95.9 ± 6.2	-	-	-
14 , 52%		40.8 ± 6.9	80.2 ± 7.4	5.5 ± 0.8	>99%	27 , 42%		87.5 ± 3.8	-	-	-
15 , 54%		107.9 ± 3.9	-	-	-	28 , 61%		63.6 ± 3.9	-	-	-



Cpd, Yield (%)	R ₁	% SOCE residual activity (10 μM)	% Viability (10 μM)	IC ₅₀ (μM)	MLS9 stability (residual substrate)
-------------------	----------------	---	---------------------------	--------------------------	--

Cpd, Yield (%)	R ₁	% SOCE residual activity (10 μM)	% Viability (10 μM)	IC ₅₀ (μM)	MLS9 stability (residual substrate)
-------------------	----------------	---	---------------------------	--------------------------	--

16, 56%



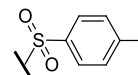
49.6 ± 6.5

100.8 ± 6.7

9.7 ± 2.3

73%

29, 45%



47.6 ± 4.2

79.4 ± 4.2

9.5 ± 1.7

76%

4.2 Experimental part

General Experimental Methods. Commercially available reagents and solvents were used as purchased without further purification. When needed, solvents were distilled and stored on molecular sieves. Column chromatography was performed on silica gel. Thin layer chromatography (TLC) was carried out on 5 cm × 20 cm plates with a layer thickness of 0.25 mm. When necessary, TLC plates were visualized with aqueous KMnO₄ or with aqueous acidic solution of cerium sulfate and ammonium molybdate. Melting points were determined in open glass capillary with a Stuart scientific SMP3 apparatus. All the target compounds were checked by IR (FT-IR Bruker Alpha II), ¹H-NMR (Bruker Avance Neo 400 MHz; Jeol ECP 300 MHz), ¹³C-NMR (Bruker Avance Neo 400 MHz), and mass spectrometry (Thermo Scientific Q-Exactive Plus) equipped with an HESI source. Chemical shifts are reported in parts per million (ppm). Carboxylic acids are commercially available, with the only exception of 3-(*N*-(2-methoxyphenyl)sulfamoyl)-4-methylbenzoic acid that was synthesized as reported below.

4-(4-(3-Methyl-1,2,4-oxadiazol-5-yl)-5-(trifluoromethyl)-1*H*-pyrazol-1-yl)aniline, (5).

A suspension of NaH (361 mg, 60% in mineral oil, 9.03 mmol) was added portionwise to a round bottom flask containing dry THF (120 mL) and *N*-hydroxyacetamide (669 mg, 9.03 mmol) was added at 0 °C and under nitrogen. The mixture was left to reach rt and heated at 50 °C for 1 h. Then, ethyl 1-(4-aminophenyl)-5-(trifluoromethyl)-1*H*-pyrazole-4-carboxylate (2.70 g, 9.03 mmol) was added and the reaction was heated at 50 °C for 3 h, diluted with EtOAc and washed with water (2x). The organic layer was dried over sodium sulfate and evaporated, yielded compound **5** as a yellow solid (2.12 g, 6.86 mmol, 76%). ¹H-NMR (400 MHz; CDCl₃): δ 8.19 (s, 1H), 7.18 (d, *J* = 8.6 Hz, 2H), 6.66 (d, *J* = 8.6 Hz, 2H), 4.07 (br s, 2H), 2.43 (s, 3H). MS (ESI): *m/z* 310 [M+H]⁺.

General procedure for the synthesis of compounds 6-29.

4-(4-(3-Methyl-1,2,4-oxadiazol-5-yl)-5-(trifluoromethyl)-1*H*-pyrazol-1-yl)aniline **5** (100 mg, 0.32 mmol) was solubilized in dry CH₂Cl₂ (2.5 mL) and DIPEA (109 μL 0.64 mmol), PyBOP (166 mg, 0.32 mmol) and the carboxylic acid (0.35 mmol, 1.1 eq) were added in order and under nitrogen. With the only exceptions of compounds **11**, **15** and **28**, after 16 h, an addition of DIPEA (0.6 eq), PyBOP (0.6 eq) and the carboxylic acid (0.3 eq) was usually necessary. The mixture was then stirred for additional 16 h and a second addition of DIPEA (0.3 eq), PyBOP (0.3 eq) and the carboxylic acid (0.3 eq) was done. After stirring for additional 16 h, the reaction was worked-up. The mixture was diluted with CH₂Cl₂ and washed with water (2x). The organic layer was dried over sodium sulfate and evaporated. The crude product was purified by column chromatography.

3-((4-(4-(3-Methyl-1,2,4-oxadiazol-5-yl)-5-(trifluoromethyl)-1*H*-pyrazol-1-yl)phenyl)carbamoyl)benzoic acid, (6).

Methyl 3-((4-(4-(3-methyl-1,2,4-oxadiazol-5-yl)-5-(trifluoromethyl)-1*H*-pyrazol-1-yl)phenyl)carbamoyl)benzoate was prepared following the general procedure starting from amine **5** (100 mg, 0.32 mmol) and 3-(methoxycarbonyl)benzoic acid (63 mg, 0.35 mmol). Purification by column chromatography using PE/EtOAc 6:4 afforded the desired compound as a white solid (104 mg, 0.22 mmol, 69%). The intermediate was then solubilized in THF (2 mL) and water (2 mL) and NaOH (17.6 mg, 0.44 mmol) were added. After 5 h, the mixture was diluted with water and HCl 3N was added until pH 4. The aqueous layer was extracted with EtOAc (2x). The collected organic layers were dried over sodium sulfate and evaporated. The crude material was purified by column chromatography using PE/EtOAc 3:7 as eluent affording compound **6** (99 mg, 0.22 mmol, 98%) as an amorphous white solid. ¹H-NMR (400 MHz; CD₃OD): δ 8.65 (s, 1H), 8.38 (s, 1H), 8.26 (d, *J* = 7.8 Hz, 1H), 8.21 (d, *J* = 7.8 Hz, 1H), 8.02 (d, *J* = 8.8 Hz, 2H), 7.67 (t, *J* = 7.8 Hz, 1H), 7.56 (d, *J* = 8.8 Hz, 2H), 2.48 (s, 3H). ¹³C-NMR (101 MHz; CD₃OD): δ 168.7, 167.8, 167.5, 166.7, 141.0, 140.6, 135.1, 134.6, 132.6, 131.6, 131.2 (q, *J* = 45.4 Hz), 128.6, 128.6, 126.7, 126.4, 120.8, 119.2 (q, *J* = 271.6 Hz), 108.9, 9.9. IR (neat): $\tilde{\nu}$ = 3270, 2922,

2853, 1700, 1650, 1519, 1298, 1141, 947, 808 cm^{-1} . HRMS (ESI) m/z (M+H)⁺ calcd for $\text{C}_{21}\text{H}_{15}\text{F}_3\text{N}_5\text{O}_4$ 458.1071, found 458.1071.

Characterization of compounds 7-28.

3-Fluoro-*N*-(4-(4-(3-methyl-1,2,4-oxadiazol-5-yl)-5-(trifluoromethyl)-1*H*-pyrazol-1-yl)phenyl)isonicotinamide, (7).

White solid (134 mg, 0.31 mmol, 97%); Chromatography: PE/EtOAc 5:5; mp: 185-186 °C, dec. ¹H-NMR (400 MHz; $(\text{CD}_3)_2\text{CO}$): δ 8.70-8.63 (m, 2H), 8.39 (s, 1H), 8.08 (d, $J = 7.7$ Hz, 2H), 7.81 (s, 1H), 7.67 (d, $J = 7.7$ Hz, 2H), 7.43 (br s, 1H), 2.46 (s, 3H). ¹³C-NMR (101 MHz; $(\text{CD}_3)_2\text{CO}$): δ 168.6, 167.9, 161.0, 155.7 (d, $J = 253.3$ Hz), 146.4 (d, $J = 5.2$ Hz), 141.1, 140.2, 139.1 (d, $J = 24.7$ Hz), 138.4 (d, $J = 23.5$ Hz), 135.0, 130.6 (q, $J = 32.4$ Hz), 126.9, 123.4, 120.3, 119.3 (q, $J = 271.9$ Hz), 109.2, 10.6. IR (neat): $\tilde{\nu} = 3487, 2922, 2852, 1630, 1516, 1422, 1296, 1146, 844, 508$ cm^{-1} . HRMS (ESI) m/z (M+H)⁺ calcd for $\text{C}_{19}\text{H}_{13}\text{F}_4\text{N}_6\text{O}_2$ 433.1031, found 433.1027.

2-Fluoro-6-methyl-*N*-(4-(4-(3-methyl-1,2,4-oxadiazol-5-yl)-5-(trifluoromethyl)-1*H*-pyrazol-1-yl)phenyl)benzamide, (8).

White solid (71 mg, 0.16 mmol, 50%); Chromatography: PE/EtOAc 9:1; mp: 218-219 °C ¹H-NMR (400 MHz; CDCl_3): δ 8.26 (s, 1H), 7.84 (d, $J = 8.4$ Hz, 2H), 7.50 (d, $J = 8.4$ Hz, 2H), 7.37-7.32 (m, 1H), 7.10 (d, $J = 7.6$ Hz, 1H), 7.04-6.99 (m, 1H), 2.50-2.48 (m, 6H). ¹³C-NMR (101 MHz; CDCl_3): δ 168.6, 167.8, 163.4, 159.3 (d, $J = 247.0$ Hz), 141.3, 139.3, 139.2 (d, $J = 2.3$ Hz), 134.9, 131.4 (q, $J = 40.7$ Hz), 131.3 (d, $J = 9.0$ Hz), 126.7, 126.6, 124.1 (d, $J = 16.7$ Hz), 120.1, 118.9 (q, $J = 272.8$ Hz), 113.3 (d, $J = 22.2$ Hz), 109.3, 19.5, 11.6. IR (neat): $\tilde{\nu} = 3246, 2918, 2850, 1656, 1512, 1298, 1136, 944, 792, 588$ cm^{-1} . HRMS (ESI) m/z (M+H)⁺ calcd for $\text{C}_{21}\text{H}_{16}\text{F}_4\text{N}_5\text{O}_2$ 446.1235, found 446.1231.

2,6-Difluoro-*N*-(4-(4-(3-methyl-1,2,4-oxadiazol-5-yl)-5-(trifluoromethyl)-1*H*-pyrazol-1-yl)phenyl)benzamide, (9).

White solid (95 mg, 0.21 mmol, 66%); Chromatography: PE/EtOAc 7:3; mp: 180-181 °C. ¹H-NMR 400 MHz; CDCl_3): δ 8.25 (s, 1H), 8.16 (br s, 1H), 7.83 (d, $J = 7.4$ Hz, 2H), 7.48-7.42 (m, 3H), 7.01-6.99 (m, 2H), 2.51 (s, 3H). ¹³C-NMR (101 MHz;

CDCl₃): δ 168.6, 167.8, 160.0 (dd, $J_s = 254.4, 6.5$ Hz), 158.6, 141.3, 139.1, 135.1, 132.5 (t, $J = 10.4$ Hz), 131.4 (q, $J = 41.2$ Hz), 126.7, 120.4, 119.4 (q, $J = 272.3$ Hz), 113.9 (t, $J = 18.9$ Hz), 112.3 (d, $J = 25.5$ Hz), 109.3, 11.6. IR (neat): $\tilde{\nu} = 3282, 2922, 2852, 1656, 1513, 1467, 1145, 1007, 794, 658$ cm⁻¹. HRMS (ESI) m/z (M+H)⁺ calcd for C₂₀H₁₃F₅N₅O₂ 450.0984, found 450.0981.

4-Chloro-*N*-(4-(4-(3-methyl-1,2,4-oxadiazol-5-yl)-5-(trifluoromethyl)-1*H*-pyrazol-1-yl)phenyl)benzamide, (10).

White solid (76 mg, 0.17 mmol, 53%); Chromatography: PE/EtOAc 7:3; mp: 208-209 °C, dec. ¹H-NMR (400 MHz; CDCl₃): δ 8.28 (s, 1H), 8.07 (br s, 1H), 7.87-7.84 (m, 4H), 7.52-7.50 (m, 4H), 2.52 (s, 3H). ¹³C-NMR (101 MHz; CDCl₃): δ 168.5, 167.9, 164.9, 141.3, 139.5, 138.9, 134.8, 132.8, 131.4 (q, $J = 40.4$ Hz), 129.2, 128.5, 126.7, 120.4, 119.0 (q, $J = 273.7$ Hz), 109.3, 11.6. IR (neat): $\tilde{\nu} = 3273, 2923, 2852, 1650, 1518, 1300, 1130, 840, 756, 535$ cm⁻¹. HRMS (ESI) m/z (M+H)⁺ calcd for C₂₀H₁₄ClF₃N₅O₂ 448.0783, found 448.0782.

2-(4-Chlorophenyl)-*N*-(4-(4-(3-methyl-1,2,4-oxadiazol-5-yl)-5-(trifluoromethyl)-1*H*-pyrazol-1-yl)phenyl)acetamide, (11).

White solid (127 mg, 0.28 mmol, 86%); Chromatography: PE/EtOAc 6:4; mp: 169-171 °C, dec. ¹H-NMR (400 MHz; (CD₃)₂CO): δ 9.73 (br s, 1H), 8.38 (s, 1H), 7.91 (d, $J = 8.0$ Hz, 2H), 7.56 (d, $J = 8.0$ Hz, 2H), 7.44 (d, $J = 8.0$ Hz, 2H), 7.38 (d, $J = 8.0$ Hz, 2H), 3.80 (s, 2H), 2.45 (s, 3H). ¹³C-NMR (101 MHz; (CD₃)₂CO): δ 169.0, 168.6, 167.8, 141.0, 134.5, 134.1, 132.2, 131.0, 130.8 (q, $J = 43.8$ Hz), 128.3, 126.7, 124.4, 119.4, 119.3 (q, $J = 271.8$ Hz), 109.4, 42.8, 10.6. IR (neat): $\tilde{\nu} = 3254, 2922, 2852, 1664, 1651, 1625, 1601, 1519, 977, 606$ cm⁻¹. HRMS (ESI) m/z (M+H)⁺ calcd for C₂₁H₁₆ClF₃N₅O₂ 462.0939, found 462.0935.

***N*-(4-(4-(3-Methyl-1,2,4-oxadiazol-5-yl)-5-(trifluoromethyl)-1*H*-pyrazol-1-yl)phenyl)-4-(trifluoromethyl)benzamide, (12).**

White solid (81 mg, 0.17 mmol, 53%); Chromatography: PE/EtOAc 8:2; mp: 190-192 °C, dec. ¹H-NMR (400 MHz; CDCl₃, *: referred to the main rotamer): δ 8.26 (s, 1H), 8.05-8.03 (m, 3H)*, 7.89 (d, $J = 8.7$ Hz, 2H), 7.81 (d, $J = 8.2$ Hz, 2H)*, 7.54

(d, $J = 8.7$ Hz, 2H), 2.52 (s, 3H). ^{13}C -NMR (101 MHz; $(\text{CD}_3)_2\text{CO}$): δ 168.6, 167.5, 164.7, 141.1, 140.8, 134.6, 133.6 (q, $J = 32.3$ Hz), 132.6 (q, $J = 32.5$ Hz), 130.3, 128.4, 126.7, 125.5, 121.7 (q, $J = 202.9$ Hz), 120.4, 119.6 (q, $J = 271.6$ Hz), 109.2, 10.6. IR (neat): $\tilde{\nu} = 3248, 3098, 1655, 1628, 1518, 1287, 1139, 1104, 978, 699$ cm^{-1} . HRMS (ESI) m/z ($\text{M}+\text{H}$) $^+$ calcd for $\text{C}_{21}\text{H}_{14}\text{F}_6\text{N}_5\text{O}_2$ 482.1046, found 482.1047.

4-(1,1,1,3,3,3-Hexafluoro-2-hydroxypropan-2-yl)-*N*-(4-(4-(3-methyl-1,2,4-oxadiazol-5-yl)-5-(trifluoromethyl)-1*H*-pyrazol-1-yl)phenyl)benzamide, (13).

White solid (89 mg, 0.15 mmol, 48%); Chromatography: PE/EtOAc 8:2; mp: 180-182 °C, ^1H -NMR (400 MHz; CDCl_3 , *: referred to the main rotamer): δ 8.29 (s, 1H), 8.01-7.99 (m, 3H), 7.92 (d, $J = 8.2$ Hz, 2H), 7.87 (d, $J = 8.5$ Hz, 2H), 7.54 (d, $J = 8.5$ Hz, 2H), 2.52 (s, 3H). ^{13}C -NMR (101 MHz; $(\text{CD}_3)_2\text{CO}$, *: referred to the main rotamer): δ 168.6, 167.9, 165.2, 141.0, 136.9, 134.5, 130.8 (q, $J = 40.2$ Hz), 129.7, 127.8, 127.2, 126.7, 123.5 (q, $J = 37.7$ Hz), 123.0 (q, $J = 288.5$ Hz), 120.3, 120.2, 119.3 (q, $J = 271.9$ Hz), 109.2, 10.5. IR (neat): $\tilde{\nu} = 3302, 1666, 1630, 1324, 1151, 1114, 975, 933, 718$ cm^{-1} . HRMS (ESI) m/z ($\text{M}+\text{H}$) $^+$ calcd for $\text{C}_{23}\text{H}_{15}\text{F}_9\text{N}_5\text{O}_3$ 580.1026, found 580.1024.

***N*-(4-(4-(3-Methyl-1,2,4-oxadiazol-5-yl)-5-(trifluoromethyl)-1*H*-pyrazol-1-yl)phenyl)-4-nitrobenzamide, (14).**

White solid (76 mg, 0.17 mmol, 52%); Chromatography: PE/EtOAc 7:3; mp: 153-155 °C, dec. ^1H -NMR (400 MHz; CDCl_3): δ 8.40 (d, $J = 8.5$ Hz, 2H), 8.29 (s, 1H), 8.10 (d, $J = 8.5$ Hz, 2H), 8.07 (br s, 1H), 7.88 (d, $J = 8.7$ Hz, 2H), 7.55 (d, $J = 8.7$ Hz, 2H), 2.52 (s, 3H). ^{13}C -NMR (101 MHz; CDCl_3): δ 168.5, 167.9, 163.8, 150.1, 141.4, 139.9, 138.9, 135.3, 131.4 (q, $J = 40.4$ Hz), 128.4, 126.9, 124.2, 120.5, 122.3 (q, $J = 272.7$ Hz), 109.5, 11.6. IR (neat): $\tilde{\nu} = 3236, 3092, 1655, 1632, 1598, 1518, 1140, 979, 834, 701$ cm^{-1} . HRMS (ESI) m/z ($\text{M}+\text{H}$) $^+$ calcd for $\text{C}_{20}\text{H}_{14}\text{F}_3\text{N}_6\text{O}_4$ 459.1023, found 459.1021.

***N*-(4-(4-(3-Methyl-1,2,4-oxadiazol-5-yl)-5-(trifluoromethyl)-1*H*-pyrazol-1-yl)phenyl)-2-(4-nitrophenyl)acetamide, (15).**

White solid (81.6 mg, 0.17 mmol, 54%); Chromatography: PE/EtOAc 6:4; mp: 171-173 °C. ¹H-NMR (400 MHz; CDCl₃): δ 8.27-8.25 (m, 3H), 7.70 (d, *J* = 8.2 Hz, 2H), 7.60 (br s, 1H), 7.56 (d, *J* = 8.2 Hz, 2H), 7.45 (d, *J* = 8.0 Hz, 2H), 3.90 (s, 2H), 2.51 (s, 3H). ¹³C-NMR (101 MHz; ; (CD₃)₂CO): δ 168.6, 168.2, 167.8, 147.1, 143.3, 141.0, 140.8, 134.2, 130.7 (q, *J* = 42.6 Hz), 130.6, 126.7, 123.3, 119.4, 119.2 (q, *J* = 271.5 Hz), 109.1, 43.1, 10.6. IR (neat): $\tilde{\nu}$ = 3255, 3115, 3080, 1662, 1629, 1599, 1535, 1518, 1133 cm⁻¹. HRMS (ESI) *m/z* (M+H)⁺ calcd for C₂₁H₁₆F₃N₆O₄ 473.1180, found 473.1180.

4-Cyano-3-fluoro-*N*-(4-(4-(3-methyl-1,2,4-oxadiazol-5-yl)-5-(trifluoromethyl)-1*H*-pyrazol-1-yl)phenyl)benzamide, (16).

White solid (82 mg, 0.18 mmol, 56%); Chromatography: PE/EtOAc 7:3; mp: 160-162 °C, dec. ¹H-NMR (400 MHz; CDCl₃): δ 8.30 (s, 1H), 7.87 (br s, 1H), 7.85-7.80 (m, 5H), 7.56 (d, *J* = 8.8 Hz, 2H), 2.52 (s, 3H). ¹³C-NMR (101 MHz; DMSO-*d*₆): δ 168.6, 168.2, 163.8, 162.7 (d, *J* = 257.5 Hz), 141.9 (d, *J* = 7.1 Hz), 141.8, 140.7, 134.8, 134.5, 130.8 (q, *J* = 40.4 Hz), 127.2, 125.2 (d, *J* = 3.0 Hz), 121.1, 119.4 (q, *J* = 271.7 Hz), 116.2 (d, *J* = 22.2 Hz), 114.0, 108.9, 103.4 (d, *J* = 15.1 Hz), 11.6.

IR (neat): $\tilde{\nu}$ = 3364, 3080, 2921, 2239, 2197, 1680, 1632, 1139, 977, 757 cm⁻¹. HRMS (ESI) *m/z* (M+H)⁺ calcd for C₂₁H₁₃F₄N₆O₂ 457.1031, found 457.1029.

2-Iodo-*N*-(4-(4-(3-methyl-1,2,4-oxadiazol-5-yl)-5-(trifluoromethyl)-1*H*-pyrazol-1-yl)phenyl)benzamide, (17).

White solid (103 mg, 0.19 mmol, 60%); Chromatography: PE/EtOAc 7:3; mp: 201-203 °C, ¹H-NMR (400 MHz; CDCl₃): δ 8.27 (s, 1H), 7.96 (d, *J* = 7.9 Hz, 1H), 7.85 (d, *J* = 8.4 Hz, 2H), 7.70 (br s, 1H), 7.59 (d, *J* = 7.9 Hz, 1H), 7.53-7.47 (m, 3H), 7.21 (t, *J* = 7.9 Hz, 1H), 2.52 (s, 3H). ¹³C-NMR (101 MHz; CDCl₃): δ 168.6, 167.8, 167.3, 141.7, 141.3, 140.2, 139.3, 134.9, 131.8, 131.4 (q, *J* = 40.8 Hz), 128.6, 128.4, 127.9, 126.7, 120.2, 119.0 (q, *J* = 272.6 Hz), 109.3, 92.3, 11.6. IR (neat): $\tilde{\nu}$ = 3310, 3097, 2921, 2851, 1687, 1631, 1153, 977, 756, 546 cm⁻¹. HRMS (ESI) *m/z* (M+H)⁺ calcd for C₂₀H₁₄F₃IN₅O₂ 540.0139, found 540.0137.

***N*-(4-(4-(3-Methyl-1,2,4-oxadiazol-5-yl)-5-(trifluoromethyl)-1*H*-pyrazol-1-yl)phenyl)-1*H*-benzo[*d*]imidazole-6-carboxamide, (18).**

White solid (84 mg, 0.19 mmol, 58%); Chromatography: PE/EtOAc 1:9; mp: 235-236 °C. ¹H-NMR (400 MHz; CD₃OD): δ 8.38-8.33 (m, 2H), 8.03-8.01 (m, 3H), 7.96 (d, *J* = 8.5 Hz, 1H), 7.76 (dd, *J*_s = 7.5, 1.6 Hz, 1H), 7.57 (d, *J* = 6.8 Hz, 2H), 2.48 (s, 3H). ¹³C-NMR (101 MHz; DMSO-*d*₆): δ 168.6, 168.2, 166.9, 141.8 (2C), 133.8 (2C), 130.8 (q, *J* = 40.0 Hz), 128.5, 127.0 (2C), 123.1, 120.9, 119.5, 119.4 (q, *J* = 272.2 Hz), 117.6, 112.0, 108.9, 11.6. IR (neat): $\tilde{\nu}$ = 3637, 2921, 2851, 1626, 1519, 1293, 1140, 946, 830, 547 cm⁻¹. HRMS (ESI) *m/z* (M+H)⁺ calcd for C₂₁H₁₅F₃N₇O₂ 454.1234, found 454.1231.

***3,5*-Dimethyl-*N*-(4-(4-(3-methyl-1,2,4-oxadiazol-5-yl)-5-(trifluoromethyl)-1*H*-pyrazol-1-yl)phenyl)isoxazole-4-carboxamide, (19).**

White solid (111 mg, 0.26 mmol, 80%); Chromatography: PE/EtOAc 8:2; mp: 177-178 °C, dec. ¹H-NMR (400 MHz; CDCl₃): δ 8.27 (s, 1H), 7.89 (br s, 1H), 7.78 (d, *J* = 6.6 Hz, 2H), 7.49 (d, *J* = 6.6 Hz, 2H), 2.68 (s, 3H), 2.50 (s, 3H), 2.48 (s, 3H). ¹³C-NMR (101 MHz; CDCl₃): δ 172.0, 168.5, 167.8, 160.3, 157.6, 141.3, 139.1, 134.9, 131.4 (q, *J* = 40.6 Hz), 126.8, 120.4, 118.8 (q, *J* = 272.7 Hz), 112.4, 109.4, 13.0, 11.6, 11.5. IR (neat): $\tilde{\nu}$ = 3307, 2923, 2853, 1649, 1522, 1219, 1132, 825, 740, 507 cm⁻¹. HRMS (ESI) *m/z* (M+H)⁺ calcd for C₁₉H₁₆F₃N₆O₃ 433.1231, found 433.1227.

***4*-Methyl-*N*-(4-(4-(3-methyl-1,2,4-oxadiazol-5-yl)-5-(trifluoromethyl)-1*H*-pyrazol-1-yl)phenyl)-1,2,3-thiadiazole-5-carboxamide, (20).**

Yellow solid (111 mg, 0.26 mmol, 80%); Chromatography: PE/EtOAc 8:2; mp: 143-144 °C, dec. ¹H-NMR (400 MHz; CDCl₃): δ 8.28 (s, 1H), 7.82 (d, *J* = 7.4 Hz, 2H), 7.52 (d, *J* = 7.4 Hz, 2H), 2.98 (s, 3H), 2.50 (s, 3H). ¹³C-NMR (101 MHz; CDCl₃): δ 168.5, 167.9, 160.1, 157.6, 143.1, 141.4, 138.5, 135.6, 131.5 (q, *J* = 41.4 Hz), 126.9, 120.8, 116.3 (q, *J* = 272.7 Hz), 109.5, 13.8, 11.6. IR (neat): $\tilde{\nu}$ = 3267, 2927, 2852, 1650, 1519, 1324, 1135, 979, 835, 554 cm⁻¹. HRMS (ESI) *m/z* (M+H)⁺ calcd for C₁₇H₁₃F₃N₇O₂S 436.0798, found 436.0797.

***N*-(4-(4-(3-methyl-1,2,4-oxadiazol-5-yl)-5-(trifluoromethyl)-1*H*-pyrazol-1-yl)phenyl)furan-2-carboxamide, (21).**

White solid (70 mg, 0.17 mmol, 54%); Chromatography: PE/EtOAc 8:2; mp: 140-141 °C, ¹H-NMR (400 MHz; CDCl₃): δ 8.28 (s, 1H), 8.26 (br s, 1H), 7.87 (d, *J* = 8.8 Hz, 2H), 7.57 (d, *J* = 1.7 Hz, 1H), 7.50 (d, *J* = 8.8 Hz, 2H), 7.31 (d, *J* = 3.5 Hz, 1H), 6.62 (dd, *J*_s = 3.5, 1.7 Hz, 1H), 2.51 (s, 3H). ¹³C-NMR (101 MHz; CDCl₃): δ 168.6, 167.8, 156.1, 147.4, 144.5, 141.3, 139.2, 134.6, 131.4 (q, *J* = 40.7 Hz), 126.7, 120.0, 119.0, 114.9, 112.8, 109.3, 11.6. IR (neat): $\tilde{\nu}$ = 3395, 3324, 3107, 2921, 2851, 1669, 1630, 1541, 1515, 980 cm⁻¹. HRMS (ESI) *m/z* (M+H)⁺ calcd for C₁₈H₁₃F₃N₅O₃ 404.0965, found 404.0963.

***4*-Bromo-*N*-(4-(4-(3-methyl-1,2,4-oxadiazol-5-yl)-5-(trifluoromethyl)-1*H*-pyrazol-1-yl)phenyl)-1*H*-pyrrole-2-carboxamide, (22).**

Yellow solid (85 mg, 0.18 mmol, 55%); Chromatography: PE/EtOAc 8:2; mp: 171-173 °C, dec. ¹H-NMR (400 MHz; (CD₃)₂CO): δ 11.27 (br s, 1H), 9.56 (br s, 1H), 8.40 (s, 1H), 8.05 (d, *J* = 8.0 Hz, 2H), 7.61 (d, *J* = 8.0 Hz, 2H), 7.20 (s, 1 H), 7.13 (s, 1H), 2.45 (s, 3H). ¹³C-NMR (101 MHz; (CD₃)₂CO): δ 168.6, 167.8, 158.2, 141.0, 134.1, 130.8 (q, *J* = 40.3 Hz), 128.9, 126.6, 124.9, 122.7, 119.8, 119.0 (q, *J* = 271.7 Hz), 112.6, 108.9, 96.2, 10.5. IR (neat): $\tilde{\nu}$ = 3273, 3094, 3051, 2971, 2926, 2873, 1660, 1631, 978, 834, 802 cm⁻¹. HRMS (ESI) *m/z* (M+H)⁺ calcd for C₁₈H₁₃BrF₃N₆O₂ 481.0230 and 483.0209, found 481.0232 and 483.0211.

Synthesis of 3-(*N*-(2-methoxyphenyl)sulfamoyl)-4-methylbenzoic acid.

To a solution of 2-methoxyaniline (157 mg, 1.28 mmol) in dry CH₂Cl₂ (4 mL), pyridine (309 μL, 3.84 mmol) and 3-(chlorosulfonyl)-4-methylbenzoic acid (300 mg, 1.28 mmol) were added at 0 °C. After 5 h at 0 °C, the reaction was not concluded and 2-methoxyaniline (0.5 eq) and pyridine (1.5 eq) were added. After stirring for additional 4 h at 0 °C, the reaction was concluded. The mixture was diluted with CH₂Cl₂, washed with HCl 3N (2x) and the organic layer was dried over sodium sulfate and evaporated, affording 3-(*N*-(2-methoxyphenyl)sulfamoyl)-4-methylbenzoic acid (152 mg, 0.47 mmol, 37%) as a pink solid. ¹H-NMR (300 MHz;

CDCl₃): δ 8.62 (s, 1H), 8.08 (d, $J = 7.7$ Hz, 1H), 7.43 (d, $J = 7.4$ Hz, 1H), 7.38 (d, $J = 7.4$ Hz, 1H), 7.01 (d, $J = 6.8$ Hz, 1H), 6.86 (t, $J = 6.8$ Hz, 1H), 6.78 (d, $J = 6.8$ Hz, 1H), 3.77 (s, 3H), 2.74 (s, 3H). MS (ESI): m/z 320 [M-H]⁻.

Synthesis of 3-(*N*-(2-methoxyphenyl)sulfamoyl)-4-methyl-*N*-(4-(4-(3-methyl-1,2,4-oxadiazol-5-yl)-5-(trifluoromethyl)-1*H*-pyrazol-1-yl)phenyl)benzamide, (23).

Compound **23** was synthesized following the general procedure, starting from amine **5** and 3-(*N*-(2-methoxyphenyl)sulfamoyl)-4-methylbenzoic acid (112 mg, 0.35 mmol) reacted with (100 mg, 0.32 mmol). Purification by column chromatography using PE/EtOAc 7:3 afforded the desired compound **23** as a white solid (129 mg, 0.21 mmol, 66%). Mp: 205-206 °C. ¹H-NMR (400 MHz; (CD₃)₂CO): δ 10.03 (br s, 1H), 8.47 (s, 1H), 8.39 (s, 1H), 8.30 (br s, 1H), 8.15 (d, $J = 7.9$ Hz, 1H), 8.09 (d, $J = 6.9$ Hz, 2H), 7.62 (d, $J = 6.9$ Hz, 2H), 7.55 (d, $J = 8.0$ Hz, 1H), 7.43 (d, $J = 7.9$ Hz, 1H), 7.09 (t, $J = 7.9$ Hz, 1H), 6.92-6.86 (m, 2H), 3.70 (s, 3H), 2.77 (s, 3H), 2.45 (s, 3H). ¹³C-NMR (101 MHz; (CD₃)₂CO): δ 168.6, 167.8, 164.3, 151.3, 141.6, 141.0, 140.9, 138.9, 134.5, 132.7, 132.6, 131.6, 130.8 (q, $J = 40.2$ Hz), 128.8, 126.6, 126.1, 125.6, 123.1, 120.7, 120.4, 119.7 (q, $J = 271.6$ Hz), 111.2, 109.2, 55.1, 19.5, 10.6. IR (neat): $\tilde{\nu} = 3387, 2922, 2852, 1666, 1518, 1298, 1152, 835, 737, 577$ cm⁻¹. HRMS (ESI) m/z (M+H)⁺ calcd for C₂₈H₂₄F₃N₆O₅S 613.1475, found 613.1475.

***N*-(4-(4-(3-Methyl-1,2,4-oxadiazol-5-yl)-5-(trifluoromethyl)-1*H*-pyrazol-1-yl)phenyl)hexanamide, (24).**

White solid (73 mg, 0.18 mmol, 56%); Chromatography: PE/EtOAc 8:2; mp: 176-178 °C, dec. ¹H-NMR (400 MHz; CDCl₃): δ 8.27 (s, 1H), 7.73 (d, $J = 8.8$ Hz, 2H), 7.45 (d, $J = 8.8$ Hz, 2H), 2.52 (s, 3H), 2.43 (t, $J = 7.4$ Hz, 2H), 1.79 (quint, $J = 7.4$ Hz, 2H), 1.43-1.39 (m, 4H), 0.94 (t, $J = 7.4$ Hz, 3H). ¹³C-NMR (101 MHz; CDCl₃): δ 171.7, 168.6, 167.8, 141.2, 139.8, 134.3, 131.4 (q, $J = 40.4$ Hz), 126.6, 119.8, 119.0 (q, $J = 272.7$ Hz), 109.3, 37.8, 31.4, 25.2, 22.4, 13.9, 11.6. IR (neat): $\tilde{\nu} = 3270, 3092, 2952, 2929, 2866, 1667, 1630, 1519, 1496, 978$ cm⁻¹. HRMS (ESI) m/z (M+H)⁺ calcd for C₁₉H₂₁F₃N₅O₂ 408.1642, found 408.1640.

***N*-(4-(4-(3-Methyl-1,2,4-oxadiazol-5-yl)-5-(trifluoromethyl)-1*H*-pyrazol-1-yl)phenyl)dodecanamide, (25).**

White solid (86 mg, 0.18 mmol, 55%); Chromatography: PE/EtOAc 8:2; mp: 138-140 °C, ¹H-NMR (400 MHz; CDCl₃): δ 8.26 (s, 1H), 7.73 (d, *J* = 8.7 Hz, 2H), 7.45-7.43 (m, 3H), 2.51 (s, 3H), 2.42 (t, *J* = 7.4 Hz, 2H), 1.77 (quint, *J* = 7.4 Hz, 2H), 1.32-1.29 (m, 16H), 0.90 (t, *J* = 7.4 Hz, 3H). ¹³C-NMR (101 MHz; CDCl₃): δ 172.1, 171.8, 167.8, 141.2, 139.9, 131.4 (q, *J* = 40.9 Hz), 127.0, 126.5, 119.7, 118.9 (q, *J* = 272.6 Hz), 109.2, 46.7, 37.8, 34.9, 31.9, 29.6, 26.1, 25.5, 25.0, 24.4, 22.7, 14.1, 11.6. IR (neat): $\tilde{\nu}$ = 3278, 3096, 2918, 2848, 1629, 1522, 1466, 1134, 979, 842 cm⁻¹. HRMS (ESI) *m/z* (M+H)⁺ calcd for C₂₅H₃₃F₃N₅O₂ 492.2581, found 492.2577.

***N*-(4-(4-(3-Methyl-1,2,4-oxadiazol-5-yl)-5-(trifluoromethyl)-1*H*-pyrazol-1-yl)phenyl)-3-morpholinopropanamide, (26).**

White solid (58 mg, 0.13 mmol, 40%); Chromatography: EtOAc; mp: 147-149 °C. ¹H-NMR (400 MHz; CDCl₃): δ 8.26 (s, 1H), 7.75 (d, *J* = 8.8 Hz, 2H), 7.44 (d, *J* = 8.8 Hz, 2H), 3.90 (t, *J* = 4.4 Hz, 4H), 2.91 (t, *J* = 5.4 Hz, 2H), 2.78-2.75 (m, 4H), 2.70 (t, *J* = 5.4 Hz, 2H), 2.51 (s, 3H). ¹³C-NMR (101 MHz; CDCl₃): δ 170.2, 168.6, 167.8, 141.2, 140.2, 134.1, 131.4 (q, *J* = 40.7 Hz), 126.6, 120.4, 118.9 (q, *J* = 272.5 Hz), 109.2, 66.6, 54.0, 52.8, 32.0, 11.6. IR (neat): $\tilde{\nu}$ = 3275, 3090, 2921, 2851, 1659, 1519, 1133, 977, 722, 703 cm⁻¹. HRMS (ESI) *m/z* (M+H)⁺ calcd for C₂₀H₂₂F₃N₆O₃ 451.1700, found 451.1695.

***N*-(4-(4-(3-Methyl-1,2,4-oxadiazol-5-yl)-5-(trifluoromethyl)-1*H*-pyrazol-1-yl)phenyl)tetrahydro-2*H*-thiopyran-4-carboxamide 1,1-dioxide, (27).**

White solid (63 mg, 0.13 mmol, 42%); Chromatography: PE/EtOAc 3:7; mp: 153.5-154.5 °C, ¹H-NMR (400 MHz; DMSO-*d*₆): δ 10.38 (br s, 1H), 8.55 (s, 1H), 7.82 (d, *J* = 8.9 Hz, 2H), 7.55 (d, *J* = 8.9 Hz, 2H), 3.29-3.19 (m, 4H), 2.23 (s, 3H), 2.21-2.18 (m, 2H), 2.15-2.09 (m, 2H). ¹³C-NMR (101 MHz; DMSO-*d*₆): δ 172.9, 168.6, 168.2, 141.7, 141.2, 133.7, 130.7 (q, *J* = 39.8 Hz), 127.2, 119.9, 119.4 (q, *J* = 272.2 Hz), 108.9, 49.9, 41.5, 27.5, 11.6. IR (neat): $\tilde{\nu}$ = 3301, 3092, 2947, 2929, 1649, 1633,

1523, 1323, 1143, 977 cm^{-1} . HRMS (ESI) m/z (M+H)⁺ calcd for C₁₉H₁₉F₃N₅O₄S 470.1104, found 470.1106.

***N*-(4-(4-(3-Methyl-1,2,4-oxadiazol-5-yl)-5-(trifluoromethyl)-1*H*-pyrazol-1-yl)phenyl)-2-phenoxyacetamide, (28).**

White solid (86 mg, 0.19 mmol, 61%); Chromatography: PE/EtOAc 7:3; mp: 160-161 °C, dec. ¹H-NMR (400 MHz; CDCl₃): δ 8.48 (br s, 1H), 8.28 (s, 1H), 7.82 (d, $J = 8.8$ Hz, 2H), 7.50 (d, $J = 8.8$ Hz, 2H), 7.40 (t, $J = 7.6$ Hz, 2H), 7.11 (t, $J = 7.6$ Hz, 1H), 7.04 (d, $J = 7.6$ Hz, 2H), 4.69 (s, 2H), 2.52 (s, 3H). ¹³C-NMR (101 MHz; CDCl₃): δ 168.6, 167.8, 166.6, 156.9, 141.3, 138.6, 135.0, 131.4 (q, $J = 40.7$ Hz), 130.0, 126.7, 122.7, 120.2, 119.0 (q, $J = 272.4$ Hz), 114.9, 109.4, 42.8, 10.6. IR (neat): $\tilde{\nu} = 3356, 3103, 3087, 2922, 2903, 1674, 1631, 1229, 1128, 982$ cm^{-1} . HRMS (ESI) m/z (M+H)⁺ calcd for C₂₁H₁₇F₃N₅O₃ 444.1278, found 444.1280.

Synthesis of 4-methyl-*N*-(4-(4-(3-methyl-1,2,4-oxadiazol-5-yl)-5-(trifluoromethyl)-1*H*-pyrazol-1-yl)phenyl)benzenesulfonamide, (29).

4-(4-(3-Methyl-1,2,4-oxadiazol-5-yl)-5-(trifluoromethyl)-1*H*-pyrazol-1-yl)aniline **5** (100 mg, 0.32 mmol) was solubilized in dry CH₂Cl₂ (2.5 mL) and pyridine (77 μL , 0.96 mmol) and *p*-toluenesulfonyl chloride (TsCl) (72 mg, 0.38 mmol) were added in order at 0 °C. The mixture was allowed to reach room temperature and stirred for 5 h. Then, the reaction was diluted with CH₂Cl₂, washed with HCl 3N (2x), dried over sodium sulfate and evaporated. Purification by column chromatography using PE/EtOAc 7:3 as eluent afforded the desired compound **29** (67 mg, 0.14 mmol, 45%) as a yellow solid. Mp: 149-150 °C. ¹H-NMR (400 MHz; CDCl₃): δ 8.25 (s, 1H), 7.75 (d, $J = 7.4$ Hz, 2H), 7.54 (br s, 1H), 7.36 (d, $J = 7.9$ Hz, 2H), 7.29-7.26 (m, 4H), 2.50 (s, 3H), 2.41 (s, 3H). ¹³C-NMR (101 MHz; CDCl₃): δ 168.5, 167.9, 144.5, 141.3, 138.6, 135.7, 135.3, 131.4 (q, $J = 40.4$ Hz), 129.9, 127.3, 127.0, 120.9, 118.9 (q, $J = 272.7$ Hz), 109.4, 21.5, 11.6. IR (neat): $\tilde{\nu} = 3173, 2922, 2852, 1631, 1514, 1324, 1147, 919, 809, 541$ cm^{-1} . HRMS (ESI) m/z (M+H)⁺ calcd for C₂₀H₁₇F₃N₅O₃S 464.0999, found 464.0998.

4.3 References

1. a) Boström, J.; Hogner, A.; Llinàs, A.; Wellner, E.; Plowright, A. T. Oxadiazoles in medicinal chemistry. *J. Med. Chem.* **2012**, *55*, 1817-1830; b) Goldberg, K.; Groombridge, S.; Hudson, J.; Leach, A. G.; MacFaul, P. A.; Pickup, A.; Poultney, R.; Scott, J. S.; Svenssonb, P. H.; Sweeney, J. Oxadiazole isomers: all bioisosteres are not created equal. *Med. Chem. Commun.* **2012**, *3*, 600-604.
2. a) Riva, B., Griglio, A.; Serafini, M.; Cordero-Sanchez, C.; Aprile, S.; Di Paola, R.; Gugliandolo, E.; Alansary, D.; Biocotino, I.; Lim, D.; Grosa, G.; Galli, U.; Niemeyer, B.; Sorba, G.; Canonico, P. L.; Cuzzocrea, S.; Genazzani, A. A.; Pirali, T. Pyrtriazoles, a novel class of store-operated calcium entry modulators: discovery, biological profiling, and in vivo proof-of-concept efficacy in acute pancreatitis. *J. Med. Chem.* **2018**, *61*, 9756-9783; b) Pirali, T.; Riva, B.; Genazzani, A. A. Modulators of SOCE, Compositions and use thereof. W.O. Patent 212,414, Dec 14, 2017.
3. a) Serafini, M.; Cordero-Sanchez, C.; Di Paola, R.; Bhela, I. P.; Aprile, S.; Purghè, B.; Fusco, R.; Cuzzocrea, S.; Genazzani, A. A.; Riva, B.; Pirali, T. Store-Operated Calcium Entry (SOCE) as a therapeutic target in acute pancreatitis: discovery and development of drug-like SOCE inhibitor. *J. Med. Chem.* **2020**, *63*, 14761-14779; b) Pirali, T.; Riva, B.; Serafini, M.; Aprile, S.; Cordero Sanchez, C. Biphenyl compounds as SOCE modulators, compositions and uses thereof. Filed on February 21, 2020, n. 102020000003692.
4. Azimi, I.; Stevenson, R. J.; Zhang, X.; Meizoso-Huesca, A.; Xin, P.; Johnson, M.; Flanagan, J. U.; Chalmers, S. B.; Yoast, R. E.; Kapure, J. S.; Ross, B. P.; Vetter, I.; Ashton, M. R.; Launikonis, B. S.; Denny, W. A.; Trebak, M.; Monteith, G. R. A new selective pharmacological enhancer of the Orai1 Ca^{2+}

- channel reveals roles for Orai1 in smooth and skeletal muscle functions. *ACS Pharmacol. Transl. Sci.* **2020**, *3*, 135-147.
5. Motiani, R. K.; Abdullaev, I. F.; Trebak, M. A novel native store-operated calcium channel encoded by Orai3: selective requirement of Orai3 versus Orai1 in estrogen receptor-positive versus estrogen receptor-negative breast cancer cells. *J. Biol. Chem.* **2010**, *285*, 19173-19183.
 6. Waldherr, L.; Tiffner, A.; Mishra, D.; Sallinger, M.; Schober, R.; Frischauf, I.; Schmidt, T.; Handl, V.; Sagmeister, P.; Köckinger, M.; Derler, I.; Üçal, M.; Bonhenry, D.; Patz, S.; Schindl, R. Blockage of store-operated Ca²⁺ influx by Synta66 is mediated by direct inhibition of the Ca²⁺ selective Orai1 pore. *Cancers* **2020**, *12*, 2876-2895.
 7. Yang, X.; Ma, G.; Zheng, S.; Qin, X.; Li, X.; Du, L.; Wang, Y.; Zhou, Y.; Li, M. Optical control of CRAC channels using photoswitchable azopyrazoles. *J. Am. Chem. Soc.* **2020**, *142*, 9460-9470.

4.4 Contributions and collaborations

The compounds described in this chapter have been partially synthesized first-hand by me or have been the object of co-supervision of Master students that have carried out their Thesis project in Prof. Pirali's laboratory.

Metabolic stability has been evaluated by Dr. Aprile.

The *in vitro* cellular activity of the compounds, MTT assay and IC₅₀ calculation have been performed in collaboration with Prof. Genazzani and Dr. Riva.

PART II
INDOLEAMINE 2,3-
DIOXYGENASE INHIBITORS

5.1 A brief introduction on indoleamine 2,3-dioxygenase

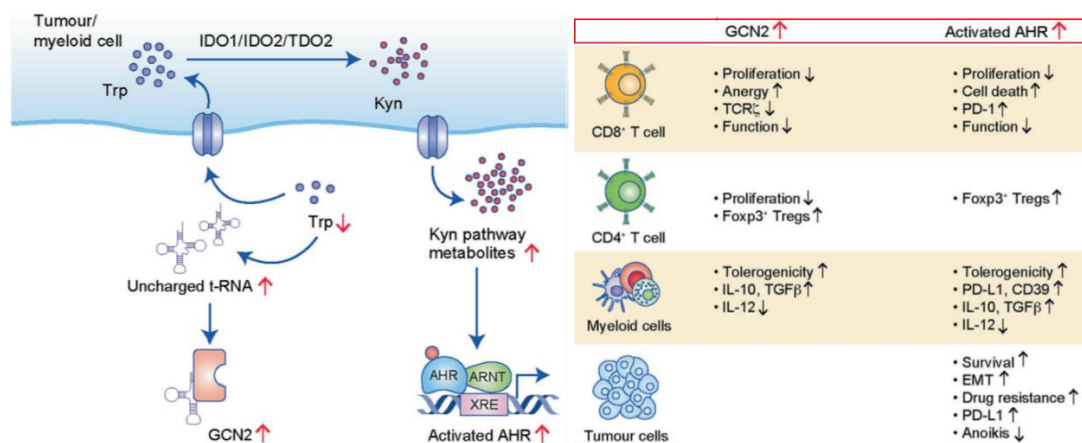
The metabolic pathway that leads to the catabolism of tryptophan (Trp), known as the kynurenine (Kyn) pathway, has drawn attention in the last decades for its central role in the escape of tumour cells from the immune surveillance. Both the depletion of Trp and the increase in Kyn and in its mainstream metabolites are associated with aggressive cancer phenotype, with enhanced inflammation in the tumor microenvironment, formation of an immune-permissive milieu¹ and promotion of neo-angiogenesis.²

More in detail, local deprivation of Trp and accumulation of Kyn cause the activation of the general control non-derepressible 2 (GCN2) kinase³ and the aryl hydrocarbon receptor (AhR),⁴ respectively. Overall, these signalling pathways lead to an inhibition of effector CD8+ T cells, with anergy and apoptosis. Also, insufficient Trp concentrations have been linked to inhibition of mTORC1⁵ and promotion of differentiation to immunosuppressive T-regulatory cells (Figure 1).⁶

The first and rate-limiting step along the kynurenine pathway is represented by the conversion of Trp to *N*-formyl-L-kynurenine and is catalysed by a family of heme-containing enzymes named dioxygenases: indoleamine 2,3-dioxygenase 1 (IDO1) and its isoform 2 (IDO2) and tryptophan 2,3-dioxygenase (TDO).⁷ While it has been shown that all the three enzymes are involved in tumour immune escape, the best known and well characterized isoform is IDO1.

The overexpression of IDO1, correlating with reduction in the overall survival of patients and in poor prognosis, has been found in a set of human tumours, including pancreatic cancer, non-small cell lung cancer and breast cancer among the others.⁸

Figure 1. The kynurenine pathway in the tumour microenvironment (*Taken and modified from Opitz et al. 2020*).⁷



Thousands of specific IDO1 inhibitors have been reported in the literature, most of them remaining at the preclinical development. Nine different compounds have entered clinical trials so far, but none have reached approval, pointing at the discovery of novel IDO1 inhibitors as an open challenge (Table 1).⁹

Epacadostat, the most advanced clinical candidate so far, entered phase 3 in combination with pembrolizumab in metastatic and non-resectable melanoma. Unfortunately, in 2018 the compound failed to show an added clinical benefit compared to pembrolizumab alone, leading to the interruption of other trials involving IDO1 inhibitors and questioning whether some elements, especially in the design of the clinical trial, had been overlooked.¹⁰

Since then, another inhibitor, linrodostat (BMS-98620) has proceeded in phase 3 trial. This compound is a suicide inhibitor able to bound to the apo-IDO1 form *i.e.* the protein lacking the heme group.¹¹ Indeed, in the last years, a more accurate appraisal of the different binding modes of IDO1 inhibitors has been undertaken and a classification of the known inhibitors based on their preferred binding mode has been proposed¹²: oxygen-bound holo-IDO1 (type I inhibitors), ferrous holo-IDO1 (type II), ferric holo-IDO1 (type III) and apo-IDO1 (type IV). The catalytically active

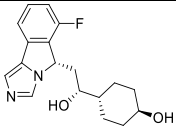
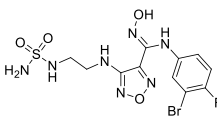
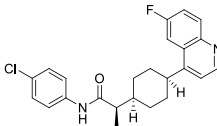
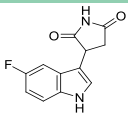
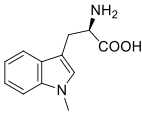
form of IDO1 sees the heme iron in its ferrous state and the first step is represented by the binding of the oxygen to this ion that is antecedent the binding with L-Trp.¹³ The Trp analogue 1-methyl-L-Trp is competitive for L-Trp and has been classified as type I inhibitor, while epacadostat and its analogues have been allocated among the type II, being competitive for oxygen.¹⁴ Type III inhibitors are those directed toward the inactive ferric form of the heme group¹⁵ and type IV target IDO1 in its apo form. Ferrous IDO1 represents the resting state (known as holo-IDO1) of the enzyme and binds ten-fold more tightly the heme group compared to the catalytically inactive ferric form.¹¹ In cells, IDO1 can exist either as holo or apo, being the binding with heme labile, dynamic, reversible and dependent on the oxidation state.

Finally, besides carrying out its catalytical functions at the C-termini, human IDO1 is also a signal-transducing molecule at its N-terminal, where a small domain with its two immunoreceptor tyrosine-based inhibitory motifs (ITIMs) is located. Phosphorylation of the tyrosine residues of ITIMs mediates the signalling function of IDO1 and the interaction with molecular partners of the enzyme, such as SOCS3 or phosphotyrosine phosphatases SHP-1 and 2 and inositolphosphatase SHIP.¹⁶

Depending on external stimuli, binding to these molecular partners is able to reduce or prolong, respectively, the half-life of the enzyme. Indeed, binding to SOCS3 is able to recruit the E3 ubiquitin ligase complex, which poly-ubiquitinates IDO1, mediating its proteasomal degradation.¹⁷ On the contrary, IDO1/SHPs axis mediates the activation of signal transduction pathways, such as the noncanonical NF- κ B route,¹⁸ which induces the production of IFN- γ and TGF- β , resulting in the upregulation of *Ido1* expression and in the *de novo* synthesis of the enzyme.^{16a} It follows that the identification of compounds able to reduce the IDO1 signalling activity and to mediate the sustained degradation of the enzyme might be an added value in the identification of IDO1 inhibitors.

It appears clear therefore that some progresses have been made in the field, paving the way for the rational design of novel and innovative IDO1 inhibitors endowed with different modes of action.

Table 1. IDO1 inhibitors in clinical trials. The “Most advanced phase of development” corresponds to the phase of clinical trials reached, as reported in Clinicaltrials.gov website.¹⁹ When more than one trials were present, the active ones have been chosen.

Compound	Structure	Mechanism of action	Most advanced phase of development	Indication
Navoximod (NLG-919)		Forms direct bond to ferric heme iron	Not registered on clinicaltrials.gov	-
epacadostat (INCB024360)		Trp-competitive inhibitor Forms direct bond to ferrous heme iron	Seven phase 3 studies (completed, active, not recruiting and terminated) Five phase 2 studies (recruiting)	Urothelial, head and neck, lung cancers, renal carcinoma and melanoma Glioblastoma, pancreatic adenocarcinoma, head and neck, breast and prostate cancers
linrodostat (BMS-986205)		Suicide inhibitor Binds to heme-free apo IDO1	Phase 3 (recruiting) Phase 3 (active, not recruiting)	Bladder cancer Melanoma
EOS200271/ PF-06840003		Catalytic inhibitor, non-competitive for L-Trp	Phase 1 (terminated)	Malignant glioma
KHK2455	NA	Binds to heme-free apo IDO1	Phase 1 (recruiting)	Urothelial carcinoma
LY3381916	NA	Binds to heme-free apo IDO1	Phase 1 (terminated)	Solid tumours
MK-7162	NA	NA	Phase 1 (active, not recruiting)	Solid tumours
indoximod (NLG8189)		Stimulates mTORC1 pathway	Phase 2 (recruiting) Phase 2 (recruiting)	Metastatic breast cancer Paediatric glioblastoma, medulloblastoma, ependymoma
NLG802	NA	Prodrug of indoximod	Phase 1 (completed)	Solid tumours

5.2 Outline of the project

By exploiting multicomponent reactions, our research group has previously reported two different classes of IDO catalytic inhibitors, displaying the imidazole²⁰ and the imidazothiazole²¹ scaffolds, respectively.

In the latter project, Passerini three-component and Ugi four-component reactions have been exploited to obtain imidazothiazoles (Figure 2) able to inhibit IDO1 in an enzyme-based assay with IC₅₀ values in the low micromolar range. While the compounds were not active in the cell-based assay as they were not able to cross the plasma membrane, docking studies revealed that the long chain of this class of molecules protrudes in a region, named by us pocket C, which had never been exploited by other reported inhibitors. Here, a crucial hydrogen bond is formed with Lys238, affording an improvement in the inhibitory activity.

The recent failure of epacadostat has clearly underlined that additional efforts in the IDO1 field, also from a medicinal chemistry point of view, are strongly needed. In this context, a better comprehension of the possible interactions with the aminoacidic residues in the IDO1 active site would guide the rational design of novel and potent inhibitors. Therefore, with the aim to probe the interactions in pocket C, another medicinal chemistry campaign was undertaken and, starting from the class of imidazothiazoles published in 2018,²¹ I decided to apply click chemistry to replace the benzylamide moiety displayed by imidazothiazoles a 1,4-disubstituted 1,2,3-triazole ring²² (both portions are highlighted in green in Figure 2). This class of IDO1 inhibitors resulted in a publication in *Molecules* (Chapter 6).

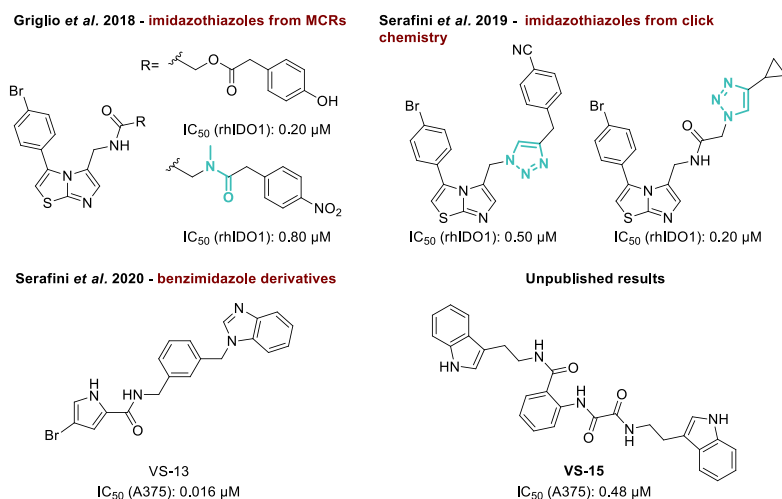
The acquired information on pocket C was then integrated in a structure-based virtual screening performed by our research group. This approach led to the discovery of two hit compounds, named **VS-13** and **VS-15** (Figure 2).

Compound **VS-13** was the most potent in inhibiting IDO1 with an IC₅₀ of 16 nM and therefore was chosen as the ideal starting point of our medicinal chemistry project, resulting in a publication in *Journal of Medicinal Chemistry* (Chapter 7).²³

Unfortunately, the compound is highly susceptible toward oxidative metabolism, resulting in dozens of metabolites formed and making the chemical refinement of this molecule highly challenging. Nevertheless, as proposed in the final part of the manuscript, one of the possible approaches in the future is represented by the use of the deuterium²⁴ to substitute part of the metabolically labile hydrogens of **VS-13**, while other soft spots might be isosterically replaced with fluorine.

However, in the meanwhile, the other hit compound identified, **VS-15**, besides displaying a high potency on IDO1, revealed a very promising biological profile, as described in Chapter 8. This evidence prompted me to focus my efforts on this candidate.

Figure 2. Outline of the project.



5.3 References

1. Prendergast, G. C.; Mondal, A.; Dey, S.; Laury-Kleintop, L. D.; Muller, A. J. Inflammatory reprogramming with IDO1 inhibitors: turning immunologically unresponsive ‘cold’ tumors ‘hot’. *Trends Cancer* **2018**, *4*, 38-58.
2. Mondal, A.; Smith, C.; DuHadaway, J. B.; Sutanto-Ward, E.; Prendergast, G. C.; Bravo-Nuevo, A.; Muller, A. J. IDO1 is an integral mediator of inflammatory neovascularization. *EBioMedicine* **2016**, *14*, 74-82.
3. Munn, D. H.; Sharma, M. D.; Baban, B.; Harding, H. P.; Zhang, Y.; Ron, D.; Mellor, A. L. GCN2 kinase in T cells mediates proliferative arrest and anergy induction in response to indoleamine 2,3-dioxygenase. *Immunity* **2005**, *22*, 633-642.
4. Vogel, C. F.; Goth, S. R.; Dong, B.; Pessah, I. N.; Matsumura, F. Aryl hydrocarbon receptor signaling mediates expression of indoleamine 2,3-dioxygenase. *Biochem. Biophys. Res. Commun.* **2008**, *375*, 331-335.
5. Metz, R.; Rust, S.; Duhadaway, J. B.; Mautino, M. R.; Munn, D. H.; Vahanian, N. N.; Link, C. J.; Prendergast, G. C. IDO inhibits a tryptophan sufficiency signal that stimulates mTOR: a novel IDO effector pathway targeted by d-1-methyl-tryptophan. *Oncoimmunology* **2012**, *1*, 1460-1468.
6. a) Grohmann, U.; Fallarino, F.; Puccetti, P. Tolerance, DCs and tryptophan: much about IDO. *Trends Immunol.* **2003**, *24*, 242-248; b) Moon, Y. W.; Hajjar, J.; Hwu, P.; Naing, A. Targeting the indoleamine 2,3-dioxygenase pathway in cancer. *J. Immunother. Cancer* **2015**, *3*, 51; c) Platten, M.; Doeberitz, N.V.K.; Oezen, I.; Wick, W.; Ochs, K. Cancer immunotherapy by targeting IDO1/TDO and their downstream effectors. *Front. Immunol.* **2015**, *5*, 1-7.
7. Opitz, C. A.; Patterson, L. F. S.; Mohapatra, S. R.; Dewi, D. L.; Sadik, A.; Platten, M.; Trump, S. The therapeutic potential of targeting tryptophan catabolism in cancer. *Br. J. Cancer* **2020**, *122*, 30-44.

8. Godin-Ethier, J.; Hanafi, L. A.; Piccirillo, C. A.; Lapointe, R. Indoleamine 2,3-dioxygenase expression in human cancers: clinical and immunologic perspectives. *Clin. Cancer Res.* **2011**, *17*, 6985-6991.
9. Prendergast, G. C.; Malachowski, W. P.; DuHadaway, J. B.; Muller, A. J. Discovery of IDO1 inhibitors: from bench to bedside. *Cancer Res.* **2017**, *77*, 6795-6811.
10. Long, G. V.; Dummer, R.; Hamid, O.; Gajewski, T.; Caglevic, C.; Dalle, S.; Arance, A.; Carlino, M. S.; Grob, J.-J.; Kim, T. M.; Demidov, L. V.; Robert, C.; Larkin, J. M. G.; Anderson, J.; Maleski, J. E.; Jones, M. M.; Diede, S. J.; Mitchell, T. C. Epcadostat (E) plus pembrolizumab (P) versus pembrolizumab alone in patients (pts) with unresectable or metastatic melanoma: Results of the phase 3 ECHO-301/KEYNOTE-252 study. *J. Clin. Oncol.* **2018**, *36*, (suppl; abstr 108); b) Garber, K. A new cancer immunotherapy suffers a setback. *Science* **2018**, *360*, 588.
11. a) Nelp, M. T.; Kates, P. A.; Hunt, J. T.; Newitt, J. A.; Balog, A.; Maley, D.; Zhu, X.; Abell, L.; Allentoff, A.; Borzilleri, R.; Lewis, H. A.; Lin, Z.; Seitz, S. P.; Yan, C.; Groves, J. T. Immune-modulating enzyme indoleamine 2,3-dioxygenase is effectively inhibited by targeting its apo-form. *Proc. Natl. Acad. Sci. U.S.A.* **2018**, *115*, 3249-3254; b) Ortiz-Meoz, R. F.; Wang, L.; Matico, R.; Rutkowska, A.; la Rosa, M.; Bedard, S.; Midgett, R.; Strohmer, K.; Thomson, D.; Zhang, C.; Guss, J.; Totoritis, R.; Consler, T.; Campobasso, N.; Taylor, D.; Lewis, T.; Weaver, K.; Mulbaier, M.; Seal, J.; Dunham, R.; Kazmierski, W.; Favre, D.; Bergamini, G.; Shewchuk, L.; Rendina, A.; Zhang, G. Characterization of novel inhibition of indoleamine 2,3-dioxygenase by targeting its apo form. **2018**, bioRxiv:324947.
12. Röhrig, U. F.; Reynaud, A.; Majjigapu, S. R.; Vogel, P.; Pojer, F.; Zoete, V. Inhibition mechanisms of indoleamine 2,3-dioxygenase 1 (IDO1). *J. Med. Chem.* **2019**, *62*, 8784-8795.

13. Efimov, I.; Basran, J.; Sun, X.; Chauhan, N.; Chapman, S. K.; Mowat, C. G.; Raven, E. L. The mechanism of substrate inhibition in human indoleamine 2,3-dioxygenase. *J. Am. Chem. Soc.* **2012**, *134*, 3034-3041.
14. a) Lewis-Ballester, A.; Pham, K. N.; Batabyal, D.; Karkashon, S.; Bonanno, J. B.; Poulos, T. L.; Yeh, S. R. Structural insights into substrate and inhibitor binding sites in human indoleamine 2,3-dioxygenase 1. *Nat. Commun.* **2017**, *8*, 1693-1700; b) Kolawole, A. O.; Hixon, B. P.; Dameron, L. S.; Chrisman, I. M.; Smirnov, V. V. Catalytic activity of human indoleamine 2,3-dioxygenase (HIDO1) at low oxygen. *Arch. Biochem. Biophys.* **2015**, *570*, 47-57.
15. Sono, M.; Cady, S. G. Enzyme kinetic and spectroscopic studies of inhibitor and effector interactions with indoleamine 2,3-dioxygenase 1. Norharman and 4-phenylimidazole binding to the enzyme as inhibitors and heme ligands. *Biochemistry* **1989**, *28*, 5392-5399.
16. a) Orabona, C.; Pallotta, M. T.; Grohmann, U. Different partners, opposite outcomes: a new perspective of the immunobiology of indoleamine 2,3-dioxygenase. *Mol. Med.* **2012**, *18*, 834-842; b) Pallotta, M. T.; Orabona, C.; Volpi, C.; Vacca, C.; Belladonna, M. L.; Bianchi, R.; Servillo, G.; Brunacci, C.; Calvitti, M.; Bicciato, S.; Mazza, E. M. C.; Boon, L.; Grassi, F.; Fioretti, M. C.; Fallarino, F.; Puccetti, P.; Grohmann, U. Indoleamine 2,3-dioxygenase is a signaling protein in long-term tolerance by dendritic cells. *Nat. Immunol.* **2011**, *12*, 870-878.
17. Orabona, C.; Pallotta, M. T.; Volpi, C.; Fallarino, F.; Vacca, C.; Bianchi, R.; Belladonna, M. L.; Fioretti, M. C.; Grohmann, U.; Puccetti, P. SOCS3 drives proteasomal degradation of indoleamine 2,3-dioxygenase (IDO) and antagonizes IDO-dependent tolerogenesis. *Proc. Natl. Acad. Sci. U. S. A.* **2008**, *105*, 20828-20833.
18. Puccetti, P.; Grohmann, U. IDO and regulatory T cells: a role for reverse signalling and noncanonical NF- κ B activation. *Nat. Rev. Immunol.* **2007**, *7*, 817-823.

19. <https://clinicaltrials.gov/> (accessed on Nov 9, 2020)
20. Fallarini, S.; Massarotti, A.; Gesù, A.; Giovarruscio, S.; Coda Zabetta, G.; Bergo, R.; Giannelli, B.; Brunco, A.; Lombardi, G.; Sorba, G.; Pirali T. In silico-driven multicomponent synthesis of 4,5- and 1,5-disubstituted imidazoles as indoleamine 2,3-dioxygenase inhibitors. *MedChemComm* **2016**, *7*, 409-419.
21. Griglio, A.; Torre, E.; Serafini, M.; Bianchi, A.; Schmid, R.; Coda Zabetta, G.; Massarotti, A.; Sorba, G.; Pirali, T.; Fallarini, S. A multicomponent approach in the discovery of indoleamine 2,3-dioxygenase 1 inhibitors: synthesis, biological investigation and docking studies. *Bioorg. Med. Chem. Lett.* **2018**, *28*, 651-657.
22. Serafini, M.; Torre, E.; Aprile, S.; Massarotti, A.; Fallarini, S.; Pirali T. Synthesis, docking and biological evaluation of a novel class of imidazothiazoles as IDO1 inhibitors. *Molecules* **2019**, *24*, pii: E1874.
23. Serafini, M.; Torre, E.; Aprile, S.; Del Grosso, E.; Gesù, A.; Griglio, A.; Colombo, G.; Travelli, C.; Paiella, S.; Adamo, A.; Orecchini, E.; Coletti, A.; Pallotta, M. T.; Ugel, S.; Massarotti, A.; Pirali, T.; Fallarini, S. Discovery of highly potent benzimidazole derivatives as indoleamine 2, 3-dioxygenase-1 (IDO1) inhibitors: from structure-based virtual screening to in vivo pharmacodynamic activity. *J. Med. Chem.* **2020**, *63*, 3047-3065.
24. Pirali, T.; Serafini, M.; Cargnin, S.; Genazzani, A. Applications of deuterium in medicinal chemistry. *J. Med. Chem.* **2019**, *62*, 5276-5297.

Chapter 6

**Synthesis, docking and biological
evaluation of a novel class of
imidazothiazoles as IDO1 inhibitors**

Synthesis, Docking and Biological Evaluation of a Novel Class of Imidazothiazoles as IDO1 Inhibitors

Marta Serafini †, Enza Torre †, Silvio Aprile, Alberto Massarotti, Silvia Fallarini and Tracey Pirali *

Department of Pharmaceutical Sciences; Università del Piemonte Orientale, Largo Donegani 2, 28100, Novara, Italy; marta.serafini@uniupo.it (M.S.)

* Correspondence: tracey.pirali@uniupo.it; Tel.: +39-0321-375-852 (T.P.)

† These authors contributed equally to this work.

Received: date; Accepted: date; Published: date

Abstract: IDO1, a key dioxygenase in tryptophan-kynurenine metabolism, appeared in the last 10 years at the vanguard of druggable targets in cancer therapy due to its well-established role both in immune escape and inflammatory neovascularization. Among the pool of IDO1 inhibitors that have entered clinical trials, none have reached approval. The identification of novel inhibitors endowed with better clinical profile, together with the further comprehension of the interactions with residues in IDO1 active site, are still a need. In this context, we have synthesized a novel class of imidazothiazole derivatives as IDO1 inhibitors and identified three compounds with inhibitory potency in the low micromolar range. This report strengthens the role played by pocket C in the active site of IDO1, providing novel directions in the design of IDO1 inhibitors.

Keywords: indoleamine 2,3-dioxygenase 1; click chemistry; imidazothiazoles; docking

1. Introduction

The tryptophan to kynurenine catabolism and the dioxygenases that catalyse the first and rate-limiting step along the kynurenine pathway play a crucial role in the pathological immune escape [1-3]. Depletion of tryptophan and the consequent increase in kynurenines in the tumour microenvironment have been shown to enhance inflammation and lead to an immune-permissive milieu [4] as well as to promote neo-angiogenesis [5]. Among the three different isoforms of dioxygenases, IDO1, IDO2 and TDO, the former has appeared at centre-stage in the cancer field with hundreds of IDO1 inhibitors discovered in the past [6].

In the last decades checkpoint inhibitors (*i.e.* anti PD-1/PD-L1) have revolutionized the scenario of cancer immunotherapy [7]. Nevertheless, it is becoming apparent that molecules able to boost the effects of cancer immunotherapy can potentially provide superior response rates, considering that a significant proportion of patients do not respond to these drugs. Great hopes have been placed on IDO1 inhibitors with five different molecules (indoximod, navoximod, epacadostat, BMS-986205, PF-06840003) that have entered clinical trials. Currently, navoximod and PF-06840003 are in Phase I trials, while indoximod, BMS-986205

and epacadostat have reached Phase III trials for the treatment of different types of cancers (e.g. melanoma, solid tumors, malignant glioma) [6].

In 2018 the report at the [ASCO Annual Meeting](#) that epacadostat failed to show a clinical benefit in combination to pembrolizumab in unresectable or metastatic melanoma suggested to reconsider if some elements have been neglected in IDO1 landscape [8].

From a clinical point of view, the best combination regimen, the most responsive patients and the biomarkers that allow to identify them, and the most responsive tumor settings still need to be identified [9]. Additional efforts in the IDO1 field are required even from a medicinal chemistry point of view. A major challenge is the discovery of IDO1 inhibitors with optimal profiles for clinical development, especially in relation to achievement of bioavailability, maintenance of inhibition levels *in vivo*, crossing of the BBB to target brain metastases, and in-depth functional characterization. Moreover, the correlation between inhibition kinetics and *in vivo* antitumor activity is still not clear and the data that will arise during clinical trials will help to clarify if it is more effective a competitive, a non-competitive or an irreversible inhibitor. Finally, a better comprehension of the possible interactions with the residues in the IDO1 active site is needed in order to guide the rational design of other novel and potent IDO1 inhibitors.

2. Results

2.1. Chemistry

In 2014, imidazothiazole compounds were reported by Tojo *et al.* as potent IDO1 inhibitors, with the reference compound **1** (Figure 1) displaying an IC₅₀ value of 1.9 μM (rhIDO1) [10]. Taking advantage of our extensive experience both in multicomponent reactions [11,12] and click chemistry approach [13], as well as their exploitation in drug discovery [14-17], we decided to synthesize in parallel two series of imidazothiazole analogues.

The first series, published in 2018 [18], was obtained using Passerini three-component and Ugi four-component reactions. The most potent compounds are represented by **2** and **3** (Figure 1) with IC₅₀ values of 0.20 μM and 0.80 μM, respectively. Docking studies have suggested the ability of the imidazole nitrogen to coordinate the iron moiety in the heme group (Figure 2). Furthermore, the long chain protrudes in a region, named pocket C, which has never been considered by previous IDO inhibitors and a crucial hydrogen bond with Lys238 favours the inhibitory activity.

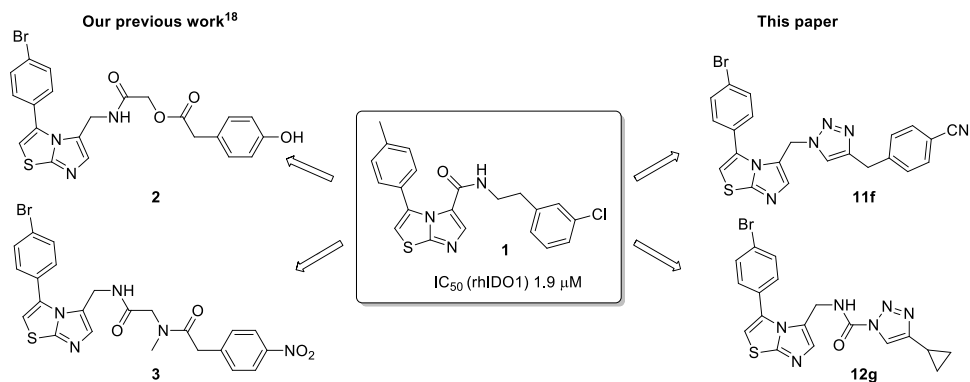


Figure 1. Structure of imidazothiazole compounds **1**, **2**, **3**, **11f** and **12g**.

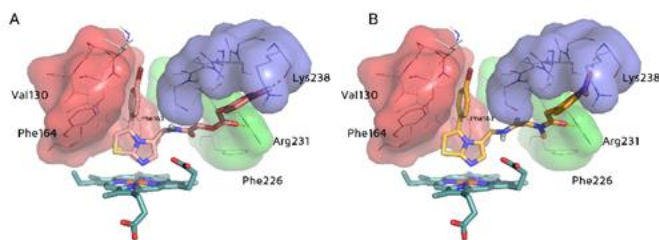
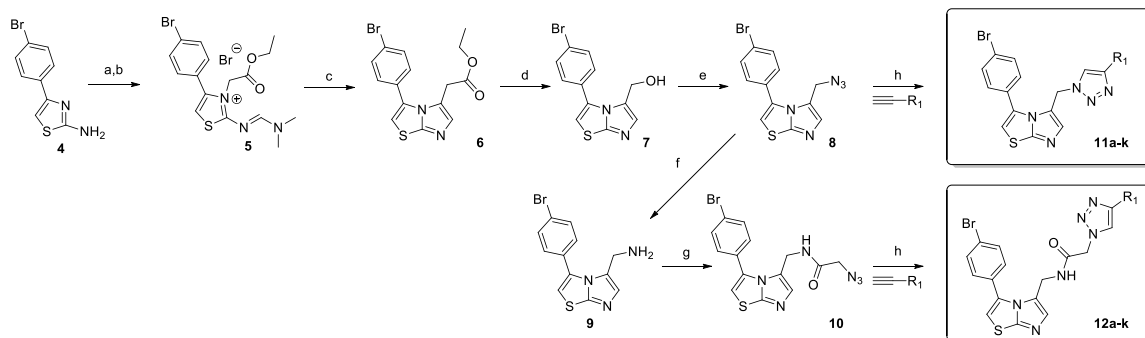


Figure 2. Docking poses of compounds **2** (A) and **3** (B). Structures are depicted as pink and orange sticks, respectively, while heme is depicted as cyan sticks. Red surface: pocket A; green surface: pocket B; blue surface: pocket C.

In the meanwhile, we wondered whether the benzamide, displayed by compounds **2** and **3**, could be isosterically replaced by a 1,4-disubstituted 1,2,3-triazole ring. It must be acknowledged that the triazole moiety has been previously described by Röhrig *et al.* [19] in IDO1 inhibitors and, more recently, in inhibitors selective for IDO2 [20]. In 2018 other triazole-displaying IDO1 inhibitors were reported [21]. In all the described examples, the nitrogen of the triazole ring makes a bond with the iron of the heme group.

With the aim to further probe interactions of the side chain of imidazothiazoles with the active site of IDO1 enzyme, and especially with pocket C, we synthesized two classes of imidazothiazoles, the first one starting from azide **8** and the second from azide **10** (Scheme 1).



Scheme 1. Reagents and conditions: (a) DMF-DMA, DMF, 80 °C, 99%; (b) ethyl bromoacetate, 80 °C, 76%; (c) DBU, DMF, 60 °C, 99%; (d) LiAlH₄, dry THF, 0 °C, 81%; (e) DPPA, DBU, DMF, 60 °C, 67%; (f) PPh₃, H₂O, THF, 45 °C, 96%; (g) 2-azidoacetic acid, EDCl, DMAP, TEA, CH₂Cl₂, 66%; (h) sodium ascorbate, CuSO₄•5H₂O, *t*-BuOH, H₂O, rt, , 41-87%.

Both the imidazothiazole azides can be easily obtained by exploiting a common synthetic route starting from 4-(4-bromophenyl)thiazol-2-amine **4** that reacts with DMF-DMA and with ethyl bromoacetate to afford intermediate **5**. **5** undergoes an intramolecular cyclization and a reduction to yield compound **7** that reacts in the presence of DPPA to form the required azide **8**. The latter is reduced *via* a Staudinger reaction and then compound **9** is coupled with 2-azidoacetic acid to form azide **10** (Scheme 1).


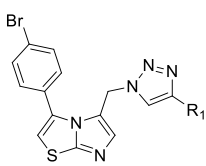
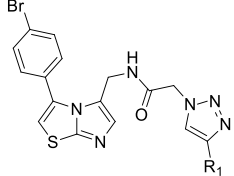
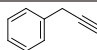
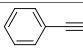
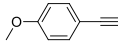
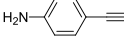
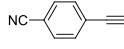
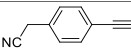

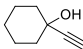
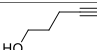
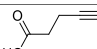
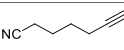
With the aim to maximize the interaction of the products in IDO1 active site, the synthetic effort was *in silico*-guided. To this end, alkynes purchasable and/or previously synthesized in our lab were virtually combined with azides **8** and **10** to generate a small library of 88 candidates that were screened in the IDO1 active site. The compounds were then ranked according to their binding energies in the IDO1 protein and the virtual candidates displaying the highest score per each of the two classes were inspected. Finally, the corresponding alkyne was selected for being coupled with both the azides **8** and **10**, for reasons of systematicity and completeness.

Following this approach, 11 alkynes were chosen, and 22 compounds were prepared exploiting the click chemistry reaction under classical conditions, eleven from azide **8** (**11a-k**) and eleven from azide **10** (**12a-k**). Products precipitated from the reaction mixture and, after filtration, were purified by column chromatography.

2.2. Biological Evaluation

All the 22 synthesized compounds were then biologically evaluated (Table 1).

Table 1. Structure and biological profile of imidazothiazoles.

R ₁ 				
	Cpd, Yield (%)	Enzymatic assay inhibition (%) at 1 μM ^a	Cpd, Yield (%)	Enzymatic assay inhibition (%) at 1 μM ^a
 a	11a , 77%	30 ± 6.7	12a , 81%	63 ± 4.3
 b	11b , 51%	35 ± 2.7	12b , 77%	61 ± 5.5
 c	11c , 87%	57 ± 13	12c , 46%	5 ± 1.2
 d	11d , 43%	17 ± 1.2	12d , 83%	56 ± 4.7
 e	11e , 83%	28 ± 1.5	12e , 76%	50 ± 4.5
 f	11f , 76%	74 ± 5.8	12f , 68%	55 ± 7.2
 g	11g , 44%	61 ± 7.1	12g , 46%	70 ± 9.2
 h	11h , 68%	35 ± 2.4	12h , 26%	63 ± 4.1
 i	11i , 45%	0	12i , 82%	45 ± 2.8
 j	11j , 41%	81 ± 7.9	12j , 42%	33 ± 4.5
 k	11k , 48%	62 ± 5.6	12k , 55%	50 ± 11

^a: the values are the mean ± SE of two independent experiments. .

The compounds were tested for their ability to inhibit human IDO1 in an enzyme-based assay using a purified recombinant human IDO1 (rhIDO1) enzyme (Table 1). Each compound (1 μM) was added to the reaction buffer and the rhIDO1 conversion of L-Trp to

L-KYN was determined spectrophotometrically using *p*-dimethylaminobenzaldehyde. As reference, imidazothiazole compound 1-((3-(4-bromophenyl)-3a*H*-thieno[2,3-*b*]pyrrol-4-yl)methyl)-3-(4-cyanophenyl)urea [10], displaying an IC₅₀ value of 0.08 μM, was chosen.

In series **11a-k**, among the aromatic substituents on the triazole ring only cyanomethylphenyl ring confers significant inhibitory activity at 1 μM (**11f**, 74%), while within the aliphatic substructures both the propanoyl and the 5-cyanopentanoyl lead to good inhibition (**11j** and **11k**, 81 and 62%, respectively). In series **12a-k** the best activity is given by the cyclopropyl substituent (**12g**, 70%), while benzyl and 1-hydroxycyclohexanyl (**12a** and **12h**) are able to give a 63% of inhibition.

IC₅₀ values were determined for compounds that displayed an inhibition above 70% (**11f**, **11j** and **12g**). Compound **11f** has an IC₅₀ value of 0.5 ± 0.04 μM, **11j** displays IC₅₀ value of 1.1 ± 0.07 μM and compound **12g** of 0.2 ± 0.01 μM.

2.3. Molecular Docking Study

Molecular modelling was exploited to understand the potential pose of imidazothiazoles in the IDO1 binding site. Docking studies were carried out using the software OMEGA2 [22-24] and FRED [25,26], showing that the most potent imidazothiazoles (**11f** and **12g**) lay with a partially different orientation than compound **2-3** (Figure 2). The *p*-bromophenyl ring of both **11f** and **12g** is accommodated in the hydrophobic pocket A (Tyr126, Cys129, Val130, Phe163 and Phe164), as for compounds **2** and **3**, while the imidazothiazole core is able to form a nitrogen-iron bond with the heme group. The triazole group extends in proximity to pocket B (Phe226 and Arg231) while the side chain derived by alkyne reagent protrudes in the direction of pocket C (Leu234, Ser235, Gly236, Lys238, Ala260, Gly261 and Gly262), without fully occupying this external part of the IDO binding site as shown by **2** and **3**. All the other compounds display similar binding modes (Supporting information Table S1): the interactions in pocket A and B are conserved among all the evaluated structures, while binding to pocket C is more compound-dependent.

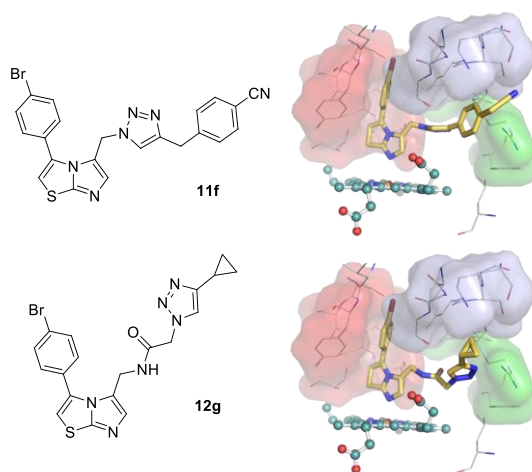


Figure 3. Structure and docking pose of the most potent imidazothiazoles **11f** and **12g**. Structures of docking poses are depicted as gold sticks, while heme is depicted as cyan

sticks. Amino acids of pocket A, B and C are depicted as red, green and blue lines shape, respectively.

3. Materials and Methods

3.1. Chemistry

3.1.1. General Chemistry

Commercially available reagents and solvents were purchased from Sigma-Aldrich and Alfa Aesar and used without further purification. Column chromatography was performed on silica gel Merck Kieselgel 70-230 mesh ASTM. Thin layer chromatography (TLC) was carried out on 5 cm × 20 cm plates with a layer thickness of 0.25 mm (Merck silica gel 60 F254). When necessary, TLC plates were visualized with aqueous KMnO₄ or with aqueous Pancaldi solution. Melting points were determined in open glass capillary with a Stuart scientific SMP3 apparatus. All the target compounds were checked by IR (FT-IR Thermo-Nicolet Avatar), ¹H- and ¹³C-NMR (Jeol ECP 300 MHz), and mass spectrometry (Thermo Finnigan LCQ-deca XP-plus) equipped with an ESI source and an ion trap detector. Chemical shifts are reported in parts per million (ppm). The purity of compounds was determined by high performance liquid chromatography (HPLC). Purity of final compounds was 95% or higher.

3.1.2. Synthesis of 2-azido-N-((3-(4-bromophenyl)imidazo[2,1-b]thiazol-5-yl)methyl)acetamide, (10).

The amine 9 (700 mg, 2.27 mmol, 1 eq) was dissolved in dry CH₂Cl₂ (12 mL) under nitrogen atmosphere. 2-Azidoacetic acid (229 mg, 2.27 mmol, 1 eq), EDCI (352 mg, 2.27 mmol, 1 eq), DMAP (28 mg, 0.23 mmol, 0.1 eq) and TEA (316 μL, 2.27 mmol, 1 eq) were added in order. The resulting mixture was stirred overnight. When the reaction was finished, CH₂Cl₂ was added and the organic layer was washed with water (2x), dried over sodium sulfate and evaporated. The crude material was purified by column chromatography using EtOAc and EtOAc/MeOH 95:5 as eluents, affording 2-azido-N-((3-(4-bromophenyl)imidazo[2,1-b]thiazol-5-yl)methyl)acetamide 10 as a white solid (66%). ¹H NMR (300 MHz, CD₃OD): δ 7.68 (d, *J* = 8.2 Hz, 2H), 7.49 (d, *J* = 8.2, 2H), 7.24 (s, 1H), 7.06 (s, 1H), 4.23 (s, 2H), 3.59 (s, 2H).

3.1.3. General procedure for the synthesis of compounds 11a-k and 12a-k

To a suspension of azide (0.29 mmol, 1 eq) in water (570 μL) and *t*-BuOH (570 μL) alkyne (0.29 mmol, 1 eq) was added. Then, 30 μL of aqueous solution of sodium ascorbate 1M and copper sulfate pentahydrate (0.0029 mmol, 0.01 eq) were added and the mixture was maintained under vigorous stirring overnight. The reaction was normally completed between 3 and 24 hours. Ice was added and the precipitate was filtered and rinsed with water and heptane. In some cases (11a, 11e, 11g, 12a, 12b, 12d, 12e, 12f, 12g, 12i, 12j, 12k) product precipitated and the precipitated solid was collected by filtration using a Buchner funnel and rinsed with ethyl acetate. In case that no precipitation was observed (11b, 11c,

11d, 11f, 11h, 11i, 11j, 11k, 12c, 12h) solvent was evaporated and the crude material was purified by column chromatography using the eluent indicated in the analytical data section.

3.1.4 Characterization of compounds **11a-k** and **12a-k**

5-((4-Benzyl-1H-1,2,3-triazol-1-yl)methyl)-3-(4-bromophenyl)imidazo[2,1-b]thiazole, (**11a**). Yellow solid. Yield: 77%. mp 106.5-107.5 °C. ¹H NMR (300 MHz, DMSO-*d*₆): δ 7.45 (d, *J* = 6.6 Hz, 2H), 7.30-7.18 (m, 9H), 7.01 (s, 1H), 5.41 (s, 2H), 3.82 (s, 2H). IR (KBr): $\tilde{\nu}$ = 3113, 2931, 1541, 1455, 1145, 1044, 1013, 844, 815 cm⁻¹. MS (ESI) *m/z* 451 [M+H]⁺.

3-(4-Bromophenyl)-5-((4-phenyl-1H-1,2,3-triazol-1-yl)methyl)imidazo[2,1-b]thiazole, (**11b**). White solid. Yield: 51%. PE/EtOAc 2:8. mp 199-199.5 °C dec. ¹H NMR (300 MHz, CD₃OD): δ 7.67 (d, *J* = 6.9 Hz, 2H), 7.50 (s, 1H), 7.47 (d, *J* = 8.5 Hz, 2H), 7.39-7.34 (m, 4H), 7.22 (d, *J* = 8.5 Hz, 2H), 6.99 (s, 1H), 5.51 (s, 2H). IR (KBr): $\tilde{\nu}$ = 3084, 2923, 2855, 1574, 1458, 1297, 1140, 1070, 755 cm⁻¹. MS (ESI) *m/z* 437 [M+H]⁺.

3-(4-Bromophenyl)-5-((4-(4-methoxyphenyl)-1H-1,2,3-triazol-1-yl)methyl)imidazo[2,1-b]thiazole, (**11c**). Yellow solid. Yield: 87%. PE/EtOAc 3:7. mp 118-119 °C dec. ¹H NMR (300 MHz, DMSO-*d*₆): δ 7.63-7.60 (m, 3H), 7.52 (d, *J* = 6.6 Hz, 2H), 7.39 (s, 1H), 7.32 (d, *J* = 7.1 Hz, 2H), 7.14 (s, 1H), 6.97 (d, *J* = 7.1 Hz, 2H), 5.61 (s, 2H), 3.78 (s, 3H). IR (KBr): $\tilde{\nu}$ = 3018, 2928, 1563, 1459, 1251, 1027, 833, 794 cm⁻¹. MS (ESI) *m/z* 467 [M+H]⁺.

4-(1-((3-(4-Bromophenyl)imidazo[2,1-b]thiazol-5-yl)methyl)-1H-1,2,3-triazol-4-yl)aniline, (**11d**). Yellow solid. Yield: 43%. EtOAc. mp 117-118 °C dec. ¹H NMR (300 MHz, DMSO-*d*₆): δ 7.55 (s, 1H), 7.43-7.35 (m, 7H), 7.17 (s, 1H), 6.60 (d, *J* = 5.5 Hz, 2H), 5.46 (s, 2H), 5.14 (br s, 2H). IR (KBr): $\tilde{\nu}$ = 3329, 3103, 2925, 1729, 1500, 1457, 1294, 836, 763 cm⁻¹. MS (ESI) *m/z* 452 [M+H]⁺.

4-(1-((3-(4-Bromophenyl)imidazo[2,1-b]thiazol-5-yl)methyl)-1H-1,2,3-triazol-4-yl)benzotrile, (**11e**). Yellow solid. Yield: 83%. mp 190-191 °C dec. ¹H NMR (300 MHz, DMSO-*d*₆): δ 8.00 (s, 1H), 7.90-7.88 (m, 5H), 7.47 (d, *J* = 7.7 Hz, 2H), 7.31 (d, *J* = 7.9 Hz, 2H), 7.18 (s, 1H), 5.60 (s, 2H). IR (KBr): $\tilde{\nu}$ = 3076, 2219, 1928, 1612, 1445, 1147, 844, 803, 555 cm⁻¹. MS (ESI) *m/z* 462 [M+H]⁺.

2-(4-(1-((3-(4-Bromophenyl)imidazo[2,1-b]thiazol-5-yl)methyl)-1H-1,2,3-triazol-4-yl)phenyl)acetonitrile, (**11f**). Yellow solid. Yield: 76%. PE/EtOAc 1:9. mp 121.5-122.5 °C. ¹H NMR (300 MHz, DMSO-*d*₆): δ 7.75-7.71 (m, 4H), 7.51 (d, *J* = 7.3 Hz, 2H), 7.40-7.30 (m, 4H), 7.19 (s, 1H), 5.58 (s, 2H), 4.06 (s, 2H). ¹³C NMR (75 MHz, DMSO-*d*₆): δ 146.1, 132.1 (3C), 131.7 (2C), 131.2, 130.5, 129.1 (2C), 126.3 (2C), 123.8, 121.2, 119.7, 112.3, 41.2, 22.8. IR (KBr): $\tilde{\nu}$ = 3100, 2963, 2105, 1487, 1456, 1149, 840, 810, 752 cm⁻¹. MS (ESI) *m/z* 476 [M+H]⁺.

3-(4-Bromophenyl)-5-((4-cyclopropyl-1H-1,2,3-triazol-1-yl)methyl)imidazo[2,1-b]thiazole, (**11g**). Yellow solid. Yield: 44%. mp 145.5-146.5 °C. ¹H NMR (300 MHz, DMSO-*d*₆): δ 7.57 (d, *J* = 8.2 Hz, 2H), 7.38 (s, 1H), 7.33 (d, *J* = 8.2 Hz, 2H), 7.18 (s, 1H), 6.97 (s, 1H), 5.38 (s, 2H), 1.76 (quint, *J* = 6.6 Hz, 1H), 0.82 (d, *J* = 6.6 Hz, 2H), 0.55 (d, *J* = 4.6 Hz, 2H). IR (KBr): $\tilde{\nu}$ = 3012, 2922, 2856, 1733, 1457, 1142, 1041, 1013, 929, 814 cm⁻¹. MS (ESI) *m/z* 401 [M+H]⁺.

1-(1-((3-(4-Bromophenyl)imidazo[2,1-b]thiazol-5-yl)methyl)-1H-1,2,3-triazol-4-yl)cyclohexanol, (**11h**). Yellow solid. Yield: 68%. PE/EtOAc 2:8. mp 163.5-164.5 °C dec. ¹H NMR (300 MHz, DMSO-*d*₆): δ 7.58 (d, *J* = 7.9 Hz, 2H), 7.43 (s, 1H), 7.35 (d, *J* = 7.9 Hz, 2H), 7.21 (s, 1H), 7.08 (s, 1H), 5.42 (s, 2H), 4.61 (br s, 1H), 1.75-1.61 (m, 6H), 1.38-1.29 (m, 4H). IR (KBr): $\tilde{\nu}$ = 3276, 2927, 1573, 1458, 1254, 979, 846, 744 cm⁻¹. MS (ESI) *m/z* 459 [M+H]⁺.

3-(1-((3-(4-Bromophenyl)imidazo[2,1-b]thiazol-5-yl)methyl)-1H-1,2,3-triazol-4-yl)propan-1-ol, (**11i**). Yellow oil. Yield: 45%. EtOAc/MeOH 8:2. ¹H NMR (300 MHz, DMSO-*d*₆): δ ¹H NMR (300 MHz, DMSO-*d*₆): δ 7.55-7.40 (m, 4H), 7.18 (d, *J* = 8.2 Hz, 2H), 6.88 (s, 1H), 5.40 (s, 2H), 5.12 (br s, 1H), 4.42 (t, *J* = 7.4 Hz, 2H), 2.53-2.51 (m, 2H), 1.64 (t, *J* = 7.4 Hz, 2H). IR (neat): $\tilde{\nu}$ = 3306, 2924, 2854, 1663, 1456, 1088, 922, 888, 701, 603 cm⁻¹. MS (ESI) *m/z* 419 [M+H]⁺.

3-(1-((3-(4-Bromophenyl)imidazo[2,1-b]thiazol-5-yl)methyl)-1H-1,2,3-triazol-4-yl)propanoic acid, (**11j**). Dark yellow solid. Yield: 41%. EtOAc:MeOH 9:1. mp 148-148.5 °C dec. ¹H NMR (300 MHz, DMSO-*d*₆): δ 7.42-7.37 (m, 4H), 7.17 (d, *J* = 8.9 Hz, 2H), 7.08 (s, 1H), 5.40 (s, 2H), 2.71 (t, *J* = 6.7 Hz, 2H), 2.45 (t, *J* = 6.7 Hz, 2H). IR (KBr): $\tilde{\nu}$ = 3180, 2923, 2853, 1715, 1457, 1307, 819, 766 cm⁻¹. MS (ESI) *m/z* 433 [M+H]⁺.

5-(1-((3-(4-Bromophenyl)imidazo[2,1-b]thiazol-5-yl)methyl)-1H-1,2,3-triazol-4-yl)pentanenitrile, (**11k**). Amorphous yellow solid. Yield: 48%. EtOAc. ¹H NMR (300 MHz, DMSO-*d*₆): δ 7.57 (s, 1H), 7.41-7.32 (m, 3H), 7.17 (d, *J* = 8.8 Hz, 2H), 7.07 (s, 1H), 5.42 (s, 2H), 2.60-2.58 (m, 2H), 1.64-1.56 (m, 6H). IR (neat): $\tilde{\nu}$ = 2932, 2258, 1573, 1454, 1144, 1045, 812, 734 cm⁻¹. MS (ESI) *m/z* 442 [M+H]⁺.

2-(4-Benzyl-1H-1,2,3-triazol-1-yl)-N-((3-(4-bromophenyl)imidazo[2,1-b]thiazol-5-yl)methyl)acetamide, (**12a**). White solid. Yield: 81%. mp 177-177.5 °C. ¹H NMR (300 MHz, DMSO-*d*₆): δ 8.34 (br s, 1H), 7.66-7.64 (m, 3H), 7.53 (d, *J* = 7.1 Hz, 2H), 7.30-7.21 (m, 6H), 4.81 (s, 2H), 4.08 (s, 2H), 4.00 (s, 2H). IR (KBr): $\tilde{\nu}$ = 3027, 2904, 2858, 1676, 1458, 1218, 1143, 1074, 1016, 815, 715 cm⁻¹. MS (ESI) *m/z* 508 [M+H]⁺.

N-((3-(4-Bromophenyl)imidazo[2,1-b]thiazol-5-yl)methyl)-2-(4-phenyl-1H-1,2,3-triazol-1-yl)acetamide, (**12b**). Yellow solid. Yield: 77%. mp 251.5-252.5 °C dec. ¹H NMR (300 MHz, DMSO-*d*₆): δ 8.44 (s, 1H), 8.37 (s, 1H), 7.85 (d, *J* = 8.2 Hz, 2H), 7.65 (d, *J* = 7.4 Hz, 2H), 7.56 (d, *J* = 8.2 Hz, 2H), 7.46 (t, *J* = 7.4 Hz, 2H), 7.36 (t, *J* = 7.4 Hz, 1H), 7.22 (s, 1H), 4.93 (s, 2H), 4.09 (s, 2H). IR (KBr): $\tilde{\nu}$ = 3283, 3063, 2931, 2785, 1652, 1548, 1454, 1149, 1072, 762, 690 cm⁻¹. MS (ESI) *m/z* 494 [M+H]⁺.

N-((3-(4-Bromophenyl)imidazo[2,1-b]thiazol-5-yl)methyl)-2-(4-(4-methoxyphenyl)-1H-1,2,3-triazol-1-yl)acetamide, (**12c**). White solid. Yield: 46%. PE/EtOAc 2:8. mp 183-184 °C. ¹H NMR (300 MHz, DMSO-*d*₆): δ 8.38 (s, 1H), 8.25 (s, 1H), 7.78 (d, *J* = 8.2 Hz, 2H), 7.68 (d, *J* = 7.9 Hz, 2H), 7.56 (d, *J* = 7.9 Hz, 2H), 7.22 (s, 1H), 7.02 (d, *J* = 8.2 Hz, 2H), 4.92 (s, 2H), 4.08 (s, 2H), 3.80 (s, 3H). IR (KBr): $\tilde{\nu}$ = 3182, 2924, 1684, 1560, 1454, 1261, 973, 833, 800 cm⁻¹. MS (ESI) *m/z* 524 [M+H]⁺.

2-(4-(4-Aminophenyl)-1H-1,2,3-triazol-1-yl)-N-((3-(4-bromophenyl)imidazo[2,1-b]thiazol-5-yl)methyl)acetamide, (**12d**). Grey solid. Yield: 83%. mp 217-218 °C dec. ¹H NMR (300 MHz, DMSO-*d*₆): δ 8.31 (s, 1H), 8.05 (s, 1H), 7.68 (d, *J* = 8.1 Hz, 2H), 7.53-7.50 (m, 4H), 7.16 (s, 1H),

6.64 (d, $J = 7.4$ Hz, 2H), 5.16 (br s, 1H), 4.87 (s, 2H), 4.35 (s, 2H). IR (KBr): $\tilde{\nu} = 3342, 3193, 2931, 1682, 1560, 1502, 1456, 1013, 835, 814$ cm⁻¹. MS (ESI) m/z 509 [M+H]⁺.

N-((3-(4-Bromophenyl)imidazo[2,1-*b*]thiazol-5-yl)methyl)-2-(4-(4-cyanophenyl)-1*H*-1,2,3-triazol-1-yl)acetamide, (**12e**). Yellow solid. Yield: 76%. mp 267-267.5 °C dec. ¹H NMR (300 MHz, DMSO-*d*₆): δ 8.60 (s, 1H), 8.47 (s, 1H), 8.07 (d, $J = 8.2$ Hz, 2H), 7.93 (d, $J = 7.9$ Hz, 2H), 7.67 (d, $J = 8.2$ Hz, 2H), 7.56 (d, $J = 7.7$ Hz, 2H), 7.23 (s, 1H), 4.97 (s, 2H), 4.09 (s, 2H). IR (KBr): $\tilde{\nu} = 3298, 3084, 3044, 2223, 1648, 1536, 1454, 1146, 846, 813$ cm⁻¹. MS (ESI) m/z 519 [M+H]⁺.

N-((3-(4-Bromophenyl)imidazo[2,1-*b*]thiazol-5-yl)methyl)-2-(4-(4-(cyanomethyl)phenyl)-1*H*-1,2,3-triazol-1-yl)acetamide, (**12f**). Yellow solid. Yield: 68%. mp 231-231.5 °C. ¹H NMR (300 MHz, DMSO-*d*₆): δ 8.44 (br s, 1H), 8.42-8.40 (m, 2H), 7.89 (d, $J = 7.7$ Hz, 2H), 7.68 (d, $J = 7.1$ Hz, 2H), 7.55 (d, $J = 7.1$ Hz, 2H), 7.43 (d, $J = 7.7$ Hz, 2H), 7.22 (s, 1H), 4.93 (s, 2H), 4.15 (s, 2H), 4.07 (s, 2H). IR (KBr): $\tilde{\nu} = 3063, 2936, 2244, 1659, 1548, 1455, 1229, 1071, 1013, 820, 794$ cm⁻¹. MS (ESI) m/z 533 [M+H]⁺.

N-((3-(4-Bromophenyl)imidazo[2,1-*b*]thiazol-5-yl)methyl)-2-(4-(cyclopropyl)-1*H*-1,2,3-triazol-1-yl)acetamide, (**12g**). White solid. Yield: 46%. mp 225-225.5 °C dec. ¹H NMR (300 MHz, DMSO-*d*₆): δ 8.35 (s, 1H), 7.68-7.63 (m, 3H), 7.54 (d, $J = 7.4$ Hz, 2H), 7.21 (s, 1H), 4.78 (s, 2H), 4.03 (s, 2H), 1.94 (quint, $J = 7.1$ Hz, 1H), 0.90 (q, $J = 7.1$ Hz, 2H), 0.72 (q, $J = 7.3$ Hz, 2H). ¹³C NMR (75 MHz, DMSO-*d*₆): δ 165.1, 146.7, 132.1 (2C), 131.9, 131.3, 129.5, 128.4, 125.7, 123.9, 123.3, 111.9, 51.6, 42.6, 8.2, 7.1. IR (KBr): $\tilde{\nu} = 3104, 2950, 2858, 1681, 1548, 1460, 1449, 1218, 1145, 1014, 818$ cm⁻¹. MS (ESI) m/z 458 [M+H]⁺.

N-((3-(4-Bromophenyl)imidazo[2,1-*b*]thiazol-5-yl)methyl)-2-(4-(1-hydroxycyclohexyl)-1*H*-1,2,3-triazol-1-yl)acetamide, (**12h**). Yellow solid. Yield: 26%. EtOAc/MeOH 9:1. mp 165-166 °C. ¹H NMR (300 MHz, DMSO-*d*₆): δ 8.35 (s, 1H), 7.73-7.70 (m, 3H), 7.58 (d, $J = 7.9$ Hz, 2H), 7.23 (s, 1H), 4.85 (s, 2H), 4.06 (s, 2H), 2.00-1.92 (m, 4H), 1.73-1.64 (m, 4H), 1.46-1.42 (m, 2H). IR (KBr): $\tilde{\nu} = 3144, 3043, 2933, 1697, 1558, 1458, 1251, 1071, 846, 809$ cm⁻¹. MS (ESI) m/z 516 [M+H]⁺.

N-((3-(4-Bromophenyl)imidazo[2,1-*b*]thiazol-5-yl)methyl)-2-(4-(3-hydroxypropyl)-1*H*-1,2,3-triazol-1-yl)acetamide, (**12i**). White solid. Yield: 82%. mp 169-170 °C dec. ¹H NMR (300 MHz, DMSO-*d*₆): δ 8.30 (s, 1H), 7.68-7.66 (m, 3H), 7.54 (d, $J = 7.8$ Hz, 2H), 7.19 (s, 1H), 4.82 (s, 2H), 4.43 (br s, 1H), 4.17 (s, 2H), 3.46 (t, $J = 7.1$ Hz, 2H), 2.67 (quint, $J = 7.1$ Hz, 2H), 1.76 (t, $J = 7.1$ Hz, 2H). IR (KBr): $\tilde{\nu} = 3250, 3107, 2935, 1679, 1544, 1459, 1219, 1072, 816$ cm⁻¹. MS (ESI) m/z 476 [M+H]⁺.

3-(1-(2-(((3-(4-Bromophenyl)imidazo[2,1-*b*]thiazol-5-yl)methyl)amino)-2-oxoethyl)-1*H*-1,2,3-triazol-4-yl)propanoic acid, (**12j**). White solid. Yield: 42%. mp 153-154 °C dec. ¹H NMR (300 MHz, DMSO-*d*₆): δ 8.02 (s, 1H), 7.70-7.67 (m, 3H), 7.53 (d, $J = 8.0$ Hz, 2H), 7.19 (s, 1H), 4.81 (s, 2H), 4.12 (s, 2H), 3.51 (t, $J = 6.2$ Hz, 2H), 2.64-2.58 (m, 2H). IR (KBr): $\tilde{\nu} = 3265, 3056, 1663, 1551, 1457, 1144, 838, 813$ cm⁻¹. MS (ESI) m/z 490 [M+H]⁺.

N-((3-(4-Bromophenyl)imidazo[2,1-*b*]thiazol-5-yl)methyl)-2-(4-(4-cyanobutyl)-1*H*-1,2,3-triazol-1-yl)acetamide, (**12k**). White solid. Yield: 55%. mp 179.5-180.5 °C. ¹H NMR (300 MHz, DMSO-*d*₆): δ 8.32 (s, 1H), 7.70-7.67 (m, 3H), 7.56 (d, $J = 7.1$ Hz, 2H), 7.22 (s, 1H), 4.85 (s, 2H), 4.09 (s,

2H), 2.69 (t, $J = 6.1$ Hz, 2H), 1.69-1.64 (m, 6H). IR (KBr): $\tilde{\nu} = 3280, 2929, 2244, 1680, 1655, 1547, 1452, 1219, 1014, 817$ cm⁻¹. MS (ESI) m/z 499 [M+H]⁺.

3.2. Biology

rhIDO1 enzymatic assay. rhIDO1 activity was determined as follows. In brief, the standard reaction mixture (200 μ L) contained 50 mM potassium phosphate buffer (KPB) (pH 6.5), 20 mM ascorbic acid (neutralized with NaOH and HCl) (Sigma Aldrich), 100 μ g/mL catalase (Sigma Aldrich), 10 μ M methylene blue (Alfa Aesar, Heysham, Lancashire, United Kingdom), 100 μ M L-tryptophan (Sigma Aldrich), 50 nM rhIDO1 (Origene, Bologna, Italy), and dimethyl sulfoxide (DMSO) solution of the compound (4 μ L). The reaction was carried out at 37 °C for 60 min and stopped by the addition of 40 μ L of 30% (w/v) CCl₃COOH. After heating at 50 °C for 15 min, the reaction mixture was centrifuged at 1500 g for 10 min. The supernatant (150 μ L) was transferred into a well of a 96-well microplate and mixed with 150 μ L of 2% (w/v) *p*-dimethylaminobenzaldehyde (Ehrlich's reagent) in acetic acid. The yellow pigment derived from kynurenine was measured at 490 nm using an Ultramark Microplate Imaging System (Bio-Rad). IC₅₀ values were calculated from concentration-response curves obtained in at least three different experiments run in triplicate.

3.3. Docking Study

Protein preparation. Crystal structure of human IDO1 in complex with compound **1** (PDB ID: 4PK6) [10], resolved using X-ray diffraction method with a resolution of 3.45 Å, was retrieved from Protein Data Bank (www.rcsb.org). Despite other X-ray crystal structures have been reported with a better resolution value, the considered crystal structure has a different conformation of the aminoacids in the binding site (mostly in pocket B) that, as already reported, can better accommodate the parental compounds **2-3**, since they were designed on structure **1**, the co-crystallized compound in PDB 4PK6. Retrieved structure has been further modified for docking calculations as follows: compound **1** was removed, polar hydrogens were added to the protein complex and the resulting polar hydrogens were optimized using the MolProbability server [27].

Compound preparation. Alkynes available in house (44 compounds) were considered and virtually combined with azides **8** and **10**. The generated virtual library (88 compounds) was prepared according to our previously reported docking procedure [17], 3D conformations of compounds were generated with the program OMEGA2 [22-24].

Docking procedure. The FRED software was used in order to dock the compounds in the IDO1 binding site [25, 26]. The center of the binding pocket considered in the study was set in the geometrical center of the original co-crystallized compound (Cmp. **1**), standard setting of FRED was used and the Chemgauss4 scores were considered to evaluate the docking poses. The representation of protein structures and docking results were generated using PyMOL software [28].

4. Conclusions

In conclusion, following a common synthetic route, two series of imidazothiazoles have been synthesized by a click chemistry approach. Three compounds show inhibitory activity

on IDO1 in the enzyme-based assay in the low micromolar range. Compound **12g** displays a ten-fold higher inhibitory activity ($IC_{50} = 0.2 \mu\text{M}$) compared to the starting compound ($IC_{50} = 1.9 \mu\text{M}$). Moreover, it is characterized by a peculiar binding mode that sees the side chain protruding into an additional pocket, named C and located in the most external part of the IDO binding site. Unfortunately, and similarly to what was observed in the case of imidazothiazoles reported by Tojo [10] and of compounds **2** and **3** discovered in our laboratory [18], these molecules are not able to significantly permeate the cell and to inhibit IDO1 in a cell-based assay (data not shown).

Overall, the information acquired both in this study and in our previous work [18] provides new insights in the field of IDO1 inhibitors. Indeed, we have demonstrated that pocket C can be exploited in the design of next generations of IDO1 inhibitors. The integration of this information in a structure-based virtual screening performed in our laboratory has recently led to the identification of structurally novel IDO1 inhibitors with cellular potency in the low nanomolar level and improved clinical potential. These further studies will be reported in due course.

Supplementary Materials: The following are available online. Table S1: Structure and biological profile of compounds evaluated by molecular docking.

Author Contributions: M.S., E.T. and S.A. performed the experiments; A.M., S.F., and T.P. designed the experiment, analysed the data and wrote the manuscript.

Funding: This research was funded by Università del Piemonte Orientale (Ricerca Locale DSF 2016). M.S. is supported by Associazione Italiana per la Ricerca sul Cancro (AIRC) fellowship for Italy.

Conflicts of Interest: The authors declare no conflict of interest.

References

1. Platten, M.; Wick, W.; Van den Eynde, B. J. Tryptophan Catabolism in Cancer: Beyond IDO and Tryptophan Depletion. *Cancer Res.* **2012**, *72*, 5435-5440.
2. Prendergast, G. C.; Smith, C.; Thomas, S.; Mandik-Nayak, L.; Laury-Kleintop, L.; Metz, R.; Muller, A. J. Indoleamine 2,3-dioxygenase Pathways of Pathogenic Inflammation and Immune Escape in Cancer. *Cancer Immunol. Immunother.* **2014**, *63*, 721-735.
3. Gostner, J. M.; Becker, K.; Uberall, F.; Fuchs, D. The Potential of Targeting Indoleamine 2,3-dioxygenase for Cancer Treatment. *Expert Opin. Ther. Targets* **2015**, *19*, 606-615.
4. Prendergast, G. C.; Mondal, A.; Dey, S.; Laury-Kleintop, L. D.; Muller, A. J. Inflammatory Reprogramming with IDO1 Inhibitors: Turning Immunologically Unresponsive 'Cold' Tumors 'Hot'. *Trends Cancer* **2018**, *4*, 38-58.
5. Mondal, A.; Smith, C.; DuHadaway, J. B.; Sutanto-Ward, E.; Prendergast, G. C.; Bravo-Nuevo, A.; Muller, A. J. IDO1 is an Integral Mediator of Inflammatory Neovascularization. *EBioMedicine* **2016**, *14*, 74-82.
6. Prendergast, G. C.; Malachowski, W. P.; DuHadaway, J. B.; Muller, A. J. Discovery of IDO1 Inhibitors: From Bench to Bedside. *Cancer Res.* **2017**, *77*, 6795-6811.
7. Ribas, A.; Wolchok, J. D. Cancer Immunotherapy Using Checkpoint Blockade. *Science* **2018**, *359*, 1350-1355.

8. Epacadostat (E) plus pembrolizumab (P) versus pembrolizumab alone in patients (pts) with unresectable or metastatic melanoma: Results of the phase 3 ECHO-301/KEYNOTE-252 study. *2018 ASCO Annual Meeting, J. Clin. Oncol.* **2018**, *36*,(suppl; abstr 108).
9. Garber, K. A New Cancer Immunotherapy Suffers a Setback. *Science* **2018**, *360*, 588.
10. Tojo, S.; Kohno, T.; Tanaka, T.; Kamioka, S.; Ota, Y.; Ishii, T.; Kamimoto, K.; Asano, S.; Isobe, Y. Crystal Structures and Structure-Activity Relationships of Imidazothiazole Derivatives as IDO1 Inhibitors. *ACS Med. Chem. Lett.* **2014**, *5*, 1119–1123.
11. Dömling, A.; Wang, W.; Wang, K. Chemistry and Biology Of Multicomponent Reactions. *Chem. Rev.* **2012**, *112*, 3083-3135.
12. Zarganes-Tzizikas, T.; Dömling, A. Modern Multicomponent Reactions for Better Drug Syntheses. *Org. Chem. Front.* **2014**, *1*, 834-837.
13. Tron, G. C.; Pirali, T.; Billington, R. A.; Canonico, P. L.; Sorba, G.; Genazzani, A. A. Click Chemistry Reactions in Medicinal Chemistry: Applications Of the 1,3-Dipolar Cycloaddition Between Azides and Alkynes. *Med. Res. Rev.* **2008**, *28*, 278-308.
14. Riva, B.; Griglio, A.; Serafini, M.; Cordero-Sanchez, C.; Aprile, S.; Di Paola, R.; Gugliandolo, E.; Alansary, D.; Biocotino, I.; Lim, D.; Grosa, G.; Galli, U.; Niemeyer, B.; Sorba, G.; Canonico, P. L.; Cuzzocrea, S.; Genazzani, A. A.; Pirali, T. Pyrtriazoles, a Novel Class of Store-Operated Calcium Entry Modulators: Discovery, Biological Profiling, and in Vivo Proof-of-Concept Efficacy in Acute Pancreatitis. *J. Med. Chem.* **2018**, *61*, 9756-9783.
15. Serafini, M.; Griglio, A.; Aprile, S.; Seiti, F.; Travelli, C.; Pattarino, F.; Grosa, G.; Sorba, G.; Genazzani, A. A.; Gonzalez-Rodriguez, S.; Butron, L.; Devesa, I.; Fernandez-Carvajal, A.; Pirali, T.; Ferrer-Montiel, A. Targeting Transient Receptor Potential Vanilloid 1 (TRPV1) Channel Softly: The Discovery of Passerini Adducts as a Topical Treatment for Inflammatory Skin Disorders. *J. Med. Chem.* **2018**, *61*, 4436-4455.
16. Pirali, T.; Ciraolo, E.; Aprile, S.; Massarotti, A.; Berndt, A.; Griglio, A.; Serafini, M.; Mercalli, V.; Landoni, C.; Campa, C. C.; Margaria, J. P.; Silva, R. L.; Grosa, G.; Sorba, G.; Williams, R.; Hirsch, E.; Tron, G. C. Identification of a Potent Phosphoinositide 3-Kinase Pan Inhibitor Displaying a Strategic Carboxylic Acid Group and Development of Its Prodrugs. *ChemMedChem* **2017**, *12*, 1542-1554.
17. Fallarini, S.; Massarotti, A.; Gesù, A.; Giovarruscio, S.; Coda Zabetta, G.; Bergo, R.; Giannelli, B.; Brunco, A.; Lombardi, G.; Sorba, G.; Pirali, T. *In Silico*-Driven Multicomponent Synthesis Of 4,5- and 1,5-Disubstituted Imidazoles as Indoleamine 2,3-Dioxygenase Inhibitors. *Med. Chem. Commun.* **2016**, *7*, 409-419.
18. Griglio, A.; Torre, E.; Serafini, M.; Bianchi, A.; Schmid, R.; Coda Zabetta, G.; Massarotti, A.; Sorba, G.; Pirali, T.; Fallarini, S. A Multicomponent Approach in the Discovery of Indoleamine 2,3-Dioxygenase 1 Inhibitors: Synthesis, Biological Investigation and Docking Studies. *Bioorg. Med. Chem. Lett.* **2018**, *28*, 651-657.
19. Röhrig, U. F.; Majjigapu, S. R.; Grosdidier, A.; Bron, S.; Stroobant, V.; Pilotte, L.; Colau, D.; Vogel, P.; Van den Eynde, B. J.; Zoete, V.; Michielin, O. Rational Design of 4-Aryl-1,2,3-Triazoles for Indoleamine 2,3-Dioxygenase 1 Inhibition. *J. Med. Chem.* **2012**, *55*, 5270-5290.
20. Röhrig, U. F.; Majjigapu, S. R.; Caldelari, D.; Dilek, N.; Reichenbach, P.; Ascencao, K.; Irving, M.; Coukos, G.; Vogel, P.; Zoete, V.; Michielin, O. 1,2,3-Triazoles as Inhibitors Of Indoleamine 2,3-Dioxygenase 2 (IDO2). *Bioorg. Med. Chem. Lett.* **2016**, *26*, 4330-4333.
21. Alexandre, J. A.; Swan, M. K.; Latchem, M. J.; Boyall, D.; Pollard, J. R.; Hughes, S. W.; Westcott, J. New 4-Amino-1,2,3-Triazole Inhibitors of Indoleamine 2,3-Dioxygenase Form a Long-Lived

- Complex with the Enzyme and Display Exquisite Cellular Potency. *ChemBioChem* **2018**, *19*, 552-561.
22. OMEGA, version 2.4.6, OpenEye Scientific Software, Santa Fe, NM, <http://www.eyesopen.com>.
 23. Hawkins, P. C. D.; Skillman, A. G.; Warren, G. L.; Ellingson, B. A.; Stahl, M. T. Conformer Generation with OMEGA: Algorithm and Validation Using High Quality Structures from the Protein Databank and Cambridge Structural Database. *J. Chem. Inf. Model.* **2010**, *50*, 572–584.
 24. Hawkins, P. C. D.; Nicholls, A. Conformer Generation with OMEGA: Learning from the Data Set and the Analysis of Failures. *J. Chem. Inf. Model.* **2012**, *52*, 2919-2936.
 25. FRED, version 3.0.0, OpenEye Scientific Software, Santa Fe, NM, <http://www.eyesopen.com>.
 26. McGann, M. FRED Pose Prediction and Virtual Screening Accuracy. *J. Chem. Inf. Model.* **2011**, *51*, 578–596.
 27. Davis, I. W.; Leaver-Fay, A.; Chen, V. B.; Block, J. N.; Kapral, G. J.; Wang, X.; Murray, L. W.; Arendall, W. B.; Snoeyink, J.; Richardson, J. S.; Richardson, D. C. MolProbity: All-Atom Contacts and Structure Validation for Proteins and Nucleic Acids. *Nucleic Acids Res.* **2007**, *35*, 375–383.
 28. The PyMOL Molecular Graphics System, version 1.3, Schrödinger LLC, 2010.

Sample Availability: Samples of the compounds **11f** and **12g** are available from the authors.

Author contributions

Article: Synthesis, docking and biological evaluation of a novel class of imidazothiazoles as IDO1 inhibitors. *Molecules* **2019**, *24*, pii: E1874.

Author 1: Marta Serafini

Performed the synthesis of the compounds, wrote the paper

Author 2: Enza Torre

Performed the *in vitro* characterization of the compounds, wrote the paper

Author 3: Silvio Aprile

Performed the analysis

Author 4: Alberto Massarotti

Performed the *in-silico* experiments

Author 5: Silvia Fallarini

Supervision, project administration

Author 6: Tracey Pirali

Designed the experiments, funding acquisition, wrote the paper

Chapter 7

Discovery of highly potent benzimidazole derivatives as indoleamine 2,3-dioxygenase-1 (IDO1) inhibitors: from structure-based virtual screening to *in vivo* pharmacodynamic activity

Discovery of highly potent benzimidazole derivatives as indoleamine 2,3-dioxygenase-1 (IDO1) inhibitors: from structure-based virtual screening to *in vivo* pharmacodynamic activity

Marta Serafini,^{1‡} Enza Torre,^{1‡} Silvio Aprile,¹ Erika Del Grosso,¹ Alessandro Gesù,¹ Alessia Griglio,¹ Giorgia Colombo,¹ Cristina Travelli,² Salvatore Paiella,³ Annalisa Adamo,⁴ Elena Orecchini,⁵ Alice Coletti,⁶ Maria Teresa Pallotta,⁵ Stefano Ugel,⁴ Alberto Massarotti,^{1*} Tracey Pirali^{1*} and Silvia Fallarini¹

¹ Department of Pharmaceutical Sciences; Università del Piemonte Orientale; Novara, 28100; Italy; ² Department of Pharmaceutical Sciences, Università degli Studi di Pavia, Pavia, 27100, Italy; ³ General and Pancreatic Surgery, Pancreas Institute; University of Verona, Verona, Italy 37134; ⁴ University Hospital and Department of Medicine, Section of Immunology; University of Verona, Verona, Italy 37126; ⁵ Department of Experimental Medicine; University of Perugia; Perugia, 06132; Italy; ⁶ Department of Medicine; University of Perugia, Piazza Lucio Severi 1, 06132 Perugia, Italy

ABSTRACT

In this study, a successful medicinal chemistry campaign that exploited virtual, biophysical and biological investigations led to the identification of a novel class of IDO1 inhibitors based on a benzimidazole substructure. This family of compounds is endowed with an extensive bonding network in the protein active site, including the interaction with pocket C, a region not commonly exploited by previously reported IDO1 inhibitors. The tight packing of selected compounds within the enzyme contributes to the strong binding interaction with IDO1, to the inhibitory potency at the low nanomolar level in several tumoral settings and to the selectivity towards IDO1 over TDO and CYPs. Notably, a significant reduction of L-Kyn levels in plasma, together with a potent effect on abrogating immunosuppressive properties of MDSC-like cells isolated from patients affected by pancreatic ductal adenocarcinoma, were observed, pointing to this class of molecules as a valuable template for boosting the antitumor immune system.

Introduction

Cancer immunotherapy is well-established as an effective clinical option for cancer treatment, alongside surgery, chemotherapy and radiation.¹ Indeed, immune checkpoint inhibitors (targeting CTLA-4 or PD-1/PD-L1 pathways) have become first-line therapies in advanced non-small cell lung cancer and melanoma.²

Nevertheless, this approach has shown substantial benefit to only some of the patients, while the rest do not respond, and even the patients that have initially a benefit might fail to respond in later stages. Mechanisms underlying resistance to cancer immunotherapy are complex and still under debate, but most of them rely on the immunosuppressive tumor microenvironment.³ Therefore, the search for novel strategies able to boost the antitumor immune system and make cancer immunotherapy more versatile, durable and effective is an urgent need.⁴ In this context, among the different combinatorial approaches that reverse tumor immunosuppression, the inhibition of indoleamine 2,3-dioxygenase-1 (IDO1) has taken center stage.

IDO1 is an intracellular enzyme catalyzing the first, rate-limiting step of tryptophan (L-Trp) catabolism resulting in the production of L-kynurenine (L-Kyn). IDO1 is expressed by primary and metastatic tumor cells, intra-tumoral endothelial cells, immune cells of peri-tumoral stroma and tumor-draining lymph nodes. This enzyme is a key mediator in the establishment of tumor immune escape through different mechanisms.⁵ In particular, L-Trp degradation and L-Kyn production induce: a) inhibition of mTOR1⁶ and activation of GCN2,⁷ resulting in dysfunction and apoptosis of T effector cells; b) suppression of NK cell proliferation and functions;⁸ c) differentiation and activation of regulatory T (Treg) cells,⁹ tolerogenic dendritic (DC)¹⁰ and myeloid-derived suppressor cells (MDSCs);¹¹ d) tumor neovascularization.¹² Moreover, IDO1 expression and/or activity have been

observed in several cancer types and are well correlated with poor prognosis and low survival of patients.¹³

Recently, a better understanding of the molecular pathways linking L-Trp catabolism and tumor immune tolerance has provided novel potential targets. In particular, L-Trp dioxygenase (TDO), initially thought to be expressed only in liver, can be found in some other tumor types (*e.g.* glioblastoma, breast cancer). Furthermore, preliminary *in vitro* studies revealed its involvement in tumor induce immune tolerance,¹⁴ tumor cell resistance to *anoikis*, and metastatic prowess.¹⁵ Besides TDO, IDO2, whose functions are currently under investigation, is overexpressed in tumor microenvironment, functionally enabling IDO1-dependent Treg and tolerogenic DC generation and contributing to B cell-mediated autoantibody production. This latter aspect is an important issue in the development of those types of cancer that rely upon B-cell to induce inflammation.¹⁶

Among the three L-Trp metabolizing enzymes, most attention has been paid to IDO1 and over the last decades thousands of compounds have been reported as IDO1 selective inhibitors in cancer immunotherapy.¹⁷ Only few have reached clinical trials, and none of these has been approved so far, suggesting that the identification of potent and clinically useful IDO1 inhibitors is an open challenge.¹⁸ Epacadostat (**1**, INCB024360, Figure 1),¹⁹ indoximod (**2**, 1-methyl-D-tryptophan, Figure 1),²⁰ navoximod (**3**, NLG-919, Figure 1),²¹ EOS-200271 (**4**, PF-06840003, Figure 1)²² and BMS-986205 (**5**, Figure 1) have been/are currently being tested in human clinical trials.

Based on promising results in Phase 1/2 studies, epacadostat has proceeded to Phase 3 trial (ECHO-301) in combination with pembrolizumab in metastatic melanoma.²³ Recent results coming from the pivotal Phase 3 of ECHO-301 have shown no indication that epacadostat provides an increased benefit compared to pembrolizumab alone, questioning the effectiveness of IDO1 inhibitors.²⁴ This failure led to the interruption of other phase III trials and to reconsider whether some elements had been neglected in the landscape of IDO1 inhibitors.²⁵ Among them, a nodal point lies in the identification of biomarkers to stratify patients that respond better to this therapy. In this regard, the detection of IDO1 expression and L-Kyn/L-Trp levels in tumor and metastatic cells, as well as in peripheral blood mononuclear cells (PBMCs), would represent good prognostic and response markers.²⁶

On a different note, availability of novel IDO1 inhibitors with different profiles in terms of PD and PK properties may be necessary to restore hope to IDO1 inhibition and achieve clinical benefit. Prompted by the challenge of discovering novel and effective IDO1 inhibitors, we have performed a medicinal chemistry campaign that has started with a structure-based virtual screening approach and has led to the identification of potent benzimidazole derivatives.

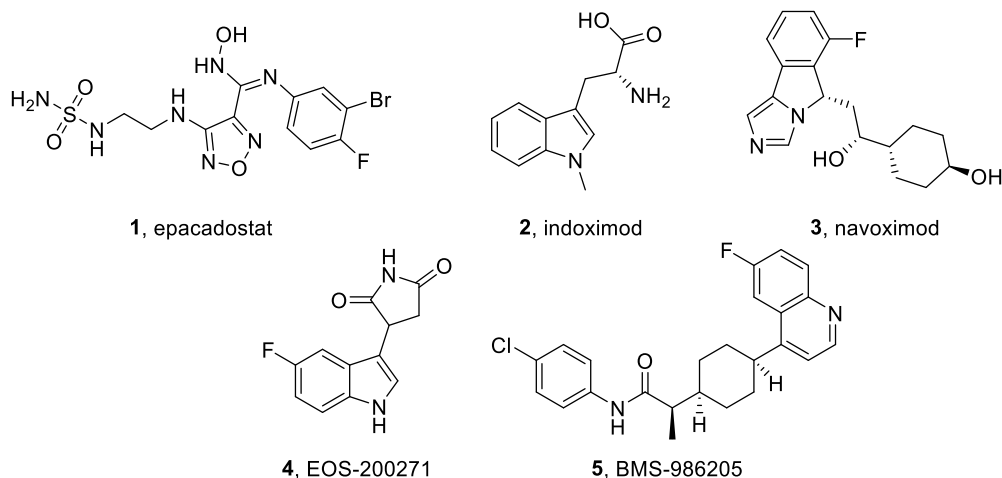


Figure 1. Chemical structures of IDO inhibitors that have reached clinical development.

Results

Structure-based virtual screening

Most IDO1 inhibitors are characterized by a binding mode that exploits the coordination with heme iron and the interaction with pocket A, a large lipophilic pocket localized above the sixth coordination site of the iron-heme, and pocket B, a lipophilic area located at the binding site entrance (for a representation of IDO1 active site see Figure 2).^{18b} In 2018 our research group published a class of imidazothiazoles featuring a peculiar binding mode in the IDO1 active site, with the side chain protruding into an additional pocket, named C, where a crucial hydrogen bond is formed with Lys238.²⁷ We therefore integrated this novel information in a structure-based virtual screening. To this aim, all the bioactivity data of already known tested molecules were extracted and downloaded from scientific literature,

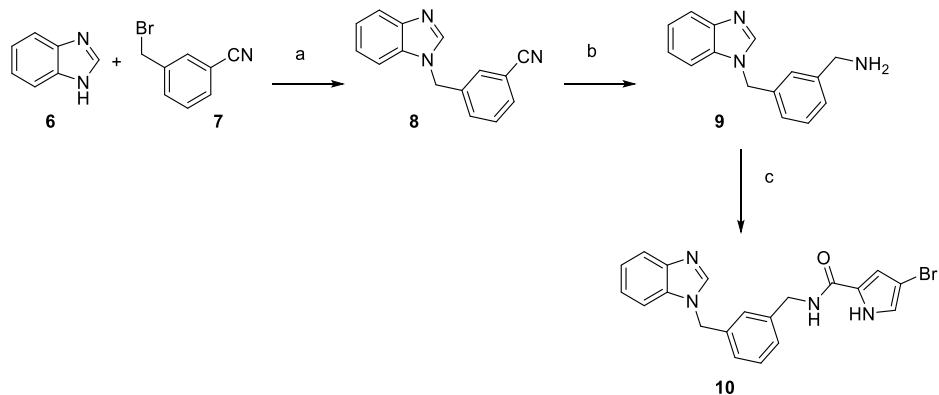
following an approach already reported in our previous paper,²⁸ in order to validate the protocol. The database chosen for our screening purpose was ZINC15,²⁹ which contains readily purchasable and drug-like compounds. OMEGA2 program was used to generate a maximum of 500 conformations for each molecule with a root mean square deviation (RMSD) of 0.8 Å between conformers. The processed database was docked into IDO1 active site (PDB structure 2D0T) with HYBRID³⁰ using default parameters, the results were sorted using the predicted binding energy (Chemgauss4), and duplicates were removed. The top ranked 500 molecules were analyzed by visual inspection and by evaluating their pose in the active site of IDO1. Among them, the first 50 commercially available molecules were selected and purchased from eMolecules®.³¹

Evaluation of cellular inhibitory activity and identification of compound 10

All the purchased molecules were tested for their IDO1 inhibition activity in a cell-based assay. The melanoma derived A375 cell line was used as cellular model, since it expresses high levels of IDO1 (RT-PCR) and L-Kyn (HPLC) when treated with recombinant human IFN- γ .^{27a} For the first screening, A375 cells were untreated/treated with 10 μ M of each compound for 48 h and L-Kyn levels were measured. A number of ten compounds out of 50 displayed an inhibitory activity >30% at the tested concentration and in all cases cell viability was >85%, confirming that the observed reduction in L-Kyn levels was not related to direct compound cytotoxicity. For the seven most active compounds, the IC₅₀ value was determined

in the cell-based assay (see Supporting Information for the IC₅₀ values) and ranged from 4.4 μM to 0.0016 μM. The seven identified compounds displayed no similarities in their structures and, among them, the most potent molecule was **10** (Figure 2B), with an IC₅₀ value of 16 nM. We therefore decided to focus our efforts on this hit, prompted by the fact that it was a novel chemotype (while other emerged compounds had already been reported in the literature), that it was far more potent than the other identified molecules (with at least a ten-fold lower IC₅₀ compared to the other emerged compounds), and that no IDO1 inhibitor with similar structure had been previously described.

To validate our discovery, the hit was synthesized in our laboratory according to Scheme 1. The synthetic protocol afforded the desired amine **9** in two steps: substitution between 1*H*-benzo[*d*]imidazole and 3-(bromomethyl)benzotrile and subsequent reduction of the aromatic nitrile **8**. Coupling between intermediate **9** and 4-bromo-1*H*-pyrrole-2-carboxylic acid provided **10** in good yield, highlighting the high synthetic feasibility displayed by our hit. The compound was re-tested at the same conditions and its potency was in accordance with the compound purchased from eMolecules[®].



Scheme 1. Re-synthesis of the hit compound **10**.

Reagents and conditions: (a) KOH, acetone, 60 °C, 4 h, 99%. (b) LiAlH₄, dry THF, 65 °C - rt, 18 h, 70%. (c) TEA, HOBt, EDCI, 4-bromo-1*H*-pyrrole-2-carboxylic acid, dry CH₂Cl₂, rt, 18 h, 50%.

Ligand binding experiments

In order to confirm target engagement of IDO1 by compound **10**, binding experiments were carried out using MicroScale Thermophoresis (MST) assays on recombinant human IDO1.³² Epacadostat (**1**) was used as positive control in this assay. As a result, a low dissociation constant was found for **10** ($K_d = 0.55 \pm 0.36$ μM; see Supporting Information), whereas a higher dissociation constant was determined for epacadostat (**1**, $K_d = 3.46 \pm 0.86$ μM, see Supporting Information). The K_d value of compound **10** suggests that it does bind to IDO1, and therefore proves a direct target engagement, accounting for the potent reduction of L-Kyn production in melanoma derived A375 cell line.

Docking pose and SAR study of compound 10

The docking pose of **10** (Figure 2) reveals a peculiar putative binding mode: the benzimidazole group is accommodated in pocket A (Tyr126, Cys129, Val130, Phe163 and Phe164) and its nitrogen coordinates the iron of the heme group. In contrast with other reported inhibitors, pocket B (Phe226, Arg231 and Ser235) is not fully exploited since the phenyl ring is located in the proximity of this pocket. Here, the carbonyl group establishes a hydrogen bond with Ser235. Two additional hydrogen bonds are formed between the carboxylic moiety of the heme group and both the amide and the pyrrole NH moieties. The long side-chain protrudes from the solvent-exposed region of the active site towards pocket C, with the bromine that forms a putative halogen bond with the close carbonyl group of Lys238.³³

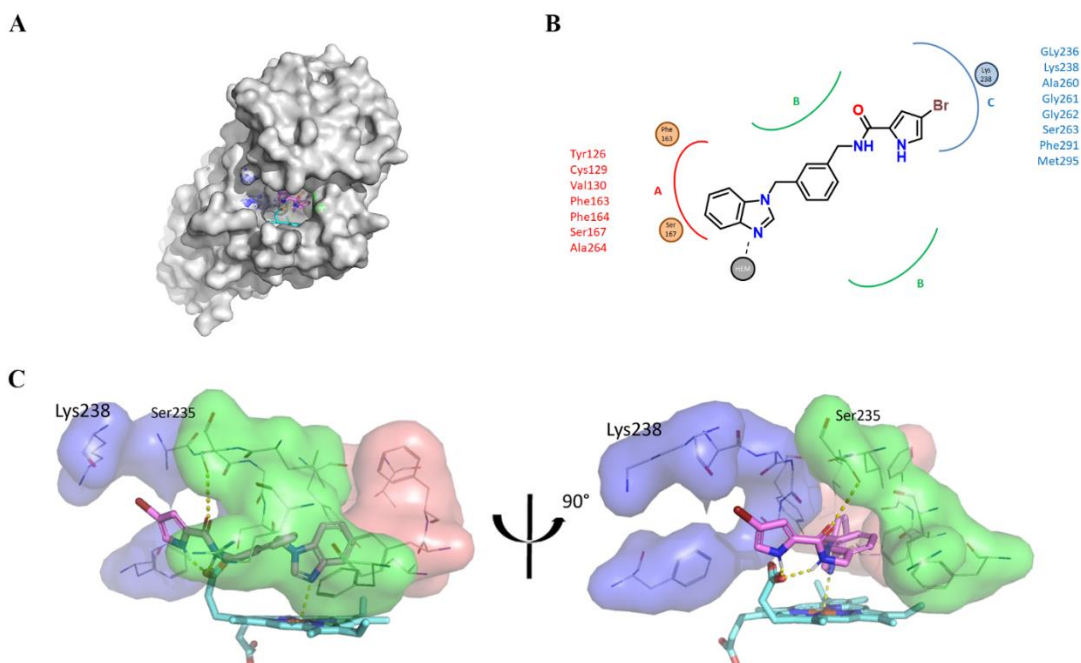
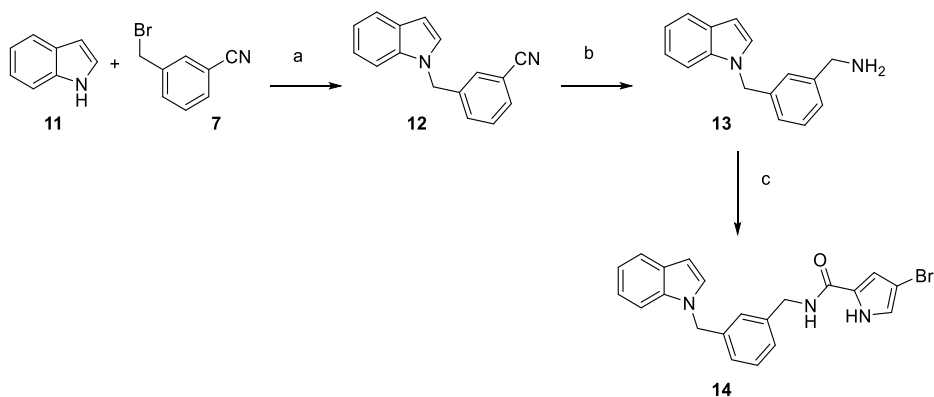


Figure 2. Structure and docking pose of the identified hit compound **10**. (A) Location of the binding region on IDO1 crystal structure (PDB id: 2D0T); (B) Schematic representation of predicted interactions of compound **10** within IDO1 binding pockets; (C) Docking pose of hit compound **10**. Aminoacids of pocket A, pocket B and pocket C are depicted in red, green and blue respectively. Heme group and compound **10** are depicted as cyan and pink sticks.

Starting from the scaffold of compound **10** and its putative binding mode, a SAR study was undertaken, with the aim of validating the predicted interactions by chemical modification of **10** and biological evaluation of the obtained analogues. The synthesized analogues were tested as IDO1 inhibitors in a cellular-based assay. The A375 cells unstimulated/stimulated with recombinant human IFN- γ were untreated/treated with 1 μ M of each compound for 48 h and L-Kyn levels were measured by HPLC.^{27a} For compounds showing an inhibitory activity >80% and cell viability >80% the concentration/response curves were determined and IC₅₀ values calculated (Table 1).

First of all, in order to investigate the role of the nitrogen of the benzimidazole in the coordination with the iron of the heme group, compound **14** was synthesized. Substitution between 1*H*-indole and 3-(bromomethyl)benzonitrile and subsequent reduction of the nitrile group afforded the intermediate **13**, that, after coupling with 4-bromo-1*H*-pyrrole-2-carboxylic acid, yielded compound **14** (Scheme 2). As expected, the inhibitory activity was completely abolished (0% of inhibition, Table

1), confirming that the presence of the benzimidazole ring is crucial for the coordination with the heme group in the active site.

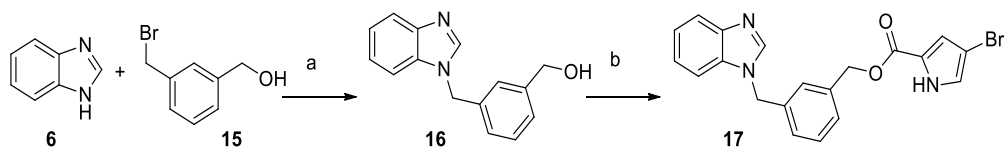


Scheme 2. Synthesis of compound 14.

Reagents and conditions: (a) KOH, acetone, 60 °C, 4 h, 71%. (b) LiAlH₄, dry THF, 65 °C - rt, 18 h, 46%. (c) TEA, HOBT, EDCI, 4-bromo-1*H*-pyrrole-2-carboxylic acid, dry CH₂Cl₂, rt, 18 h, 54%.

Next, the role of the key hydrogen bond between the amide and the carboxylic moiety of the heme group was confirmed by the synthesis and evaluation of compound 17, where the -NH- of the secondary amide is substituted with the -O- of the ester. 17 was prepared according to Scheme 3, starting from 1*H*-benzo[*d*]imidazole and (3-(bromomethyl)phenyl)methanol to afford intermediate 16 that underwent esterification with 4-bromo-1*H*-pyrrole-2-carboxylic acid to provide the desired compound. 17 is devoid of inhibitory activity at 1 μM, substantiating that the -NH-

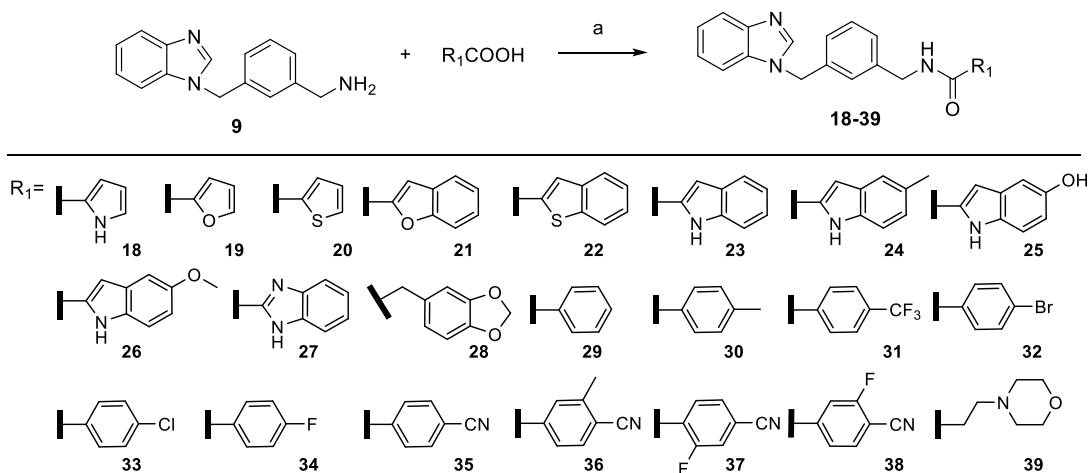
of the secondary amide is involved in the formation of a pivotal hydrogen bond within the IDO1 active site.



Scheme 3. Synthesis of compound **17**.

Reagents and conditions: (a) KOH, acetone, 60 °C, 2 h, 34%. (b) TEA, DMAP, EDCI, 4-bromo-1*H*-pyrrole-2-carboxylic acid, dry CH₂Cl₂, rt, 18 h, 40%.

Furthermore, the importance of the halogen bond between the bromine at 3 position on the pyrrole ring and the close carbonyl group of Lys238 was investigated by the synthesis of compound **18** that was obtained by coupling the amine **9** with the appropriate carboxylic acid, according to Scheme 4. As suggested by the docking pose, the presence of the bromine contributes to the binding as its removal leads to a decrease in activity (**18**, 72% of inhibition).



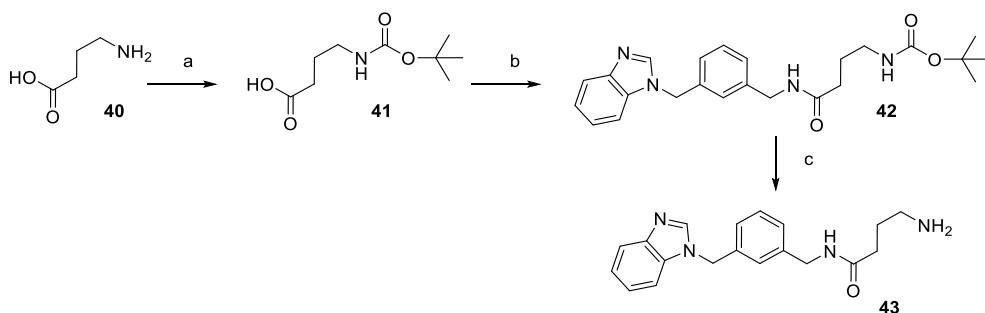
Scheme 4. Synthesis of compounds **18-39**.

Reagents and conditions: (a) TEA, HOBT, EDCI, dry CH₂Cl₂, rt, 18 h, 13-86%.

Finally, compounds **19** and **20**, displaying a furan and a thiophene ring, respectively, were prepared as described in Scheme 4 and evaluated with the aim of confirming the role of the -NH- of the pyrrole ring of **10** in establishing the hydrogen bond with the carboxylic moiety of the heme group. As expected, a decrease in the inhibitory activity occurs in both cases (**19** and **20**, 25% and 62% of inhibition, respectively). Besides the above SAR study, in order to investigate the role of the 4-bromopyrrole moiety placed in pocket C and further improve the potency of compound **10**, a series of analogues was *in silico*-designed and synthesized (**21-39**, **43**, **46**, **47**). To this aim, about 44,000 purchasable carboxylic acids have been virtually combined with compound **9**, and the resulted library of candidates has been screened in the IDO1 active site, using the same virtual screening procedure described before. Compounds have been ranked according to their binding energies in the protein, as well as their

drug-like profiles. The virtual candidates that displayed the highest score have been selected for synthesis.

By coupling amine **9** with different carboxylic acids (Scheme 4), 19 benzimidazoles have been obtained in good to excellent yields (**22-24**, **26-39**, **43**), with only two exceptions (**21**, **25**) showing poor yield (Table 1). For the synthesis of compound **43** protection and deprotection of the additional amine group were necessary, according to Scheme 5.



Scheme 5. Synthesis of compound **43**.

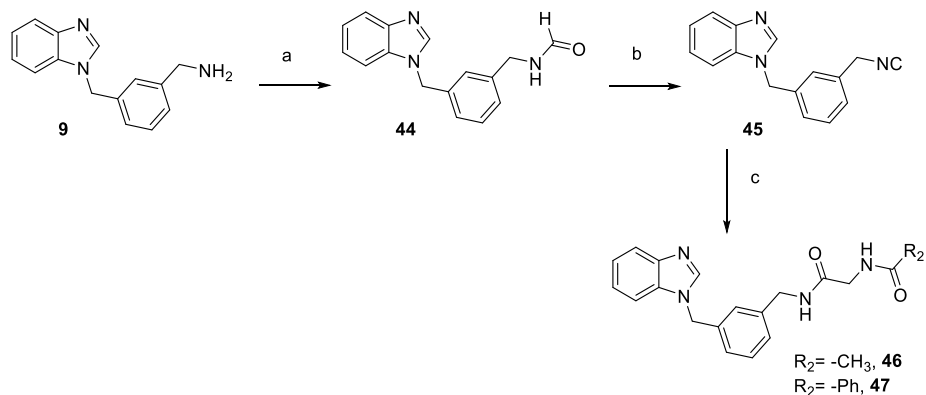
Reagents and conditions: (a) 2 M aq. NaOH, Boc_2O , THF, 16 h, 86%. (b) Compound **9**, TEA, HOBT, EDCI, dry CH_2Cl_2 , rt, 18 h, 57%. (c) CF_3COOH , dry CH_2Cl_2 , 0°C , 30 min, 71%.

Benzofuran **21** shows an IC_{50} value of 413 nM, while benzothiophene (**22**) provides a lower inhibitory activity (77% of inhibition). If pyrrole is fused with both a non-substituted (**23**) or a substituted (**24**, **25**) phenyl ring, the activity is retained (IC_{50} = 72, 636, 781 nM, respectively), while when a 5-methoxy-1*H*-indole substituent is present (**26**) a significant cytotoxicity is observed (55% of viability at 1 μM). Finally,

the benzimidazole **27** is well tolerated ($IC_{50} = 407$ nM), while a benzodioxolane ring is not (**28**, 5% of inhibition).

The SAR study reveals that for the analogues displaying a phenyl ring at the R_1 position (**29-38**), when unsubstituted, the inhibitory activity is lost (**29**, 32% of inhibition). Electron-donating (**30**) and electron-withdrawing groups such as trifluoromethyl (**31**), bromine (**32**), chlorine (**33**) and fluorine (**34**) at position 4' reduce potency compared to **10**. On the other hand, compound **35** displaying a cyano group at position 4' retains a good potency ($IC_{50} = 90$ nM), while the activity is lower when other substituents are added on the -CN substituted phenyl ring (**36, 37, 38**).

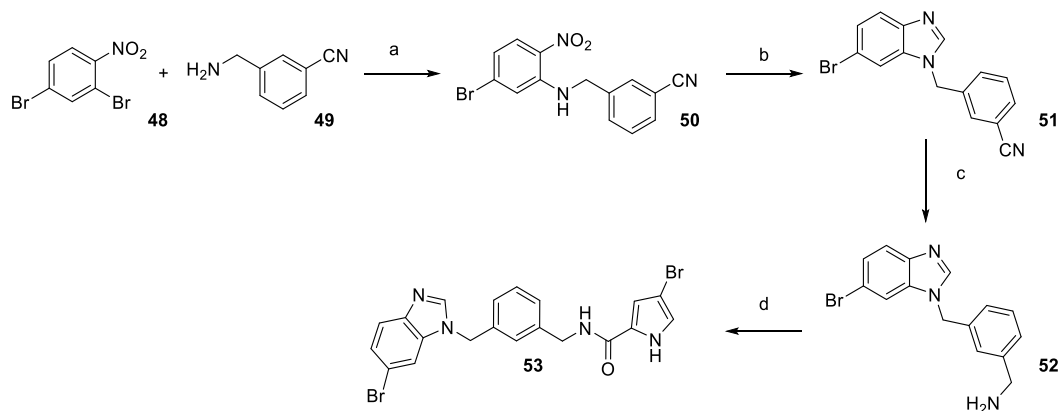
Compounds **46** and **47** have been synthesized by using Ugi multicomponent reaction (MCR) and exploiting ammonium chloride as a nitrogen source. The required isocyanide **45** has been synthesized starting from amine **9** that was formylated and dehydrated. Then, two MCRs have been set up using isocyanide **45**, paraformaldehyde, ammonium chloride and acetic or benzoic acid, yielding compounds **46** and **47**, respectively (Scheme 6). The yields of both reactions were very poor (30-32%), not surprisingly since it is well known that Ugi MCR does not work well when ammonia is employed as nitrogen source.³⁴ The introduction of a polar moiety (**39, 43**) at R_1 position or a peptidic substructure (**46, 47**) in the side chain are not tolerated, inducing a drop in activity.



Scheme 6. Synthesis of compounds **46** and **47**.

Reagents and conditions: (a) Ac_2O , HCOOH , 3 h, 98%. (b) TEA, POCl_3 , dry CH_2Cl_2 , $0\text{ }^\circ\text{C}$, 2.5 h, 44%. (c) NH_4Cl , CH_2O , TEA, R_2COOH , MeOH, H_2O , $65\text{ }^\circ\text{C}$, 8 h, 30-32%.

Since pocket A is not completely occupied by compound **10** and other reported IDO1 inhibitors display halogen atoms to increase the affinity with this buried pocket, a bromine atom was introduced at position 6 of the benzimidazole core with the aim of improving the affinity with pocket A. Compound **53** was synthesized following the synthetic route outlined in Scheme 7. The desired amine **52** was prepared *via* a three-step procedure: nucleophilic aromatic substitution, cyclization and reduction of the nitrile group (Scheme 7).



Scheme 7. Synthesis of compound **53**.

Reagents and conditions: (a) K_2CO_3 , DMSO, 72 °C, 16 h, 13%. (b) formic acid, Fe, 85 °C, 16 h, 69%. (c) $LiAlH_4$, dry THF, rt, 16 h, 40%. (d) TEA, HOBT, EDCI, dry CH_2Cl_2 , rt, 18 h, 39%.

Compound **53** shows an IC_{50} value of 19 nM, but its chemical instability together with the lack of improvement in ADME properties compared to the hit compound (data not shown) have prompted us to discard the compound.

Taking into consideration all these data, the main findings are represented in Figure 3 and the compounds **10**, **23** and **35** that display no significant cytotoxicity and IC_{50} values of 16, 72 and 90 nM, respectively, have been selected for further evaluation.

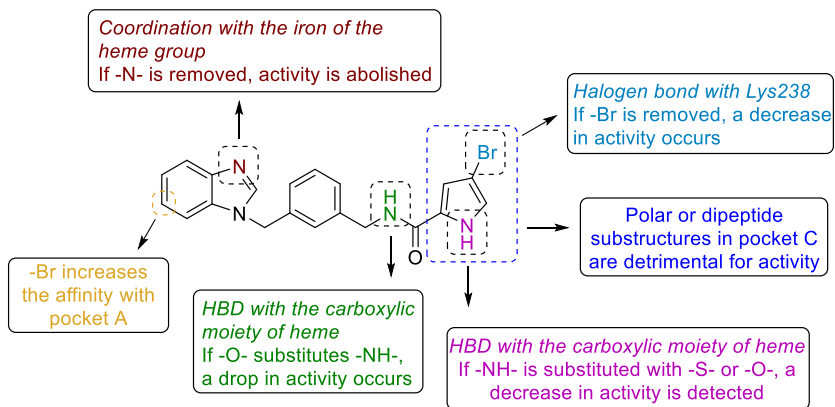
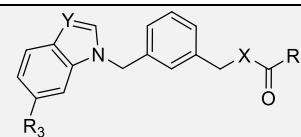
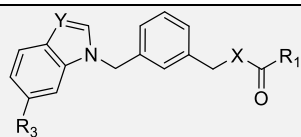


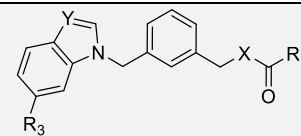
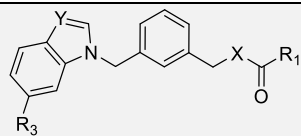
Figure 3. Graphical representation of SAR study around compound 10.

Table 1. SAR study around compound **10**.

Cpd, Yield (%)	X	Y	R ₁	R ₃	Cell viability (%) @ 1 μM ± SD	IDO cellular assay inhibition (%) @ 1 μM	IC ₅₀ (nM)	Cpd, Yield (%)	X	Y	R ₁	R ₃	Cell viability (%) @ 1 μM ± SD	IDO cellular assay inhibition (%) @ 1 μM	IC ₅₀ (nM)
1	-	-	-	-	97 ± 2.5	92 ± 3.6	7.7	29 , 54%	NH	N		H	98 ± 2	32 ± 15	-
10 , 50%	NH	N		H	100 ± 0.5	96 ± 0.2	16	30 , 69%	NH	N		H	94 ± 3	88 ± 2.1	327
14 , 54%	NH	H		H	100 ± 0	0 ± 4	-	31 , 82%	NH	H		H	97 ± 3	81 ± 4.9	-
17 , 40%	O	N		H	100 ± 0	0 ± 2	-	32 , 77%	NH	N		H	96 ± 4	98 ± 1.4	134
18 , 62%	NH	N		H	94 ± 6	72 ± 2.1	-	33 , 60%	NH	N		H	96 ± 4	99 ± 0	477
19 , 65%	NH	N		H	100 ± 0	25 ± 11.4	-	34 , 78%	NH	N		H	89 ± 7	88 ± 7.1	961



Cpd, Yield (%)	X	Y	R ₁	R ₃	Cell viability (%) @ 1 μM ± SD	IDO cellular assay inhibition (%) @ 1 μM	IC ₅₀ (nM)	Cpd, Yield (%)	X	Y	R ₁	R ₃	Cell viability (%) @ 1 μM ± SD	IDO cellular assay inhibition (%) @ 1 μM	IC ₅₀ (nM)
20 , 78%	NH	N		H	98 ± 1	62 ± 9.9	-	35 , 77%	NH	N		H	100 ± 1	88 ± 6.9	90
21 , 37%	NH	N		H	100 ± 0	91 ± 4	413	36 , 51%	NH	N		H	94 ± 1	44 ± 16.9	-
22 , 52%	NH	N		H	88 ± 1	77 ± 1.2	-	37 , 60%	NH	N		H	99 ± 1	37 ± 0	-
23 , 54%	NH	N		H	99 ± 4	94 ± 3.5	72	38 , 48%	NH	N		H	100 ± 0	32 ± 14.5	-
24 , 49%	NH	N		H	99 ± 1	90 ± 7.5	636	39 , 55%	NH	N		H	100 ± 1	0 ± 0	-
25 , 13%	NH	N		H	99 ± 1	71 ± 15.5	781	43 , 71%	NH	N		H	100 ± 0	0 ± 0	-
26 , 56%	NH	N		H	55 ± 11	-	-	46 , 30%	NH	N		H	100 ± 0	0 ± 0	-
27 , 86%	NH	N		H	100 ± 0	83 ± 10.6	407	47 , 32%	NH	N		H	99 ± 0	13 ± 0.7	-



Cpd, Yield (%)	X	Y	R ₁	R ₃	Cell viability (%) @ 1 μM ± SD	IDO cellular assay inhibition (%) @ 1 μM	IC ₅₀ (nM)	Cpd, Yield (%)	X	Y	R ₁	R ₃	Cell viability (%) @ 1 μM ± SD	IDO cellular assay inhibition (%) @ 1 μM	IC ₅₀ (nM)
28 , 84%	NH	N		H	96 ± 3	5 ± 6.4	-	53 , 39%	NH	N		Br	99 ± 1	98 ± 1.7	19 nM

Profiling of compounds 10, 23 and 35

IDO1 and TDO selectivity

The three selected compounds were tested in a mastocytoma cell line stably expressing mouse IDO1 (P1.IDO1) or TDO (P1.TDO) in order to evaluate their selectivity. To this aim, cells P1.IDO1 and P1.TDO were treated with different dilutions of **10**, **23** and **35** for 16 h and L-Kyn secretion in cell culture supernatants was detected by HPLC analysis. In these settings, the compounds behaved as selective inhibitors of IDO1 against TDO at 1 μM , yet when the concentration was increased up to 10 μM , an inhibition of TDO was observed to some extent. We measured the IC_{50} value of each compound in the two cell lines and we found that IC_{50} of compound **10** is 12.7 nM in P1.IDO1 and 5.46 μM in P1.TDO. Moreover, for **23** IC_{50} is 9.3 nM in P1.IDO1 and 13.2 μM in P1.TDO, whereas for **35** IC_{50} is 111.7 nM and 32.3 μM , respectively, suggesting a high selectivity of the three compounds towards IDO1 over TDO .

IDO1 inhibitory activity in a set of different tumoral cell lines

Compared to epacadostat (**1**, Figure 1), compound **10** showed a very similar activity in the A375 cell line, with IC_{50} values of 7.7 nM and 16 nM, respectively. The cellular potency of **10** in inhibiting L-Kyn production was further investigated using several human cell lines, including cervical cancer derived HeLa cells, lung cancer derived LXF-289 cells, breast cancer derived MCF-7 cells, liver cancer derived HepG2 cells and pancreas cancer derived DAN-G cells. As shown in Table 2, compound **10** is

able to inhibit L-Kyn production in most cell lines with potency comparable with that observed in A375 cell line, suggesting that it effectively inhibits IDO1 enzyme activity regardless of cell source. Compared to the other cell lines, in the pancreatic derived DAN-G cells **10** showed an IC₅₀ value of one order of magnitude greater (0.605 μM ± 0.0626) than those observed in the other cells. This result could be ascribed to the concomitant expression of other Trp degrading enzymes such as TDO, as suggested by Western Blot analysis (data not shown), or IDO2, and to the fact that, as reported above, compound **10** is a selective inhibitor of IDO1.

Table 2. Potency of compound **10** on different cell lines.

Cell line	IC ₅₀ (μM)
A375	0.016 ± 0.0004
HeLa	0.064 ± 0.0018
LXF-289	0.014 ± 0.0002
MCF-7	0.021 ± 0.0006
HepG2	0.043 ± 0.0016
DAN-G	0.605 ± 0.0626

On the same note, the activity of **23** and **35** was measured on human breast derived MCF-7 and human pancreas derived DAN-G cell lines as *in vitro* models. As shown in Table 3, the IC₅₀ values obtained in MCF-7 cell line were slightly increased for both compounds (0.083 μM ± 0.005 and 0.11 μM ± 0.23 for **23** and **35**, respectively).

As observed for compound **10**, the IC₅₀ values measured in DAN-G cell line were higher than those observed in A375 cell line for both compounds, in particular of one and two order of magnitude greater for compounds **23** and **35**, respectively.

Table 3. Potency of compounds **23** and **35** on different cell lines.

Compound Cell line	IC ₅₀ (μM) 23	IC ₅₀ (μM) 35
A375	0.072 ± 0.002	0.09 ± 0.006
MCF-7	0.083 ± 0.005	0.11 ± 0.23
DAN-G	0.14 ± 0.007	1.94 ± 0.23

Molecular dynamics

The docking results of compounds **10** (Figure 2), **23** and **35** (see Supporting Information) were further analyzed with Molecular Dynamics (MD) simulations using Desmond package.³⁵ The MD of IDO1/compound complexes were simulated for 100 ns at 300 K using a standard protocol. The protein structure was stabilized, as shown in the RMSDs for both the IDO1 Cα and the ligand (see Supporting Information). In the MD simulation the benzimidazole moiety of **10** is stabilized in pocket A, where it is able to interact, for the majority of time, with the amino acidic residues of Phe163 and Tyr126, as well as with the heme group. This behavior is consistent with the docking results, as well as the contacts near the pocket B, such as

with Arg231. On the other hand, the hydrogen bond interaction with Ser235 occurs for only the 50% of the simulation time. The pyrrole group of **10** makes interactions with the amino acids in pocket C, that are present for up to 10% of the simulation time. The conformation of hIDO1 changes during the MD, and in this relaxed/dynamic situation the side-chain of **10** that is more exposed to the solvent is shifted near the pocket B. In this new conformation, the pyrrole group can give a cation- π interaction with Arg231.

Compound **23** adopts two different poses during the MD, one within pocket C and the other near pocket B, and, as for compound **10**, a cation- π interaction with Arg231 is formed for the 80% of the simulation time. Similarly, compound **35** can adopt two different poses: half of the time it maintains the interaction with pocket C, while in the other half the aromatic ring bearing a nitrile group is located near Phe227.

In vitro metabolic stability

The *in vitro* metabolic stability of **10**, **23** and **35** was evaluated in mouse liver microsomes (MLM) activated by NADPH by measuring the substrate residual after one hour of incubation. All three compounds undergo oxidative metabolism, with a residual substrate of 32%, 65% and 59%, respectively. Similar percentages have been observed in the incubation mixtures supplied with glutathione (GSH). Next, we performed the metabolites structural characterization by high resolution mass spectrometry (HRMS), processing the raw data with a workflow aimed for drug

metabolites discovery provided by Compound Discoverer™ 3.0 software (Thermo Scientific™). Overall, the three compounds undergo two main transformations (Figure 4): benzimidazole oxidation at different positions and oxidative *N*-dealkylation at both the benzylic carbon atoms, the latter leading to the formation of the corresponding carboxylic acid further reduced to aldehyde and alcohol. Despite a higher metabolic stability compared to the other two analogues, the indole heterocycle of **23** is susceptible to microsomal oxidation and at least three metabolites have been detected. Interestingly, data analysis did not highlight the formation of GSH adducts, suggesting that metabolism is not driven toward the formation of reactive species. Full data of metabolites structures and mass spectral data, as well as the metabolic pathways, are given in the Supporting Information. Based on the observed liability, strategies aimed at reducing the susceptibility toward metabolism might be worth of investigation. The blockage of the putative sites of hydroxylation by using fluorine or deuterium atoms would presumably not impair the activity of the compounds on IDO1, while improving resistance toward metabolism (Figure 4). While the use of fluorine is well established in medicinal chemistry, deuterium incorporation has only recently exploded,³⁶ after the approval by FDA of the first deuterated drug. Within our class of molecules, the deuterium kinetic isotope effect (DKIE) might be exploited to mitigate both the aldehyde oxidase (AO)-driven oxidation of benzimidazole ring and the amide *N*-dealkylation.³⁷

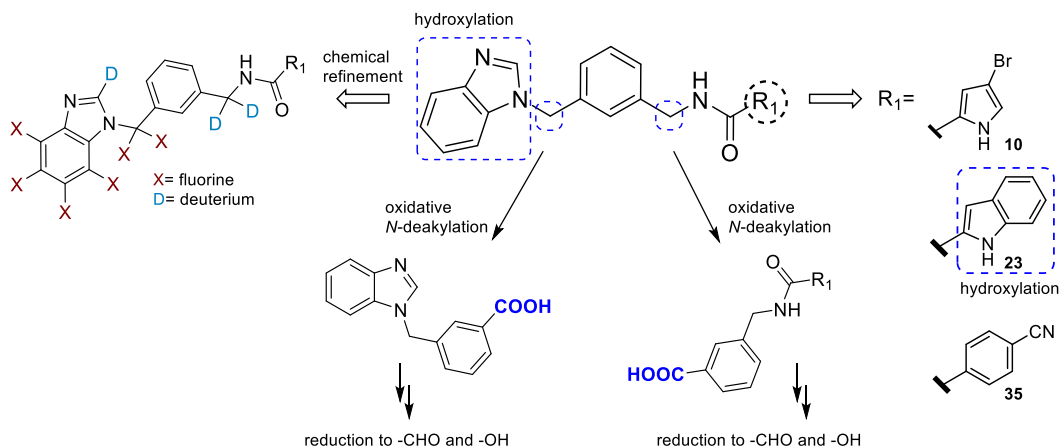


Figure 4. Metabolic pathways of compounds **10**, **23** and **35** in MLM and possible strategies to improve metabolic stability. The labile soft spots are highlighted in blue.

CYP inhibition

Since cytochrome P450 (CYP) family shares with IDO1 the iron-containing heme group, all the candidates have been evaluated for their inhibitory activity on these enzymes. Aminopyrine *N*-demethylase assay was performed in order to evaluate the inhibition of CYPs by **10**, **23** and **35** and to predict the risk of pharmacokinetic drug interactions. **10** showed a mild inhibitory activity with an IC₅₀ value of 67.7 μM compared to incubations with ketoconazole (CYP3A inhibitor), which gave an IC₅₀ value of 6.4 μM in our assay. For **23** and **35**, IC₅₀s curves could not be fitted for the absence of the bottom plateau phase which is related to their inability to inhibit CYP.

Inhibition of immunosuppressive activity of human monocytes from PDAC patients

In order to further validate the activity of our compounds, the two hits, **10** and **23**, were evaluated for their ability to inhibit the immunosuppressive activity of monocytes from patients affected by pancreatic ductal adenocarcinoma (PDAC) towards proliferation of T cells. PDAC represents the fourth leading cause of cancer death especially because of its high resistance to therapy.³⁸ PDAC cells release several pro-inflammatory molecules, thus favoring the expansion and accumulation of monocytic MDSCs that are strongly involved in promoting immune escape mechanisms exploited by cancer. We validated the immunosuppressive activity of monocytes isolated from PDAC patients (n=16). As previously shown by Trovato *et al.*,³⁹ on the basis of such immunosuppressive activity, our cohort of PDAC patients could be divided into two sub-groups: “suppressive PDAC” (n=11, red), whose monocytes were able to reduce T cell proliferation, and “non-suppressive PDAC” (n=5, blue), whose monocytes did not inhibit T cell proliferation, similarly to healthy donor (HD)-derived monocytes (n=7, black) (Figure 5A). In order to evaluate the capability of IDO1 inhibitors to reduce the immunosuppressive activity of monocytes from PDAC patients, we first selected the higher concentration that would not affect the viability of both monocytes isolated from HD (30 μ M) (Figure 5B) and PDAC patients (Figure 5C). Interestingly, the treatment of suppressive monocytes with IDO1 inhibitors **1**, **10** and **23** significantly reduced their capacity to restrict T cell proliferation (Figure 5D), suggesting the impact of IDO1 in driving the

inhibitory function of PDAC-isolated suppressive monocytes. Notably, compound **10** showed a higher effect compared to epacadostat **1**. Finally, as expected, both **10** and **23** inhibitors resulted ineffective on non-suppressive PDAC-isolated monocytes (Figure 5E).

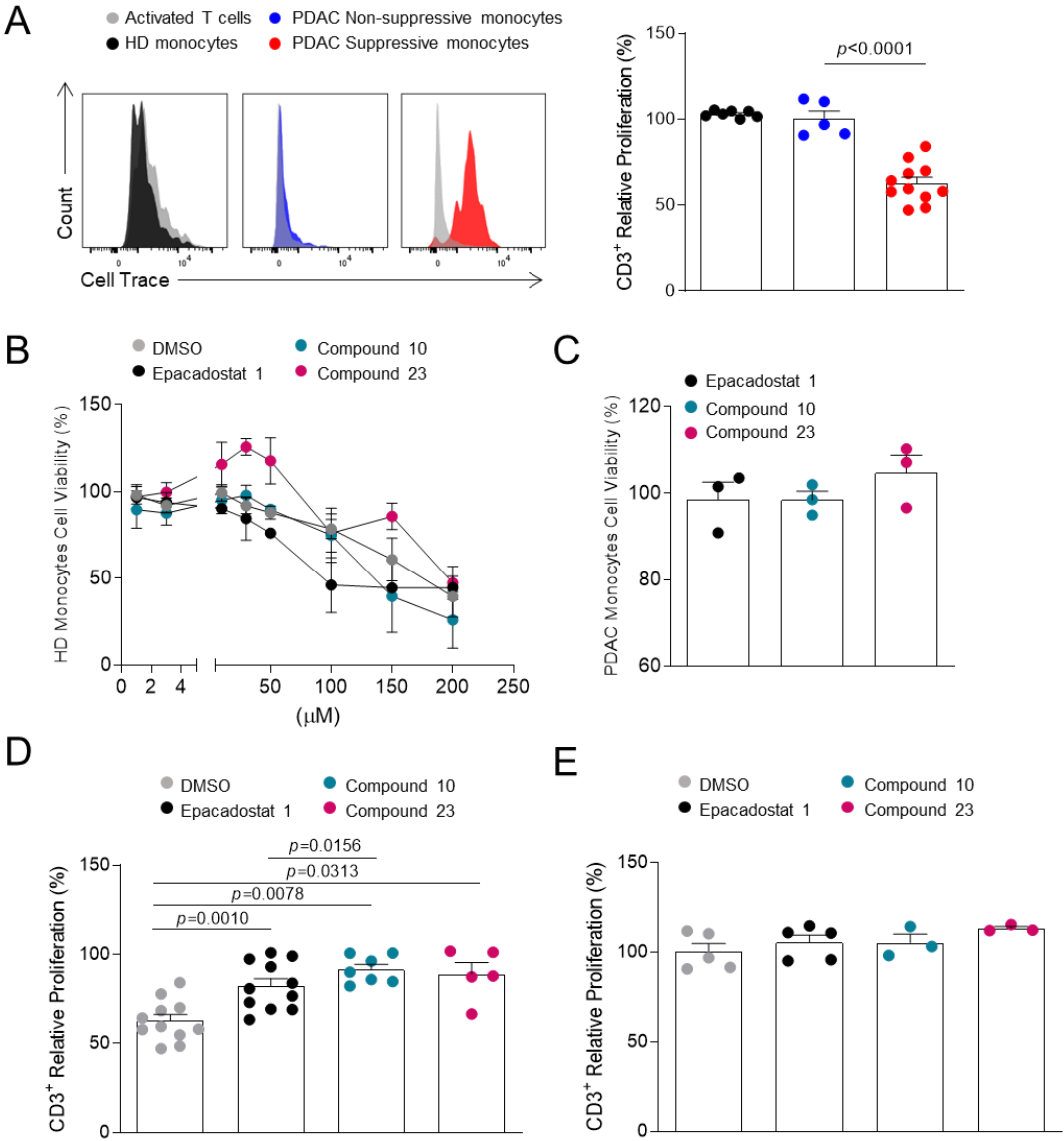


Figure 5. IDO-inhibitors abrogate immunosuppressive function of PDAC-derived monocytes. **(A)** Representative proliferation peaks of Cell Trace⁺CD3⁺ T lymphocytes following the co-culture with HD (black), PDAC non-suppressive (blue), and PDAC suppressive monocytes (red) (left panel) and relative proliferation percentage of CD3⁺T cells after the co-culture with HD (n=7, black), PDAC non-suppressive (n=5, blue), and PDAC suppressive monocytes (n=11, red) (right panel). All values are normalized on activated T cells in the absence of myeloid cells. **(B)** HD monocytes (n=3) viability after a 24 h treatment with different concentrations of epacadostat **1** (black), compound **10** (light blue), compound **23** (purple) and DMSO (grey) as control. All values are normalized on untreated cells. **(C)** PDAC monocytes (n=3) viability after a 24 h treatment with 30 μ M of epacadostat (black), compound **10** (light blue) and compound **23** (purple). **(D, E)** Relative proliferation percentage of CD3⁺ T cells after 4 days of co-culture with PDAC suppressive **(D)** and PDAC non-suppressive **(E)** monocytes pre-treated with 30 μ M of epacadostat **1** (black), compound **10** (light blue), compound **23** (purple) and DMSO (grey) as control. All values are normalized on activated T cells in the absence of myeloid cells. Data are expressed as mean \pm SEM. Statistical analyses were performed using Mann-Whitney test. HD: healthy donor PDAC: pancreatic ductal adenocarcinoma.

***In vivo* PK/PD of compound 23**

Considering the slightly higher *in vitro* metabolic stability shown by compound **23** compared to **10**, we proceeded evaluating its pharmacokinetic parameters in mice.

Briefly, mice were injected with **23** (*i.v.* 10 mg/kg, once) and serial blood sampling was performed. **23** showed a half-life of 0.65 h, with a clearance of 7.5 mL/min/Kg, a volume of distribution of 6.6 L/Kg and a C_{\max} of 2684 $\mu\text{g/L}$ (see Supporting Information for the full set of PK parameters).

At selected time points, and in particular at 0, 2, 5, 15, 30 min and 8 h after the injection of the compound, the L-Kyn plasmatic levels were measured. As expected, according to the short half-life of **10**, L-Kyn levels rapidly decreased up to 2 min and remained below the basal level until 30 min, while restoring the basal level in 8 h (see Supporting Information).

These data were benchmarked against epacadostat **1**, evaluating L-Kyn levels after oral administration of compound **1**: a tendency in decreasing L-Kyn levels was observed, in agreement with literature data.⁴⁰

Discussion and Conclusions

In this study, structure-based virtual screening was instrumental to identify a potent benzimidazole compound (**10**) that is endowed with attractive features. It is a novel chemotype, not sharing structural similarities with previously reported IDO1 inhibitors, and displays high synthetic feasibility, together with a peculiar predicted binding mode in the active site compared to the previously reported IDO1 inhibitors. The benzimidazole group is accommodated in pocket A, the nitrogen of the benzimidazole ring coordinates the heme group and the long side chain protrudes towards pocket C. The tight packing within the enzyme allows for an extensive

bonding network, including one halogen and three hydrogen bonds that contribute to a strong binding interaction ($K_d = 0.36 \mu\text{M}$) and a high inhibition potency ($\text{IC}_{50} = 16 \text{ nM}$ in A375). Interestingly, MD analysis reveals that this pocket is not constantly occupied as **10** flips between two poses: one where it interacts with pocket C and the other where it is shifted towards pocket B, in proximity to Arg231. The *in silico*-aided SAR study around **10** afforded a derivative, **23**, in which the bromopyrrole moiety displayed by **10** is replaced by an indole group, that according to docking analysis is located between pocket B and pocket C, and is able to form two hydrogen bonds with the carboxylic moiety of the heme group. MD analysis highlights that **23** can flip between two different poses, but simulation time spent near Arg231 is greater than compound **10**. **23** is able to inhibit IDO1 at the low nanomolar level in different tumour cell lines, is not cytotoxic up to $30 \mu\text{M}$, is specific for IDO1 over TDO (>1000-fold) and does not interfere with CYPs. Last, the compound can be prepared through three high-yielding synthetic steps and is synthetically tractable. The *in vitro* metabolic stability underlined that **23** undergoes oxidative metabolism, a liability that was further confirmed by a short *in vivo* half-life. In spite of this, a significant reduction of L-Kyn levels in plasma was observed when the compound was injected *i.v.* at a dose of 10 mg/kg in mice, confirming the molecule as a potent IDO1 inhibitor also under *in vivo* settings. Finally, we demonstrated that compound **23** has a potent effect on abrogating immunosuppressive properties of MDSC-like cells isolated from PDAC patients to an extent similar to epacadostat.

In conclusion, a novel class of potent IDO1 inhibitors that displays a peculiar profile compared to the known IDO1 inhibitors in terms of chemical structure, pose in the active site, synthetic feasibility and specificity over TDO, has been discovered by a structure-based virtual screening. All the accumulated data strongly suggest that these compounds might lay the basis for an improvement of the effectiveness of IDO1-targeting immunotherapy. Current efforts aimed at optimizing the PK profile are ongoing in our laboratory and will be reported in due course.

EXPERIMENTAL SECTION

Molecular modelling

All molecular modelling studies were performed on a Tesla workstation equipped with two Intel Xeon X5650 2.67 GHz processors and with Ubuntu 14.04 (<http://www.ubuntu.com>). Protein structures and 3D chemical structures were generated in PyMOL.⁴¹

Compound sources

The collection of compounds was retrieved from ZINC15, a searchable database that includes chemical structures available from vendors.²⁹ The “in stock”-“drug-now” subset, that contains molecules with drug-like properties (molecular weight <500 Da and >150, logP ≤5, number of rotatable bonds ≤7, polar surface area <150, number of hydrogen bond donor ≤5 and number of hydrogen bond acceptor ≤10), was downloaded. Using these criteria, 8.2 million structures were retrieved. An in-house Perl script was used in order to standardize charges, enumerate ionization states and

generate tautomers at physiological pH range using QUACPAC software from OpenEye.⁴² The latter operation was followed by a 3D structure optimization and generation of conformers using OMEGA2 software.⁴³

Virtual screening procedure

In this study the X-ray structure of the 4-phenylimidazole-IDO1 complex was used (entry code 2D0T).⁴⁴ Water molecules were removed, and all the hydrogen atoms and MMFF94 charges were added. Then, the complex was transferred into fred_receptor and prepared for docking with FRED.³⁰ The interaction between the iron moiety of the heme group and the target molecule was used as a constraint: if an atom of the molecule was within an acceptable distance to it, the docking pose was retained; if not, the compound was discarded. Docked conformations were scored using Chemgauss4.

Compound 10 focused library

All the available compounds bearing an acid moiety were retrieved from the ZINC database. Only three vendors were considered (SigmaAldrich, AlfaAesar, Fluorochem) and 44,066 structures were obtained. All the compounds were virtually combined with compound **9** using an *in-house* python script to obtain the corresponding amides. The resulting molecules were filtered using the virtual screening procedure already discussed in this manuscript.

Molecular dynamics (MD) simulation

The MD simulations were carried out using Desmond simulation package of Schrödinger LLC.³⁵ The NPT ensemble with a temperature of 300 K and a pressure

of 1 bar was applied in all runs. The simulation length was 100 ns with a relaxation time 1 ps. The OPLS_2005 force field parameters were used in all the simulations.⁴⁵ The long-range electrostatic interactions were calculated using the particle mesh Ewald method.⁴⁶ The cut-off radius in Coulomb interactions was 9.0 Å. The water molecules were explicitly described using the simple point charge model.⁴⁷ The Martyna–Tuckerman–Klein chain coupling scheme⁴⁸ with a coupling constant of 2.0 ps was used for the pressure control and the Nosé–Hoover chain coupling scheme⁴⁹ for the temperature control. Nonbonded forces were calculated using an r-RESPA integrator where the short-range forces were updated every step and the long-range forces were updated every three steps. The trajectory sampling was done at an interval of 1.0 ps. The behavior and the interactions between the ligands and protein were analyzed using the Simulation Interaction Diagram tool implemented in Desmond MD package. The stability of MD simulations was monitored considering the RMSD of the ligand and protein atom positions over time.

Chemistry

General Experimental Methods. Commercially available reagents and solvents were used as purchased without further purification. When needed, solvents were distilled and stored on molecular sieves. Column chromatography was performed on silica gel. Thin layer chromatography (TLC) was carried out on 5 cm × 20 cm plates with a layer thickness of 0.25 mm. When necessary, TLC plates were visualized with aqueous KMnO₄ or with aqueous Pancaldi solution. Melting points were determined in open glass capillary with a Stuart scientific SMP3 apparatus. All the target

compounds were checked by IR (FT-IR Thermo-Nicolet Avatar), ¹H-NMR (Bruker Avance Neo 400 MHz; Jeol ECP 300 MHz), ¹³C-NMR (Bruker Avance Neo 400 MHz; Jeol ECP 300 MHz), and mass spectrometry (Thermo Finnigan LCQ-deca XP-plus) equipped with an ESI source and an ion trap detector. Chemical shifts are reported in parts per million (ppm).

The purity of lead compounds was determined by high performance liquid chromatography (HPLC) using a Shimadzu HPLC system (Shimadzu, Kyoto, Japan) equipped with a *Synegi Polar 150 × 4.6 mm (4 μm d.p.)* stationary phase (Phenomenex Torrance, CA, USA) and using 0.2% formic acid in water and 0.2% formic acid in acetonitrile as eluents (for further details see Supporting Information). Purity of all lead compounds is 95% or higher.

3-((1*H*-Benzo[*d*]imidazol-1-yl)methyl)benzonitrile, (8).

To a solution of 1*H*-benzo[*d*]imidazole (3.00 g, 25.39 mmol, 1 eq) in acetone (83 mL) KOH (2.90 g, 50.79 mmol, 2 eq) and 3-(bromomethyl)benzonitrile (4.98 g, 25.39 mmol, 1 eq) were added in order. The reaction mixture was heated at 60 °C for 4 h. Then, acetone was removed in vacuo, water was added and the aqueous layer was extracted with EtOAc (x1). The organic extract was dried over Na₂SO₄, filtered and concentrated in vacuo. Purification by silica gel column chromatography using PE/EtOAc 3:7 provided the desired compound (5.86 g, 25.14 mmol, 99%) as a yellow solid. Mp 110-112 °C. ¹H-NMR (300 MHz, CDCl₃): δ = 7.98 (s, 1H), 7.83 (d, *J* = 7.7 Hz, 1H), 7.59 (d, *J* = 7.7 Hz, 1H), 7.76 (s, 1H), 7.43 (d, *J* = 7.4 Hz, 1H), 7.33-7.25 (m, 3H), 7.22 (t, *J* = 7.4 Hz, 1H), 5.40 (s, 2H). ¹³C-NMR (75 MHz,

CD₃OD): δ = 143.9, 143.3, 137.4, 133.6, 131.9, 131.4, 130.4, 130.0, 123.6, 122.7, 120.5, 118.4, 113.0, 110.0, 47.9. IR (KBr): $\tilde{\nu}$ = 3099, 3077, 3051, 2865, 2757, 2560, 1496, 1439, 743 cm⁻¹. MS (ESI): m/z 234 [M + H]⁺.

(3-((1*H*-Benzo[*d*]imidazol-1-yl)methyl)phenyl)methanamine, (9).

Compound **8** (1.50 g, 6.43 mmol, 1 eq) was solubilized in dry THF (49 mL). The solution was cooled to 0 °C and LiAlH₄ (0.49 g, 16.09 mmol, 2.5 eq) was slowly added. The mixture was stirred at rt overnight and then heated at 65 °C for 2 h. Then, the reaction was quenched with EtOAc and with saturated aqueous solution of Na₂SO₄. The mixture was filtered over a pad of celite and rinsed with EtOAc. Purification by silica gel column chromatography using EtOAc /MeOH 7:3 as eluent provided the title compound (1.07 g, 4.50 mmol, 70%) as a yellow oil. ¹H-NMR (300 MHz, CD₃OD): δ = 8.28 (s, 1H), 7.66 (t, J = 7.2 Hz, 1H), 7.43 (t, J = 7.2 Hz, 1H), 7.30-7.15 (m, 6H), 5.74 (s, 2H), 3.75 (s, 2H). ¹³C-NMR (75 MHz, CD₃OD): δ = 143.9, 143.2, 137.4, 133.6, 131.9, 131.4, 130.4, 130.0, 123.6, 122.7, 120.5, 118.4, 113.0, 110.0, 47.8. IR (KBr): $\tilde{\nu}$ = 3359, 3048, 2984, 1730, 1494, 1438, 1286, 1201, 741 cm⁻¹. MS (ESI): m/z 238 [M + H]⁺.

General procedure for the synthesis of compounds 10, 14, 18-39, 53.

To a solution of compound **9** (167.11 mg, 0.7 mmol, 1 eq) in dry CH₂Cl₂ (5 mL) TEA (220 μ L, 1.54 mmol, 2.2 eq), EDCI (161.28 mg, 0.84 mmol, 1.2 eq), HOBT (113.51 mg, 0.84 mmol, 1.2 eq) and carboxylic acid (0.84 mmol, 1.2 eq) were added in order. The resulting mixture was stirred at room temperature for 16 h. CH₂Cl₂ was added and the organic phase was washed with aqueous saturated NH₄Cl solution

(x1), dried over Na₂SO₄ and evaporated. Purification by silica gel column chromatography afforded compounds **10**, **14**, **18-39**, **53**.

***N*-(3-((1*H*-Benzo[*d*]imidazol-1-yl)methyl)benzyl)-4-bromo-1*H*-pyrrole-2-carboxamide, (10).**

The title compound was synthesized following the general procedure, starting from compound **9** (90 mg, 0.38 mmol) and 4-bromo-1*H*-pyrrole-2-carboxylic acid (86 mg, 0.46 mmol). The crude material was purified by column chromatography using PE/EtOAc 2:8 as eluent to afford compound **10** (77 mg, 0.19 mmol, 50%) as a white solid. Mp 212-214 °C. ¹H-NMR (400 MHz, CD₃OD): δ = 8.21 (s, 1H), 7.65 (d, *J* = 7.4 Hz, 1H), 7.38 (d, *J* = 7.6 Hz, 1H), 7.31-7.12 (m, 6H), 6.90 (s, 1H), 6.73 (s, 1H), 5.44 (s, 2H), 4.44 (s, 2H). ¹³C-NMR (100.6 MHz, DMSO-*d*₆): δ = 160.1, 144.6, 144.1, 140.8, 137.5, 134.1, 129.2, 127.2, 127.1, 126.8, 126.4, 122.8, 122.0, 121.8, 119.9, 112.1, 111.2, 95.5, 48.1, 42.3. IR (KBr): $\tilde{\nu}$ = 3285, 3118, 2913, 2850, 2446, 2360, 3242, 1945, 1722, 748 cm⁻¹. MS (ESI): *m/z* 409 [M + H]⁺.

3-((1*H*-Indol-1-yl)methyl)benzotrile, (12).

To a solution of 1*H*-indole **11** (300 mg, 2.56 mmol, 1 eq) in acetone (6 mL) KOH (287 mg, 5.12 mmol, 2 eq) and 3-(bromomethyl)benzotrile (502 mg, 2.56 mmol, 1 eq) were added in order. The reaction mixture was heated at 60 °C for 4 h. Then, acetone was removed in vacuo, water was added and the aqueous layer was extracted with EtOAc (x3). The organic extract was dried over Na₂SO₄, filtered and concentrated in vacuo. Purification by silica gel column chromatography using PE/EtOAc 9:1 provided the desired compound (425 mg, 1.83 mmol, 71%) as a

yellow oil. $^1\text{H-NMR}$ (400 MHz, CDCl_3): $\delta = 7.79$ (d, $J = 7.5$ Hz, 1H), 7.53 (d, $J = 7.5$ Hz, 1H), 7.40 (s, 1H), 7.35 (t, $J = 7.5$ Hz, 1H), 7.30-7.26 (m, 4H), 7.18 (d, $J = 3.2$ Hz, 1H), 6.71 (d, $J = 3.2$ Hz, 1H), 5.30 (s, 2H). $^{13}\text{C-NMR}$ (100.6 MHz, CDCl_3): $\delta = 139.7, 136.2, 135.8, 134.8, 130.1, 129.8, 128.2, 126.7, 123.6, 122.7, 120.5, 119.6, 118.3, 112.9, 100.9, 51.9$. IR (neat): $\tilde{\nu} = 3053, 2918, 2228, 1483, 1461, 1314, 471, 685$ cm^{-1} . MS (ESI): m/z 233 $[\text{M} + \text{H}]^+$.

(3-((1*H*-Indol-1-yl)methyl)phenyl)methanamine, (13).

Compound **12** (416 mg, 1.79 mmol, 1 eq) was solubilized in dry THF (6 mL). The solution was cooled to 0 °C and LiAlH_4 (170 mg, 4.48 mmol, 2.5 eq) was slowly added. The mixture was heated at 65 °C for 7 h and then was stirred at rt overnight. The reaction was quenched with EtOAc and then with saturated aqueous solution of Na_2SO_4 . The mixture was filtered over a pad of celite and rinsed with EtOAc. Purification by silica gel column chromatography using EtOAc/MeOH 7:3 as eluent provided the title compound (194 mg, 0.82 mmol, 46%) as a colorless oil. $^1\text{H-NMR}$ (400 MHz, CDCl_3): $\delta = 7.76$ (d, $J = 7.8$ Hz, 1H), 7.38 (d, $J = 7.8$ Hz, 1H), 7.37-7.19 (m, 6H), 7.05 (d, $J = 6.8$ Hz, 1H), 6.66 (s, 1H), 5.33 (s, 2H), 3.83 (s, 2H). $^{13}\text{C-NMR}$ (100.6 MHz, CDCl_3): $\delta = 138.1, 136.3, 129.2, 129.1, 128.8, 128.2, 127.7, 126.8, 125.8, 121.7, 121.0, 119.6, 109.7, 101.7, 64.7, 50.0$. IR (neat): $\tilde{\nu} = 3049, 2917, 2852, 1461, 1313, 735, 693$ cm^{-1} . MS (ESI): m/z 237 $[\text{M} + \text{H}]^+$.

***N*-3-((1*H*-Indol-1-yl)methyl)benzyl)-4-bromo-1*H*-pyrrole-2-carboxamide, (14).**

The title compound was synthesized following the general procedure, starting from compound **13** (186 mg, 0.79 mmol) and 4-bromo-1*H*-pyrrole-2-carboxylic acid (179 mg, 0.94 mmol). The crude material was purified by column chromatography using PE/EtOAc 5:5 as eluent to afford compound **14** (178 mg, 0.43 mmol, 54%) as a white solid. Mp 80-81 °C. ¹H-NMR (400 MHz, CDCl₃): δ = 9.89 (br s, 1H), 7.67 (d, *J* = 7.2 Hz, 1H), 7.28-7.26 (m, 2H), 7.23 (s, 1H), 7.15-7.13 (m, 3H), 7.06-7.04 (m, 2H), 6.87 (s, 1H), 6.56 (d, *J* = 3.1 Hz, 1H), 6.49 (s, 1H), 6.11 (br s, 1H), 5.33 (s, 2H), 4.52 (d, *J* = 5.8 Hz, 2H). IR (neat): $\tilde{\nu}$ = 3052, 2919, 2854, 1623, 1557, 1509, 1314, 919, 738 cm⁻¹. MS (ESI): *m/z* 409 [M + H]⁺.

(3-((1*H*-Benzo[*d*]imidazol-1-yl)methyl)phenyl)methanol, (16).

To a solution of 1*H*-benzo[*d*]imidazole (118 mg, 1.00 mmol, 1 eq) in acetone (4 mL) KOH (112 mg, 2.00 mmol, 2 eq) and (3-(bromomethyl)phenyl)methanol **15** (201 mg, 1.00 mmol, 1 eq) were added in order. The reaction mixture was heated at 60 °C for 2 h. Then, acetone was removed in vacuo, water was added and the aqueous layer was extracted with EtOAc (x3). The organic extract was dried over Na₂SO₄, filtered and concentrated in vacuo. Purification by silica gel column chromatography using EtOAc/MeOH 9:1 provided the desired compound (81 mg, 0.34 mmol, 34%) as a yellow oil. ¹H-NMR (400 MHz, CDCl₃): δ = 7.85 (s, 1H), 7.73 (d, *J* = 6.8 Hz, 1H), 7.29-7.28 (m, 3H), 7.26-7.23 (m, 3H), 7.06 (d, *J* = 6.4 Hz, 1H), 5.26 (s, 2H), 4.67 (s, 2H). ¹³C-NMR (100.6 MHz, CDCl₃): δ = 143.0, 142.6, 135.4, 133.7, 129.1, 126.8, 126.1, 125.6 (2C), 123.3, 122.6, 119.9, 110.2, 64.2, 48.9. IR (neat): $\tilde{\nu}$ = 3093, 2922, 2853, 1733, 1492, 735, 691 cm⁻¹. MS (ESI): *m/z* 239 [M + H]⁺.

3-((1*H*-Benzo[*d*]imidazol-1-yl)methyl)benzyl**4-bromo-1*H*-pyrrole-2-****carboxylate, (17).**

To a solution of compound **16** (70 mg, 0.29 mmol, 1 eq) in dry CH₂Cl₂ (2 mL) TEA (45 μL, 0.32 mmol, 1.1 eq), EDCI (61.3 mg, 0.32 mmol, 1.1 eq), DMAP (3.5 mg, 0.029 mmol, 0.1 eq) and 4-bromo-1*H*-pyrrole-2-carboxylic acid (55 mg, 0.29 mmol, 1 eq) were added in order. The resulting mixture was stirred at room temperature for 18 h. Then, CH₂Cl₂ was added and the organic phase was washed with water (x1), dried over Na₂SO₄ and evaporated. Purification by silica gel column chromatography using PE/EtOAc 2:8 provided the desired compound (48 mg, 0.12 mmol, 40%) as a white solid. Mp 171-172 °C. ¹H-NMR (400 MHz, CD₃OD): δ = 8.29 (s, 1H), 7.69 (d, *J* = 7.0 Hz, 1H), 7.43 (d, *J* = 6.9 Hz, 1H), 7.39-7.35 (m, 3H), 7.28-7.23 (m, 3H), 6.98 (d, *J* = 1.56 Hz, 1H), 6.78 (d, *J* = 1.56 Hz, 1H), 5.54 (s, 2H), 5.27 (s, 2H). IR (neat): $\tilde{\nu}$ = 2922, 2851, 1701, 1398, 1186, 1135, 775, 741 cm⁻¹. MS (ESI): *m/z* 411 [M + H]⁺.

***N*-(3-((1*H*-Benzo[*d*]imidazol-1-yl)methyl)benzyl)-1*H*-pyrrole-2-carboxamide, (18).**

The title compound was synthesized following the general procedure, starting from compound **9** (166 mg, 0.70 mmol) and 1*H*-pyrrole-2-carboxylic acid (93 mg, 0.84 mmol). The crude material was purified by column chromatography using PE/EtOAc 2:8 as eluent to afford compound **18** (143 mg, 0.43 mmol, 62%) as a yellow solid. Mp 206-208 °C. ¹H-NMR (300 MHz, CD₃OD): δ = 8.23 (s, 1H), 7.64 (dd, *J*_s = 1.0, 8.3 Hz), 7.39 (d, *J* = 6.9 Hz, 1H), 7.26-7.13 (m, 7H), 7.76 (s, 1H), 6.16 (d, *J* = 2.5

Hz, 1H), 5.43 (s, 2H), 5.36 (s, 2H). IR (KBr): $\tilde{\nu}$ = 3220, 3087, 2935, 2701, 2563, 1628, 1560, 1491, 1437, 1438, 776, 745 cm^{-1} . MS (ESI): m/z 331 $[\text{M} + \text{H}]^+$.

***N*-(3-((1*H*-Benzo[*d*]imidazol-1-yl)methyl)benzyl)furan-2-carboxamide, (19).**

The title compound was synthesized following the general procedure, starting from compound **9** (166 mg, 0.70 mmol) and furan-2-carboxylic acid (94 mg, 0.84 mmol).

The crude material was purified by column chromatography using PE/EtOAc 4:6 as eluent to afford compound **19** (150 mg, 0.46 mmol, 65%) as a white solid. Mp 153-154 °C. $^1\text{H-NMR}$ (300 MHz, CD_3OD): δ = 8.19 (s, 1H), 7.64-7.57 (m, 3H), 7.34 (d, J = 7.4 Hz, 1H), 7.35-7.04 (m, 7H), 5.36 (s, 2H), 4.44 (s, 2H). IR (KBr): $\tilde{\nu}$ = 3477, 3231, 3070, 2977, 2926, 1742, 1638, 1495, 1442, 1365, 1015, 769, 745 cm^{-1} . MS (ESI): m/z 332 $[\text{M} + \text{H}]^+$.

***N*-(3-((1*H*-Benzo[*d*]imidazol-1-yl)methyl)benzyl)thiophene-2-carboxamide, (20).**

The title compound was synthesized following the general procedure, starting from compound **9** (160 mg, 0.67 mmol) and thiophene-2-carboxylic acid (103 mg, 0.81 mmol). The crude material was purified by column chromatography using PE/EtOAc 3:7 as eluent to afford compound **20** (182 mg, 0.52 mmol, 78%) as a yellow solid. Mp 171-173 °C. $^1\text{H-NMR}$ (300 MHz, CD_3OD): δ = 8.19 (s, 1H), 7.64-7.57 (m, 3H), 7.34 (d, J = 7.4 Hz, 1H), 7.35-7.04 (m, 7H), 5.36 (s, 2H), 4.44 (s, 2H). IR (KBr): $\tilde{\nu}$ = 3555, 3414, 3263, 3070, 2892, 1636, 1618, 1498, 1365, 744 cm^{-1} . MS (ESI): m/z 348 $[\text{M} + \text{H}]^+$.

***N*-((1*H*-Benzo[*d*]imidazol-1-yl)methyl)benzyl)benzofuran-2-carboxamide, (21).**

The title compound was synthesized following the general procedure, starting from compound **9** (166 mg, 0.70 mmol) and benzofuran-2-carboxylic acid (136 mg, 0.84 mmol). The crude material was purified by column chromatography using PE/EtOAc 3:7 as eluent to afford compound **21** (98 mg, 0.26 mmol, 37%) as a yellow solid. Mp 161-163 °C. ¹H-NMR (300 MHz, CD₃OD): δ = 8.26 (s, 1H), 7.65 (d, *J* = 7.9 Hz, 1H), 7.60-7.57 (s, 1H), 7.50 (d, *J* = 7.9 Hz, 1H), 7.41 (m, 2H), 7.36-7.31 (m, 2H), 7.25 (m, 3H), 7.13-7.10 (m, 3H), 5.43 (s, 2H), 4.52 (s, 2H). ¹³C-NMR (100.6 MHz, DMSO-*d*₆): δ = 158.6, 154.7, 149.5, 140.3 (2C), 137.5 (2C), 133.9, 129.2, 127.6, 127.3, 127.3, 126.9, 126.5, 124.2, 123.2, 122.8, 122.1, 119.9, 112.3, 111.2, 110.0, 48.1, 42.5. IR (KBr): $\tilde{\nu}$ = 3892, 3801, 3735, 2927, 2850, 1734, 1590, 1560, 1496, 1474, 747 cm⁻¹. MS (ESI): 382 *m/z* [M + H]⁺.

***N*-((1*H*-Benzo[*d*]imidazol-1-yl)methyl)benzyl)benzo[*b*]thiophene-2-carboxamide, (22).**

The title compound was synthesized following the general procedure, starting from compound **9** (166 mg, 0.70 mmol) and benzo[*b*]thiophene-2-carboxylic acid (149 mg, 0.84 mmol). The crude material was purified by column chromatography using PE/EtOAc 5:5 as eluent to afford compound **22** (144 mg, 0.36 mmol, 52%) as a white solid. Mp 185-187 °C. ¹H-NMR (300 MHz, acetone-*d*₆): δ = 8.48 (s, 1H), 8.23 (s, 1H), 8.00-7.98 (m, 2H), 7.89 (dd, *J*_S = 1.9, 7.1 Hz, 1H), 7.77-7.63 (m, 1H), 7.48-7.47 (m, 2H), 7.44-7.41 (m, 2H), 7.33-7.28 (d, *J* = 5.8 Hz, 2H), 7.21-7.11 (m, 2H), 5.50

(s, 2H), 4.59 (s, 2H). IR (KBr): $\tilde{\nu}$ = 3183, 3055, 1642, 1560, 1495, 1458, 1290, 742 cm^{-1} . MS (ESI): m/z 398 [M + H]⁺.

***N*-((3-((1*H*-Benzo[*d*]imidazol-1-yl)methyl)benzyl)-1*H*-indole-2-carboxamide, (23).**

The title compound was synthesized following the general procedure, starting from compound **9** (166 mg, 0.70 mmol) and 1*H*-indole-2-carboxylic acid (135 mg, 0.84 mmol). The crude material was purified by column chromatography using PE/EtOAc 4:6 as eluent to afford compound **23** (144 mg, 0.38 mmol, 54%) as a yellow solid. Mp 231-233 °C. ¹H-NMR (400 MHz, DMSO-*d*₆): δ = 11.53 (br s, 1H), 8.94 (br s, 1H), 8.37 (s, 1H), 7.68-7.55 (m, 2H), 7.53-7.40 (m, 2H), 7.37 (s, 1H), 7.31-7.26 (m, 2H), 7.21-7.15, (m, 5H), 7.04 (t, J = 7.9 Hz, 1H), 5.49 (s, 2H), 4.48 (s, 2H). ¹³C-NMR (100.6 MHz, DMSO-*d*₆): δ = 161.6, 144.7, 144.1, 140.7, 137.5, 136.9, 134.2, 132.0, 129.2, 127.6, 127.2, 126.9, 126.4, 123.8, 122.8, 122.0, 121.9, 120.2, 119.9, 112.8, 111.2, 103.1, 48.1, 42.5. IR (KBr): $\tilde{\nu}$ = 3218, 3053, 2926, 2853, 2721, 2648, 1638, 1564, 1495, 1310, 746 cm^{-1} . MS (ESI): m/z 381 [M + H]⁺.

***N*-((3-((1*H*-Benzo[*d*]imidazol-1-yl)methyl)benzyl)-5-methyl-1*H*-indole-2-carboxamide, (24).**

The title compound was synthesized following the general procedure, starting from compound **9** (166 mg, 0.70 mmol) and 5-methyl-1*H*-indole-2-carboxylic acid (147 mg, 0.84 mmol). The crude material was purified by column chromatography using PE/EtOAc 3:7 as eluent to afford compound **24** (134 mg, 0.34 mmol, 49%) as a white solid. Mp 222-224 °C. ¹H-NMR (300 MHz, CD₃OD): δ = 8.25 (s, 1H), 7.62 (dd, J s

= 1.9, 7.7 Hz, 1H), 7.41-7.28 (m, 6H), 7.18-7.16 (m, 3H), 7.61 (d, $J = 7.7$ Hz, 1H), 6.93 (s, 1H), 5.48 (s, 2H), 4.53 (s, 2H), 2.40 (s, 3H). ^{13}C -NMR (100.6 MHz, $\text{DMSO-}d_6$): $\delta = 161.7, 144.7, 144.0, 140.8, 137.5, 135.4, 134.1, 132.0, 129.2, 128.7, 127.8, 127.2, 126.9, 126.4, 125.6, 122.8, 122.0, 121.2, 119.9, 112.5, 111.2, 102.6, 48.1, 42.5, 21.6$. IR (KBr): $\tilde{\nu} = 3232, 3090, 3061, 2922, 1637, 1560, 1496, 1419, 802, 736$ cm^{-1} . MS (ESI): m/z 395 $[\text{M} + \text{H}]^+$.

***N*-(3-((1*H*-Benzo[*d*]imidazol-1-yl)methyl)benzyl)-5-hydroxy-1*H*-indole-2-carboxamide, (25).**

The title compound was synthesized following the general procedure, starting from compound **9** (166 mg, 0.70 mmol) and 5-hydroxy-1*H*-indole-2-carboxylic acid (148 mg, 0.84 mmol). The crude material was purified by column chromatography using PE/EtOAc 3:7 as eluent to afford compound **25** (35 mg, 0.09 mmol, 13%) as a yellow solid. Mp 210-212 °C. ^1H -NMR (300 MHz, acetone- d_6): $\delta = 10.42$ (br s, 1H), 8.32 (s, 1H), 7.52 (dd, $J_S = 1.7, 7.1$ Hz, 1H), 7.32-7.20 (m, 6H), 7.18-7.15 (m, 3H), 7.59 (d, $J = 7.7$ Hz, 1H), 7.01 (s, 1H), 5.67 (br s, 1H), 5.50 (s, 2H), 4.58 (s, 2H), 3.31 (br s, 1H). IR (KBr): $\tilde{\nu} = 3745, 2359, 2342, 1742, 1557, 1496, 1362, 1257$ cm^{-1} . MS (ESI): m/z 397 $[\text{M} + \text{H}]^+$.

***N*-(3-((1*H*-Benzo[*d*]imidazol-1-yl)methyl)benzyl)-5-methoxy-1*H*-indole-2-carboxamide, (26).**

The title compound was synthesized following the general procedure, starting from compound **9** (166 mg, 0.70 mmol) and 5-methoxy-1*H*-indole-2-carboxylic acid (160 mg, 0.84 mmol). The crude material was purified by column chromatography using

PE/EtOAc 2:8 as eluent to afford compound **26** (160 mg, 0.39 mmol, 56%) as a yellow solid. Mp 225-227 °C. ¹H-NMR (300 MHz, DMSO-*d*₆): δ = 11.43 (br s, 1H), 8.97 (s, 1H), 8.39 (s, 1H), 7.65 (d, *J* = 7.1 Hz, 1H), 7.50 (d, *J* = 7.1 Hz, 1H), 7.33 (t, *J* = 6.3 Hz, 1H), 7.27 (d, *J* = 6.3 Hz, 2H), 7.22-7.18 (m, 3H), 7.06 (d, *J* = 6.3 Hz, 2H), 6.83 (d, *J* = 8.5 Hz, 1H), 5.48 (s, 2H), 4.47 (s, 2H), 3.75 (s, 3H). IR (KBr): $\tilde{\nu}$ = 3246, 3087, 3004, 2926, 2803, 1637, 1559, 1497, 1359, 1269, 163, 742 cm⁻¹. MS (ESI): 411 *m/z* [M + H]⁺.

***N*-(3-((1*H*-Benzo[*d*]imidazol-1-yl)methyl)benzyl)-1*H*-benzo[*d*]imidazole-2-carboxamide, (27).**

The title compound was synthesized following the general procedure, starting from compound **9** (166 mg, 0.70 mmol) and 1*H*-benzo[*d*]imidazole-2-carboxylic acid (136 mg, 0.84 mmol). The crude material was purified by column chromatography using PE/EtOAc 4:6 as eluent to afford compound **27** (229 mg, 0.60 mmol, 86%) as a white solid. Mp 226-227 °C. ¹H-NMR (300 MHz, DMSO-*d*₆): δ = 9.40 (br s, 1H), 8.34 (s, 1H), 7.77-7.58 (m, 3H), 7.47 (d, *J* = 7.2 Hz, 1H), 7.36 (s, 1H), 7.27-7.21 (m, 4H), 7.16-7.06 (m, 3H), 5.46 (s, 2H), 4.46 (s, 2H). ¹³C-NMR (100.6 MHz, DMSO-*d*₆): δ = 159.5, 146.2, 144.7 (2C), 144.2, 140.4, 137.5, 134.3, 129.3, 127.4 (2C), 127.1 (2C), 126.5, 123.9, 122.9, 122.3, 122.1, 120.0 (2C), 111.2, 48.3, 42.8. IR (KBr): $\tilde{\nu}$ = 3418, 3047, 1666, 1507, 1494, 1436, 1330, 744 cm⁻¹. MS (ESI): *m/z* 382 [M + H]⁺.

***N*-(3-((1*H*-Benzo[*d*]imidazol-1-yl)methyl)benzyl)-2-(benzo[*d*][1,3]dioxol-5-yl)acetamide, (28).**

The title compound was synthesized following the general procedure, starting from compound **9** (166 mg, 0.70 mmol) and 2-(benzo[*d*][1,3]dioxol-5-yl)acetic acid (151 mg, 0.84 mmol). The crude material was purified by column chromatography using PE/EtOAc 3:7 as eluent to afford compound **28** (235 mg, 0.59 mmol, 84%) as an amorphous yellow solid. ¹H-NMR (300 MHz, CD₃OD): δ = 8.13 (s, 1H), 7.66 (d, *J* = 8.0 Hz, 1H), 7.29 (d, *J* = 8.0 Hz, 1H), 7.30-7.00 (m, 7H), 6.74 (s, 1H), 6.66 (s, 1H), 5.76 (s, 2H), 5.27 (s, 2H), 4.23 (s, 2H), 3.30 (s, 2H). IR (KBr): $\tilde{\nu}$ = 3735, 3629, 3255, 2887, 2790, 1845, 1654, 1500, 1442, 1260, 1190, 1040, 668 cm⁻¹. MS (ESI): *m/z* 400 [M + H]⁺.

***N*-(3-((1*H*-Benzo[*d*]imidazol-1-yl)methyl)benzyl)benzamide, (29).**

The title compound was synthesized following the general procedure, starting from compound **9** (166 mg, 0.70 mmol) and benzoic acid (102 mg, 0.84 mmol). The crude material was purified by column chromatography using PE/EtOAc 3:7 as eluent to afford compound **29** (128 mg, 0.39 mmol, 54%) as a white solid. ¹H-NMR (300 MHz, CD₃OD): δ = 8.24 (s, 1H), 7.75 (d, *J* = 8.2 Hz, 2H), 7.64 (d, *J* = 8.2 Hz, 1H), 7.55-7.49 (m, 1H), 7.43 (t, *J* = 7.7 Hz, 1H), 7.38 (d, *J* = 7.7 Hz, 1H), 7.31-7.15 (m, 7H), 5.45 (s, 2H), 4.51 (s, 2H). MS (ESI): *m/z* 342 [M + H]⁺.

***N*-(3-((1*H*-Benzo[*d*]imidazol-1-yl)methyl)benzyl)-4-methylbenzamide, (30).**

The title compound was synthesized following the general procedure, starting from compound **9** (76 mg, 0.32 mmol) and 2-oxo-2-(*p*-tolyl)acetic acid (52 mg, 0.38 mmol). The crude material was purified by column chromatography using PE/EtOAc 3:7 as eluent to afford compound **30** (79 mg, 0.21 mmol, 69%) as a white solid. Mp

137-139 °C. ¹H-NMR (300 MHz, CD₃OD): δ = 8.22 (s, 1H), 7.81-7.58 (m, 3H), 7.38 (d, *J* = 7.6 Hz, 1H), 7.36-7.06 (m, 8H), 5.43 (s, 2H), 4.90 (s, 2H), 2.36 (s, 3H). ¹³C-NMR (100.6 MHz, DMSO-*d*₆): δ = 166.6, 144.7, 144.0, 141.5, 140.9, 137.4, 134.1, 132.0, 129.3 (2C), 129.2, 127.7 (2C), 127.1, 126.8, 126.3, 122.8, 122.0, 119.9, 111.2, 48.1, 42.9, 21.4. MS (ESI): 356 *m/z* [M + H]⁺.

***N*-(3-((1*H*-Benzo[*d*]imidazol-1-yl)methyl)benzyl)-4-(trifluoromethyl)benzamide, (31).**

The title compound was synthesized following the general procedure, starting from compound **9** (60 mg, 0.25 mmol) and 4-(trifluoromethyl)benzoic acid (57 mg, 0.30 mmol). The crude material was purified by column chromatography using PE/EtOAc 3:7 as eluent to afford compound **31** (84 mg, 0.21 mmol, 82%) as a white solid. Mp 154-156 °C. ¹H-NMR (300 MHz, CD₃OD): δ = 8.27 (s, 1H), 7.89 (d, *J* = 8.2 Hz, 2H), 7.75 (d, *J* = 8.2 Hz, 2H), 7.64 (d, *J* = 7.4 Hz, 1H), 7.39 (d, *J* = 8.2 Hz, 1H), 7.33-7.12 (m, 6H), 5.49 (s, 2H), 4.52 (s, 2H). ¹³C-NMR (100.6 MHz, DMSO-*d*₆): δ = 165.6, 144.7, 144.0, 141.3 (q, *J* = 441.6 Hz), 140.4 (2C), 137.5 (2C), 131.6 (q, *J* = 32.2 Hz), 129.2, 128.6, 127.1, 126.7, 126.5, 125.8 (q, *J* = 4.0 Hz), 122.8, 122.0, 119.9, 111.1, 48.1, 43.0. MS (ESI): 410 *m/z* [M + H]⁺.

***N*-(3-((1*H*-Benzo[*d*]imidazol-1-yl)methyl)benzyl)-4-bromobenzamide, (32).**

The title compound was synthesized following the general procedure, starting from compound **9** (60 mg, 0.25 mmol) and 4-bromobenzoic acid (61 mg, 0.30 mmol). The crude material was purified by column chromatography using PE/EtOAc 3:7 as eluent to afford compound **32** (81 mg, 0.19 mmol, 77%) as a white solid. Mp 151-

153 °C. ¹H-NMR (300 MHz, CD₃OD): δ = 8.27 (s, 1H), 7.73-7.56 (m, 5H), 7.41 (d, *J* = 7.1 Hz, 1H), 7.35 (d, *J* = 7.4 Hz, 2H), 7.29-7.18 (m, 4H), 5.50 (s, 2H), 4.61 (s, 2H). ¹³C-NMR (100.6 MHz, DMSO-*d*₆): δ = 165.8, 144.7, 144.0, 140.5, 137.5, 134.1, 133.9, 131.8, 129.9, 129.2, 127.1, 126.7, 126.4, 125.4, 122.8, 122.0, 119.9, 111.2, 48.1, 42.9. MS (ESI): 420 *m/z* [M + H]⁺.

***N*-(3-((1*H*-Benzo[*d*]imidazol-1-yl)methyl)benzyl)-4-chlorobenzamide, (33).**

The title compound was synthesized following the general procedure, starting from compound **9** (60 mg, 0.25 mmol) and 4-chlorobenzoic acid (47 mg, 0.30 mmol). The crude material was purified by column chromatography using PE/EtOAc 3:7 as eluent to afford compound **33** (57 mg, 0.15 mmol, 60%) as a white solid. Mp 125-127 °C. ¹H-NMR (300 MHz, CD₃OD): δ = 8.25 (s, 1H), 7.73 (d, *J* = 8.5 Hz, 2H), 7.65 (d, *J* = 7.1 Hz, 1H), 7.49-7.37 (m, 3H), 7.33-7.09 (m, 6H), 5.48 (s, 2H), 4.50 (s, 2H). ¹³C-NMR (100.6 MHz, DMSO-*d*₆): δ = 165.7, 144.7, 144.0, 140.6, 137.5, 136.5, 134.1, 133.5, 129.7, 129.2, 128.9, 127.1, 126.7, 126.4, 122.8, 122.0, 119.9, 111.2, 48.1, 42.9. MS (ESI): 376 *m/z* [M + H]⁺.

***N*-(3-((1*H*-Benzo[*d*]imidazol-1-yl)methyl)benzyl)-4-fluorobenzamide, (34).**

The title compound was synthesized following the general procedure, starting from compound **9** (60 mg, 0.25 mmol) and 4-fluorobenzoic acid (43 mg, 0.30 mmol). The crude material was purified by column chromatography using PE/EtOAc 3:7 as eluent to afford compound **34** (70 mg, 0.19 mmol, 78%) as a grey solid. Mp 116-118 °C. ¹H-NMR (300 MHz, CD₃OD): δ = 8.26 (s, 1H), 7.87-7.78 (m, 2H), 7.65 (d, *J* = 6.8 Hz, 1H), 7.41 (d, *J* = 6.8 Hz, 1H), 7.35 (d, *J* = 8.0 Hz, 2H), 7.27-7.09 (m, 6H),

5.49 (s, 2H), 4.52 (s, 2H). ^{13}C -NMR (100.6 MHz, DMSO- d_6): δ = 165.7, 164.3 (d, J = 248.8 Hz), 144.7, 144.0, 140.7, 137.5, 134.1, 131.2 (d, J = 3.0 Hz), 130.3 (d, J = 9.0 Hz), 129.2, 127.1, 126.7, 126.4, 122.8, 122.0, 119.9, 115.7 (d, J = 21.1 Hz), 111.2, 48.1, 42.9. MS (ESI): 360 m/z [M + H] $^+$.

***N*-(3-((1*H*-Benzo[*d*]imidazol-1-yl)methyl)benzyl)-4-cyanobenzamide, (35).**

The title compound was synthesized following the general procedure, starting from compound **9** (166 mg, 0.70 mmol) and 4-cyanobenzoic acid (123 mg, 0.84 mmol). The crude material was purified by column chromatography using PE/EtOAc 3:7 as eluent to afford compound **35** (197 mg, 0.54 mmol, 77%) as a white solid. Mp 192-194 °C. ^1H -NMR (400 MHz, CD $_3$ OD): δ = 8.25 (s, 1H), 7.90-7.79 (m, 4H), 7.64 (d, J = 6.8 Hz, 1H), 7.39 (d, J = 6.8 Hz, 1H), 7.35-7.16 (m, 6H), 5.49 (s, 2H), 4.52 (s, 2H). ^{13}C -NMR (100.6 MHz, DMSO- d_6): δ = 165.4, 144.7, 144.0, 140.3, 138.8, 137.5, 134.1, 132.9 (2C), 129.2, 128.6 (2C), 127.2, 126.7, 126.5, 122.8, 122.0, 119.9, 118.8, 114.1, 111.1, 48.1, 43.1. IR (KBr): $\tilde{\nu}$ 3553, 3414, 3348, 3082, 2923, 2358, 2227, 1638, 1546, 1492, 1443, 736, 742 cm^{-1} . MS (ESI): m/z 367 [M + H] $^+$.

***N*-(3-((1*H*-Benzo[*d*]imidazol-1-yl)methyl)benzyl)-4-cyano-3-methylbenzamide, (36).**

The title compound was synthesized following the general procedure, starting from compound **9** (60 mg, 0.25 mmol) and 4-cyano-3-methylbenzoic acid (49 mg, 0.30 mmol). The crude material was purified by column chromatography using PE/EtOAc 3:7 as eluent to afford compound **36** (48 mg, 0.13 mmol, 51%) as a yellow solid. Mp 178-180 °C. ^1H -NMR (300 MHz, DMSO- d_6): δ = 9.21 (br s, 1H), 8.40 (s, 1H), 7.90

(d, $J = 6.9$ Hz, 2H), 7.78 (d, $J = 8.0$ Hz, 1H), 7.65 (d, $J = 5.0$ Hz, 1H), 7.51 (d, $J = 5.0$ Hz, 1H), 7.34-7.27 (m, 2H), 7.21-7.17 (m, 4H), 5.48 (s, 2H), 4.50 (s, 2H). MS (ESI): 381 m/z $[M + H]^+$.

***N*-(3-((1*H*-Benzo[*d*]imidazol-1-yl)methyl)benzyl)-4-cyano-2-fluorobenzamide, (37).**

The title compound was synthesized following the general procedure, starting from compound **9** (60 mg, 0.25 mmol) and 4-cyano-2-fluorobenzoic acid (49 mg, 0.30 mmol). The crude material was purified by column chromatography using PE/EtOAc 3:7 as eluent to afford compound **37** (58 mg, 0.15 mmol, 60%) as a white solid. Mp 103-105 °C. ¹H-NMR (300 MHz, CD₃OD): $\delta = 8.28$ (s, 1H), 7.79-7.57 (m, 4H), 7.42 (d, $J = 5.2$ Hz, 1H), 7.34 (d, $J = 8.5$ Hz, 2H), 7.27-7.19 (m, 4H), 5.51 (s, 2H), 4.53 (s, 2H). MS (ESI): 385 m/z $[M + H]^+$.

***N*-(3-((1*H*-Benzo[*d*]imidazol-1-yl)methyl)benzyl)-4-cyano-3-fluorobenzamide, (38).**

The title compound was synthesized following the general procedure, starting from compound **9** (60 mg, 0.25 mmol) and 4-cyano-3-fluorobenzoic acid (50 mg, 0.30 mmol). The crude material was purified by column chromatography using PE/EtOAc 3:7 as eluent to afford compound **38** (46 mg, 0.11 mmol, 48%) as a yellow solid. Mp 192-194 °C. ¹H-NMR (300 MHz, DMSO-*d*₆): $\delta = 9.37$ (br s, 1H), 8.58 (s, 1H), 8.08 (t, $J = 8.08$ Hz, 1H), 7.95-7.80 (m, 2H), 7.65 (d, $J = 7.6$ Hz, 1H), 7.56 (d, $J = 7.6$ Hz, 1H), 7.43-7.16 (m, 6H), 5.53 (s, 2H), 4.45 (s, 2H). MS (ESI): 385 m/z $[M + H]^+$.

***N*-(3-((1*H*-Benzo[*d*]imidazol-1-yl)methyl)benzyl)-3-morpholinopropanamide, (39).**

The title compound was synthesized following the general procedure, starting from compound **9** (166 mg, 0.70 mmol) and 3-morpholinopropanoic acid (133 mg, 0.84 mmol). The crude material was purified by column chromatography using EtOAc/MeOH 9:1 as eluent to afford compound **39** (146 mg, 0.39 mmol, 55%) as an amorphous yellow solid. ¹H-NMR (300 MHz, CD₃OD): δ = 8.25 (s, 1H), 7.68 (t, *J* = 3.0 Hz, 1H), 7.43 (t, *J* = 3.0 Hz, 1H), 7.34-7.24 (m, 5H), 7.18 (d, *J* = 6.9 Hz, 1H), 5.48 (s, 2H), 4.34 (s, 2H), 3.58-3.50 (m, 4H), 2.60 (t, *J* = 7.0 Hz, 2H), 2.42- 2.39 (m, 4H), 2.36 (t, *J* = 7.0 Hz, 2H). IR (neat): $\tilde{\nu}$ = 3268, 2062, 1649, 1550, 1495, 1457, 1287, 1114, 743 cm⁻¹. MS (ESI): *m/z* 379 [M + H]⁺.

4-((*Tert*-butoxycarbonyl)amino)butanoic acid, (41).

To a solution of 4-aminobutanoic acid **40** (200 mg, 1.94 mmol, 1 eq) in 2 M aq. NaOH (3 mL), a solution of Boc₂O (507.50 mg, 2.33 mmol, 1.2 eq) in THF (5 mL) was added dropwise and the reaction was stirred at rt overnight. The solvent was removed in vacuo. The aqueous layer was acidified with 2M aq. HCl until pH 4 and extracted with EtOAc (6x). Additionally, the aqueous layer was saturated with NaCl and extracted with THF (3x). The combined organic layers were dried over Na₂SO₄, filtrated and concentrate in vacuo yielding the desired compound (339 mg, 1.67 mmol, 86%) as a yellow oil, which was used directly in the next step without further purification. ¹H-NMR (300 MHz, DMSO-*d*₆): δ = 6.77 (br s, 1H), 2.92 (t, *J* = 6.3 Hz,

2H), 2.16 (t, $J = 6.3$ Hz, 2H), 1.58 (quint, $J = 6.9$ Hz, 2H), 1.41 (s, 9H). MS (ESI): 204 m/z $[M + H]^+$.

***N*-(3-((1*H*-Benzo[*d*]imidazol-1-yl)methyl)benzyl)-4-aminobutanamide, (43).**

Step 1: To a solution of compound **9** (166.11 mg, 0.70 mmol, 1 eq) in dry CH_2Cl_2 (5 mL) TEA (220 μL , 1.54 mmol, 2.2 eq), EDCI (161.28 mg, 0.84 mmol, 1.2 eq), HOBT (113.51 mg, 0.84 mmol, 1.2 eq) and compound **41** (170.71 mg, 0.84 mmol, 1.2 eq) were added in order. The resulting mixture was stirred at room temperature for 16 h. CH_2Cl_2 was added and the organic phase was washed with H_2O (x3), dried over Na_2SO_4 and evaporated. Purification by column chromatography using EtOAc as eluent afforded compound **42** (168 mg, 0.40 mmol, 57%) as a yellow solid.

Step 2: To a solution of compound **42** (148 mg, 0.35 mmol, 1 eq) in CH_2Cl_2 (2.5 mL) at 0 °C CF_3COOH (1.23 mL) was added. The reaction mixture was stirred at the same temperature for 30 min and then for 3 h at rt. 2 M aq. NaOH was added until pH 7 and the aqueous layer was extracted with EtOAc (x3). The collected organic layers were dried over Na_2SO_4 , filtrated and concentrated in vacuo. Purification by column chromatography using $\text{CH}_3\text{CN}/\text{NH}_3$ 9:1 as eluent afforded compound **43** (80 mg, 0.25 mmol, 71%) as a yellow oil. $^1\text{H-NMR}$ (300 MHz, CD_3OD): $\delta = 8.24$ (s, 1H), 7.67 (d, $J = 7.6$ Hz, 1H), 7.36 (d, $J = 7.6$ Hz, 1H), 7.23-7.13 (m, 6H), 5.41 (s, 2H), 4.30 (s, 2H), 2.61 (t, $J = 7.4$ Hz, 2H), 2.19 (t, $J = 7.4$ Hz, 2H), 1.70 (quint, $J = 6.8$ Hz, 2H). IR (KBr): $\tilde{\nu} = 3478, 2621, 1617, 1521, 1540, 1456, 615$ cm^{-1} . MS (ESI): 323 m/z $[M + H]^+$.

***N*-(3-((1*H*-Benzo[*d*]imidazol-1-yl)methyl)benzyl)formamide, (44).**

To a solution of amine **9** (500 mg, 2.11 mmol, 1 eq) in formic acid (1.86 mL) acetic anhydride (1.58 mL, 16.86 mmol, 8 eq) was added dropwise at 0 °C. After ten min, the mixture was allowed to reach room temperature and was stirred for 3 h. Then, water was added and the mixture was stirred for additional 10 min. The volatile was removed, affording compound **44** (548 mg, 2.07 mmol, 98%) as a yellow oil. ¹H-NMR (300 MHz, CD₃OD): δ = 8.20 (s, 1H), 8.12 (s, 1H), 7.66 (d, *J* = 7.5 Hz, 1H), 7.31 (d, *J* = 7.8 Hz, 1H), 7.18-7.14 (m, 5H), 7.03 (s, 1H), 5.27 (s, 2H), 4.28 (s, 2H). IR (neat): $\tilde{\nu}$ = 3256, 3051, 2861, 1664, 1494, 1457, 1381, 1261, 1007, 738, 698 cm⁻¹. MS (ESI): 266 *m/z* [M + H]⁺.

1-(3-(Isocyanomethyl)benzyl)-1*H*-benzo[*d*]imidazole, (45).

Compound **44** (500 mg, 1.89 mmol, 1 eq) was dissolved in dry CH₂Cl₂ (7 mL) and TEA (1.3 mL, 9.43 mmol, 5 eq) was added at 0 °C and under nitrogen. A solution of POCl₃ (259 μL, 2.83 mmol, 1.5 eq) in dry CH₂Cl₂ (4 mL) was added dropwise and the reaction was stirred for 1.5 h at 0 °C. Aqueous saturated NaHCO₃ solution was then added and the mixture was left to reach room temperature and stirred for additional 10 min. Then, the reaction was extracted with CH₂Cl₂, dried over Na₂SO₄ and evaporated, yielding compound **45** (205.4 mg, 0.83 mmol, 44%) as an amorphous yellow solid. ¹H-NMR (300 MHz, CD₃OD): δ = 7.88 (s, 1H), 7.45 (dd, *J*_s = 6.8, 2.5 Hz, 1H), 7.29-7.17 (m, 5H), 7.04 (m, 2H), 5.23 (s, 2H), 4.45 (s, 2H). IR (KBr): $\tilde{\nu}$ = 2927, 2854, 2671, 2159, 1617, 1494, 1437, 1266, 746 cm⁻¹.

***N*-(3-((1*H*-Benzo[*d*]imidazol-1-yl)methyl)benzyl)-2-acetamidoacetamide, (46).**

To a solution of compound **45** (197.6 mg, 0.8 mmol, 1 eq) in MeOH (1.4 mL) and water (0.5 mL) acetic acid (45 μ L, 0.8 mmol, 1 eq), NH₄Cl (128.3 mg, 2.4 mmol, 3 eq), TEA (111 μ L, 0.8 mmol, 1 eq) and paraformaldehyde (38.4 mg, 0.80 mmol, 1 eq) were added in order. The mixture was heated at 65 °C for 8 h. Then, water was added and the aqueous phase was extracted with EtOAc (3x). The organic phases were collected, dried over Na₂SO₄ and evaporated. The crude product was purified by column chromatography using EtOAc/MeOH 9:1 as eluent, affording compound **46** (80 mg, 0.25 mmol, 30%) as a white solid. Mp 164-166 °C. ¹H-NMR (300 MHz, CD₃OD): δ = 8.30 (s, 1H), 7.66 (d, *J* = 6.7 Hz, 1H), 7.41 (d, *J* = 6.2 Hz, 1H), 7.24-7.18 (m, 5H), 7.15 (s, 1H), 5.44 (s, 2H), 4.35 (s, 2H), 3.85 (s, 2H), 1.99 (s, 3H). IR (KBr): $\tilde{\nu}$ = 3476, 3415, 3228, 3054, 2927, 2811, 1617, 1548, 1286 cm⁻¹. MS (ESI): 337 *m/z* [M + H]⁺.

***N*-(2-(((3-((1*H*-Benzo[*d*]imidazol-1-yl)methyl)benzyl)amino)-2-oxoethyl)benzamide, (**47**).**

The title compound was synthesized following the procedure described for compound **46**. The crude material was purified by column chromatography using EtOAc/MeOH 9:1 as eluent to afford compound **47** (101.9 mg, 0.26 mmol, 32%) as a white solid. Mp 136-138 °C. ¹H-NMR (300 MHz, CD₃OD): δ = 8.28 (s, 1H), 7.89 (d, *J* = 7.9 Hz, 2H), 7.66 (d, *J* = 7.7 Hz, 1H), 7.52-7.42 (m, 3H), 7.26-7.18 (m, 6H), 7.12 (s, 1H), 5.46 (s, 2H), 4.37 (s, 2H), 4.07 (s, 2H). IR (KBr): $\tilde{\nu}$ = 3465, 3415, 3081, 2931, 1686, 1453, 1437, 1207, 1142, 737, 725 cm⁻¹. MS (ESI): 399 *m/z* [M + H]⁺.

3-(((5-Bromo-2-nitrophenyl)amino)methyl)benzonitrile, (50**).**

To a solution of 2,4-dibromo-1-nitrobenzene **48** (100 mg, 0.36 mmol, 1 eq) in DMSO (1 mL), K₂CO₃ (73 mg, 0.53 mmol, 1.5 eq) and 3-(aminomethyl)benzotrile **49** (51 mg, 0.39 mmol, 1.01 eq) were added in order. The reaction mixture was stirred at 72 °C overnight. EtOAc was added and the organic layer was washed with aqueous saturated NaHCO₃ (3x), dried over Na₂SO₄, filtered and concentrated in vacuo. Purification by silica gel column chromatography using PE/EtOAc 95:5 as eluent afforded compound **50** (15 mg, 0.05 mmol, 13%) as a yellow solid. Mp 196-198 °C. ¹H-NMR (300 MHz, CDCl₃): δ = 8.42 (s, 1H), 8.08 (d, *J* = 7.8 Hz, 1H), 7.62-7.49 (m, 2H), 7.51 (d, *J* = 7.8 Hz, 1H), 6.88-6.83 (m, 2H), 4.57 (d, *J* = 4.7 Hz, 2H). IR (KBr): $\tilde{\nu}$ = 3390, 2921, 2229, 1962, 1890, 1520, 1408, 1257, 1049, 750, 618 cm⁻¹. MS (ESI): 332 *m/z* [M + H]⁺.

3-((6-Bromo-1*H*-benzo[*d*]imidazol-1-yl)methyl)benzotrile, (51).

To a solution of compound **50** (0.93 g, 56.24 mmol, 1 eq) in formic acid (29 mL), Fe (3.14 g, 56.24 mmol, 20 eq) was added. The reaction mixture was heated to 85 °C for 16 h. MeOH (29 mL) was added, the reaction was filtered and the filtrate concentrate in vacuo. The crude material was purified by silica gel column chromatography using PE/EtOAc 4:6 as eluent yielding a yellow solid (1.21 g, 38.81 mmol, 69%). Mp 123-125 °C. ¹H-NMR (300 MHz, CDCl₃): δ = 8.00 (s, 1H), 7.62 (m, 2H), 7.42-7.26 (m, 5H), 5.35 (s, 2H). IR (KBr): $\tilde{\nu}$ = 3063, 2921, 2722, 2356, 2228, 1699, 1493, 1462, 1361, 1283, 767, 690 cm⁻¹. MS (ESI): 313 *m/z* [M + H]⁺.

(3-((6-Bromo-1*H*-benzo[*d*]imidazol-1-yl)methyl)phenyl)methanamine, (52).

Compound **52** was synthesized as previously reported for the preparation of compound **9**, starting from compound **51** (350 mg, 1.17 mmol). The crude material was purified by column chromatography using EtOAc/MeOH 7:3 to obtain the desired compound (147 mg, 0.47 mmol, 40%) as a yellow oil. ¹H-NMR (300 MHz, CD₃OD): δ = 8.21 (s, 1H), 7.55 (t, *J* = 7.1 Hz, 1H), 7.36 (dd, *J*_s = 1.4, 7.4 Hz, 1H), 7.23-7.17 (m, 4H), 7.05 (s, 1H), 5.32 (s, 2H), 3.7 (s, 2H). IR (KBr): $\tilde{\nu}$ = 3521, 3444, 2922, 2855, 1496, 1562, 1458, 1367, 745 cm⁻¹. MS (ESI): 316 *m/z* [M + H]⁺.

4-Bromo-*N*-(3-((6-bromo-1*H*-benzo[*d*]imidazol-1-yl)methyl)benzyl)-1*H*-pyrrole-2-carboxamide, (53**).**

The title compound was synthesized following the general procedure, starting from compound **52** (100 mg, 0.32 mmol) and 4-bromo-1*H*-pyrrole-2-carboxylic acid (71 mg, 0.38 mmol). The crude material was purified by column chromatography using PE/EtOAc 3:7 as eluent to afford compound **53** (61 mg, 0.12 mmol, 39%) as a white solid. Mp 200-202 °C. ¹H-NMR (300 MHz, CD₃OD): δ = 8.26 (s, 1H), 7.65 (d, *J* = 7.7 Hz, 1H), 7.55 (d, *J* = 7.7 Hz, 1H) 7.31-7.13 (m, 5H), 6.91 (s, 1H), 6.73 (s, 1H), 7.15 (s, 2H), 4.45 (s, 2H). ¹³C-NMR (100.6 MHz, DMSO-*d*₆): δ = 161.2, 144.8, 144.0, 140.3, 138.0, 134.7, 129.7, 127.0, 126.9, 126.8, 125.2, 122.8, 122.2, 121.8, 118.7, 117.9, 111.2, 94.8, 50.4, 42.9. IR (KBr): $\tilde{\nu}$ = 3484, 3407, 3224, 3119, 3291, 2769, 1564, 1525, 1459, 749 cm⁻¹. MS (ESI): 489 *m/z* [M + H]⁺.

In vitro metabolism studies

***In vitro* metabolism in mouse liver microsomes**

Mouse liver microsomes (MLM), (pooled male mouse CD-1, protein concentration: 20 mg/mL) were purchased from Corning B.V. Life Sciences (Amsterdam, The Netherlands) and used throughout this study. The standard incubation mixture (250 μ L final volume), was carried out in a 50 mM TRIS (tris[hydroxymethyl]aminomethane) buffer (pH 7.4) containing 3.3 mM $MgCl_2$, 1.3 mM β -NADP- Na_2 , 3.3 mM glucose 6-phosphate, 0.4 Units/mL glucose 6-phosphate dehydrogenase (NADPH regenerating system), 5 μ L of acetonitrile (1% of total volume), and the substrate compounds at a concentration of 50 μ M. After pre-equilibration of the mixture, an appropriate volume of MLM suspension was added to give a final protein concentration of 1 mg/mL. The mixture was shaken for 60 min at 37 $^{\circ}C$. Control incubations were carried out without the presence of MLM suspension or cofactors. When metabolic activation was studied, 3 mM GSH trapping agent was added in the incubation mixture. Each incubation was stopped by addition of 250 μ L ice-cold acetonitrile, vortexed and centrifuged at 13000 r.p.m. for 10 min.

CYP inhibition: aminopyrine *N*-demethylase assay

Aminopyrine *N*-demethylase activity was determined by detecting the amount of formaldehyde produced by rat liver microsomes (RLM). The incubation was carried out in Tris-HCl buffer (50 mM, pH 7.4) supplemented with 150 mM KCl and 10 mM $MgCl_2$. The incubation contained 1 mM aminopyrine, acetonitrile (1% final volume), and 1 mg/mL of RLM in a total volume of 180 μ L. Increasing concentrations of **10**, **23** and **35** (0.01, 1, 5, 10, 25, 50, 75, and 100 μ M) were added

to the incubation mixture to inhibit aminopyrine *N*-demethylase activity. After 3 min pre-incubation at 37 °C, the reaction was initiated by adding the β -NADPH (3 mM) and carried out at 37 °C for 15 min with moderate shaking. The reaction was then quenched by addition of 90 μ L of 20% (*w/v*) cold TCA solution. After centrifugation at 13000 r.p.m. for 10 min, a 240 μ L aliquot of the protein-free supernatant was treated with 120 μ L of Nash reagent and incubated at 37 °C for 40 min. The absorbance intensity of the resultant solution was determined at 412 nm, subtracting the blank sample absorbance (without β -NADPH). The concentration of formaldehyde was quantified (nmol/min/mg) by comparison with a standard curve prepared from commercially available formaldehyde solution freshly standardized by iodometric titration. IC₅₀ values were calculated by using GraphPad Prism software (GraphPad Software, Inc., USA). Nash reagent: 3.75 g ammonium acetate, 50 μ l glacial acetic acid, and 75 μ L acetylacetone were dissolved in 25 mL of deionized water. The solution was freshly prepared and used only for one day.

Biology

Ligand binding experiments

Recombinant human IDO1 (rhIDO1) was purchased from Proteros Biostructures GmbH, (Martinsried, Germany). Experiments to assess K_d values were conducted using Monolith NT.115 instrument (NanoTemper Technologies, Munich, Germany). Fluorescence labeling of rhIDO1 was performed following the protocol for *N*-hydroxysuccinimide (NHS) coupling of RED dye NT650 (NanoTemper Technologies, Munich, Germany) to lysine residues. Briefly, 100 μ L of a 20 μ M

solution of rhIDO1 protein in MES buffer (25 mM MES, 150 mM KCl, pH 6.5) was mixed with 100 μ L of 80 μ M NT650-NHS fluorophore (NanoTemper Technologies, Munich, Germany) and incubated for 30 min at room temperature in the dark. Unbound fluorophores were removed by size-exclusion chromatography with MST buffer (50 mM TRIS, 150 mM NaCl, 10 mM MgCl₂, pH 7.4, 0.05% Tween20) as running buffer. The real concentration of each element of the sample, such as protein, heme group and RED dye, and the *degree of labeling (DoL)* were determined using extinction coefficient $\epsilon_{280} = 51,380 \text{ M}^{-1} \text{ cm}^{-1}$ for rhIDO1, $\epsilon_{405} = 159,000 \text{ M}^{-1} \text{ cm}^{-1}$ for rhIDO1 heme group and $\epsilon_{650} = 195,000 \text{ M}^{-1} \text{ cm}^{-1}$ for NT650 fluorophore, with a correction factor (F_{corr}) of 0.04 at 280 nm, using $C_{\text{prot}} = [A_{280} - (A_{650} \times F_{\text{corr}}) / \epsilon_{280} \times l]$, and *DoL* resulted between 0.6 and 0.8. Compound pre-dilutions were prepared for MST experiments by 16-fold 1:1 serial dilutions in assay buffer containing 4% DMSO in PCR tubes supplied by NanoTemper Technologies to yield final volumes of 10 μ L. NT650-rhIDO1 solution 10 μ L was added to each compound dilution and mixed to reach a final NT650-rhIDO1 concentration of 50 nM, including 2% DMSO, 2 mM DTT and a reaction volume of 20 μ L. After 10 min incubation, these samples were loaded into 16 premium-coated capillaries and inserted in the chip tray of the MST instrument for thermophoresis analysis and K_d evaluation. MST signals were recorded at Medium MST power (compounds **1** and **10**) and 20% LED power. Each compound was tested in three independent experiments and recorded data were processed with NanoTemper *MO.Affinity Analysis* software v2.3 in *Manual* mode setting the hot region between 19-20 seconds. Confidence values (\pm)

are indicated next to K_d value, showing the range where the K_d falls with a 68% of certainty.

Cell culture

Human A375 cells were cultured in DMEM medium with high glucose (4.5 g/L), containing 10% heat inactivated fetal bovine serum (FBS), 2 mM L-glutamine 100 U/mL of penicillin and 10 μ g/mL of streptomycin (GE Healthcare, Milan, Italy).

Human HeLa, HepG2 and MCF-7 cells were cultured in EMEM medium containing 10% FBS, 2 mM L-glutamine 100 U/mL of penicillin and 10 μ g/mL of streptomycin (GE Healthcare, Milan, Italy). Human LXF-289 and DAN-G cells were cultured in RPMI medium containing 10% FBS, 2 mM L-glutamine 100 U/mL of penicillin and 10 μ g/mL of streptomycin (GE Healthcare, Milan, Italy).

Cells of P1.HTR, a highly transfectable clonal variant of mouse mastocytoma P815,⁵⁰ were transfected by electroporation with plasmid constructs coding for mouse IDO1 (P1.IDO1) or TDO (P1.TDO). Stable transfectant cell lines were obtained by puromycin selection. Both cell lines were cultured in Iscove's Modified Dulbecco's Medium (Gibco, Invitrogen CA, USA) supplemented with 10% FCS (Gibco, Invitrogen CA, USA), 1 mM glutamine (Gibco, Invitrogen CA, USA) and penicillin/streptomycin (Gibco, Invitrogen CA, USA).

Peripheral blood samples were collected from a cohort of 16 patients with different stages of pancreatic ductal adenocarcinoma admitted at the Unit of General and Pancreatic Surgery of the Azienda Ospedaliera Universitaria Integrata of Verona before surgical resection or from healthy donors. No subject was undergoing therapy

at the time of sample collection. PBMCs were isolated by Ficoll-Hypaque (GE Healthcare). Monocytes were isolated from PBMCs by using CD14 MicroBeads (Miltenyi Biotech) according to manufacturer's instructions with at least 95% cell purity, as evaluated by flow cytometry. Cells were cultured in a humidified atmosphere (5% CO₂, 37 °C).

Cell cytotoxicity

Cell viability was measured by the 3-(4,5-dimethylthiazol-2-yl)-2,5-diphenyl-tetrazolium bromide (MTT) assay, as previously described.⁵¹ A375 cells were seeded (0.5 x 10⁵ cells/well) in 24-well plates and treated with each compound (1 μM) for 48 h at 37 °C in a 5% CO₂ humidified incubator. The percentage of cell viability was calculated as $[100 (x-y) / (z-y)]$, where x, y, and z were the absorbance read in compound-treated, resting and compound-untreated cells, respectively.

Monocytes viability assay

Purified monocytes from HD were treated or not with increasing concentration of epacadostat, compounds **10** and **23**. Purified monocytes from PDAC patients were treated or not with 30 μM epacadostat, compounds **10** and **23**. Following 24 h, cells were stained with Annexin V using the Annexin V Apoptosis Detection Kit APC (eBioscience, Thermo Fisher Scientific) and 7-AAD (BD Biosciences). Cell viability was evaluated on AnnexinV^{neg}7AAD^{neg} monocytes by flow cytometry and FlowJo software (TreeStar).

Cellular IDO1 enzymatic assay

The enzymatic activity of IDO1 was evaluated by measuring the levels of L-Kyn into A375 cell media, as previously described.⁵² A375 cells (3×10^4) were seeded in a 24-well culture plate (500 μ L/well) and grown overnight. DMSO dilutions (1 μ M) of each compound in a total volume of 500 μ L culture medium including human IFN- γ (1000 U/mL final concentration) per well were added into wells containing the cells. All compounds were dissolved in DMSO (Sigma–Aldrich). The DMSO final concentration in cell culture medium was always 0.1%. Equivalent amount of DMSO was always added to drug untreated controls. After 48 h incubation, cell medium was collected, deproteinized by 20% (v/v) aqueous CCl_3COOH , centrifuged at 13,200 rpm for 10 min, and the amounts of L-Kyn in A375 cell media were quantified with HPLC. 20 μ L of supernatants were injected by a multi-sampler (Beckman Coulter, Milan, Italy) into a HPLC-UV system (System Gold, Beckman Coulter), equipped with a C-18 sphereClone ODS analytical column (5 μ m particle size, 250 mm x 4.0 mm; Phenomenex, Torrance, CA, USA). The mobile phase (50 mM potassium dihydrogen phosphate, 10% v/v acetonitrile; pH 4.8) was delivered at a flow-rate of 1 mL/min at room temperature, and the absorbance was measured at 330 nm. Amounts of L-Kyn in A375 cell media were quantified on the basis of a calibration curve obtained using the same HPLC-UV experimental setting. To calculate IC_{50} values, IFN- γ -stimulated A375 cells were incubated with increasing concentrations (0.001-3 μ M) of compounds for 48 h and L-Kyn levels were evaluated by HPLC, as reported above. The determination of inhibitors activity on

Hela, HepG2, LXF-289, MCF-7 and DAN-G cell lines was performed similarly to A375 cells.

IDO1 and TDO selectivity assay

In every cellular assay, P1 transfected cells were used at a passage number not exceeding the 10th. Dose-response curves for extrapolating the cellular IC₅₀ were built by incubating 1×10⁵ P1.IDO1 or P1.TDO cells in a final volume of 400 µL with 3-fold serial dilutions of each compound for 16 h in a 48-well plate. The control was represented by cells incubated with an equivalent volume of DMSO, the vehicle in which compounds have been solubilized. After the incubation, supernatants of cell cultures were recovered and L-Kyn concentration was detected by HPLC-UV. Every cell assay was conducted in triplicate and repeated three times. Detection of L-Kyn concentrations was performed by using a Perkin Elmer, series 200 HPLC instrument (MA, USA). A Kinetex® C18 column (250×4.6 mm, 5 µm, 100 Å; Phenomenex, USA), maintained at the temperature of 25 °C and pressure of 1800 PSI, was used. A sample volume of 300 µL was injected and eluted by a mobile phase containing 10 mM NaH₂PO₄ pH 3.0 (99%) and methanol (1%) (Sigma-Aldrich, MO, USA), with a flow rate of 1 mL/min. L-Kyn was detected at 360 nm by an UV detector. The software TURBOCHROM 4 was used for evaluating the concentration of L-Kyn in samples by mean of a calibration curve. The detection limit of the analysis was 0.05 µM.

T cell proliferation assay

PBMCs were isolated from leukocytes-enriched buffy coats from HD (Transfusion Centre, University and Hospital Trust of Verona, Italy), stained with 1 μ M of CellTrace Violet (Thermo Fisher Scientific) in PBS and followed by 5 min incubation at 37 °C, protected from light. Labelled PBMCs were stimulated with coated 0.6 μ g/mL anti-CD3 (clone OKT-3, eBioscience, Thermo Fisher Scientific) and 5 μ g/mL anti-CD28 (clone CD28.2, eBioscience, Thermo Fisher Scientific) for 4 days and co-cultured with monocytes pre-treated or not with 30 μ M of epacadostat **1**, compounds **10** and **23** for 24 h at 3:1 ratio (monocyte:PBMCs). Cell cultures were incubated at 37 °C and 8% CO₂ in L-arginine and L-glutamine-free-RPMI (Biochrom), supplemented with 2 mM L-glutamine (Euroclone), 150 μ M L-arginine (Sigma-Aldrich), 10% FBS (Superior, Merck), 10 U/mL penicillin and streptomycin (Euroclone), and 0.1 mM HEPES (Euroclone). At the end of the co-culture, cells were stained with PE-Cy7 conjugated anti-CD3 (UCHT1, eBioscience, Thermo Fisher Scientific), and CellTrace signal of CD3⁺ gated lymphocytes were analysed by flow cytometry and FlowJo software (Tree Star).

Western Blot

5x10⁶ monocytes isolated from HD and PDAC samples were lysed in RIPA buffer with the addition of protease inhibitor cocktail tablets (Roche) and sodium vanadate. SDS-PAGE was performed loading 40 μ g of protein lysates on 10% denaturing SDS polyacrylamide gel and transferred on PVDF membrane (Millipore). Membrane was blocked in Tris-buffered saline plus 0.01% Tween-20 and 5% non-fat milk and incubated with rabbit anti-human IDO (D5J4E, Cell Signaling Technologies),

followed by the secondary incubation with goat anti-rabbit IgG antibody, horseradish peroxidase (HRP)-conjugated (Millipore).

Animal studies

Animal care was in compliance with Italian regulations on protection of animals used for experimental purposes and were authorized by the Ministry of Health (259/2019 DB064.44 of 28/03/2019).

Pharmacokinetic-Pharmacodynamic studies

8 Weeks-old male BALB/C mice (n=8; Envigo) were maintained under 12-h light/dark cycle at 21 ± 1 °C and $50 \pm 5\%$ humidity. Mice were starved 8 h before the single dose administration of epacadostat (INCB24360) and **23**.⁴⁰ INCB24360, used as a positive control, was administered 50 mg/kg and **23** intravenously at the dose of 10 mg/kg. The blood was collected from the eye by a retro-orbital puncture at different time points (2, 5, 15, 30 min, 1 h, 3 h, 8 h, 24 h), centrifuged at 8679 rpm for 15', separating the clot from the plasma, and then used for LC/MS analysis.

Pharmacokinetic analysis

After 10 mg/Kg endovenous administration of **10** and **23** blood was drawn after 2, 5, 15, 30, 60, 180 min and 24 h. Aliquots of plasma samples (50 μ L) were diluted by adding 100 μ L of acetonitrile. Samples were homogenized and centrifuged at 13000 r.p.m. for ten min and supernatants (5 μ L) were injected into LC-HRMS system. Plasma calibration standards were prepared by spiking appropriate amounts of analytes into blank plasma. The calibration curves ($y = ax + b$), were constructed

from the peak area versus plasma concentration using the weighted ($1/x$) linear least-squares regression method (calibration range 0.1-5000 $\mu\text{g/L}$).

L-Kyn levels analysis

After 10 mg/kg endovenous administration of **10**, **23**, epacadostat (control) blood was drawn after 2, 5, 15, 30, 60, 180 min and 24 h. Aliquots of plasma samples (50 μL) were diluted by adding 100 μL of acetonitrile. Samples were homogenized and centrifuged at 13000 r.p.m. for 10 min and supernatants (5 μL) were injected into LC-HRMS system. The % of L-Kyn was calculated considering 100% the area of the analyte before the administration.

ASSOCIATED CONTENT

Supporting Information.

The Supporting Information is available free of charge.

Molecular modelling, NMR spectra of compounds **10**, **23** and **35**, dose-response curves of the selected compounds in A375, P1.IDO1 and P1.TDO cell lines, metabolic stability data, structural characterization of metabolites by HRMS and *in vivo* PK/PD evaluation of compound **23**.

Molecular formula strings.

AUTHOR INFORMATION

Corresponding Authors

Dr. Alberto Massarotti

Dept. of Pharmaceutical Sciences
Università del Piemonte Orientale
Largo Donegani, 2 – 28100 Novara
Phone: 0039-0321-375753
Fax: 0039-0321-375821
e-mail: alberto.massarotti@uniupo.it

Prof. Tracey Pirali
Dept. of Pharmaceutical Sciences
Università del Piemonte Orientale
Largo Donegani, 2 – 28100 Novara
Phone: 0039-0321-375852
Fax: 0039-0321-375821
e-mail: tracey.pirali@uniupo.it

Author Contributions

The manuscript was written through contributions of all authors. All authors have given approval to the final version of the manuscript. ‡These authors contributed equally. *These authors contributed equally.

Notes

The authors declare no competing financial interest.

ACKNOWLEDGMENT

We gratefully acknowledge Salvatore Terrazzino for support in the PK data analysis. M. S. is supported by Fondazione AIRC (Associazione Italiana per la Ricerca sul Cancro) fellowship for Italy (Rif. 22568). T.P., S.A., S.F., M.T.P. and S.U. gratefully acknowledge Ministero dell'Istruzione, dell'Università e della Ricerca (MIUR) for financial support (PRIN 2017 N° 2017WJZ9W9). This work was partially supported by S.U. grant (21509) from Fondazione AIRC.

ABBREVIATIONS

AO, aldehyde oxidase; Boc₂O, di-*tert*-butyl dicarbonate; CD3, cluster of differentiation 3; CD28, cluster of differentiation 28; CDCl₃, deuterated chloroform; CD₃OD, deuterated methanol; CH₂Cl₂, dichloromethane; CTLA-4, cytotoxic T-lymphocyte antigen 4; CYP, cytochrome P450; DC, dendritic cells; DKIE, deuterium kinetic isotope effect; DMEM, Dulbecco's modified eagle medium; DMSO-*d*₆, deuterated dimethyl sulfoxide; DoL, degree of labeling; EDCI, 1-ethyl-3-(3-dimethylaminopropyl)carbodiimide; EtOAc, ethyl acetate; FBS, fetal bovine serum; GCN2, general control nonderepressible 2; GSH, glutathione; HOBt, hydroxybenzotriazole; HD, healthy donor; HPLC, high performance liquid chromatography; HRP, horseradish peroxidase; IC₅₀, half maximum inhibitory concentration; IDO1, indoleamine 2,3-dioxygenase-1; IDO2, indoleamine 2,3-dioxygenase-2; IFN γ , interferon gamma; IR, infrared; L-Kyn, L-kynurenine; LC-HRMS, liquid chromatography - high resolution mass spectrometry; HPLC-UV,

high pressure liquid chromatography - ultraviolet; MCR, multicomponent reaction; MD, Molecular dynamics; MDSCs, monocytic myeloid-derived suppressor cells; MeOH, methanol; MLM, mouse liver microsomes; Mp, melting point; mTOR1, mammalian target of rapamycin complex 1; MST, MicroScale Thermophoresis; MTT, 3-(4,5-dimethylthiazol-2-yl)-2,5-diphenyl-tetrazolium bromide; NADPH, nicotinamide adenine dinucleotide phosphate; NHS, *N*-hydroxysuccinimide; PBMCs, peripheral blood mononuclear cells; PBS, phosphate-buffered saline, PDAC, pancreatic ductal adenocarcinoma; PD, pharmacodynamics; PD-1, programmed cell death protein 1; PE, petroleum ether; PK, pharmacokinetic; rhIDO1, recombinant human IDO1; RIPA, radioimmunoprecipitation assay; RMSD, root mean square deviation; RLM, rat liver microsomes; RT-PCR, reverse transcriptase-polymerase chain reaction; SAR, structure activity relationship; SEM, standard error of the mean; SDS, sodium dodecyl sulphate; TEA, triethylamine; THF, tetrahydrofuran; TLC, thin layer chromatography; Treg, regulatory T cells; L-Trp, L-tryptophan; TDO, tryptophan 2,3-dioxygenase.

REFERENCES

1. a) Ribas, A.; Wolchok, J. D. Cancer immunotherapy using checkpoint blockade. *Science* **2018**, *359*, 1350-1355;

- b) Wilkinson, R. W.; Leishman, A. J. Further advances in cancer immunotherapy: going beyond checkpoint blockade. *Front. Immunol.* **2018**, *9*, 1082-1085.
2. a) Hodi, F. S.; O'Day, S. J.; McDermott, D. F.; Weber, R. W.; Sosman, J. A.; Haanen, J. B.; Gonzalez, R.; Robert, C.; Schadendorf, D.; Hassel, J. C.; Akerley, W.; van den Eertwegh, A. J. M.; Lutzky, J.; Lorigan, P.; Vaubel, J. M.; Linette, G. P.; Hogg, D.; Ottensmeier, C. H.; Lebbe, C.; Peschel, C.; Quirt, I.; Clark, J. I.; Wolchok, J. D.; Weber, J. S.; Tian, J.; Yellin, M. J.; Nichol, G. M.; Hoos, A.; Urba, W. J. Improved survival with ipilimumab in patients with metastatic melanoma. *N. Engl. J. Med.* **2010**, *363*, 711-723; b) Robert, C.; Schachter, J.; Long, G. V.; Arance, A.; Grob, J. J.; Mortier, L.; Daud, A.; Carlino, M. S.; McNeil, C.; Lotem, M.; Larkin, J.; Lorigan, P.; Neyns, B.; Blank, C. U.; Hamid, O.; Mateus, C.; Shapira-Frommer, R.; Kosh, M.; Zhou, H.; Ibrahim, N.; Ebbinghaus, S.; Ribas, A. Pembrolizumab versus ipilimumab in advanced melanoma. *N. Engl. J. Med.* **2015**, *372*, 2521-2532; c) Kazandjian, D.; Suzman, D. L.; Blumenthal, G.; Mushti, S.; He, K.; Libeg, M.; Keegan, P.; Pazdur, R. FDA approval summary: nivolumab for the treatment of metastatic non-small cell lung cancer with progression on or after platinum-based chemotherapy. *Oncologist* **2016**, *21*, 634-642. d) Pacheco, J. M.; Camidge, D. R.; Doebele, R. C.; Schenk, E. A changing of the guard: immune checkpoint inhibitors with and without chemotherapy as first line treatment for metastatic non-small cell lung cancer. *Front. Oncol.* **2019**, *9*, 195-207.

3. a) Jenkins, R. W.; Barbie, D. A.; Flaherty, K. T. Mechanisms of resistance to immune checkpoint inhibitors. *Br. J. Cancer* **2018**, *118*, 9-16; b) Sharma, P.; Hu-Lieskovan, S.; Wargo, J. A.; Ribas, A. Primary, adaptive, and acquired resistance to cancer immunotherapy. *Cell* **2017**, *168*, 707-723. c) Restifo, N. P.; Smyth, M. J.; Snyder A. Acquired resistance to immunotherapy and future challenges. *Nat. Rev. Cancer* **2016**, *16*, 121-126.
4. a) Weinmann, H. Cancer immunotherapy: selected targets and small-molecule modulators. *ChemMedChem* **2016**, *11*, 450-466; b) Melero, I.; Berman, D. M.; Aznar, M. A.; Korman, A. J.; Pérez Gracia, J. L.; Haanen, J. Evolving synergistic combinations of targeted immunotherapies to combat cancer. *Nat. Rev. Cancer* **2015**, *15*, 457-472; c) Antonia, S. J.; Larkin, J.; Ascierto, P. A. Immuno-oncology combinations: a review of clinical experience and future prospects. *Clin. Cancer Res.* **2014**, *20*, 6258-6268.
5. a) Prendergast, G. C.; Mondal, A.; Dey, S.; Laury-Kleintop, L. D.; Muller, A. J. Inflammatory reprogramming with IDO1 inhibitors: turning immunologically unresponsive 'cold' tumors 'hot'. *Trends Cancer* **2018**, *4*, 38-58; b) Munn, D. H.; Mellor, A. L. IDO and tolerance to tumors. *Trends Mol. Med.* **2004**, *10*, 15-18; c) Uyttenhove, C.; Pilotte, L.; Theate, I.; Stroobant, V.; Colau, D.; Parmentier, N.; Boon, T.; Van den Eynde, B. J. Evidence for a tumoral immune resistance mechanism based on tryptophan degradation by indoleamine 2,3-dioxygenase. *Nat. Med.* **2003**, *9*, 1269-1274.

6. Metz, R.; Rust, S.; Duhadaway, J. B.; Mautino, M. R.; Munn, D. H.; Vahanian, N. N.; Link, C. J.; Prendergast, G. C. IDO inhibits a tryptophan sufficiency signal that stimulates mTOR: A novel IDO effector pathway targeted by D-1-methyl-tryptophan. *Oncoimmunology* **2012**, *1*, 1460-1468.
7. a) Fallarino, F.; Grohmann, U.; You, S.; McGrath, B. C.; Cavener, D. R.; Vacca, C.; Orabona, C.; Bianchi, R.; Belladonna, M. L.; Volpi, C.; Santamaria, P.; Fioretti, M. C.; Puccetti, P. The combined effects of tryptophan starvation and tryptophan catabolites down-regulate T cell receptor zeta-chain and induce a regulatory phenotype in naive T cells. *J. Immunol.* **2006**, *176*, 6752-6761; b) Munn, D. H.; Sharma, M. D.; Baban, B.; Harding, H. P.; Zhang, Y.; Ron, D.; Mellor, A. L. GCN2 kinase in T cells mediates proliferative arrest and anergy induction in response to indoleamine 2,3-dioxygenase. *Immunity* **2005**, *22*, 633-642.
8. a) Della Chiesa, M.; Carlomagno, S.; Frumento, G.; Balsamo, M.; Cantoni, C.; Conte, R.; Moretta, L.; Moretta, A.; Vitale M. The tryptophan catabolite L-kynurenine inhibits the surface expression of NKp46- and NKG2D-activating receptors and regulates NK-cell function. *Blood* **2006**, *108*, 4118-4125; b) Frumento, G.; Rotondo, R.; Tonetti, M.; Damonte, G.; Benatti, U.; Ferrara, G. B. Tryptophan-derived catabolites are responsible for inhibition of T and natural killer cell proliferation induced by indoleamine 2,3-dioxygenase. *J. Exp. Med.* **2002**, *196*, 459-468.

9. Sharma, M. D.; Baban, B.; Chandler, P.; Hou, D. Y.; Singh, N.; Yagita, H.; Azuma, M.; Blazar, B. R.; Mellor, A. L.; Munn, D. H. Plasmacytoid dendritic cells from mouse tumor-draining lymph nodes directly activate mature Tregs via indoleamine 2,3-dioxygenase. *J. Clin. Invest.* **2007**, *117*, 2570-2582.
10. Manlapat, A. K.; Kahler, D. J.; Chandler, P. R.; Munn, D. H.; Mellor, A. L. Cell-autonomous control of interferon type I expression by indoleamine 2,3-dioxygenase in regulatory CD19+ dendritic cells. *Eur. J. Immunol.* **2007**, *37*, 1064-1071.
11. Holmgaard, R. B.; Zamarin, D.; Li, Y.; Gasmi, B.; Munn, D. H.; Allison, J. P.; Merghoub, T.; Wolchok, J. D. Tumor-expressed IDO recruits and activates MDSCs in a Treg-dependent manner. *Cell Rep.* **2015**, *13*, 412-424.
12. Mondal, A.; Smith, C.; DuHadaway, J. B.; Sutanto-Ward, E.; Prendergast, G. C.; Bravo-Nuevo, A.; Muller, A. J. IDO1 is an integral mediator of inflammatory neovascularization. *EBioMedicine* **2016**, *14*, 74-82.
13. Godin-Ethier, J.; Hanafi, L. A.; Piccirillo, C. A.; Lapointe, R. Indoleamine 2,3-dioxygenase expression in human cancers: clinical and immunologic perspectives. *Clin. Cancer Res.* **2011**, *17*, 6985-6991.
14. a) Greene, L. I.; Bruno, T. C.; Christenson, J. L.; D'Alessandro, A.; Culp-Hill, R.; Torkko, K.; Borges, V. F.; Slansky, J. E.; Richer, J. K. A Role for tryptophan-2,3-dioxygenase in CD8 T-cell suppression and evidence of tryptophan catabolism in breast cancer patient plasma. *Mol. Cancer Res.* **2019**, *17*, 131-139;

- b) Pilotte, L.; Larrieu, P.; Stroobant, V.; Colau, D.; Dolušić, E.; Frédérick, R.; De Plaen, E.; Uyttenhove, C.; Wouters, J.; Masereel, B.; Van den Eynde, B. J. Reversal of tumoral immune resistance by inhibition of tryptophan 2,3-dioxygenase. *Proc. Natl. Acad. Sci. U. S. A.* **2012**, *109*, 2497-2502.
15. D'Amato, N. C.; Rogers, T. J.; Gordon, M. A.; Greene, L. I.; Cochrane, D. R.; Spoelstra, . S.; Nemkov, T. G.; D'Alessandro, A.; Hansen, K. C.; Richer, J. K. A TDO2-AhR signaling axis facilitates *anoikis* resistance and metastasis in triple-negative breast cancer. *Cancer Res.* **2015**, *75*, 4651-4664.
16. Merlo, L. M.; DuHadaway, J. B.; Grabler, S.; Prendergast, G. C.; Muller, A. J.; Mandik-Nayak, L. IDO2 modulates T cell-dependent autoimmune responses through a B cell-intrinsic mechanism. *J. Immunol.* **2016**, *196*, 4487-4497.
17. a) Weng, T.; Qiu, X.; Wang, J.; Li, Z.; Bian, J. Recent discovery of indoleamine-2,3-dioxygenase 1 inhibitors targeting cancer immunotherapy. *Eur. J. Med. Chem.* **2018**, *143*, 656-669; b) Coletti, A.; Greco, F. A.; Dolciemi, D.; Camaioni, E.; Sardella, R.; Pallotta, M. T.; Volpi, C.; Orabona, C.; Grohmann, U.; Macchiarulo, A. Advances in indoleamine 2,3-dioxygenase 1 medicinal chemistry. *Medchemcomm.* **2017**, *8*, 1378-1392.
18. a) Prendergast, G. C., Malachowski, W. P. DuHadaway, J. B.; Muller, A. J. Discovery of IDO1 inhibitors: from bench to bedside. *Cancer Res.* **2017**, *77*, 6795-6811; b) Röhrig, U. F.; Majjigapu, S. R.; Vogel, P.; Zoete, V.; Michielin, O. Challenges in the discovery of indoleamine 2,3-dioxygenase 1 (IDO1) inhibitors. *J. Med. Chem.* **2015**, *58*, 9421-9437; c) Dounay, A. B.; Tuttle, J. B.;

- Verhoest, P. R. Challenges and opportunities in the discovery of new therapeutics targeting the kynurenine pathway. *J. Med. Chem.* **2015**, *58*, 8762-8782.
19. Yue, E. W.; Sparks, R.; Polam, P.; Modi, D.; Douty, B.; Wayland, B.; Glass, B.; Takvorian, A.; Glenn, J.; Zhu, W.; Bower, M.; Liu, X.; Leffet, L.; Wang, Q.; Bowman, K. J.; Hansbury, M. J.; Wei, M.; Li, Y.; Wynn, R.; Burn, T. C.; Koblish, H. K.; Fridman, J. S.; Emm, T.; Scherle, P. A.; Metcalf, B.; Combs, A. P. INCB24360 (epacadostat), a highly potent and selective indoleamine-2,3-dioxygenase 1 (IDO1) inhibitor for immuno-oncology. *ACS Med. Chem. Lett.* **2017**, *8*, 486-491.
20. Soliman, H. H.; Antonia, S.; Sullivan, D.; Vanahanian, N.; Link, C. Overcoming coming tumor antigen anergy in human malignancies using the novel indoleamine 2,3-dioxygenase (IDO) enzyme inhibitor, 1-methyl-D-tryptophan (1MT). *J. Clin. Oncol.* **2009**, *27* (suppl 15; abstr 3004).
21. a) Kumar, S.; Waldo, J. P.; Jaipuri, F. A.; Marcinowicz, A.; Van Allen, C.; Adams, J.; Kesharwani, T.; Zhang, X.; Metz, R.; Oh, A. J.; Harris, S. F.; Mautino, M. R. Discovery of clinical candidate (1*R*,4*r*)-4-((*R*)-2-((*S*)-6-Fluoro-5*H*-imidazo[5,1-*a*]isoindol-5-yl)-1-hydroxyethyl)cyclohexan-1-ol (navoximod), a potent and selective inhibitor of indoleamine 2,3-dioxygenase 1. *J. Med. Chem.* **2019**, *62*, 6705-6733; b) Peng, Y. H.; Ueng, S. H.; Tseng, C. T.; Hung, M. S.; Song, J. S.; Wu, J. S.; Liao, F. Y.; Fan, Y. S.; Wu, M. H.; Hsiao, W. C.; Hsueh, C. C.; Lin, S. Y.; Cheng, C. Y.; Tu, C. H.; Lee, L. C.; Cheng, M. F.; Shia, K. S.;

- Shih, C.; Wu, S. Y. Important hydrogen bond networks in indoleamine 2,3-dioxygenase 1 (IDO1) inhibitor design revealed by crystal structures of imidazoleisoindole derivatives with IDO1. *J. Med. Chem.* **2016**, *59*, 282-293.
22. Crosignani, S.; Bingham, P.; Botteman, P.; Cannelle, H.; Cauwenberghs, S.; Cordonnier, M.; Dalvie, D.; Deroose, F.; Feng, J. L.; Gomes, B.; Greasley, S.; Kaiser, S. E.; Kraus, M.; Négrerie, M.; Maegley, K.; Miller, N.; Murray, B. W.; Schneider, M.; Soloweij, J.; Stewart, A. E.; Tumang, J.; Torti, V. R.; Van Den Eynde, B.; Wythes, M. Discovery of a novel and selective indoleamine 2,3-dioxygenase (IDO-1) inhibitor 3-(5-Fluoro-1*H*-indol-3-yl)pyrrolidine-2,5-dione (EOS200271/PF-06840003) and its characterization as a potential clinical candidate. *J. Med. Chem.* **2017**, *60*, 9617-9629.
23. a) Gangadhar, T. C.; Hamid, O.; Smith, D. C.; Bauer, T. M.; Waser, J. S.; Luke, J. J.; Balmanoukian, A. S.; Kaufman, D. R.; Zhao, Y.; Maleski, J.; Leopold, L.; Gajewski, T. F. Preliminary results from a phase I/II study of epacadostat (INCB024360) in combination with pembrolizumab in patients with selected advanced cancers. *J. Immunother. Cancer* **2015**, *3* (suppl 2), 07; b) A Phase 3 Study of Pembrolizumab + Epacadostat or Placebo in Subjects With Unresectable or Metastatic Melanoma (Keynote-252 / ECHO-301). ClinicalTrials.gov Identifier: NCT02752074. Last update: September 04, 2019 (accessed on Oct 23, 2019).
24. Long, G. V.; Dummer, R.; Hamid, O.; Gajewski, T.; Caglevic, C.; Dalle, S.; Arance, A.; Carlino, M. S.; Grob, J.-J.; Kim, T. M.; Demidov, L. V.; Robert, C.;

- Larkin, J. M. G.; Anderson, J.; Maleski, J. E.; Jones, M. M.; Diede, S. J.; Mitchell, T. C. Epacadostat (E) plus pembrolizumab (P) versus pembrolizumab alone in patients (pts) with unresectable or metastatic melanoma: Results of the phase 3 ECHO-301/KEYNOTE-252 study. 2018 ASCO Annual Meeting, *J. Clin. Oncol.* **2018**, *36*, (suppl 15; abstr 108).
25. a) Sondak, V. K.; Khushalani, N. Y. Echoes of a failure: what lessons can we learn? *Lancet Oncol.* **2019**, *20*, 1037-1039; b) Garber K. A new cancer immunotherapy suffers a setback. *Science* **2018**, *360*, 588; c) Komiya, T.; Huang, C. H. Updates in the clinical development of epacadostat and other indoleamine 2,3-dioxygenase 1 inhibitors (IDO1) for human cancer. *Front. Oncol.* **2018**, *8*, 423-429.
26. Brochez, L.; Chevolet, I.; Kruse, V. The rationale of indoleamine 2,3-dioxygenase inhibition for cancer therapy. *Eur. J. Cancer.* **2017** *76*, 167-182.
27. a) Griglio, A.; Torre, E.; Serafini, M.; Bianchi, A.; Schmid, R.; Coda Zabetta G.; Massarotti, A.; Sorba, G.; Pirali, T.; Fallarini, S. A multicomponent approach in the discovery of indoleamine 2, 3-dioxygenase 1 inhibitors: Synthesis, biological investigation and docking studies. *Bioorg. Med. Chem. Lett.* **2018**, *28*, 651-657; b) Serafini, M.; Torre, E.; Aprile, S.; Massarotti, A.; Fallarini, S.; Pirali, T. Synthesis, docking and biological evaluation of a novel class of imidazothiazoles as IDO1 inhibitors. *Molecules* **2019**, *24*, pii: E1874.
28. Fallarini, S.; Massarotti, A.; Gesù, A.; Giovarruscio, S.; Coda Zabetta, G.; Bergo, R.; Giannelli, B.; Brunco, A.; Lombardi, G.; Sorba, G.; Pirali, T. In silico-driven

- multicomponent synthesis of 4,5- and 1,5-disubstituted imidazoles as indoleamine 2,3-dioxygenase inhibitors. *Med. Chem. Commun.* **2016**, *7*, 409-419.
29. Sterling, T.; Irwin, J. J. ZINC 15--Ligand discovery for everyone. *J. Chem. Inf. Model* **2015**, *55*, 2324-2337.
30. a) FRED, version 3.0.0, OpenEye Scientific Software, Santa Fe, NM, <http://www.eyesopen.com> (accessed on Oct 21, 2019);
- b) McGann, M. FRED pose prediction and virtual screening accuracy. *J. Chem. Inf. Model.* **2011**, *51*, 578-596.
31. <https://www.emolecules.com> (accessed on Oct 21, 2019).
32. Duhr, S.; Braun, D. Why molecules move along a temperature gradient. *Proc. Natl. Acad. Sci. U. S. A.* **2006**, *103*, 19678-19682.
33. Cavallo, G.; Metrangolo, P.; Milani, R.; Pilati, T.; Priimagi, A.; Resnati, G.; Terraneo, G. The halogen bond. *Chem. Rev.* **2016**, *116*, 2478-2601.
34. a) Pick, R.; Bauer, M.; Kazmaier, U.; Hebach, C. Ammonia in Ugi reactions - four-component versus six-component couplings. *Synlett* **2005**, *5*, 757-760; b) Kazmaier, U.; Hebach, C. Peptide syntheses via Ugi reactions with ammonia. *Synlett* **2003**, *11*, 1591-1594.
35. a) Schrödinger Release 2019-1: Desmond Molecular Dynamics System; D. E. Shaw Research: New York, NY, 2019; b) Maestro-Desmond Interoperability Tools 2019-1, Schrödinger, New York, NY, 2019.
36. Pirali, T.; Serafini, M.; Cargnin, S.; Genazzani, A. A. Applications of deuterium in medicinal chemistry. *J. Med. Chem.* **2019**, *62*, 5276-5297; b) Cargnin, S.;

- Serafini, M.; Pirali, T. A primer of deuterium in drug design. *Future Med. Chem.* **2019**, *11*, 2039-2042.
37. a) Sharma, R.; Strelevitz, T. J.; Gao, H.; Clark, A. J.; Schildknecht, K.; Obach, R. S.; Ripp, S. L.; Spracklin, D. K.; Tremaine, L. M.; Vaz, A. D. N.; Deuterium isotope effects on drug pharmacokinetics. I. System-dependent effects of specific deuteration with aldehyde oxidase cleared drugs. *Drug Metab. Dispos.* **2012**, *40*, 625-634; b) Khan, A. J.; Misenko, S. M.; Thandoni, A.; Schiff, D.; Jhawar, S. R.; Bunting, S. F.; Haffty, B. G. VX-984 is a selective inhibitor of non-homologous end joining, with possible preferential activity in transformed cells. *Oncotarget* **2018**, *9*, 25833-25841; c) Moslin, R.; Zhang, Y.; Wroblewski, S. T.; Lin, S.; Mertzman, M.; Spergel, S.; Tokarski, J. S.; Strnad, J.; Gillooly, K.; McIntyre, K. W.; Zupa-Fernandez, A.; Cheng, L.; Sun, H.; Chaudhry, C.; Huang, C.; D'Arienzo, C.; Heimrich, E.; Yang, X.; Muckelbauer, J. K.; Chang, C.; Tredup, J.; Mulligan, D.; Xie, D.; Aranibar, N.; Chiney, M.; Burke, J. R.; Lombardo, L.; Carter, P. H.; Weinstein, D. S. Identification of *N*-methyl nicotinamide and *N*-methyl pyridazine-3-carboxamide pseudokinase domain ligands as highly selective allosteric inhibitors of Tyrosine Kinase 2 (TYK2). *J. Med. Chem.* **2019**, *62*, 8953-8972.
38. a) Neoptolemos, J. P.; Palmer, D. H.; Ghaneh, P.; Psarelli, E. E.; Valle, J. W.; Halloran, C. M.; Faluyi, O.; O'Reilly, D. A.; Cunningham, D.; Wadsley, J.; Darby, S.; Meyer, T.; Gillmore, R.; Anthoney, A.; Lind, P.; Glimelius, B.; Falk, S.; Izbicki, J. R.; Middleton, G. W.; Cummins, S.; Ross, P. J.; Wasan, H.;

- McDonald, A.; Crosby, T.; Ma, Y. T.; Patel, K.; Sherriff, D.; Soomal, R.; Borg, D.; Sothi, S.; Hammel, P.; Hackert, T.; Jackson, R.; Büchler, M. W. Comparison of adjuvant gemcitabine and capecitabine with gemcitabine monotherapy in patients with resected pancreatic cancer (ESPAC-4): a multicentre, open-label, randomised, phase 3 trial. *Lancet* **2017**, *389*, 1011-1024; b) Cid-Arregui, A.; Juarez, V. Perspectives in the treatment of pancreatic adenocarcinoma. *World J. Gastroenterol.* **2015**, *21*, 9297-9316.
39. Trovato, R.; Fiore, A.; Sartori, S.; Canè, S.; Giugno, R.; Cascione, L.; Paiella, S.; Salvia, R.; De Sanctis, F.; Poffe, O.; Anselmi, C.; Hofer, F.; Sartoris, S.; Piro, G.; Carbone, C.; Corbo, V.; Lawlor, R.; Solito, S.; Pinton, L.; Mandruzzato, S.; Bassi, C.; Scarpa, A.; Bronte, V.; Ugel, S. Immunosuppression by monocytic myeloid-derived suppressor cells in patients with pancreatic ductal carcinoma is orchestrated by STAT3. *J. Immunother. Cancer* **2019**, *7*, 255-270.
40. Koblisch, H. K.; Hansbury, M. J.; Bowman, K. J.; Yang, G.; Neilan, C. L.; Haley, P. J.; Burn, T. C.; Waeltz, P.; Sparks, R. B.; Yue, E. W.; Combs, A. P.; Scherle, P. A.; Vaddi, K.; Fridman, J. S. Hydroxyamidine inhibitors of indoleamine-2,3-dioxygenase potently suppress systemic tryptophan catabolism and the growth of IDO-expressing tumors. *Mol. Cancer Ther.* **2010**, *9*, 489-498.
41. The PyMOL Molecular Graphics System, version 2.2.3, Schrödinger LLC, 2019.
42. QUACPAC, version 1.6.3.1; OpenEye Scientific Software: Santa Fe, NM, <http://www.eyesopen.com> (accessed on Oct 21, 2019).

43. a) OMEGA, version 2.4.6; OpenEye Scientific Software: Santa Fe, NM, <http://www.eyesopen.com> (accessed on Oct 21, 2019); b) Hawkins, P. C.; Nicholls, A. Conformer generation with OMEGA: learning from the data set and the analysis of failures. *J. Chem. Inf. Model.* **2012**, *52*, 2919-2936; c) Hawkins, P. C.; Skillman, A. G.; Warren, G. L.; Ellingson, B. A.; Stahl, M. T. Conformer generation with OMEGA: algorithm and validation using high quality structures from the Protein Databank and Cambridge Structural Database. *J. Chem. Inf. Model.* **2010**, *50*, 572-584.
44. Sugimoto, H.; Oda, S.; Otsuki, T.; Hino, T.; Yoshida, T.; Shiro, Y. Crystal structure of human indoleamine 2,3-dioxygenase: catalytic mechanism of O₂ incorporation by a heme-containing dioxygenase. *Proc. Natl. Acad. Sci. U. S. A.* **2006**, *103*, 2611-2616.
45. Banks, J. L.; Beard, H. S.; Cao, Y.; Cho, A. E.; Damm, W.; Farid, R.; Felts, A. K.; Halgren, T. A.; Mainz, D. T.; Maple, J. R.; Murphy, R.; Philipp, D. M.; Repasky, M. P.; Zhang, L. Y.; Berne, B. J.; Friesner, R. A.; Gallicchio, E.; Levy, R. M. Integrated modeling program, applied chemical theory (IMPACT). *J. Comput. Chem.* **2005**, *26*, 1752-1780.
46. Toukmaji, A. Y.; Board, J. A. Ewald summation techniques in perspective: a survey. *Comput. Phys. Commun.* **1996**, *95*, 73-92.
47. Zielkiewicz J. Structural properties of water: comparison of the SPC, SPCE, TIP4P, and TIP5P models of water. *J. Chem. Phys.* **2005**, *123*, 104501-104506.

48. Martyna, G. J.; Klein, M. L.; Tuckerman, M. Nosé-Hoover chains: The canonical ensemble via continuous dynamics. *J. Chem. Phys.* **1992**, *97*, 2635-2643.
49. Evans, D. J.; Holian, B. L. The Nose-Hoover thermostat. *J. Chem. Phys.* **1985**, *83*, 4069-4074.
50. Fallarino, F.; Uyttenhove, C.; Boon, T.; Gajewski, T. F. Endogenous IL-12 is necessary for rejection of P815 tumor variants in vivo. *J. Immunol.* **1996**, *156*, 1095-1100.
51. Fallarini, S.; Paoletti, T.; Battaglini, C. O.; Ronchi, P.; Lay, L.; Bonomi, R.; Jha, S.; Mancin, F.; Scrimin, P.; Lombardi, G. Factors affecting T cell responses induced by fully synthetic glyco-gold-nanoparticles. *Nanoscale* **2013**, *5*, 390-400.
52. Fallarini, S.; Paoletti, T.; Panza, L.; Lombardi, G. Alpha-galactosylceramide modulates the induction of indoleamine 2,3-dioxygenase in antigen presenting cells. *Biochem. Pharmacol.* **2008**, *76*, 738-750.

Author contributions

Article: Discovery of highly potent benzimidazole derivatives as indoleamine 2, 3-dioxygenase-1 (IDO1) inhibitors: from structure-based virtual screening to in vivo pharmacodynamic activity. *J. Med. Chem.* **2020**, *63*, 3047-3065.

Author 1: Marta Serafini

Performed the synthesis of part of the compounds, wrote the paper

Author 2: Enza Torre

Performed the *in vitro* screening of the compounds

Author 3: Silvio Aprile

Performed the evaluation of the metabolism of the compounds

Author 4: Erika Del Grosso

Evaluated the Kyn plasma levels

Author 5: Alessandro Gesù

Performed the *in-silico* experiments

Author 6: Alessia Griglio

Performed the synthesis of part of the compounds

Author 7: Giorgia Colombo

Performed the *in vivo* experiments

Author 8: Cristina Travelli

Supervision

Author 9: Salvatore Paiella

Provided the samples of PDAC patients

Author 10: Annalisa Adamo

Performed the *in vitro* characterization of PDAC samples

Author 11: Elena Orecchini

Performed the evaluation of the selectivity over TDO

Author 12: Alice Coletti

Performed the MST assay

Author 13: Maria Teresa Pallotta

Funding acquisition, supervision, designed the experiments

Author 14: Stefano Ugel

Funding acquisition, supervision, designed the experiments

Author 15: Alberto Massarotti

Supervision, designed the experiments

Author 16: Tracey Pirali

Funding acquisition, project administration, wrote the paper, designed the experiments

Author 17: Silvia Fallarini

Supervision, designed the experiments

Chapter 8

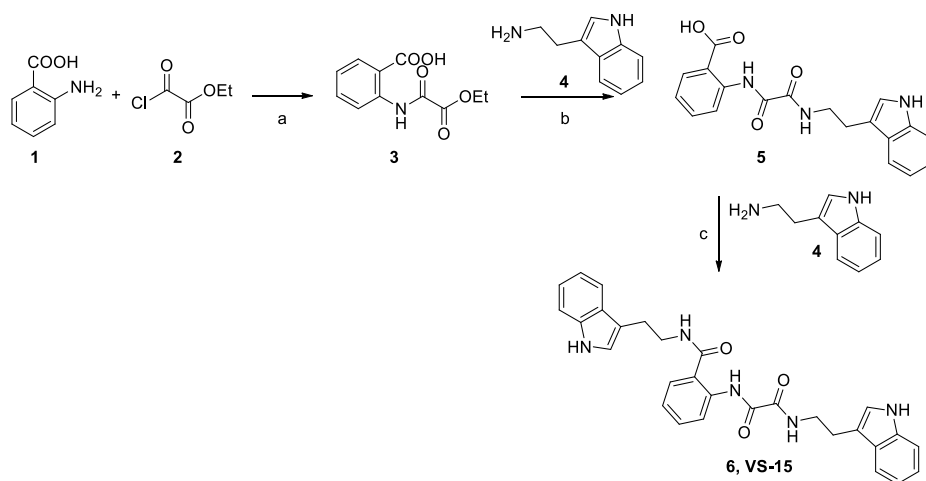
Unpublished results

8.1 Identification of compound VS-15

A second hit compound identified by virtual screening was **VS-15**.¹ This molecule displays an inhibitory activity on IDO1 of $93 \pm 3\%$ at $10 \mu\text{M}$, an IC_{50} value of $0.8 \mu\text{M}$ in A375 cell line and no detectable cytotoxicity, with a cell viability of $96 \pm 3\%$ at $10 \mu\text{M}$ after 48 hours.

Firstly, the candidate, initially purchased from eMolecules,² was re-synthesized in our laboratory according to Scheme 1. Anthranilic acid **1** reacted with ethyl 2-chloro-2-oxoacetate **2** to afford intermediate **3**, that underwent a nucleophilic attack at the carbonyl ester moiety with tryptamine, yielding intermediate **5**. After a coupling reaction between **5** and tryptamine **4**, **VS-15** (**6**) was obtained with a yield of 58%. The compound was then re-tested under the same conditions as before, confirming the inhibitory activity and potency of the compound purchased from eMolecules®.

Scheme 1. Re-synthesis of the hit compound **VS-15**.

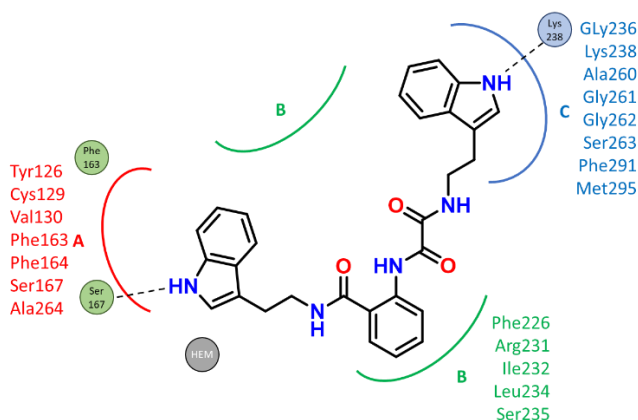


Reagents and conditions: (a) dry THF, 0°C , 2 h, 99%. (b) TEA, toluene, reflux, 18 h, 68%. (c) TEA, EDCI, HOBT, dry CH_2Cl_2 , rt, 18 h, 58%.

Docking pose of VS-15 and ligand binding experiments

The proposed docking pose in the catalytic active site of IDO1 reveals a putative binding mode in which the 2-(1*H*-indol-3-yl)ethyl)carbamoyl moiety is accommodated in pocket A (Tyr126, Cys129, Val130, Phe163, Phe164, Ser167 and Ala264) and its nitrogen establishes a hydrogen bond with Ser167. Pocket B (Phe226, Arg231, Ile232, Leu234 and Ser235) is partially exploited by the phenyl ring and the 2-((2-(1*H*-indol-3-yl)ethyl)amino)-2-oxoacetamido) side-chain is located in pocket C (Gly236, Lys238, Ala260, Gly261, Gly262, Ser263, Phe291, Met295), with the NH of the indole ring forming a hydrogen bond with Lys238 (Figure 1). Surprisingly, in the predicted docking pose there is no atom able to bind the heme group in the IDO1 active site.

Figure 1. Schematic representation of predicted interactions of **VS-15** within IDO1 binding pockets.



Considering that the docking pose of the compound was not resolute and in order to confirm target engagement of IDO1 by **VS-15**, binding experiments were carried out using MicroScale Thermophoresis (MST) assays on recombinant human IDO1.³ Both epacadostat and compound **VS-13** were used as positive control in this assay. While both compounds displayed lower dissociation constants (**VS-13**: K_d of $0.55 \pm$

0.36 μM ; epacadostat: K_d of $3.46 \pm 0.86 \mu\text{M}$) compared to **VS-15** (K_d of $24.29 \pm 3.76 \mu\text{M}$), the K_d value of this hit compound suggests that it does bind to IDO1.

Preliminary characterization of compound VS-15

IDO1 and TDO selectivity

To evaluate the selectivity over TDO, the compound was tested in a mastocytoma cell line stably expressing mouse IDO1 (P1.IDO1) or TDO (P1.TDO). To this aim, cells P1.IDO1 and P1.TDO were treated with different concentrations of **VS-15** for 16 h and Kyn secretion in cell culture supernatants was detected by HPLC analysis. In these settings, the compound behaved as selective inhibitor of IDO1 over TDO both at 1 and 10 μM . The IC_{50} value of **VS-15** was 0.63 μM in P1.IDO1, while it was not possible to calculate the IC_{50} value in P1.TDO cell line.

iNOS activity

While the compound is specific on IDO1 over TDO, its structure has been previously reported as being an iNOS inhibitor.⁴ This mechanism of action has been further confirmed by us in RAW264.7 cells of murine macrophages. The cells were treated with 10 and 20 μM of **VS-15** and, after induction with LPS and incubation for 24 h, the levels of NO production were evaluated using the colorimetric Griess method. At these concentrations, the compound is able to inhibit NO production by a percentage of 37.5% and 55% at 10 and 20 μM , respectively, compared to the untreated sample. A dose-dependent response experiment will be performed, but this preliminary result suggests that the compound might act as a dual IDO1-iNOS inhibitor.

Signalling activity

A preliminary experiment made in collaboration with Dr. Pallotta's group from the University of Perugia has suggested that the compound is also able to interfere with the IDO1 signalling functions, more than with the catalytic activity of the enzyme.⁵

The compound was incubated at 10 μ M in P1.IDO1 cells and, after immunoprecipitation of IDO1, the levels of free phosphate were evaluated by colorimetric reaction for untreated and treated cells.⁶ This indirect assay assesses the ability of IDO1 immunoprecipitates to remove phosphate groups from a co-incubated tyrosine-phosphorylated substrate. Under these conditions, **VS-15** reduced the amount of free phosphate compared to control, indicating that the compound might act as a negative modulator of the ITIMs-mediated signalling pathway of the protein. Further experiments evaluating different concentrations of the compound will be performed.

Moreover, to assess if the compound can also interfere with the degradation of the enzyme in the cells, a Western blot analysis to estimate the expression of IDO1 protein over time will be performed.

Chemical stability

One of the major concerns in the structure of **VS-15** was the presence of a possible chemically unstable substructure represented by the α,β -dicarbonyl moiety, whose cleavage could lead to the formation of tryptamine and oxalic acid, two undesired by-products, the former for its central effects on serotonin and dopaminergic systems, the latter for the formation of insoluble calcium oxalate leading to kidney failure.

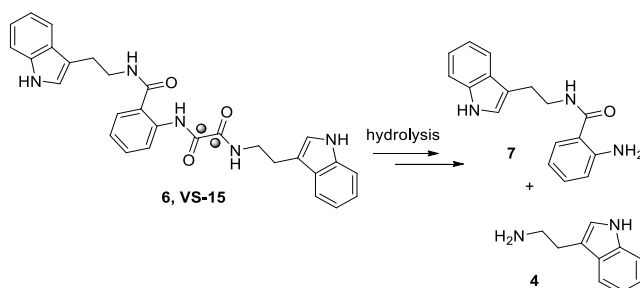
The chemical stability of the compound toward hydrolysis was verified both in a physiological 0.1 M phosphate buffer (pH=7.4) and in a 20 mM acetate buffer (pH=4.5). The stability was evaluated after one and 6 hours at 37 °C and **VS-15** was completely stable under the tested conditions.

Metabolic stability

After having confirmed the chemical stability of **VS-15**, its metabolic stability was evaluated in mouse liver S9 fraction (MLS9) activated by NADPH. Unfortunately, the compound is highly susceptible toward metabolism, with a residual substrate recovered after one hour of incubation of 15%. To design more stable analogues, we performed a structural characterization of the metabolites by mass spectrometry.

This analysis highlighted that the α,β -dicarbonyl substructure is the main soft spot, being tryptamine **4** and the aromatic amine **7** the two metabolites formed (Figure 2). Therefore, thanks to the fact that the metabolic liability is circumscribed to one soft spot, a hit to lead optimization was undertaken with the aim to increase both the metabolic stability and the potency.

Figure 2. Metabolic soft spots of compound **VS-15**.



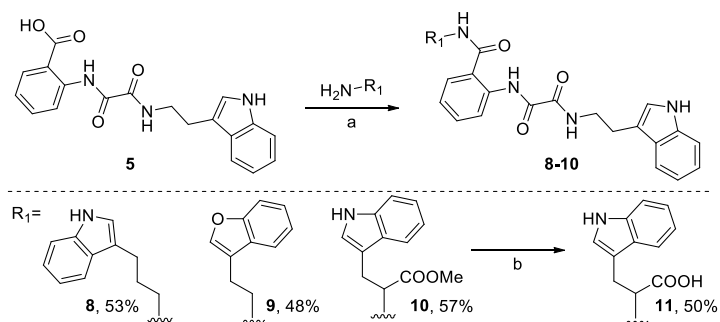
SAR study and hit to lead optimization

Starting from the scaffold of **VS-15**, a library of candidates has been synthesized with two different objectives: (i) performing a classical SAR study to better elucidate the docking pose of the compound in the IDO1 active site; (ii) improving the metabolic stability of the compound.

Modification of the moiety putatively located in pocket A

First, the molecule was made less symmetric and four compounds (**8-11**) were synthesized by modifying the tryptamine substructure putatively located in pocket A of IDO1 active site. To this aim, intermediate **5** was coupled with three different amines (Scheme 2, compounds **8-10**), while compound **11** (Scheme 2) was obtained by hydrolysis reaction of the methyl ester moiety of **10**.

Scheme 2. Synthesis of compounds **8-11**.

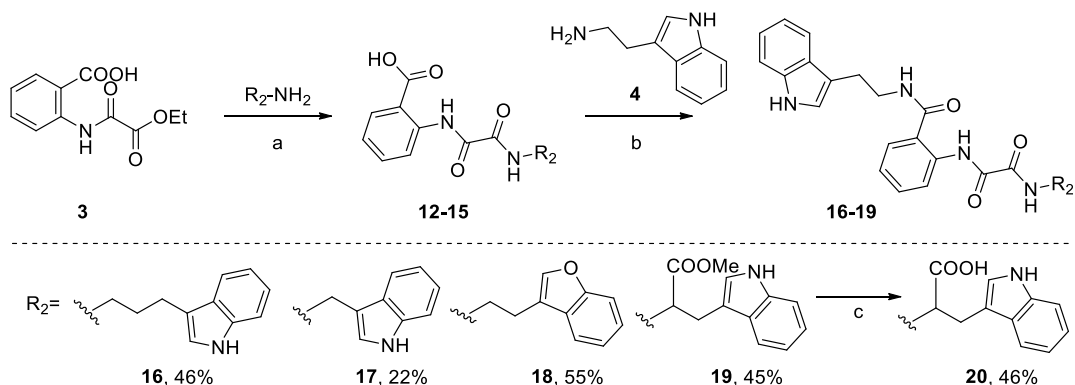


Reagents and conditions: (a) TEA, EDCI, HOBt, dry CH_2Cl_2 , rt, 18 h, 48-57%; (b) NaOH, H_2O , THF, rt, 5 h, 50%.

Modification of the moiety putatively located in pocket C

In a similar fashion, five analogues (**16-20**) were obtained by substituting the tryptamine moiety located in pocket C. Intermediate **3** reacted with four different amines, affording compounds **16-19**. After hydrolysis of the methyl ester group of **19**, compound **20** was obtained (Scheme 3).

Scheme 3. Synthesis of compounds **16-20**.

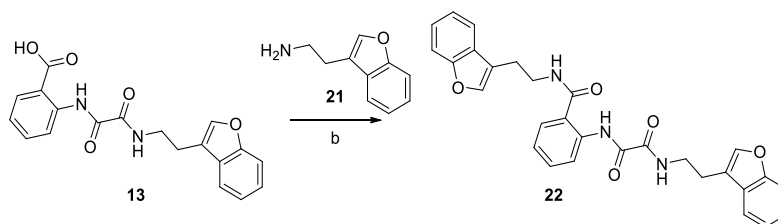


Reagents and conditions: (a) TEA, toluene, reflux, 18 h, 39-60%; (b) TEA, EDCI, HOBt, dry CH_2Cl_2 , rt, 18 h, 22-55%; (c) NaOH, H_2O , THF, rt, 5 h, 46%.

Removal of both the indole rings

Moreover, a compound (**22**) in which both the indole rings located in pocket A and C were substituted with benzofurans has been synthesized according to Scheme 4, by coupling reaction between intermediate **13** and amine **21**.

Scheme 4. Synthesis of compound **22**.

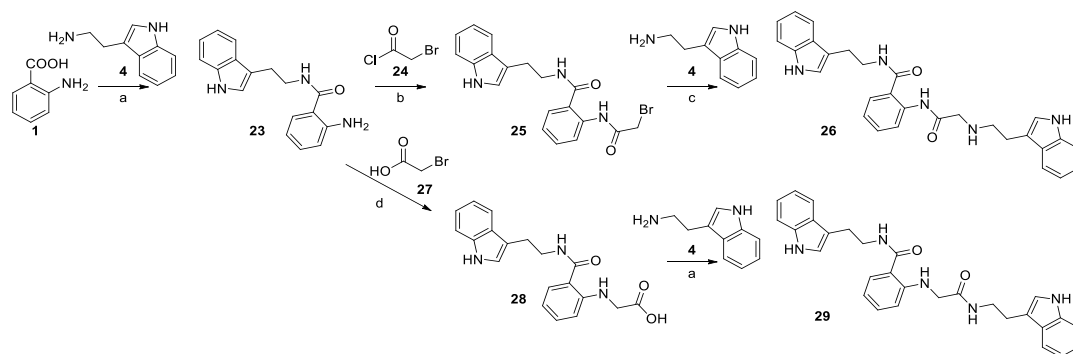


Reagents and conditions: (a) TEA, EDCI, HOBT, dry CH_2Cl_2 , rt, 18 h, 60%.

Modification of the side chain

The side chain of **VS-15**, responsible for its metabolic instability, was then extensively varied. First, the two carbonyl groups have been removed one at a time, and compounds **26** and **29** were synthesized (Scheme 5). From intermediate **23**, acylation followed by nucleophilic substitution afforded **26**, or alternatively, nucleophilic substitution followed by coupling reaction with tryptamine afforded compound **29**.

Scheme 5. Synthesis of compounds **26** and **29**.

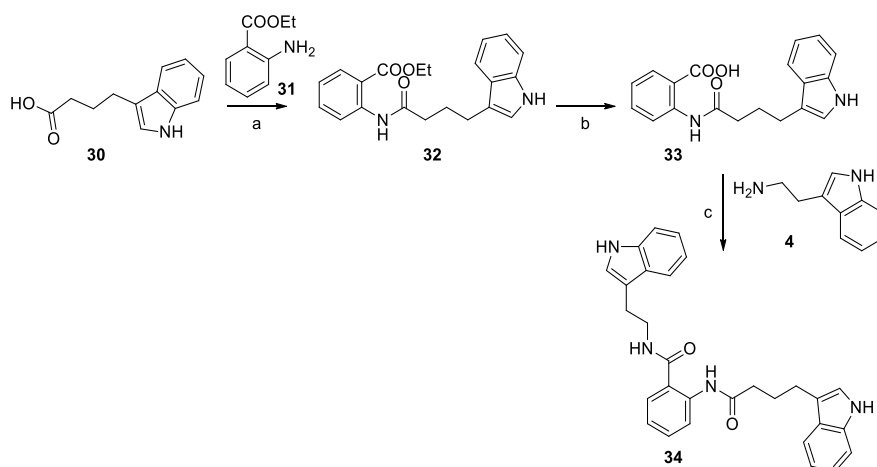


Reagents and conditions: (a) TEA, EDCI, HOBT, dry CH₂Cl₂, rt, 18 h, 62-86%; (b) TEA, dry CH₂Cl₂, 0 °C, 2 h, 67%; (c) K₂CO₃, CH₃CN, 90 °C, 18 h, 62%; (d) TEA, DMAP, EtOH, reflux, 72 h, 30%.

Similarly, the two amide groups were removed one at a time, according to Scheme 6 and 7. Coupling reaction between **30** and **31**, followed by hydrolysis of the ethyl ester group, yielded intermediate **33**, that underwent a coupling reaction with tryptamine to afford compound **34**.

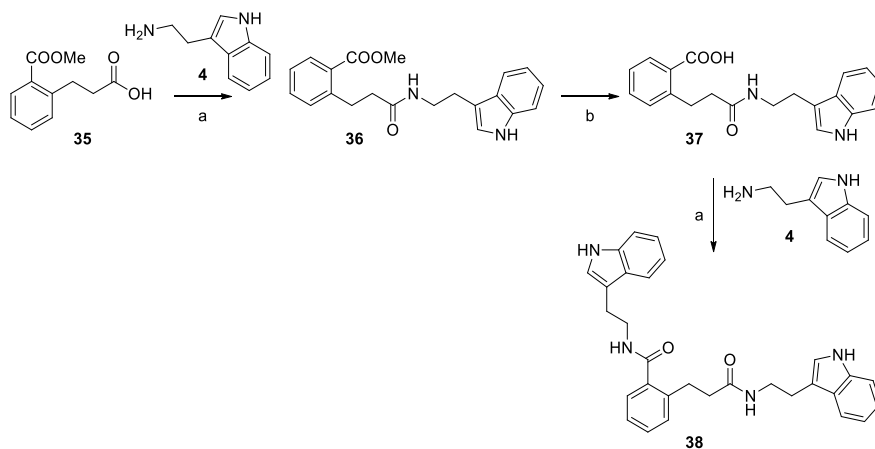
Compound **38** was obtained in a similar manner: a first coupling reaction between tryptamine and **35**, hydrolysis of the methyl ester and a final coupling with tryptamine.

Scheme 6. Synthesis of compound **34**.



Reagents and conditions: (a) DIPEA, EDCI, DMAP, dry CH₂Cl₂, rt, 72 h, 40%; (b) NaOH, H₂O, THF, 50 °C, 4 h, 54%; (c) TEA, EDCI, HOBT, dry CH₂Cl₂, rt, 18 h, 48%.

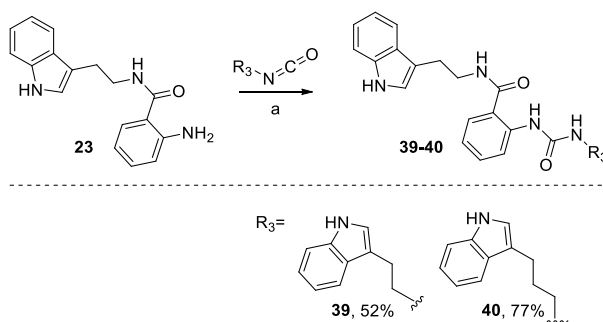
Scheme 7. Synthesis of compound **38**.



Reagents and conditions: (a) TEA, EDCI, HOBT, dry CH₂Cl₂, rt, 18 h, 71-85%; (b) NaOH, H₂O, THF, 50 °C, 8 h, 68%.

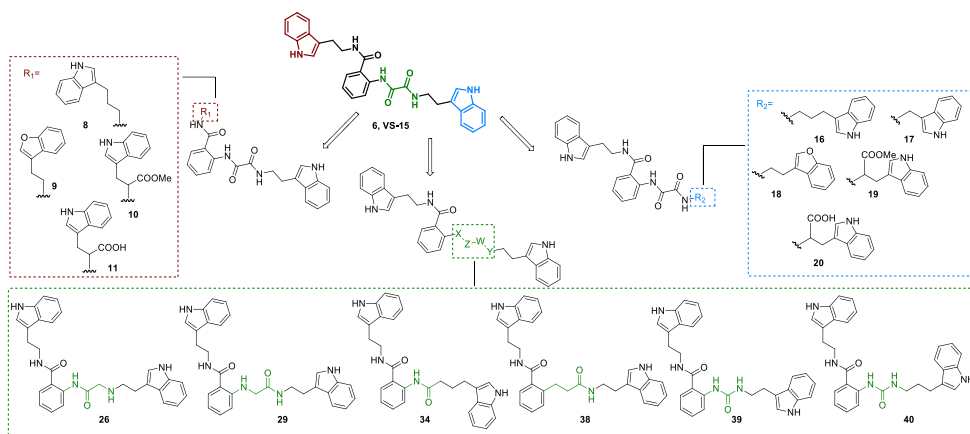
Finally, two urea derivatives were synthesized (Scheme 8). The required isocyanates were prepared as described in the experimental section and reacted with intermediate **23** to afford compounds **39** and **40**.

Scheme 8. Synthesis of compounds **39-40**.



Reagents and conditions: (a) DIPEA, dry THF, rt, 96 h, 52-77%.

Figure 3. Summary of the preliminary SAR study around compound **VS-15**.



The biological evaluation of the 16 synthesized analogues (Figure 3) was then performed. After having ruled out a cytotoxicity by MTT assay at 10 μM , the reduction of L-Kyn production after 48 hours of treatment with 10 μM of the compounds was evaluated in A375 cells. Only one compound significantly affected cell viability (**8**, $76 \pm 5\%$) and 5 analogues induced an IDO1 inhibition higher than 85% (**16**, **17**, **18**, **19**, **38**). Among these, only compound **38** displays a side chain in which the α,β -dicarbonyl soft spot has been removed and therefore its metabolic stability was evaluated. After one hour of incubation in MLS9, the residual substrate recovered was 51% and the characterization of the metabolites revealed that no hydrolysis of the amide groups occurs. In contrast to what observed for **VS-15**, the main liabilities of this molecule are represented by the oxidative metabolism of the two indole rings. To further elucidate the enhanced metabolic stability in the analogues in which the soft spot has been removed, despite not being the most active ones, 3 other candidates (**29**, **39**, **40**, Table 1) have been evaluated for their stability in MLS9 and globally all of them are more stable than **VS-15**, with a residual substrate of 49, 67 and 70%, respectively).

On the basis of this evidence further optimization of the selected compounds will be performed, also taking into consideration the biological data that are currently ongoing.

Despite the biological characterization of this class is currently under development, by these preliminary results we can draw the following conclusions: (i) the indole ring located in pocket A is crucial for IDO1 inhibition, and elongation of the carbon chain (**8**, $68 \pm 15\%$) or substitution of the moiety with a benzofuran (**9**, $6 \pm 7\%$) reduces the activity compared to **VS-15**; (ii) the substitution of the indole ring in pocket C with a benzofuran substructure (**18**, $97 \pm 3\%$) or elongation of the carbon chain (**16**, $91 \pm 3\%$) are well tolerated; (iii) the removal of the aryl amide group leads to a compound (**38**) slightly less active ($88 \pm 6\%$), but more stable (51% of residual substrate) than **VS-15** (13% of residual substrate); (iv) on the contrary, the removal of the other amide group (**34**, $46 \pm 10\%$) causes a drop-in the activity; (v) the insertion of an urea group in the side chain reduces the activity (**39**: $67 \pm 4\%$, **40**: $59 \pm 3\%$), but leads to an enhanced metabolic stability (residual substrate of 67% for **39** and 70% for **40**).

Table 1. Biological profile and metabolic stability of **VS-15** analogues.

Cpd	Cell viability (%) @ 10 μ M \pm SD	IDO1 cellular assay inhibition (%) @ 10 μ M	Residual substrate (MLS9)
VS-15	96 ± 3	93 ± 3	15%
8	76 ± 5	68 ± 15	-
9	100 ± 0	6 ± 7	-
10	93 ± 8	60 ± 2	-
11	96 ± 3	27 ± 1	-

Cpd	Cell viability (%) @ 10 μ M \pm SD	IDO1 cellular assay inhibition (%) @ 10 μ M	Residual substrate (MLS9)
16	100 \pm 0	91 \pm 3	-
17	95 \pm 5	91 \pm 1	-
18	91 \pm 6	97 \pm 3	-
19	97 \pm 3	87 \pm 10	-
20	100 \pm 0	0 \pm 0	-
22	86 \pm 7	<i>to be done</i>	-
26	97 \pm 3	61 \pm 3	-
29	92 \pm 7	57 \pm 6	49%
34	99 \pm 1	46 \pm 10	-
38	93 \pm 8	88 \pm 6	51%
39	90 \pm 1	67 \pm 4	67%
40	92 \pm 6	59 \pm 3	70%

Enzymatic activity

To determine the inhibitory activity of **VS-15** and its analogues (**8-11**, **16-20**, **26**, **34**, **38-40**) toward the purified enzyme, an enzyme-based assay using recombinant human IDO1 (rhIDO1) was performed. 10 μ M of each compound was added to the reaction buffer and the rhIDO1 conversion of Trp to Kyn was determined by HPLC. Epacadostat was chosen as reference compound. Surprisingly, while the reference compound exhibited a good activity on rhIDO1, none of the tested compounds provided a reduction in the Kyn levels in the enzyme-based assay.

On the contrary, **VS-15** has demonstrated to possess a low K_d value (24.29 ± 3.76 μM) in the MST experiment, confirming its strong binding to IDO1, and a good IC_{50} value (0.8 μM) in the cell-based assay. This unexpected result, while uncommon, is in accordance with the behaviour of the reported apo-IDO1 inhibitor linrodostat (type IV, see Chapter 5),⁷ or with the only known modulator of the signalling pathway of the protein, VIS351.^{6b} This initial result has prompted us to further explore the mechanism of action of the compound, as described in the discussion.

8.2 Experimental section

General Experimental Methods. Commercially available reagents and solvents were used as purchased without further purification. When needed, solvents were distilled and stored on molecular sieves. Column chromatography was performed on silica gel. The following instrumentation was used: Stuart scientific SMP3 apparatus (melting point), FT-IR Thermo-Nicolet Avatar, FT-IR Bruker Alpha II (IR), Bruker Avance Neo 400 MHz (^1H -NMR and ^{13}C -NMR), Thermo Finnigan LCQ-deca XP-plus equipped with an ESI source and an ion trap detector (mass spectrometry). Chemical shifts are reported in parts per million (ppm).

2-(2-Ethoxy-2-oxoacetamido)benzoic acid, (3).

2-Aminobenzoic acid (1.0 g, 7.3 mmol) was solubilized in dry THF (12 mL) and ethyl 2-chloro-2-oxoacetate (0.8 mL, 7.3 mmol) was added dropwise at 0 $^\circ\text{C}$ and under nitrogen. After 1 hour, the reaction was not concluded and 0.3 eq of ethyl 2-chloro-2-oxoacetate were added. After additional 30 minutes at 0 $^\circ\text{C}$, the reaction was concluded and the volatile was removed under vacuo, yielded the title compound as a white solid (1.73 g, 7.3 mmol). The yield was quantitative; ^1H -NMR (400 MHz, acetone- d_6): δ 12.62 (br s, 1H), 8.74 (d, $J = 7.4$ Hz, 1H), 8.19 (d, $J = 7.4$ Hz, 1H), 7.66 (t, $J = 7.4$ Hz, 1H), 7.23 (t, $J = 7.4$ Hz, 1H), 4.40 (q, $J = 7.1$ Hz, 2H), 1.40 (t, $J = 7.1$ Hz, 3H). MS (ESI): m/z 236 $[\text{M-H}]^-$.

2-(2-((2-(1H-Indol-3-yl)ethyl)amino)-2-oxoacetamido)benzoic acid, (5).

Intermediate **3** (1.85 g, 7.8 mmol) was solubilized in toluene (62 mL) and 2-(1*H*-indol-3-yl)ethanamine (1.5 g, 9.4 mmol) and TEA (2.2 mL, 15.6 mmol) were added. The reaction was heated at reflux overnight, then was diluted with EtOAc and washed with HCl 3N. Purification with column chromatography (EtOAc as eluent) afforded the title compound as a yellow solid, with a yield of 68%; ¹H-NMR (400 MHz, acetone-*d*₆): δ 9.94 (br s, 1H), 8.74 (d, *J* = 8.5 Hz, 1H), 8.29 (br s, 1H), 8.15 (d, *J* = 8.5 Hz, 1H), 7.67-7.64 (m, 2H), 7.38 (d, *J* = 7.9 Hz, 1H), 7.24-7.22 (m, 2H), 7.09-7.02 (m, 2H), 3.68 (q, *J* = 7.1 Hz, 2H), 3.07 (t, *J* = 7.1 Hz, 2H). MS (ESI): *m/z* 350 [M-H]⁻.

***N*¹-(2-(1*H*-Indol-3-yl)ethyl)-*N*²-(2-((2-(1*H*-indol-3-yl)ethyl)carbamoyl)phenyl)oxalamide, (6, VS15).**

2-(2-((2-(1*H*-Indol-3-yl)ethyl)amino)-2-oxoacetamido)benzoic acid was solubilized (100 mg, 0.28 mmol) in dry CH₂Cl₂ (2.5 mL) and TEA (90 μL, 0.63 mmol), HOBT (46.2 mg, 0.34 mmol), EDCI (65.5 mg, 0.34 mmol) and 2-(1*H*-indol-3-yl)ethanamine (54.7 mg, 0.34 mmol) were added in order under nitrogen. After stirring at room temperature overnight, the reaction was diluted with water and extracted with CH₂Cl₂. The organic layer was dried over sodium sulfate and purified by column chromatography (PE/EtOAc 6:4 as eluent), affording the title compound as yellow solid (58%); mp: 186-188 °C. ¹H-NMR (400 MHz, acetone-*d*₆): δ 9.87 (br s, 1H), 8.63 (d, *J* = 8.3 Hz, 1H), 8.26 (br s, 1H), 7.85 (br s, 1H), 7.73-7.66 (m, 3H), 7.49 (t, *J* = 7.2 Hz, 1H), 7.40-7.37 (m, 2H), 7.20-7.00 (m, 7H), 3.77-3.68 (m, 4H), 3.15-3.07 (m, 4H). IR (neat): $\tilde{\nu}$ = 3458, 3321, 2920, 2852, 1678, 1519, 1448, 1190, 735 cm⁻¹. MS (ESI): *m/z* 516 [M+Na]⁺.

***N*¹-(2-(1*H*-Indol-3-yl)ethyl)-*N*²-(2-((3-(1*H*-indol-3-yl)propyl)carbamoyl)phenyl)oxalamide, (8).**

Following the procedure described for compound **6**, the reaction of intermediate **5** and 3-(1*H*-indol-3-yl)propan-1-amine, after purification (PE/EtOAc 5:5 as eluent), yielded compound **8** as a white solid (53%); mp: 184-185 °C. ¹H-NMR (400 MHz, acetone-*d*₆): δ 12.81 (br s, 1H), 10.08 (br s, 1H), 10.00 (br s, 1H), 8.66 (d, *J* = 8.3

Hz, 1H), 8.40 (br s, 1H), 8.05 (br s, 1H), 7.75 (d, $J = 7.8$ Hz, 1H), 7.69 (d, $J = 7.8$ Hz, 1H), 7.60 (d, $J = 8.0$ Hz, 1H), 7.52 (t, $J = 7.8$ Hz, 1H), 7.42-7.39 (m, 2H), 7.19-7.00 (m, 7H), 3.70 (q, $J = 7.5$ Hz, 2H), 3.55 (q, $J = 6.6$ Hz, 2H), 3.10 (t, $J = 7.5$ Hz, 2H), 2.90 (t, $J = 6.6$ Hz, 2H), 2.07 (quint, $J = 7.5$ Hz, 2H). IR (neat): $\tilde{\nu} = 3395, 2920, 1672, 1637, 1543, 1509, 1450, 1298, 1225, 744, 580, 500$ cm⁻¹. MS (ESI): m/z 530 [M+Na]⁺.

***N*¹-(2-(1*H*-indol-3-yl)ethyl)-*N*²-(2-((2-(benzofuran-3-yl)ethyl)carbamoyl)phenyl)oxalamide, (9).**

Following the procedure described for compound **6**, the reaction of intermediate **5** and 2-(benzofuran-3-yl)ethanamine, after purification (PE/EtOAc 7:3 as eluent), yielded compound **9** as a yellow solid (48%); mp: 180-181 °C. ¹H-NMR (400 MHz, DMSO-*d*₆): δ 10.80 (br s, 1H), 9.09 (br s, 1H), 8.92 (br s, 1H), 8.54 (d, $J = 8.1$ Hz, 1H), 7.87 (s, 1H), 7.75-7.69 (m, 2H), 7.62-7.53 (m, 3H), 7.36-7.23 (m, 5H), 7.08 (t, $J = 7.1$ Hz, 1H), 7.00 (t, $J = 7.6$ Hz, 1H), 3.63 (t, $J = 6.0$ Hz, 2H), 3.51 (t, $J = 7.2$ Hz, 2H), 3.00-2.93 (m, 4H). IR (neat): $\tilde{\nu} = 3321, 1680, 1595, 1519, 1448, 1088, 740, 496, 420$ cm⁻¹. MS (ESI): m/z 495 [M+H]⁺.

Methyl 2-(2-(2-((2-(1*H*-indol-3-yl)ethyl)amino)-2-oxoacetamido)benzamido)-3-(1*H*-indol-3-yl)propanoate, (10).

Following the procedure described for compound **6**, the reaction of intermediate **5** and methyl 2-amino-3-(1*H*-indol-3-yl)propanoate, after purification (PE/EtOAc 4:6 as eluent), yielded compound **10** as a yellow solid (57%); mp: 152-153 °C. ¹H-NMR (400 MHz, CD₃OD): δ 8.51 (d, $J = 8.3$ Hz, 1H), 7.63-7.56 (m, 3H), 7.51 (t, $J = 8.1$ Hz, 1H), 7.35-7.31 (m, 2H), 7.18-7.06 (m, 5H), 7.04-9.97 (m, 2H), 4.86-4.84 (m, 1H), 3.74 (s, 3H), 3.62 (t, $J = 7.3$ Hz, 2H), 3.43-3.33 (m, 2H), 3.05 (t, $J = 7.3$ Hz, 2H). IR (neat): $\tilde{\nu} = 3416, 3359, 2921, 1678, 1507, 1441, 1365, 1215, 1184, 733, 496, 425$ cm⁻¹. MS (ESI): m/z 552 [M+H]⁺.

2-(2-(2-((2-(1*H*-Indol-3-yl)ethyl)amino)-2-oxoacetamido)benzamido)-3-(1*H*-indol-3-yl)propanoic acid, (11).

To a solution of compound **10** (165 mg, 0.3 mmol) in THF (1.5 mL), a solution of NaOH (24 mg, 0.6 mmol) in water (1.5 mL) was added. After 5 hours at room temperature, HCl 3N was added until pH 4 and the aqueous layer was extracted with EtOAc (x3). The collected organic phases were dried over sodium sulfate and evaporated. Purification by column chromatography (EtOAc as eluent) afforded the title compound (50%) as a yellow solid; mp: 182-183 °C. ¹H-NMR (400 MHz, CD₃OD): δ 8.35 (d, *J* = 8.6 Hz, 1H), 7.50-7.46 (m, 2H), 7.35-7.31 (m, 2H), 7.22 (d, *J* = 8.0 Hz, 1H), 7.16 (d, *J* = 8.0 Hz, 1H), 7.03 (s, 1H), 6.99-6.88 (m, 5H), 6.79 (t, *J* = 7.3 Hz, 1H), 4.77-4.74 (m, 1H), 3.51 (t, *J* = 7.4 Hz, 1H), 3.43 (dd, *J_s* = 14.7, 5.0 Hz, 1H), 3.26-3.24 (m, 1H), 2.93 (t, *J* = 7.4 Hz, 2H). IR (neat): $\tilde{\nu}$ = 3384, 2921, 1670, 1584, 1508, 1447, 1224, 1092, 738, 422 cm⁻¹. MS (ESI): *m/z* 538 [M+H]⁺.

2-(2-((3-(1*H*-Indol-3-yl)propyl)amino)-2-oxoacetamido)benzoic acid, (12).

Following the procedure described for compound **5**, the reaction of intermediate **3** and 3-(1*H*-indol-3-yl)propan-1-amine, after purification (PE/EtOAc 3:7 as eluent), yielded compound **12** as a yellow solid (51%); ¹H-NMR (400 MHz, CD₃OD): δ 8.71 (d, *J* = 8.3 Hz, 1H), 8.14 (d, *J* = 7.4 Hz, 1H), 7.61-7.51 (m, 2H), 7.32 (d, *J* = 8.3 Hz, 1H), 7.22 (t, *J* = 7.4 Hz, 1H), 7.09-7.06 (m, 2H), 7.00 (t, *J* = 7.4 Hz, 1H), 3.41 (t, *J* = 7.0 Hz, 2H), 2.84 (t, *J* = 7.0 Hz, 2H), 2.03 (quint, *J* = 7.0 Hz, 2H). MS (ESI): *m/z* 366 [M+H]⁺.

2-(2-(((1*H*-Indol-3-yl)methyl)amino)-2-oxoacetamido)benzoic acid, (13).

Following the procedure described for compound **5**, the reaction of intermediate **3** and (1*H*-indol-3-yl)methanamine, after purification (PE/EtOAc 7:3 as eluent), yielded compound **13** as a red solid (60%); ¹H-NMR (400 MHz, acetone-*d*₆): δ 10.14 (br s, 1H), 8.60 (d, *J* = 8.2 Hz, 1H), 8.34 (d, *J* = 7.6 Hz, 1H), 7.44-7.29 (m, 3H), 7.09 (t, *J* = 7.6 Hz, 1H), 7.11-6.92 (m, 3H), 4.21 (s, 2H). MS (ESI): *m/z* 338 [M+H]⁺.

2-(2-((2-(Benzofuran-3-yl)ethyl)amino)-2-oxoacetamido)benzoic acid, (14).

Following the procedure described for compound **5**, the reaction of intermediate **3** and 2-(benzofuran-3-yl)ethanamine, after purification (EtOAc/MeOH 9:1 as eluent), yielded compound **14** as a dark yellow solid (46%); ¹H-NMR (400 MHz, CD₃OD):

δ 8.62 (d, $J = 8.3$ Hz, 1H), 8.10 (d, $J = 7.8$ Hz, 1H), 7.69 (d, $J = 7.8$ Hz, 1H), 7.64 (s, 1H), 7.49-7.44 (m, 2H), 7.31-7.23 (m, 2H), 7.16 (t, $J = 7.8$ Hz, 1H), 3.66 (t, $J = 7.4$ Hz, 2H), 3.01 (t, $J = 7.4$ Hz, 2H). MS (ESI): m/z 353 [M+H]⁺.

2-(2-((3-(1*H*-Indol-3-yl)-1-methoxy-1-oxopropan-2-yl)amino)-2-oxoacetamido)benzoic acid, (15).

Following the procedure described for compound **5**, the reaction of intermediate **3** and methyl 2-amino-3-(1*H*-indol-3-yl)propanoate, after purification (PE/EtOAc 3:7 as eluent), yielded compound **15** as a dark yellow solid (39%); ¹H-NMR (400 MHz, CD₃OD): δ 8.52 (d, $J = 8.1$ Hz, 1H), 7.99 (d, $J = 7.2$ Hz, 1H), 7.43-7.41 (m, 2H), 7.22 (d, $J = 8.1$ Hz, 1H), 7.06 (t, $J = 7.2$ Hz, 1H), 7.00-6.95 (m, 2H), 6.89 (t, $J = 7.2$ Hz, 1H), 3.58 (s, 3H), 3.29-3.26 (m, 2H). MS (ESI): m/z 432 [M+Na]⁺.

***N*¹-(2-((2-(1*H*-Indol-3-yl)ethyl)carbamoyl)phenyl)-*N*²-(3-(1*H*-indol-3-yl)propyl)oxalamide, (16).**

Following the procedure described for compound **6**, the reaction of intermediate **12** and 2-(1*H*-indol-3-yl)ethanamine, after purification (PE/EtOAc 3:7 as eluent), yielded compound **16** as a yellow solid (46%); mp: 107-108 °C. ¹H-NMR (400 MHz, CD₃OD): δ 8.55 (d, $J = 8.3$ Hz, 1H), 7.63-7.48 (m, 4H), 7.35-7.32 (m, 2H), 7.17 (t, $J = 7.7$ Hz, 1H), 7.13 (s, 1H), 7.11-7.06 (m, 4H), 6.99 (t, $J = 7.2$ Hz, 1H), 3.70 (t, $J = 7.4$ Hz, 2H), 3.42 (t, $J = 7.3$ Hz, 2H), 3.11 (t, $J = 7.3$ Hz, 2H), 2.84 (t, $J = 7.4$ Hz, 2H), 2.01 (quint, $J = 7.3$ Hz, 2H). IR (neat): $\tilde{\nu} = 3308, 2961, 1674, 1513, 1442, 1258, 1086, 1017, 794$ cm⁻¹. MS (ESI): m/z 508 [M+H]⁺.

***N*¹-(2-((2-(1*H*-indol-3-yl)ethyl)carbamoyl)phenyl)-*N*²-((1*H*-indol-3-yl)methyl)oxalamide, (17).**

Following the procedure described for compound **6**, the reaction of intermediate **13** and 2-(1*H*-indol-3-yl)ethanamine, after purification (PE/EtOAc 7:3 as eluent), yielded compound **17** as a yellow solid (22%); mp: 97-98 °C. ¹H-NMR (400 MHz, CD₃OD): δ 8.52 (d, $J = 7.6$ Hz, 1H), 7.67-7.56 (m, 3H), 7.37-7.31 (m, 2H), 7.28 (s, 1H), 7.16-6.97 (m, 7H), 4.70 (s, 2H), 3.71 (t, $J = 7.3$ Hz, 2H), 3.11 (t, $J = 7.3$ Hz,

2H). IR (neat): $\tilde{\nu}$ = 2921, 2852, 1671, 1506, 1448, 1260, 1012, 799, 739 cm^{-1} . MS (ESI): m/z 480 $[\text{M}+\text{H}]^+$.

***N*¹-(2-((2-(1*H*-indol-3-yl)ethyl)carbamoyl)phenyl)-*N*²-(2-(benzofuran-3-yl)ethyl)oxalamide, (18).**

Following the procedure described for compound **6**, the reaction of intermediate **14** and 2-(1*H*-indol-3-yl)ethanamine, after purification (PE/EtOAc 6:4 as eluent), yielded compound **18** as a dark yellow solid (55%); mp: 189-190 °C. ¹H-NMR (400 MHz, DMSO-*d*₆): δ 12.62 (br s, 1H), 10.81 (br s, 1H), 9.19 (br s, 1H), 8.88 (br s, 1H), 8.55 (d, J = 8.3 Hz, 1H), 7.84 (s, 1H), 7.77-7.70 (m, 2H), 7.60-7.53 (m, 3H), 7.36-7.21 (m, 5H), 7.07 (t, J = 7.1 Hz, 1H), 6.98 (t, J = 7.9 Hz, 1H), 3.61-3.52 (m, 4H), 3.00 (t, J = 7.5 Hz, 2H), 2.94 (t, J = 7.2 Hz, 2H). IR (neat): $\tilde{\nu}$ = 3299, 1670, 1632, 1504, 1446, 1092, 737, 628, 425 cm^{-1} . MS (ESI): m/z 495 $[\text{M}+\text{H}]^+$.

Methyl 2-(2-((2-((2-(1*H*-indol-3-yl)ethyl)carbamoyl)phenyl)amino)-2-oxoacetamido)-3-(1*H*-indol-3-yl)propanoate, (19).

Following the procedure described for compound **6**, the reaction of intermediate **15** and 2-(1*H*-indol-3-yl)ethanamine, after purification (PE/EtOAc 3:7 as eluent), yielded compound **19** as a dark yellow solid (45%); mp: 104-105 °C. ¹H-NMR (400 MHz, CD₃OD): δ 8.44 (d, J = 8.2 Hz, 1H), 7.59-7.44 (m, 3H), 7.33-7.29 (m, 2H), 7.09-6.93 (m, 8H), 4.83 (t, J = 6.6 Hz, 1H), 3.65-3.62 (m, 5H), 3.37-3.32 (m, 2H), 3.03 (t, J = 7.3 Hz, 2H). IR (neat): $\tilde{\nu}$ = 3369, 1737, 1673, 1504, 1448, 1220, 1094, 739, 481, 424 cm^{-1} . MS (ESI): m/z 552 $[\text{M}+\text{H}]^+$.

2-(2-((2-((2-(1*H*-Indol-3-yl)ethyl)carbamoyl)phenyl)amino)-2-oxoacetamido)-3-(1*H*-indol-3-yl)propanoic acid, (20).

Following the procedure described for compound **11**, the reaction of compound **19**, after purification by column chromatography (EtOAc/MeOH 9:1 as eluent) afforded the title compound (46%) as a white solid; mp: 184-185 °C. ¹H-NMR (400 MHz, CD₃OD): δ 8.47 (d, J = 8.2 Hz, 1H), 7.65-7.55 (m, 3H), 7.47 (t, J = 7.3 Hz, 1H), 7.34-7.29 (m, 2H), 7.20-6.96 (m, 7H), 4.71 (t, J = 5.6 Hz, 1H), 3.69 (t, J = 7.3 Hz,

2H), 3.42-3.39 (m, 2H), 3.09 (t, $J = 7.2$ Hz, 2H). IR (neat): $\tilde{\nu} = 3350, 2922, 2852, 1671, 1508, 1449, 1259, 1012, 795, 739, 492$ cm⁻¹. MS (ESI): m/z 538 [M+H]⁺.

***N*¹-(2-(benzofuran-3-yl)ethyl)-*N*²-(2-((2-(benzofuran-3-yl)ethyl)carbamoyl)phenyl)oxalamide, (22).**

Following the procedure described for compound **6**, the reaction of intermediate **13** and 2-(benzofuran-3-yl)ethanamine, after purification (PE/EtOAc 8:2 as eluent), yielded compound **22** as a yellow solid (60%); ¹H-NMR (400 MHz, CDCl₃): δ 12.77 (br s, 1H), 8.62 (d, $J = 8.3$ Hz, 1H), 7.66 (br s, 1H), 7.63-7.59 (m, 2H), 7.53-7.47 (m, 5H), 7.38-7.24 (m, 5H), 7.10 (t, $J = 7.6$ Hz, 1H), 6.40 (br s, 1H), 3.85 (q, $J = 6.2$ Hz, 2H), 3.75 (q, $J = 6.7$ Hz, 2H), 3.08-3.00 (m, 4H). MS (ESI): m/z 496 [M+H]⁺.

***N*-(2-(1*H*-Indol-3-yl)ethyl)-2-aminobenzamide, (23).**

Following the procedure described for compound **6**, the reaction of 2-aminobenzoic acid and 2-(1*H*-indol-3-yl)ethanamine, after purification (PE/EtOAc 7:3 as eluent), yielded compound **23** as a yellow solid (82%); ¹H-NMR (400 MHz, CD₃OD): δ 7.48 (d, $J = 7.9$ Hz, 1H), 7.21-7.17 (m, 2H), 7.03-6.96 (m, 2H), 6.94 (s, 1H), 6.89 (t, $J = 7.9$ Hz, 1H), 6.58 (d, $J = 8.2$ Hz, 1H), 6.45 (t, $J = 8.2$ Hz, 1H), 3.49 (t, $J = 7.2$ Hz, 2H), 2.91 (t, $J = 7.2$ Hz, 2H). MS (ESI): m/z 280 [M+H]⁺.

***N*-(2-(1*H*-Indol-3-yl)ethyl)-2-(2-bromoacetamido)benzamide, (25).**

Intermediate **23** (391 mg, 1.4 mmol) was solubilized in dry CH₂Cl₂ (8 mL) and TEA (428 μ L, 3.08 mmol) was added under nitrogen. Then, 2-bromoacetyl chloride (187 μ L, 2.24 mmol) was added dropwise at 0 °C. After 2 hours, the reaction was not concluded and 1 eq of 2-bromoacetyl chloride was added. After 2 additional hours, the reaction was diluted with CH₂Cl₂ and washed with water (x3). After anidrification over sodium sulfate and evaporation, the crude material was purified by column chromatography (PE/EtOAc 6:4), affording the title compound (67%) as a yellow solid; ¹H-NMR (400 MHz, acetone-*d*₆): δ 12.07 (br s, 1H), 10.02 (br s, 1H), 8.58 (d, $J = 8.1$ Hz, 1H), 8.15 (br s, 1H), 7.73 (d, $J = 8.1$ Hz, 1H), 7.65 (d, $J = 7.2$ Hz, 1H), 7.50 (t, $J = 7.2$ Hz, 1H), 7.40 (t, $J = 8.1$ Hz, 1H), 7.24 (s, 1H), 7.15-7.10

(m, 2H), 7.03 (t, $J = 7.2$ Hz, 1H), 4.13 (s, 2H), 3.76 (q, $J = 7.1$ Hz, 2H), 3.13 (t, $J = 7.1$ Hz, 2H). MS (ESI): m/z 280 [M+H]⁺.

***N*-(2-(1*H*-Indol-3-yl)ethyl)-2-((2-(1*H*-indol-3-yl)ethyl)amino)acetamido)benzamide, (26).**

To a solution of intermediate **25** (150 mg, 0.37 mmol) in CH₃CN (3 mL), K₂CO₃ (100 mg, 0.74 mmol) and 2-(1*H*-indol-3-yl)ethanamine (120 mg, 0.74 mmol) were added. The mixture was heated at reflux overnight. Then, the volatile was removed and the reaction was diluted with EtOAc and the organic phase was washed with water, dried over sodium sulfate and evaporated. Purification by column chromatography (PE/EtOAc 5:5 as eluent) afforded the title compound as a pink solid (62%); ¹H-NMR (400 MHz, acetone-*d*₆): δ 12.05 (br s, 1H), 9.96 (br s, 1H), 8.72 (d, $J = 8.4$ Hz, 1H), 7.96 (br s, 1H), 7.71-7.64 (m, 3H), 7.44 (t, $J = 8.4$ Hz, 1H), 7.39-7.36 (m, 2H), 7.25 (s, 1H), 7.19 (s, 1H), 7.10-7.04 (m, 3H), 7.00-6.96 (m, 2H), 3.79 (q, $J = 7.1$ Hz, 2H), 3.39 (s, 2H), 3.18-3.13 (m, 4H), 3.00 (t, $J = 7.1$ Hz, 2H). MS (ESI): m/z 481 [M+H]⁺.

2-((2-(2-(1*H*-Indol-3-yl)ethyl)carbamoyl)phenyl)amino)acetic acid, (28).

Intermediate **23** (100 mg, 0.36 mmol) was solubilized in EtOH (5 mL) and 2-bromoacetic acid (38 μL, 0.54 mmol), TEA (149 μL, 1.07 mmol) and DMAP (13 mg, 0.03 mmol) were added in order. The mixture was heated at reflux for 72 hours, then the volatile was removed and EtOAc was added. The organic phase was washed with HCl 3N, dried over sodium sulfate and evaporated. Purification by column chromatography (EtOAc/MeOH 9:1 as eluent) afforded the title compound as a dark yellow solid (30%); ¹H-NMR (400 MHz, CD₃OD): δ 7.59 (d, $J = 7.8$ Hz, 1H), 7.37-7.34 (m, 2H), 7.25 (t, $J = 7.8$ Hz, 1H), 7.11-7.07 (m, 2H), 6.99 (t, $J = 7.1$ Hz, 1H), 6.62-6.58 (m, 2H), 3.65 (t, $J = 7.4$ Hz, 2H), 3.34 (s, 2H), 3.05 (t, $J = 7.4$ Hz, 2H). MS (ESI): m/z 338 [M+H]⁺.

***N*-(2-(1*H*-indol-3-yl)ethyl)-2-(((2-(1*H*-indol-3-yl)ethyl)amino)-2-oxoethyl)amino)benzamide, (29).**

Following the procedure described for compound **6**, the reaction of intermediate **28** and 2-(1*H*-indol-3-yl)ethanamine, after purification (PE/EtOAc 4:6 as eluent), yielded compound **29** as a yellow solid (62%); mp: 80-81 °C. ¹H-NMR (400 MHz, CD₃OD): δ 7.96 (br s, 1H), 7.63 (d, *J* = 7.9 Hz, 1H), 7.51 (d, *J* = 7.9 Hz, 1H), 7.39-7.30 (m, 3H), 7.20 (t, *J* = 7.0 Hz, 1H), 7.12-7.05 (m, 3H), 7.02-6.96 (m, 2H), 6.87 (s, 1H), 6.66 (t, *J* = 7.3 Hz, 1H), 6.42 (d, *J* = 7.9 Hz, 1H), 3.71 (s, 2H), 3.67 (t, *J* = 7.3 Hz, 2H), 3.50 (t, *J* = 7.1 Hz, 2H), 3.07 (t, *J* = 7.3 Hz, 2H), 2.89 (t, *J* = 7.1 Hz, 2H). IR (neat): $\tilde{\nu}$ = 3273, 2922, 2852, 1629, 1510, 1454, 1259, 1011, 798, 738, 474 cm⁻¹. MS (ESI): *m/z* 480 [M+H]⁺.

Ethyl 2-(4-(1*H*-indol-3-yl)butanamido)benzoate, (32).

4-(1*H*-Indol-3-yl)butanoic acid (300 mg, 1.48 mmol) was solubilized in dry CH₂Cl₂ and 2-aminobenzoic acid (244 mg, 1.48 mmol), EDCI (567 mg, 2.96 mmol), DIPEA (773 μL, 4.44 mmol) and DMAP (18 mg, 0.14 mmol) were added in order. After stirring at room temperature overnight, the reaction was not concluded and EDCI (1.2 eq), DIPEA (1.2 eq) and DMAP (0.1 eq) were added. After 2 days, the mixture was diluted with CH₂Cl₂ and the organic phase was washed with water, dried over sodium sulfate and evaporated. Purification by column chromatography (PE/EtOAc 8:2 as eluent) afforded the title compound as a yellow solid (40%); ¹H-NMR (400 MHz, CD₃OD): δ 8.49 (d, *J* = 8.4 Hz, 1H), 8.49 (d, *J* = 8.0 Hz, 1H), 7.58-7.53 (m, 2H), 7.32 (d, *J* = 8.0 Hz, 1H), 7.15 (t, *J* = 8.4 Hz, 1H), 7.09-7.05 (m, 2H), 6.98 (t, *J* = 8.0 Hz, 1H), 4.38 (q, *J* = 7.1 Hz, 2H), 2.87 (t, *J* = 7.3 Hz, 2H), 2.50 (t, *J* = 7.3 Hz, 2H), 2.15 (quint, *J* = 7.3 Hz, 2H), 1.39 (t, *J* = 7.1 Hz, 3H).

MS (ESI): *m/z* 351 [M+H]⁺.

2-(4-(1*H*-Indol-3-yl)butanamido)benzoic acid, (33).

Following the procedure described for compound **11**, the reaction of compound **32**, after purification by column chromatography (EtOAc as eluent) afforded the title compound (54%) as a yellow solid; ¹H-NMR (400 MHz, acetone-*d*₆): δ 9.85 (br s, 1H), 8.71 (d, *J* = 8.1 Hz, 1H), 8.28 (br s, 1H), 7.51 (d, *J* = 8.1 Hz, 1H), 7.33-7.31 (m,

2H), 7.06-6.95 (m, 5H), 2.65 (t, $J = 7.4$ Hz, 2H), 2.41-2.36 (m, 4H). MS (ESI): m/z 323 $[M+H]^+$.

2-(4-(1*H*-Indol-3-yl)butanamido)-*N*-(2-(1*H*-indol-3-yl)ethyl)benzamide, (34).

Following the procedure described for compound **6**, the reaction of intermediate **33** and 2-(1*H*-indol-3-yl)ethanamine, after purification (PE/EtOAc 7:3 as eluent), yielded compound **34** as a yellow solid (48%); mp: 188-189 °C. ¹H-NMR (400 MHz, CD₃OD): δ 8.29 (d, $J = 8.2$ Hz, 1H), 7.61-7.51 (m, 3H), 7.45 (t, $J = 7.8$ Hz, 1H), 7.34-7.31 (m, 2H), 7.14-7.05 (m, 5H), 7.00-6.95 (m, 2H), 3.68 (t, $J = 7.2$ Hz, 2H), 3.07 (t, $J = 7.2$ Hz, 2H), 2.86 (t, $J = 7.4$ Hz, 2H), 2.44 (t, $J = 7.4$ Hz, 2H), 2.12 (quint, $J = 7.4$ Hz, 2H). IR (neat): $\tilde{\nu} = 3305, 2919, 1512, 1443, 1260, 1091, 1010, 799, 737, 422$ cm⁻¹. MS (ESI): m/z 466 $[M+H]^+$.

Methyl 2-(3-((2-(1*H*-indol-3-yl)ethyl)amino)-3-oxopropyl)benzoate, (36).

Following the procedure described for compound **6**, the reaction of 3-(2-(methoxycarbonyl)phenyl)propanoic acid and 2-(1*H*-indol-3-yl)ethanamine, after purification (PE/EtOAc 5:5 as eluent), yielded compound **36** as a pale red oil (85%); ¹H-NMR (400 MHz, CD₃OD): δ 7.83 (d, $J = 6.8$ Hz, 1H), 7.54 (d, $J = 7.9$ Hz, 1H), 7.37-7.33 (m, 2H), 7.23-7.19 (m, 2H), 7.09 (t, $J = 7.9$ Hz, 1H), 7.01 (t, $J = 7.9$ Hz, 1H), 6.98 (s, 1H), 3.81 (s, 3H), 3.44 (t, $J = 7.3$ Hz, 2H), 3.20 (t, $J = 7.5$ Hz, 2H), 2.87 (t, $J = 7.3$ Hz, 2H), 2.45 (t, $J = 7.5$ Hz, 2H). MS (ESI): m/z 351 $[M+H]^+$.

2-(3-((2-(1*H*-Indol-3-yl)ethyl)amino)-3-oxopropyl)benzoic acid, (37).

To a solution of compound **36** (143 mg, 0.4 mmol) in THF (1.6 mL), a solution of NaOH (32 mg, 0.8 mmol) in water (1.6 mL) was added. After 2 hours at 50 °C, the mixture was stirred overnight at room temperature. Then, HCl 3N was added until pH 4 and the aqueous layer was extracted with EtOAc (x3). The collected organic phases were dried over sodium sulfate and evaporated, yielding the title compound (68%) as a dark yellow solid; ¹H-NMR (400 MHz, CD₃OD): δ 7.92 (d, $J = 6.3$ Hz, 1H), 7.58 (d, $J = 7.1$ Hz, 1H), 7.43 (t, $J = 6.3$ Hz, 1H), 7.39-7.30 (m, 3H), 7.11 (t, $J = 7.1$ Hz, 1H), 7.02-6.99 (m, 2H), 3.45 (t, $J = 7.2$ Hz, 2H), 3.25 (t, $J = 7.8$ Hz, 2H), 2.88 (t, $J = 7.2$ Hz, 2H), 2.52 (t, $J = 7.8$ Hz, 2H). MS (ESI): m/z 337 $[M+H]^+$.

2-(4-(1*H*-Indol-3-yl)butanamido)-*N*-(2-(1*H*-indol-3-yl)ethyl)benzamide, (38).

Following the procedure described for compound **6**, the reaction of intermediate **37** and 2-(1*H*-indol-3-yl)ethanamine, after purification (PE/EtOAc 4:6 as eluent), yielded compound **38** as a white solid (71%); mp: 98-99 °C. ¹H-NMR (400 MHz, acetone-*d*₆): δ 9.98 (br s, 1H), 9.92 (br s, 1H), 7.86 (br s, 1H), 7.68 (d, *J* = 7.8 Hz, 1H), 7.59 (d, *J* = 7.8 Hz, 1H), 7.40-7.35 (m, 3H), 7.32-7.26 (m, 3H), 7.12-7.07 (m, 4H), 7.05-6.99 (m, 2H), 3.75 (q, *J* = 7.3 Hz, 2H), 3.46 (q, *J* = 7.5 Hz, 2H), 3.13 (t, *J* = 7.3 Hz, 2H), 3.03 (t, *J* = 7.5 Hz, 2H), 2.87 (t, *J* = 7.3 Hz, 2H), 2.54 (t, *J* = 7.5 Hz, 2H). IR (neat): $\tilde{\nu}$ = 3254, 1629, 1521, 1454, 1226, 1095, 739, 423 cm⁻¹. MS (ESI): *m/z* 480 [M+H]⁺.

***N*-(2-(1*H*-Indol-3-yl)ethyl)-2-(3-(2-(1*H*-indol-3-yl)ethyl)ureido)benzamide, (39).**

2-(1*H*-Indol-3-yl)ethanamine (150 mg, 0.94 mmol) was solubilized in a solution of CH₂Cl₂ (3.3 mL) and NaHCO₃ saturated aqueous solution (6.6 mL) and the mixture was cooled at 0 °C. At this temperature, triphosgene (111 mg, 0.38 mmol) was added portionwise. After 2 hours, the mixture was diluted with CH₂Cl₂ and washed with NaHCO₃ saturated aqueous solution (3x), dried over sodium sulfate and evaporated. Purification with column chromatography (PE/EtOAc 8:2 as eluent) afforded 3-(2-isocyanatoethyl)-1*H*-indole (99%) as a dark yellow oil; ¹H-NMR (400 MHz, CDCl₃): δ 8.34 (br s, 1H), 7.63 (d, *J* = 7.8 Hz, 1H), 7.39 (d, *J* = 7.8 Hz, 1H), 7.27 (t, *J* = 7.8 Hz, 1H), 7.20 (t, *J* = 7.8 Hz, 1H), 7.08 (s, 1H), 3.60 (t, *J* = 6.7 Hz, 2H), 3.12 (t, *J* = 6.7 Hz, 2H).

Intermediate **22** (100 mg, 0.36 mmol) was solubilized in dry THF (2.5 mL) and DIPEA (81 μL) and 3-(2-isocyanatoethyl)-1*H*-indole (80 mg, 0.43 mmol) were added under nitrogen. After 4 days, the reaction is worked-up: the volatile was removed under vacuo, EtOAc was added and the organic phase was washed with NaHCO₃ saturated aqueous solution, dried over sodium sulfate and evaporated. Purification by column chromatography (PE/EtOAc 7:3 as eluent) afforded compound **39** (52%) as a yellow solid; ¹H-NMR (400 MHz, acetone-*d*₆): δ 10.52 (br

s, 1H), 10.07 (br s, 1H), 10.04 (br s, 1H), 8.05 (br s, 1H), 8.58 (d, $J = 8.4$ Hz, 1H), 7.70-7.62 (m, 3H), 7.43-7.37 (m, 3H), 7.20 (s, 1H), 7.19 (s, 1H), 7.15-7.10 (m, 2H), 7.07-7.03 (m, 2H), 6.90 (t, $J = 7.5$ Hz, 1H), 6.75 (br s, 1H), 3.73 (q, $J = 6.5$ Hz, 2H), 3.63 (q, $J = 7.5$ Hz, 2H), 3.14-3.05 (m, 4H). MS (ESI): m/z 467 [M+H]⁺.

***N*-(2-(1*H*-Indol-3-yl)ethyl)-2-(3-(3-(1*H*-indol-3-yl)propyl)ureido)benzamide, (40).**

3-(3-Isocyanatopropyl)-1*H*-indole was obtained as described for 3-(2-isocyanatoethyl)-1*H*-indole, starting from 3-(1*H*-indol-3-yl)propan-1-amine and after purification by column chromatography (PE/EtOAc 8:2), the compound was obtained as a dark yellow oil (58%); ¹H-NMR (400 MHz, CDCl₃): δ 7.91 (br s, 1H), 7.75 (d, $J = 8.1$ Hz, 1H), 7.44 (d, $J = 8.1$ Hz, 1H), 7.37 (t, $J = 8.1$ Hz, 1H), 7.30 (t, $J = 8.1$ Hz, 1H), 7.02 (s, 1H), 3.41 (t, $J = 6.6$ Hz, 2H), 2.99 (t, $J = 6.6$ Hz, 2H), 2.11 (quint, $J = 6.6$ Hz, 2H).

Compound **40** was obtained following the procedure described for compound **39**, starting from amine **22** and 3-(3-isocyanatopropyl)-1*H*-indole. After purification by column chromatography (PE/EtOAc 7:3 as eluent), the title compound was obtained (77%) as a yellow solid; ¹H-NMR (400 MHz, acetone-*d*₆): δ 10.55 (br s, 1H), 10.05 (br s, 1H), 9.96 (br s, 1H), 8.59 (d, $J = 8.4$ Hz, 1H), 8.03 (br s, 1H), 7.69 (d, $J = 7.9$ Hz, 1H), 7.63-7.61 (m, 2H), 7.44-7.37 (m, 3H), 7.19-7.03 (m, 6H), 6.91 (t, $J = 7.9$ Hz, 1H), 6.73 (br s, 1H), 3.76 (q, $J = 6.8$ Hz, 2H), 3.42 (q, $J = 7.4$ Hz, 2H), 3.14 (t, $J = 7.4$ Hz, 2H), 2.88 (t, $J = 6.8$ Hz, 2H), 2.03 (quint, $J = 7.4$ Hz, 2H). MS (ESI): m/z 481 [M+H]⁺.

8.3 References

1. Serafini, M.; Torre, E.; Aprile, S.; Del Grosso, E.; Gesù, A.; Griglio, A.; Colombo, G.; Travelli, C.; Paiella, S.; Adamo, A.; Orecchini, E.; Coletti, A.; Pallotta, M. T.; Ugel, S.; Massarotti, A.; Pirali, T.; Fallarini, S. Discovery of highly potent benzimidazole derivatives as indoleamine 2, 3-dioxygenase-1

- (IDO1) inhibitors: from structure-based virtual screening to *in vivo* pharmacodynamic activity. *J. Med. Chem.* **2020**, *63*, 3047-3065.
2. <https://www.emolecules.com> (accessed on Oct 31, 2020).
 3. Duhr, S.; Braun, D. Why molecules move along a temperature gradient. *Proc. Natl. Acad. Sci. U. S. A.* **2006**, *103*, 19678-19682.
 4. Zhong, H. J.; Liu, L. J.; Chong, C. M.; Lu, L.; Wang, M.; Chan, D. S.; Chan, P. W.; Lee, S. M.; Ma, D. L.; Leung, C. H. Discovery of a natural product-like iNOS inhibitor by molecular docking with potential neuroprotective effects *in vivo*. *PLoS One* **2014**, *9*, e92905.
 5. a) Orabona, C.; Pallotta, M. T.; Grohmann, U. Different partners, opposite outcomes: a new perspective of the immunobiology of indoleamine 2,3-dioxygenase. *Mol. Med.* **2012**, *18*, 834-842; b) Pallotta, M. T.; Orabona, C.; Volpi, C.; Vacca, C.; Belladonna, M. L.; Bianchi, R.; Servillo, G.; Brunacci, C.; Calvitti, M.; Bicciato, S.; Mazza, E. M. C.; Boon, L.; Grassi, F.; Fioretti, M. C.; Fallarino, F.; Puccetti, P.; Grohmann, U. Indoleamine 2,3-dioxygenase is a signaling protein in long-term tolerance by dendritic cells. *Nat. Immunol.* **2011**, *12*, 870-878.
 6. a) Albin, E.; Rosini, V.; Gargaro, M.; Mondanelli, G.; Belladonna, M. L.; Pallotta, M. T.; Volpi, C.; Fallarino, F.; Macchiarulo, A.; Antognelli, C.; Bianchi, R.; Vacca, C.; Puccetti, P.; Grohmann, U.; Orabona, C. Distinct roles of immunoreceptor tyrosinebased motifs in immunosuppressive indoleamine 2,3-dioxygenase 1. *J. Cell Mol. Med.* **2017**, *21*, 165-176; b) Albin, E.; Coletti, A.; Greco, F.; Pallotta, M. T.; Mondanelli, G.; Gargaro, M.; Belladonna, M. L.; Volpi, C.; Bianchi, R.; Grohmann, U.; Macchiarulo, A.; Orabona, C. Identification of a 2-propanol analogue modulating the non-enzymatic function of indoleamine 2,3-dioxygenase 1. *Biochem. Pharmacol.* **2018**, *158*, 286-297.

7. Röhrig, U. F.; Reynaud, A.; Majjigapu, S. R.; Vogel, P.; Pojer, F.; Zoete, V. Inhibition mechanisms of indoleamine 2,3-dioxygenase 1 (IDO1). *J. Med. Chem.* **2019**, *62*, 8784-8795.

8.4 Contributions and collaborations

The compounds described in this chapter have been partially synthesized first-hand by me or have been the object of co-supervision of Master students that have carried out their Thesis project in Prof. Pirali's laboratory.

The virtual screening that led to the identification of the hit compound and the evaluation of its docking pose in IDO1 active site has been performed by Prof. Massarotti from UPO. Metabolic and chemical stability have been evaluated by Dr. Aprile, while the *in vitro* screening of the compounds on A375 cell lines has been performed in collaboration with Dr. Fallarini and Dr. Torre from UPO.

The determination of the selectivity over TDO, the evaluation of the signalling modulation the iNOS inhibition have been performed thanks to the collaboration with Dr. Pallotta from the University of Perugia.

Chapter 9

Discussion and conclusions

9.1 The modulation of Store-Operated Calcium Entry as a therapeutic approach for the treatment of Tubular Aggregate Myopathy

The development of SOCE modulators is a translational project, initially born in our academic laboratories and then become the core business of ChemICare, a spin-off company of UPO, whose mission is the discovery of therapeutic approaches for patients affected by TAM.

Over time, three different classes of SOCE modulators have been discovered by us, the first represented by pytriazoles,¹ the second by biphenyl triazoles² and the last by oxadiazole-bearing pyrazoles (Figure 1).

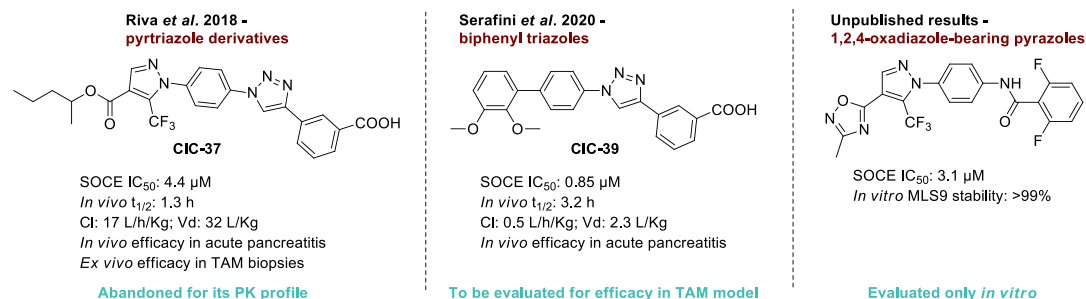
While the further development of the lead compound of pytriazoles, CIC-37, has been interrupted due to its unfavourable *in vivo* PK profile, the class of biphenyl triazoles represents the one on which our group of research and ChemICare are still focusing their efforts. Indeed, the lead compound, CIC-39, is a promising candidate for both its *in vitro* potency on SOCE (IC₅₀: 851 nM) and its *in vivo* PK profile (half-life: 3.2 h; Cl: 0.5 L/h/kg; Vd: 2.3 L/Kg). The *in vivo* proof of concept has been also provided by means of an experiment in which CIC-39 has proven to be effective in a model of acute pancreatitis.

On the basis of these results, the preclinical development of the compound has been undertaken by ChemICare, together with an external CRO, in order to assess its full toxicological profile. These planned experiments include the evaluation of the toxicokinetic profile in minipig, the Ames test, toxicity on hERG channels, the evaluation of the toxicity after a single *e.v.* administration in mini-pig and rat species, formulation studies. In the meanwhile, an *in vivo* experiment aimed at evaluating the efficacy of the candidate in the mouse model of TAM is ongoing.

Finally, while the class of oxadiazole-bearing pyrazoles has shown a promising *in vitro* profile, the *in vivo* PK evaluation of these compounds has not been performed, being our attention currently focused on the development of CIC-39. However, these

molecules represent a back-up strategy, in case our candidate fails in its development.

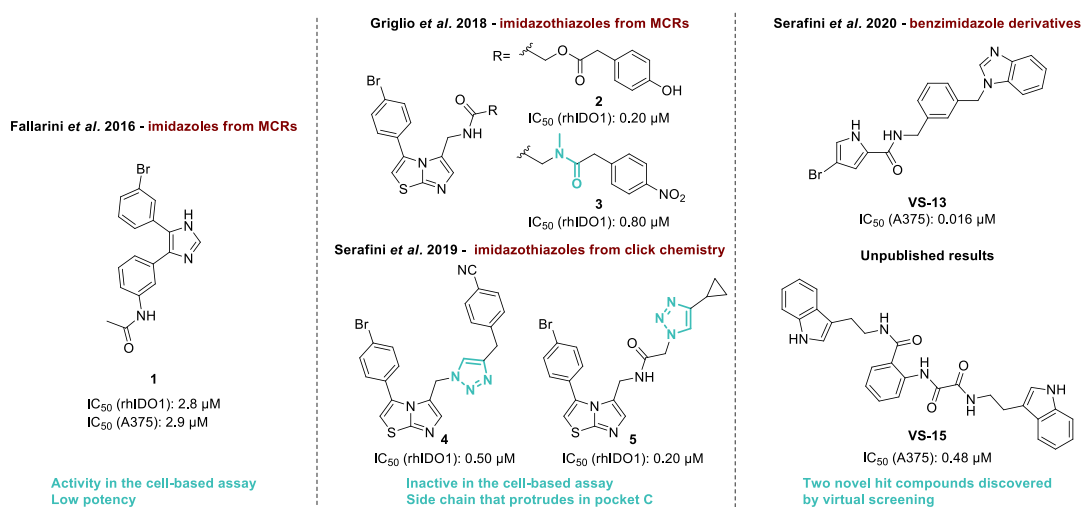
Figure 1. Structures and characteristics of the identified candidates among the three classes.



9.2 IDO1 inhibitors in cancer immunotherapy

The project on IDO1 inhibitors started in 2014,³ when the multicomponent reaction (*i.e.* the Van Leusen reaction) was exploited in the synthesis of a class of imidazoles that possessed cellular inhibitory activity on IDO1 but with low potency (**1**, Figure 2, lowest IC₅₀ value of the series: 2.8 μM (rhIDO1) and 2.9 μM (A375)). From this starting point, two classes of imidazothiazoles^{4,5} have been synthesized (**2-3** and **4-5**, Figure 2). While these classes showed a higher potency on the recombinant enzyme (lowest IC₅₀ value (rhIDO1): 0.2 μM), these compounds were not able to cross the plasma membrane and therefore they were inactive in the cell-based assay. Nevertheless, the imidazothiazole inhibitors have allowed us to get insight in the IDO1 active site and to discover an additional pocket, named C, that can be exploited in the design of novel IDO1 inhibitors. After having integrated this structural information in a virtual screening, we were able to discover two novel hit compounds, **VS-13** and **VS-15** (Figure 2).

Figure 2. A journey in the discovery of IDO1 inhibitors.



9.2.1 VS-13 is a promising candidate but is affected by a low metabolic stability

VS-13 is extremely potent against IDO1, being its IC_{50} value of 16 nM. Moreover, the compound represents a completely new chemical scaffold, never reported before.⁶

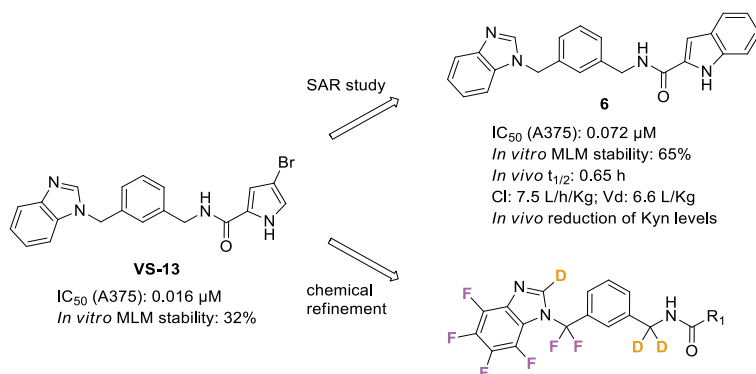
After having performed a complete SAR study, the most potent analogue of **VS-13** (**6**, Figure 3) has been selected for the evaluation of its pharmacokinetic and pharmacodynamic profile, being slightly more stable *in vitro* compared to **VS-13** (65% of residual substrate of **6** vs 32% of **VS-13** in MLM after 1 hour).

After administration in mice, the plasma levels of Kyn have been monitored and compound **6** showed a pharmacodynamic activity comparable to that of epacadostat. However, the compound is highly susceptible toward oxidative metabolism, resulting in dozens of metabolites formed and in a short half-life (less than one hour). Nevertheless, **VS-13** and its analogue are promising hit compounds, able to produce a strong reduction of Kyn levels and to abrogate the immunosuppressive properties of monocytic myeloid-derived suppressor cells (MDSC) isolated from patients affected by pancreatic ductal adenocarcinoma, with an effect comparable (or even

superior in case of **VS-13**) to epacadostat. Therefore, different strategies are being put in place to overcome the metabolic instability.

First, a chemical refinement will be performed by substitute the metabolically labile soft spots of the two molecules with either fluorine or deuterium as metabolic blockers (Figure 3). While fluorine represents a well-known isosteric replacement, deuterium incorporation has recently started to be used with the aim to bring new life to abandoned medicinal chemistry campaigns (Chapter 1). In this particular case, deuterium will be incorporated to reduce both oxidative metabolism of the benzimidazole ring mediated by aldehyde oxidase and *N*-dealkylation.⁷

Figure 3. Compound **VS-13** and its most potent analogue and possible strategies to improve the metabolic stability.



Another possibility is the use of the compound as a starting point to design PROTACs to target and promote the degradation of IDO1 in the cells. As described in Chapter 1, PROTACs are bifunctional molecules composed by a ligand for the protein of interest, such as **VS-13**, linked to a known ligand able to recruit an E3 ligase.⁸ The formation of this ternary complex (PROTAC, the protein of interest and the ligase with the E2 enzyme) induces the poly-ubiquitination of the target protein and its degradation through the proteasome system. Among the ligands that recruit the ligases, the most exploited are thalidomide and its analogues, that hijack cereblon (CRBN), and Von Hippel Lindau (VHL) ligands.

A recent study⁹ has evaluated the metabolism of 40 synthesized PROTACs in human hepatocytes and has compared their stability with that of the ligands which constitute the bifunctional molecules. This study highlighted that PROTACs are completely independent chemical entities, in which the metabolic liabilities are not retained from the parent small molecules, but largely depend on the linker features and on the site of attachment of the linker to the ligands.

Therefore, the metabolism of **VS-13**-based PROTACs could not be predicted based on the soft spots that characterized the molecule alone and its intrinsic instability could be masked by exploiting PROTACs. At the same time, to design a successful bifunctional molecule that will lead to IDO1 degradation, a SAR study will be performed by modifying the ligase-recruiting moiety, the linker portion and the site of attachment between the linker and **VS-13**.

9.2.3 VS-15 is characterized by a peculiar biological profile

VS-15 is endowed with a peculiar biological profile: while its IC₅₀ in A375 cell line is 0.48 μM and MST assay has highlighted a strong binding to IDO1 (K_d: 24.29 μM), the compound is inactive in the enzyme-based assay.

To get insight into its inhibition mechanism, a first experiment will be performed evaluating if the compound binds to IDO1 in its apo-form devoid of the heme group.¹⁰ This mechanism of action represents an off-beaten path in IDO1 field, since only two compounds¹¹ have been reported as apo-inhibitors and one of them is currently the most advanced clinical candidate linrodostat.

Also, while the compound is selective for IDO1 over TDO, it putatively acts also as an iNOS inhibitor. Inducible nitric oxide synthase (iNOS) is one of the three isoforms known to generate NO in response to external stimuli, together with the two constitutive isoforms, endothelial (eNOS) and neuronal (nNOS) nitric oxide synthases. iNOS is expressed upon cytokine exposure, produces more NO compared to the two related enzymes and promotes important tumour features, such as neoangiogenesis and metastasis.¹²

Moreover, a tight crosstalk between IDO1 and iNOS has been highlighted.¹³ Overall, therefore, the concomitant dual inhibition of both enzymes could represent an effective strategy in cancer treatment.

One of the main weaknesses of the compound is its metabolic instability, that leads to a residual substrate in MLS9 of 15% after 1 hour. However, **VS-15** has in the α,β -dicarbonyl substructure its main soft spot and therefore the chemical refinement has been already started and has led to a more metabolically stable analogue (compound **38**, Chapter 8, residual substrate in MLS9 of 51% after 1 hour). The SAR study of this class is currently ongoing, but it is likely that the metabolic weaknesses of the compound will be solved while retaining inhibitory activity.

9.3 References

1. a) Riva, B., Griglio, A.; Serafini, M.; Cordero-Sanchez, C.; Aprile, S.; Di Paola, R.; Gugliandolo, E.; Alansary, D.; Biocotino, I.; Lim, D.; Grosa, G.; Galli, U.; Niemeyer, B.; Sorba, G.; Canonico, P. L.; Cuzzocrea, S.; Genazzani, A. A.; Pirali, T. Pyrtriazoles, a novel class of store-operated calcium entry modulators: discovery, biological profiling, and *in vivo* proof-of-concept efficacy in acute pancreatitis. *J. Med. Chem.* **2018**, *61*, 9756-9783; b) Pirali, T.; Riva, B.; Genazzani, A. A. Modulators of SOCE, Compositions and use thereof. W.O. Patent 212,414, Dec 14, 2017.
2. a) Serafini, M.; Cordero-Sanchez, C.; Di Paola, R.; Bhela, I. P.; Aprile, S.; Purghe, B.; Fusco, R.; Cuzzocrea, S.; Genazzani, A. A.; Riva, B.; Pirali, T. Store-operated calcium entry (SOCE) as a therapeutic target in acute pancreatitis: discovery and development of drug-like SOCE inhibitor. *J. Med. Chem.* **2020**, *63*, 14761-14779; b) Pirali, T.; Riva, B.; Serafini, M.; Aprile, S.; Cordero Sanchez, C. Biphenyl compounds as SOCE modulators, compositions and uses thereof. Filed on February 21, 2020, n. 102020000003692.

3. Fallarini, S.; Massarotti, A.; Gesù, A.; Giovarruscio, S.; Coda Zabetta, G.; Bergo, R.; Giannelli, B.; Brunco, A.; Lombardi, G.; Sorba, G.; Piralì T. In silico-driven multicomponent synthesis of 4,5- and 1,5-disubstituted imidazoles as indoleamine 2,3-dioxygenase inhibitors. *MedChemComm* **2016**, *7*, 409-419.
4. Griglio, A.; Torre, E.; Serafini, M.; Bianchi, A.; Schmid, R.; Coda Zabetta, G.; Massarotti, A.; Sorba, G.; Piralì, T.; Fallarini, S. A multicomponent approach in the discovery of indoleamine 2,3-dioxygenase 1 inhibitors: synthesis, biological investigation and docking studies. *Bioorg. Med. Chem. Lett.* **2018**, *28*, 651-657.
5. Serafini, M.; Torre, E.; Aprile, S.; Massarotti, A.; Fallarini, S.; Piralì T. Synthesis, docking and biological evaluation of a novel class of imidazothiazoles as IDO1 inhibitors. *Molecules* **2019**, *24*, pii: E1874.
6. Serafini, M.; Torre, E.; Aprile, S.; Del Grosso, E.; Gesù, A.; Griglio, A.; Colombo, G.; Travelli, C.; Paiella, S.; Adamo, A.; Orecchini, E.; Coletti, A.; Pallotta, M. T.; Ugel, S.; Massarotti, A.; Piralì, T.; Fallarini, S. Discovery of highly potent benzimidazole derivatives as indoleamine 2, 3-dioxygenase-1 (IDO1) inhibitors: from structure-based virtual screening to *in vivo* pharmacodynamic activity. *J. Med. Chem.* **2020**, *63*, 3047-3065.
7. Piralì, T.; Serafini, M.; Cargini, S.; Genazzani, A. Applications of deuterium in medicinal chemistry. *J. Med. Chem.* **2019**, *62*, 5276-5297.
8. Toure, M.; Crews, C. M. Small-molecule PROTACS: new approaches to protein degradation. *Angew. Chem. Int. Ed. Engl.* **2016**, *55*, 1966-1973.
9. Goracci, L.; Desantis, J.; Valeri, A.; Castellani, B.; Eleuteri, M.; Cruciani, G. Understanding the metabolism of proteolysis targeting chimeras (PROTACs): the next step toward pharmaceutical applications. *J. Med. Chem.* **2020**, *63*, 11615-11638.
10. Nelp, M. T.; Kates, P. A.; Hunt, J. T.; Newitt, J. A.; Balog, A.; Maley, D.; Zhu, X.; Abell, L.; Allentoff, A.; Borzilleri, R.; Lewis, H. A.; Lin, Z.; Seitz,

S. P.; Yan, C.; Groves, J. T. Immune-modulating enzyme indoleamine 2,3-dioxygenase is effectively inhibited by targeting its apo-form. *Proc. Natl. Acad. Sci. U.S.A.* **2018**, *115*, 3249-3254.

11. Ortiz-Meoz, R. F.; Wang, L.; Matico, R.; Rutkowska, A.; la Rosa, M.; Bedard, S.; Midgett, R.; Strohmer, K.; Thomson, D.; Zhang, C.; Guss, J.; Totoritis, R.; Consler, T.; Campobasso, N.; Taylor, D.; Lewis, T.; Weaver, K.; Mulbaier, M.; Seal, J.; Dunham, R.; Kazmierski, W.; Favre, D.; Bergamini, G.; Shewchuk, L.; Rendina, A.; Zhang, G. Characterization of novel inhibition of indoleamine 2,3-dioxygenase by targeting its apo form. **2018**, bioRxiv:324947.
12. Vannini, F.; Kashfi, K.; Nathb, N. The dual role of iNOS in cancer. *Redox Biol.* **2015**, *6*, 334-343.
13. Samelson-Jones, B. J.; Yeh, S.-R. Interactions between nitric oxide and indoleamine 2,3-dioxygenase. *Biochemistry* **2006**, *45*, 8527-8538.

Publications

Publications from the thesis

1. Serafini, M.; Cordero-Sanchez, C.; Di Paola, R.; Bhela, I. P.; Aprile, S.; Purgè, B.; Fusco, R.; Cuzzocrea, S.; Genazzani, A. A.; Riva, B.; Pirali, T. Store-operated calcium entry (SOCE) as a therapeutic target in acute pancreatitis: discovery and development of drug-like SOCE inhibitor. *J. Med. Chem.* **2020**, *63*, 14761-14779.
2. Serafini, M.; Cargnin, S.; Massarotti, A.; Pirali, T.; Genazzani, A. A. Essential medicinal chemistry of essential medicines. *J. Med. Chem.* **2020**, *63*, 10170-10187.
3. Serafini, M.; Torre, E.; Aprile, S.; Del Grosso, E.; Gesù, A.; Griglio, A.; Colombo, G.; Travelli, C.; Paiella, S.; Adamo, A.; Orecchini, E.; Coletti, A.; Pallotta, M. T.; Ugel, S.; Massarotti, A.; Pirali, T.; Fallarini, S. Discovery of highly potent benzimidazole derivatives as indoleamine 2, 3-dioxygenase-1 (IDO1) inhibitors: from structure-based virtual screening to *in vivo* pharmacodynamic activity. *J. Med. Chem.* **2020**, *63*, 3047-3065.
4. Serafini, M.; Torre, E.; Aprile, S.; Massarotti, A.; Fallarini, S.; Pirali T. Synthesis, docking and biological evaluation of a novel class of imidazothiazoles as IDO1 inhibitors. *Molecules* **2019**, *24*, pii: E1874.
5. Pirali, T.; Serafini, M.; Cargnin, S.; Genazzani, A. Applications of deuterium in medicinal chemistry. *J. Med. Chem.* **2019**, *62*, 5276-5297.
6. Riva, B.; Griglio, A.; Serafini, M.; Cordero-Sanchez, C.; Aprile, S.; Di Paola, R.; Gugliandolo, E.; Alansary, D.; Biocotino, I.; Lim, D.; Grosa, G.; Galli, U.; Niemeyer, B.; Sorba, G.; Canonico, P. L.; Cuzzocrea, S.; Genazzani, A. A.; Pirali, T. Pyrtriazoles, a novel class of store-operated calcium entry modulators: Discovery, biological profiling, and *in vivo* proof-of-concept efficacy in acute pancreatitis. *J. Med. Chem.* **2018**, *61*, 9756-9783.

Publications from allied projects

7. Serafini, M.; Murgia, I.; Giustiniano, M.; Pirali, T.; Tron, G. C. The 115 year old multicomponent Bargellini reaction: perspectives and new applications. *Molecules* **2021**, *26*, 558-577.
8. Nikolaeva-Koleva, M.; Butron, L.; González-Rodríguez, S.; Devesa, I.; Valente, P.; Serafini, M.; Genazzani, A. A.; Pirali, T.; Fernández Ballester, G.; Fernández-Carvajal, A.; Ferrer-Montiel, A. A capsaicinoid-based soft drug, AG1529, for attenuating TRPV1-mediated histaminergic and inflammatory sensory neuron excitability. *Sci. Rep.* **2021**, *11*, 246-263.
9. Aprile, S.; Serafini, M.; Pirali, T. Soft drugs for dermatological applications: recent trends. *Drug Discov. Today* **2019**, *24*, 2234-2246.
10. Cargnin, S.; Serafini, M.; Pirali, T. A primer of deuterium in drug design. *Future Med. Chem.* **2019**, *11*, 2039-2042.

11. Serafini, M.; Griglio, A.; Aprile, S.; Seiti, F.; Travelli, C.; Pattarino, F.; Grosa, G.; Sorba, G.; Genazzani, A. A.; Gonzalez-Rodriguez, S.; Boutron, L.; Devesa, I.; Fernandez-Carvajal, A.; Pirali, T.; Ferrer-Montiel, A. Targeting Transient Receptor Potential Vanilloid 1 (TRPV1) channel softly: the discovery of Passerini adducts as a topical treatment for inflammatory skin disorders. *J. Med. Chem.* **2018**, *61*, 4436-4455.
12. Griglio, A.; Torre, E.; Serafini, M.; Bianchi, A.; Schmid, R.; Coda Zabetta, G.; Massarotti, A.; Sorba, G.; Pirali, T.; Fallarini, S. A multicomponent approach in the discovery of indoleamine 2,3-dioxygenase 1 inhibitors: synthesis, biological investigation and docking studies. *Bioorg. Med. Chem. Lett.* **2018**, *28*, 651-657.
13. Serafini, M.; Pirali, T. Arynes and isocyanides: two close-knit partners in multicomponent reactions. *Drug Discov. Today Technol.* **2018**, *29*, 35-41.
14. Serafini, M.; Griglio, A.; Oberto, E.; Pirali, T.; Tron, G. C. The use of 2-hydroxymethyl benzoic acid as an effective water surrogate in the Passerini reaction: a straightforward access to α -hydroxyamides. *Tetrahedron Lett.* **2017**, *58*, 4786-4789.
15. Pirali, T.; Ciruolo, E.; Aprile, S.; Massarotti, A.; Berndt, A.; Griglio, A.; Serafini, M.; Mercalli, V.; Landoni, C.; Campa, C. C.; Margaria, J. P.; Silva, R. L.; Grosa, G.; Sorba, G.; Williams, R.; Hirsch, E.; Tron, G. C. Identification of a potent phosphoinositide 3-kinase (PI3K) pan inhibitor displaying a strategic carboxylic acid group and development of its prodrugs. *ChemMedChem* **2017**, *12*, 1542-1554.
16. Serafini, M.; Griglio, A.; Viarengo, S.; Aprile, S.; Pirali, T. An aryne-based three-component access to α -aroylamino amides. *Org. Biomol. Chem.* **2017**, *15*, 6604-6612.

Book chapters:

1. Serafini M.; Pirali, T.; Tron, G. C. Click 1,2,3-triazoles in drug discovery and development: from the flask to the clinic? *Advances in Heterocyclic Chemistry* **2020**, *134* (article in press; DOI: 10.1016/bs.aihch.2020.10.001).
2. Pirali, T.; Galli, U.; Serafini, M.; Griglio, A.; Genazzani, A.A.; Tron, G.C. Drug discovery for soft drugs on TRPV1 and TRPM8 channels using the Passerini reaction. *Methods Mol. Biol.* **2019**, *1987*, 207-221.

Curriculum Vitae

Curriculum Vitae Marta Serafini

Born on April 19, 1991 in Gattinara (VC), Italy

Work address: Department of Pharmaceutical Sciences,
Università del Piemonte Orientale,
via Bovio 6, 28100 Novara (NO) Italy;

Work phone: +39 0321375852

Mobile phone: +39 3495338810

e-mail: marta.serafini@uniupo.it

Skype account: MartaSerafini.1904

Mother tongue: Italian

Other languages: English – Upper-intermediate level

Education and qualifications

11/2017 - 11/2020 PhD student in Chemistry and Biology (Medicinal Chemistry),
University of Piemonte Orientale, Novara (NO), Italy.

01/2016 - 11/2017 In-training Scholarship, University of Piemonte Orientale,
Novara (NO), Italy.

“Synthesis and scale-up of TRPV1 and cannabinoid receptors soft modulators”

11/2016 Admission to the Italian Pharmacy Board (abilitazione), University of
Piemonte Orientale, Novara (NO), Italy.

**10/2010 - 11/2015 Master’s Degree in Medicinal Chemistry and Technology
110/110 with honors**, University of Piemonte Orientale, Novara (NO), Italy. I was
awarded the prize for Student of the year from the School of Pharmacy (out of
approximately 120 students) on the basis of academic merit. The program included
a 6-month experimental project *“Synthesis of Transient Receptor Potential Channel-
1 (TRPV1) and cannabinoid receptors soft modulators”*. The results were published
on the *Journal of Medicinal Chemistry* (Serafini *et al.*, 2018).

Teaching experiences at University of Piemonte Orientale

2017 - present Co-supervisor of 11 Master’s Degree experimental thesis. As part
of my Ph.D. training, I co-supervise, together with my Ph.D. supervisor, those
students that attend a 6-month independent project in the lab.

2019 - 2020 Lectures for the EMOTION European Master (www.emotion-master.eu). In the context of an Erasmus Mundus Master Degree that my University
issues together with Spanish and Belgian universities, I have been appointed to give
4 1-hour lectures on bibliographic searches, with a particular focus on the use of
chemical databases such as SciFinder.

2016 - 2019 Laboratory assistant - I have been formally appointed to assist in the
laboratory of “drug synthetic preparation” that is held yearly for Master students and
lasts 3 weeks (50 hours). This lab allows students to set up reactions and to purify
compounds through standard chromatographic techniques. It is a rather challenging,

yet thrilling, laboratory in which every year the synthetic routes are changed and in which students work in small groups to allow a wide range of synthesis to be performed. I also participate in the planning of the proposed synthesis.

Awards and Prizes

2019 - 2020 Two-year funding for salary from the Italian Cancer Association (AIRC; 50000 euros) obtained through open competition (<https://www.direzionescientifica.airc.it/funding-for-research/fellowship/>).

2019 Best Poster Prize, “Store-Operated Calcium Entry: a new target from the cell calcium toolkit” European School of Medicinal Chemistry (ESMEC) 2019, Urbino (PU), Italy.

2018 - 2019 Travel awards to attend the following 3 conferences: National Meeting in Medicinal Chemistry (NMMC; Milano, 2019), MedChemSicily (Palermo, 2018), XXVI National Congress of Italian Chemical Society (Paestum 2017).

2015 Student of the year Award, University of Piemonte Orientale, academic year 2014/2015.

University governance

2019 - present Member of the Eligibility and Pre-admission Committee of the European Master in Translational Cosmetic and Dermatological Sciences (EMOTION Master), University of Piemonte Orientale, Novara (NO), Italy.

2019 - 2020 Elected Representative of PhD students in the Staff meeting of the Department Council of the School of Pharmaceutical Sciences, University of Piemonte Orientale, Novara (NO), Italy.

Public understanding of science

2020 I have written an article in Italian for *Cosmetic Technology*, CEC Editore, an Italian magazine on cosmetics: “The metabolism of bioactive substances”, Aprile, S.; Serafini, M.; Pirali, T. Sept-Oct 2020, 23(5), 8-14.

2019 I have written an article in Italian for a very well-known Italian magazine distributed to professionals in the chemistry field, explaining the druggability of calcium signalling pathways (Serafini and Pirali, *La Chimica & L’Industria*, 2019, N° 3).

2018 - present I have participated in a number of events to disseminate the importance of cancer prevention and oncology research, as well as my passion for it. These have been mainly organized by the Italian Association for Cancer Research, which is also the sponsor of my scholarship. In this, I have spoken in high schools, to children’s parents and to AIRC institutional and large donors. Recently, I have also been nominated by my Head of Department in the Coordination Committee to lease with Charities in the context of public understanding of science.

Additional Information

SCI (Italian Chemical Society) member since 2016, Medicinal Chemistry Division

References: References can be obtained from:

- Prof. Tracey Pirali, Dept. of Pharmaceutical Sciences, University of Piemonte Orientale, Italy
e-mail: tracey.pirali@uniupo.it; phone: +39 0321375853
- Prof. Armando Genazzani, Dept. of Pharmaceutical Sciences, University of Piemonte Orientale, Italy
e-mail: armando.genazzani@uniupo.it; phone: +39 0321375827
- Prof. Gian Cesare Tron, Dept. of Pharmaceutical Sciences, University of Piemonte Orientale, Italy
e-mail: giancesare.tron@uniupo.it; phone: +39 0321375857

Participation in conferences

2020 “Benzimidazoles as IDO1 inhibitors: from a virtual screening to a potential treatment in pancreatic ductal adenocarcinoma” **oral communication** (under invitation by SCI Giovani) at Italian Young Medicinal Chemistry Virtual Meeting (#IYMCVMEET).

2019 “Fine-tuning of Store-Operated Calcium Entry by pytriazoles as potential treatment of calcium-related rare diseases” **poster presentation** at National Meeting in Medicinal Chemistry (NMMC) 2019, Milano (MI), Italy.

2019 “Store-Operated Calcium Entry: a new target from the cell calcium toolkit” **poster presentation** at European School of Medicinal Chemistry (ESMEC) 2019, Urbino (PU), Italy.

2018 “Targeting TRPV1 softly: from the multicomponent synthesis to the preclinical validation of capsaicinoid modulators as a treatment for psoriatic pruritus” **oral communication** at MedChemSicily 2018, Palermo (PA), Italy.

2017 “Synthesis, biological evaluation and molecular docking of Ugi and Passerini products as novel indoleamine 2,3-dioxygenase 1 inhibitors” **poster presentation** at XXVI National Congress of Italian Chemical Society, Paestum (SA), Italy.

2017 “ α -Isocyanoacetamides: an investigation about their reactivity towards arynes” **poster presentation** at ISOS 2017, Gargnano (BS), Italy.

2016 “A novel three component reaction involving arynes, α -isocyanoacetamides and water” **poster presentation** at National Meeting in Medicinal Chemistry (NMMC) 2016, Perugia (PG), Italy.

Patents

- “Biphenyl compounds as SOCE modulators, compositions and uses thereof” Pirali, T.; Riva, B.; Serafini, M.; Aprile, S.; Cordero Sanchez, C. filed on February 21, 2020, n. 102020000003692.
- “Doxophylline derivatives” Giraudi, A.; Giraudi, G.; Cuzzocrea, S.; Di Paola, R.; Genazzani, A. A.; Pirali, T.; Serafini M., WO/2020/194223.